Reconstructing past Arctic sea ice and permafrost changes with lipid biomarkers: proxy development and case studies

Karen Jiaxi Wang

Sc.M. Brown University, 2019
B.S. Peking University, 2017

A dissertation submitted in partial fulfillment of the requirements for the degree of Doctor of Philosophy in the Department of Earth, Environmental and Planetary Sciences at Brown University.

Providence, Rhode Island
May 2022

© Copyright 2022 by Karen J. Wang

This dissertation by Karen Wang is accepted in its present form by the Department of Earth, Environmental and Planetary Sciences as satisfying the dissertation requirements for the degree of Doctor of Philosophy.

Date_____ _____
Yongsong Huang, Advisor

Recommended to the Graduate Council

Date _____ _____
Steven Clemens, Reader

Date _____ _____
Timothy Herbert, Reader

Date _____ _____
Victor Tsai, Reader

Date _____ _____
Tyler Kartzinel, Reader

Date _____ _____
Jonathan O'Donnell, Reader

Approved by the Graduate Council

Date _____ _____
Andrew G. Campbell, Dean of the Graduate School

KAREN JIAXI WANG

karenjxwang@gmail.com

Department of Earth, Environmental, and Planetary Sciences, Brown University, Box 1846, Providence, RI 02912

EDUCATION

Ph.D.	**Department of Earth, Environmental, and Planetary Sciences, Brown University** Focus: Climate & Environment, Advisor: Prof. Yongsong Huang	**2022** (expected)
M. Sc.	**Department of Earth, Environmental, and Planetary Sciences, Brown University** Focus: Climate & Environment, Advisor: Prof. Yongsong Huang	**2019**
B. Sc.	**School of Earth and Space Sciences, Peking University** Major: Geology	**2017**

HONORS AND AWARDS

International Meeting on Organic Geochemistry Best Student Presentation	2021
IBES Graduate Research, Training and Travel Award	2018, 2020
Brown University French Doctoral Research Fellow	2020
LacCore/CSDCO Visiting Graduate Student Travel Grant	2019
Chinese Academy of Sciences Stratigraphical Paleontology Scholarship	2016
Excellence in Undergraduate Research Training Program Award	2016
Kwang-Hua Educational Scholarship	2016
National Innovative Program Fellowship	2015

PEER-REVIEWED PUBLICATIONS

Novak, J., McGrath, S. M., **Wang, K. J.**, Liao, S., Clemens, S. C., Wolfgang, K., Holbourn, A., Huang, Y. (2022). $U^{K'}_{38ME}$ Expands the Linear Dynamic Range of the Alkenone Sea Surface Temperature Proxy. (*Geochimica et Cosmochimica Acta*, in print)

Liao, S., **Wang, K. J.**, Huang, Y. (2021). Extended chain length alkenoates differentiate three Isochrysidales groups. *Organic Geochemistry*, *161*, 104303.

Liao, S., **Wang, K. J.**, Xue, Y., Huo, J., Santos, E., Wang, J., Carsten, S. J., Huang, Y. (2021). Novel methyl-branched alkenones with up to five double bonds in saline lakes. *Organic Geochemistry, 156*, 104243.

Vachula, R. S., **Wang, K. J.**, Huang, Y., O'Donnell, J. A., (2021). New Approaches to Study Interactions Among Climate, Environment, and Humans in Arctic Alaska. *Alaska Park Science*, 20.

Wang, K. J., Huang, Y., Majaneva, M., Belt, S., Liao, S., Novak, J., Kartzinel, T. R., Herbert, T. D., Richter, N., Cabedo-Sanz, P. (2021). Group 2i Isochrysidales produce characteristic alkenones reflecting sea ice distribution. *Nature Communications, 12*, 15.

Liao, S., Yao, Y., Wang, L., **Wang, K. J.**, Amaral-Zettler, L., Longo, W. M., & Huang, Y. (2020). C41 methyl and C42 ethyl alkenones are biomarkers for Group II Isochrysidales. *Organic Geochemistry, 147*, 104081.

Wang, K. J., O'Donnell, J. A., Longo, W. M., Amaral-Zettler, L., Li, G., Yao, Y., & Huang, Y. (2019). Group I alkenones and Isochrysidales in the world's largest maar lakes and their potential paleoclimate applications. *Organic Geochemistry*, *138*, 103924.

Yao, Y., Zhao, J., Longo, W. M., Li, G., Wang, X., Vachula, R. S., **Wang, K. J.**, Huang, Y. (2019). New insights into environmental controls on the occurrence and abundance of Group I alkenones and their paleoclimate applications: Evidence from volcanic lakes of northeastern China. *Earth and Planetary Science Letters*, *527*, 115792.

Kaiser, J., **Wang, K. J.**, Rott, D., Li, G., Zheng, Y., Amaral-Zettler, L., ... & Huang, Y. (2019). Changes in long chain alkenone distributions and Isochrysidales groups along the Baltic Sea salinity gradient. *Organic geochemistry, 127*, 92-103.

Li, G., Li, L., Tarozo, R., Longo, W. M., **Wang, K. J.**, Dong, H., & Huang, Y. (2018). Microbial production of long-chain n-alkanes: Implication for interpreting sedimentary leaf wax signals. *Organic Geochemistry, 115*, 24-31.

PRESENTATIONS

Invited Talks

- Organic geochemical tools for understanding the oceans and atmosphere now and through time session invited talk, Goldschmidt2021 Conference, France, 2021
- Peking University, the Fifth International Young Scholars Geo-Symposium, 2021
- MIT, EAPS, Chemical Oceanography, Geology and Geobiology (COG3) seminar, 2021
- Chinese Society for Mineralogy Petrology and Geochemistry online lecture series, 2021
- Nanjing University, the Seventh Young Scholar Geo-Symposium, 2021
- Paleoclimate seminar, University of California Santa Cruz, 2021

Conference Presentations

- "An Annually Resolved Record of Permafrost-thaw Induced Carbon Cycling Changes for the Past 60 Years from White Fish Lake, Seward Peninsula, Alaska", AGU Fall Meeting, 2021
- "Species mixing in alkenone producers brings new opportunities in paleoclimate and paleoceanographic reconstruction", IMOG2021 Conference, France, 2021 (Best Student Presentation Award)
- "Demystifying the anomalous high-latitude marine alkenones: new paleo-sea ice proxies", AGU Fall Meeting, 2020
- "Species mixing of alkenone-producers at high latitude marginal oceans and its potential for sea ice margin reconstructions", AGU Fall Meeting, 2019
- "Freshwater alkenone producers", LacCore/CSDCO Drilling And Coring Summer Institute, 2018

- "Occurrence of Group I Isochrysidales in Alaska Maar lakes and its implications for alkenone based paleotemperature proxy", AGU Fall Meeting, 2018

TEACHING AND MENTORSHIP

Teaching Assistant

- GEOL 1370 Environmental Geochemistry (fall 2018, fall 2020)

Undergraduate Mentor

- Mentored five undergraduates (Derek Rott, Annie Huang, Rebecca Dalum, Eleanor Pereboom, Emma Kaufman) doing research with Prof. Yongsong Huang. (2018, 2019, 2020)

FIELD EXPERIENCE

Coring of Imuruk Lake, Seward Peninsula, Alaska	2019
Surface sediment sampling of White Fish Lake, Seward Peninsula, Alaska	2017
Surface sediment sampling of crater lakes, Inner Mongolia, China	2017
Geological mapping in Xingcheng, Liaoning province, China	2015

PROFESSIONAL TRAINING

Summer school

- Urbino Summer School of Paleoclimatology (USSP), 2018
- LacCore/CSDCO Drilling And Coring Summer Institute, 2018

Workshop

- PaleoHack—a hackathon exploring Python tools for paleoclimate data analysis, 2021

PROFESSIONAL SERVICE

Peer-Reviewed Articles for:

- *Earth Surface Processes and Landforms*

LANGUAGES

English (full professional proficiency), Chinese (native)

Dedicated to my grandma, and my parents.

Acknowledgements

I would like to first thank my advisor Dr. Yongsong Huang. Yongsong has not only taught me so much knowledge in the field of organic geochemistry, but also taught me how to think of big scientific questions and how to do and write research projects. Yongsong has encouraged me to think creatively, be brave to learn new skills, and be confident. I have grown so much as a scientist and also as a person in the past five years, with the challenges Yongsong encouraged me to take on. Yongsong is always rooting for his students to succeed, and I am forever grateful for the support.

I would like to thank the rest of my advisory and defense committee members: Pete Schultz, Steve Clemens, Tim Herbert, Tyler Kartzinel, Jon O'Donnell, and Victor Tsai. Over the past five years, I have worked on different projects crossing multiple disciplines. My study subjects ranged from oceans to Alaskan lakes, and the methods ranged from organic chemistry, to molecular biology, and to statistics. I am very grateful for the knowledge and expertise shared by the committee members, which made those interdisciplinary projects possible. And I'd also like to especially thank Jon for the help with field work and made sure everyone survive the Alaska wilderness.

I am very grateful for everyone in Yongsong's lab. Lab manager Marcelo Alexandre and Ewerton Santos have contributed so much to my experiments. Previous students: Will Longo, James Dillon, Yinsui Zheng, Richard Vachula, Nora Richter have all selflessly helped me, and I see them as mentors and role models. I also enjoyed doing research with my peers Sarah McGrath, Sian Liao, Ted Bobik, and Joseph Novak, they made every step less lonely. The

visiting scholars and undergraduate researcher in the lab have brought so many different perspectives to my research.

My friends in C&E and DEEPS have created a lot of great memories, from small chats at the rocks on GeoChem Green, to ski trips. And outside of the geoscience community, I want to thank my roommates: Zhiyan Wang, Wonyoung Lee, Xiaojing Du, Yanqi Liu, and Lingling Zhang, who made those rented apartments felt more like home. I also want to thank my international friends, and particularly my Chinese friends with whom I had so many hotpot parties. I want to thank my tennis friends, and the dance communities in Providence that brought so much joy and energy to my life.

Lastly, I want to thank my family that provided endless support even when far away. They showed me diligence, curiosity, persistence, ambition, and most importantly, kindness and generosity. They are the ones that I modeled after as a child, as a teenager and as an adult. I feel incredibly lucky to have them.

Table of Contents

List of Tables

List of Figures

Chapter 1: Introduction

Karen J. Wang[1,2]

[1]Department of Earth, Environmental, and Planetary Sciences, Brown University, Providence, USA
[2]Institute at Brown for Environment and Society, Brown University, Providence, USA

The Arctic is currently experiencing rapid changes with unprecedented rate and magnitude from human-induced climate warming. Profound changes in sea ice and permafrost extent are expected by 2050 under all warming scenarios (IPCC WGII, 2022). The projected warming in the Arctic is much faster than other regions, as the mean temperature change in the Arctic Ocean is around three times of global warming level (https://interactive-atlas.ipcc.ch/). The warming has radically altered the unique features in the Arctic, including, sea ice and permafrost. Specifically, Arctic sea ice cover has reduced to its lowest level since at least 1850, and an ice-free summer is projected to occur before 2050 (IPCC WGI, 2021). Sea ice plays a crucial role in the Earth's climate system as it has a much higher albedo that reflects majority of solar energy (0.65 for bare ice and 0.85 for snow-covered sea ice) compared to open seawater (0.07) (Stroeve et al., 2012). The sea-ice seasonality, extent, thickness, and melt pond proportion are important to the ocean heat budget. On the other hand, widespread permafrost warming and thawing have been occurring in the Arctic since the 1980s (IPCC WGI, 2021). Northern circumpolar surface permafrost (0-3 m) alone stores 1035 ±150 gigatons of soil organic carbon (Hugelius et al., 2014; Schuur et al., 2015). Thawing and warming of permafrost can expose this frozen carbon pool to microbial degradation and release CO_2 and CH_4, which forms positive feedback that accelerates climate warming, which in turn, promotes additional permafrost thaw (Schuur et al., 2015).

However, projections for future changes under climate forcing in Arctic sea ice and permafrost contain major uncertainties. Satellite data that provides observational constrains for sea ice is only available since 1978. Changes in sea-ice area since 1978 in response to warming is consistently underestimated in climate models, and modeling of sea ice changes in the marginal and shelf seas are especially complicated (Rosenblum & Eisenman, 2017; Horvat, 2021; Watts et al., 2021). Accurate past sea ice reconstruction on a longer timescale is needed to

parameterize and validate the model prior to future prediction. However, the existing sea ice reconstructions have largely relied upon terrestrial proxies (i.e. ice cores, tree rings, documentaries) which are indirectly related to sea ice (hence prone to errors), or marine proxies (i.e. diatoms, dinoflagellate cysts, IP_{25}) that often suffer from preservation problems (Kinnard et al., 2011; de Vernal et al., 2013). Robust, diagenetically stable marine based proxy for past sea ice reconstructions is needed.

Similarly for permafrost, modeling of permafrost thaw and associated ecosystem and carbon-cycle processes face limitations includes inadequate historical data and lack of understanding in the process (Walvoord & Kurylyk, 2016). The current permafrost carbon feedback models mainly focus on gradual (centimeters over decades) permafrost thaw near the ground-surface, and has significantly underestimated the carbon emission from permafrost thaw (Walter Anthony et al., 2018; Turetsky et al., 2020). Abrupt permafrost thaw (e.g., ground subsidence from melting ground ice, or thermokarst) that affect meters of permafrost soil in days to years has much greater greenhouse gas emission than gradual thaw, but those process are understudied (Turetsky et al., 2020). Thus, developing approaches to quantify the past changes in permafrost are crucial for understanding those physical process and estimate carbon emission from permafrost under different warming scenarios.

This dissertation consists of two sections: 1) Sea ice; and 2) permafrost. The overall objectives are to develop novel molecular and isotopic tools for sea ice and permafrost reconstructions, followed by case studies and proxy validations. I explored a series of lipid biomarkers that are produced by a broad spectrum of organisms, including Archaea, Bacteria, and Eukarya, and demonstrate that many of these biomarkers can quantitatively record past changes in Arctic sea-ice extent as well as ecological and carbon-cycling changes related to

permafrost thaw. I also applied the isotopic proxies tracking carbon-cycling to White Fish Lake, Seward, Alaska to obtain the first annually resolved record of Arctic permafrost induced biogeochemical changes during the Anthropocene.

In the first section of the thesis (Chapter 2-3), I developed a new sea ice proxy based on alkenones. Alkenones are a groups of compounds produced exclusively by algae in the order Isochrysidales. They are a class of $C_{35\text{-}42}$ methyl and ethyl ketones with two to four double bonds. The indices quantifying the unsaturation degree of C_{37} alkenones U_{37}^{K} and $U_{37}^{K'}$ are fundamental to paleo sea surface temperature (SST) reconstruction (Volkman et al., 1980; Brassell et al., 1986; Prahl & Wakeham, 1987). However, U_{37}^{K} and $U_{37}^{K'}$ often yield unrealistic SST in the northern high latitude oceans (Tierney & Tingley, 2018), and are often accompanied by the anomalously high relative abundance of the C_{37} tetra-unsaturated methyl alkenone ($\%C_{37:4}$), which is absent in mid- to low- latitude ocean. Chapter 2 challenged the conventional view that *Emiliania huxleyi* and *Gephyrocapsa oceanica* are the only alkenone producers in the ocean. Through next-generation sequencing of sediment samples, re-analyses of published environmental DNA data, and culture experiments, I identified a new lineage of Isochrysidales that is responsible for the $C_{37:4}$ production in high latitude oceans. I derived a significant positive correlation between $\%C_{37:4}$ and sea ice concentration in seawater filtered particulate organic matter and surface sediment, and applied $\%C_{37:4}$ as a sea-ice proxy in the Svalbard region downcore sediment samples spanning the past 14 kyrs. The finding demonstrates that $\%C_{37:4}$ is a promising proxy for sea ice reconstruction on thousand- and, potentially, million-year timescales.

Chapter 3 examined the global distribution and bloom phenology of Group 2i Isochrysidales in greater detail and further constrained its relationship with sea ice. In this chapter, I investigated Isochrysidales DNA and alkenones in sediment samples from Greenland fjords,

Baltic Sea, and Chesapeake Bay, which encompass three thermal regimes with the last being essentially free of sea ice. I also systematically mapped the occurrence of Group 2i based on environmental DNA data around the globe and compared it with temperature and ice occurrence. The results show that Group 2i relies on ice and its growth is hindered by warm temperature. Its bloom season is fundamentally different from other Isochrysidales that bloom in summer, as Group 2i blooms around the ice-melting season. Results from Chapter 3 supports the use of $\%C_{37:4}$ as a sea-ice proxy proposed in Chapter 2.

In the second section of the thesis (Chapter 4-5), I focused on applying lipid biomarker proxies in maar lakes in the northern Seward Peninsula, Alaska, to quantify recent climate change. Under the surface Holocene accumulation, the northern Seward Peninsula is covered by a vast, 5-50 m thick yedoma deposit, which are ice-rich fine-grained deposits with massive ice wedges formed in the late Pleistocene (Strauss et al., 2021). Abrupt thaw is extensive across this region underlain by yedoma, evidenced by widespread thermokarst lakes, thaw slumps, and peat-plateau collapse scars (Walter Anthony et al., 2018). The Espenberg volcanic field in this region created four of the world's largest maar lakes: White Fish Lake, North Killeak Lake, South Killeak Lake, and Devil Mountain Lake (Lanik et al., 2019). Those maar lakes provide valuable archives for the climate reconstruction in this region, in particular, White Fish Lake has much higher sedimentation rates than nearby ocean sites. In Chapter 4, I examined alkenones, sedimentary DNA, and water chemistry data across three maar lakes: White Fish Lake, North Killeak Lake, and Devil Mountain Lake. The results showed that alkenones are abundant in all three lakes, and Group I Isochrysidales are the producers of alkenones. The results also demonstrate the use of U_{37}^{K} as a proxy for the mean temperature of the spring isotherm.

Chapter 5 zooms in on a sediment core recovered from White Fish Lake and reconstructed the hydrological, ecological, and carbon-cycle changes in response to climate variations and permafrost thaw since the late 1950s at an annual resolution. This is the first time an Arctic lake with sedimentation rate high enough for annual resolution has been cored. I investigated the abundance as well as $\delta^{13}C$ of alkenones, n-alkanes, GDGTs, diploptene, and total organic carbon (TOC) in the core. The biomarkers showed changes in primary productivity, methanogenesis, methanotrophy, and vegetation in the White Fish Lake catchment since the late 1950s. In particular, the intensified carbon cycle since the 2010s coincides with the increase in Arctic air temperature and active layer depth, reflecting the unprecedented rate of change in Arctic climate during recent years.

Reference

Brassell, S. C., Eglinton, G., Marlowe, I. T., Pflaumann, U., & Sarnthein, M. (1986). Molecular stratigraphy: A new tool for climatic assessment. *Nature*, *320*(6058), 129–133. https://doi.org/10.1038/320129a0

de Vernal, A., Gersonde, R., Goosse, H., Seidenkrantz, M.-S., & Wolff, E. W. (2013). Sea ice in the paleoclimate system: The challenge of reconstructing sea ice from proxies – an introduction. *Quaternary Science Reviews*, *79*, 1–8. https://doi.org/10.1016/j.quascirev.2013.08.009

Horvat, C. (2021). Marginal ice zone fraction benchmarks sea ice and climate model skill. *Nature Communications*, *12*(1), 2221. https://doi.org/10.1038/s41467-021-22004-7

Hugelius, G., Strauss, J., Zubrzycki, S., Harden, J. W., Schuur, E. A. G., Ping, C.-L., Schirrmeister, L., Grosse, G., Michaelson, G. J., Koven, C. D., O'Donnell, J. A., Elberling, B., Mishra, U., Camill, P., Yu, Z., Palmtag, J., & Kuhry, P. (2014). Estimated stocks of circumpolar permafrost carbon with quantified uncertainty ranges and identified data gaps. *Biogeosciences*, *11*(23), 6573–6593. https://doi.org/10.5194/bg-11-6573-2014

Kinnard, C., Zdanowicz, C. M., Fisher, D. A., Isaksson, E., de Vernal, A., & Thompson, L. G. (2011). Reconstructed changes in Arctic sea ice over the past 1,450 years. *Nature*, *479*(7374), 509–512. https://doi.org/10.1038/nature10581

Prahl, F. G., & Wakeham, S. G. (1987). Calibration of unsaturation patterns in long-chain ketone compositions for palaeotemperature assessment. *Nature*, *330*(6146), 367–369. https://doi.org/10.1038/330367a0

Rosenblum, E., & Eisenman, I. (2017). Sea Ice Trends in Climate Models Only Accurate in Runs with Biased Global Warming. *Journal of Climate*, *30*(16), 6265–6278. https://doi.org/10.1175/JCLI-D-16-0455.1

Schuur, E. A. G., McGuire, A. D., Schädel, C., Grosse, G., Harden, J. W., Hayes, D. J., Hugelius, G., Koven, C. D., Kuhry, P., Lawrence, D. M., Natali, S. M., Olefeldt, D., Romanovsky, V. E., Schaefer, K., Turetsky, M. R., Treat, C. C., & Vonk, J. E. (2015). Climate change and the permafrost carbon feedback. *Nature*, *520*(7546), 171–179. https://doi.org/10.1038/nature14338

Service, N. P. (n.d.). *Bering Land Bridge National Preserve: Geologic Resources Inventory Report*. 122.

Strauss, J., Laboor, S., Schirrmeister, L., Fedorov, A. N., Fortier, D., Froese, D., Fuchs, M., Günther, F., Grigoriev, M., Harden, J., Hugelius, G., Jongejans, L. L., Kanevskiy, M., Kholodov, A., Kunitsky, V., Kraev, G., Lozhkin, A., Rivkina, E., Shur, Y., … Grosse, G. (2021). Circum-Arctic Map of the Yedoma Permafrost Domain. *Frontiers in Earth Science*, *9*, 758360. https://doi.org/10.3389/feart.2021.758360

Stroeve, J. C., Serreze, M. C., Holland, M. M., Kay, J. E., Malanik, J., & Barrett, A. P. (2012). The Arctic's rapidly shrinking sea ice cover: A research synthesis. *Climatic Change*, *110*(3–4), 1005–1027. https://doi.org/10.1007/s10584-011-0101-1

Tierney, J. E., & Tingley, M. P. (2018). BAYSPLINE: A New Calibration for the Alkenone Paleothermometer. *Paleoceanography and Paleoclimatology*, *33*(3), 281–301. https://doi.org/10.1002/2017PA003201

Turetsky, M. R., Abbott, B. W., Jones, M. C., Anthony, K. W., Olefeldt, D., Schuur, E. A. G., Grosse, G., Kuhry, P., Hugelius, G., Koven, C., Lawrence, D. M., Gibson, C., Sannel, A.

B. K., & McGuire, A. D. (2020). Carbon release through abrupt permafrost thaw. *Nature Geoscience*, *13*(2), 138–143. https://doi.org/10.1038/s41561-019-0526-0

Volkman, J. K., Eglinton, G., Corner, E. D. S., & Forsberg, T. E. V. (1980). Long-chain alkenes and alkenones in the marine coccolithophorid Emiliania huxleyi. *Phytochemistry*, *19*(12), 2619–2622. https://doi.org/10.1016/S0031-9422(00)83930-8

Walter Anthony, K., Schneider von Deimling, T., Nitze, I., Frolking, S., Emond, A., Daanen, R., Anthony, P., Lindgren, P., Jones, B., & Grosse, G. (2018). 21st-century modeled permafrost carbon emissions accelerated by abrupt thaw beneath lakes. *Nature Communications*, *9*(1). https://doi.org/10.1038/s41467-018-05738-9

Walvoord, M. A., & Kurylyk, B. L. (2016). Hydrologic Impacts of Thawing Permafrost-A Review. *Vadose Zone Journal*, *15*(6), vzj2016.01.0010. https://doi.org/10.2136/vzj2016.01.0010

Watts, M., Maslowski, W., Lee, Y. J., Kinney, J. C., & Osinski, R. (2021). A spatial evaluation of Arctic sea ice and regional limitations in CMIP6 historical simulations. *Journal of Climate*, 1–54. https://doi.org/10.1175/JCLI-D-20-0491.1

Chapter 2: Group 2i Isochrysidales produce characteristic alkenones reflecting sea ice distribution

Karen Jiaxi Wang [1,2,*], Yongsong Huang[1,2,*] ,Markus Majaneva[3], Simon T. Belt[4], Sian Liao[2,5], Joseph Novak[1], Tyler R. Kartzinel[2,6], Timothy D. Herbert[1,2], Nora Richter[1,2,7] & Patricia Cabedo-Sanz[4]

[1]Department of Earth, Environmental and Planetary Sciences, Brown University, Providence, RI 02912, USA.

[2] Institute at Brown for Environment and Society, Brown University, Providence, RI 02912, USA.

[3] Norwegian Institute for Nature Research (NINA), NO-7485 Trondheim, Norway.

[4] Biogeochemistry Research Centre, School of Geography, Earth and Environmental Sciences, Plymouth University, Plymouth PL4 8AA, UK.

[5] Department of Chemistry, Brown University, Providence, RI 02912, USA.

[6] Department of Ecology and Evolutionary Biology, Brown University, Providence, RI 02912, USA.

[7] Department of Marine Microbiology and Biogeochemistry, NIOZ Royal Netherlands Institute for Sea Research, Texel, The Netherlands.

This Chapter has been published in: *Nature Communications*

Citation: Wang, K. J., Huang, Y., Majaneva, M., Belt, S. T., Liao, S., Novak, J., ... & Cabedo-Sanz, P. (2021). Group 2i Isochrysidales produce characteristic alkenones reflecting sea ice distribution. *Nature communications*, *12*(1), 1-10.

Abstract

Alkenones are biomarkers produced solely by algae in the order Isochrysidales that have been used to reconstruct sea surface temperature (SST) since the 1980s. However, alkenone-based SST reconstructions in the northern high latitude oceans show significant bias towards warmer temperatures in core-tops, diverge from other SST proxies in down core records, and are often accompanied by anomalously high relative abundance of the C_{37} tetra-unsaturated methyl alkenone ($\%C_{37:4}$). Elevated $\%C_{37:4}$ is widely interpreted as an indicator of low sea surface salinity from polar water masses, but its biological source has thus far remained elusive. Here we identify a lineage of Isochrysidales that is responsible for elevated $C_{37:4}$ methyl alkenone in the northern high latitude oceans through next-generation sequencing and lab-culture experiments. This Isochrysidales lineage co-occurs widely with sea ice in marine environments and is distinct from other known marine alkenone-producers, namely *Emiliania huxleyi* and *Gephyrocapsa oceanica*. More importantly, the $\%C_{37:4}$ in seawater filtered particulate organic matter and surface sediments is significantly correlated with annual mean sea ice concentrations. In sediment cores from the Svalbard region, the $\%C_{37:4}$ concentration aligns with the Greenland temperature record and other qualitative regional sea ice records spanning the past 14 kyrs, reflecting sea ice concentrations quantitatively. Our findings imply that $\%C_{37:4}$ is a powerful proxy for reconstructing sea ice conditions in the high latitude oceans on thousand- and, potentially, on million-year timescales.

1.1 Introduction

Alkenones are among the best proxies for paleo-sea surface temperature (SST) reconstructions, and their exceptional diagenetic stability has enabled the generation of palaeotemperature records spanning tens of millions of years of Earth's history(Brassell et al., 1986; Herbert et al., 2016; Liu et al., 2009). They are a class of $C_{35\text{-}42}$ methyl and ethyl ketones with two to four double bonds produced exclusively by the algae in the order Isochrysidales(Brassell et al., 1986; Conte et al., 1995; Volkman et al., 1980; Xu et al., 2001; Zhao et al., 2014; Zheng et al., 2019): in ocean settings *Emiliania huxleyi* and the closely related *Gephyrocapsa oceanica* have been considered as the exclusive producers of di- ($C_{37:2}$) and tri- ($C_{37:3}$) unsaturated methyl alkenones(Brassell et al., 1986; Conte et al., 1995; Volkman et al., 1980). The unsaturation index of alkenones ($U_{37}^{K\prime}$), defined as $C_{37:2}/(C_{37:2}+C_{37:3})$, is positively correlated with temperature, as validated both by algal culture experiments and global core-top calibrations(Conte et al., 2006; P. J. Müller et al., 1998; Prahl et al., 1988; Prahl & Wakeham, 1987; Tierney & Tingley, 2018).

However, application of $U_{37}^{K\prime}$-SST calibrations in the northern high latitude oceans has encountered major difficulties. Variable warm bias in $U_{37}^{K\prime}$-based SST reconstructions is often accompanied by the occurrence of tetra-unsaturated alkenone ($C_{37:4}$), which is usually absent in mid- to low- latitude oceans and *E. huxleyi* cultures even under exceedingly low growth temperature(Zheng et al., 2019). This pattern is reported in surface sediment and seawater filtered particulate organic matter (POM) samples from the Nordic Seas and the Bering Sea(Bendle & Rosell-Melé, 2004; Harada et al., 2003; Rosell-Melé, 1998), and downcore sediment records in Okhotsk Sea during glacial periods(Harada et al., 2008; Hernández-Almeida et al., 2020; Seki et al., 2004). As a result, Rosell-Melé et al.(Rosell-Melé, 1998) concluded that $U_{37}^{K\prime}$ was unreliable

when the percentage of $C_{37:4}$ among the total C_{37} methyl alkenones ($\%C_{37:4}$) is >5%. Yet, $\%C_{37:4}$ greater than 5% is widely reported in sediment records in the northern high latitude oceans, thereby complicating SST reconstructions from these regions (Fig. 2. S. 1).

On the other hand, negative correlations between $\%C_{37:4}$ and sea surface salinity (SSS) on a regional scale were observed(Harada et al., 2003; Rosell-Melé, 1998; Sicre et al., 2002), with elevated $\%C_{37:4}$ often associated with fresher and colder water mass(Bendle et al., 2005; Rosellmele, 2002). The mechanisms for these observations, however, are poorly defined, with previous studies suggesting unknown oceanographic parameters(Rosell-Melé, 1998), and/or alkenone producers(Bendle et al., 2005) as the possible explanations. The occurrence of miscellaneous compounds that co-elute with $C_{37:4}$ alkenone in sediment samples extracts adds an additional level of complication when interpreting $\%C_{37:4}$ data.(Wang et al., 2019) Regardless of these problems, elevated $\%C_{37:4}$ is widely applied as an indicator of fresher and colder polar water mass or decreased SSS (Table 2. S. 1). More recently, it has been applied as an indicator of sea ice margin based on co-occurrence with benthic foraminifera signal suggesting sea-ice breakup(Lochte et al., 2019). The interpretation of $\%C_{37:4}$ as a proxy for SSS stands in direct contrast to results from culture experiments, which show positive, or no correlation between salinity and $\%C_{37:4}$ in marine and brackish Isochrysidales species(Chivall et al., 2014; Ono et al., n.d., 2012). Such conflict suggests that elevated $\%C_{37:4}$ is not a physiological response to decreased SSS, but rather that unidentified producers of $C_{37:4}$ occur in high latitude marine environments(Bendle et al., 2005; Rosell-Melé, 1998).

In this study, we used next-generation sequencing (NGS) to identify Isochrysidales in water column, sea ice, and sediment samples in northern high latitude marine environments. We show that Isochrysidales communities in subarctic regions are composed of a lineage that is distinct from

E. huxleyi and any other described species. Culture of this lineage isolated from sea ice demonstrate they are prolific producers of $C_{37:4}$. $\%C_{37:4}$ in POM and surface sediments in northern high latitude oceans show strong correlation with annual mean sea ice concentrations, which is further corroborated by downcore sediment records from the Svalbard region spanning the past 14 kyr. Our results suggest $\%C_{37:4}$ has great potential as a paleo sea ice proxy, which may provide crucial information about sea ice distributions prior to satellite observations.

2. Methods and Materials

2.1 Sample collection

Surface sediment samples for both DNA sequencing and alkenone analyses were collected from Canadian Arctic Archipelago during Amundsen 2018. The samples were stored at -20˚C before DNA extraction. Other surface sediment samples for alkenone analyses were collected during several cruises including M86/1 (R/V Meteor; 2011), P435 (R/V Poseidon; 2012), EMB046 (R/V Elisabeth Mann Borgese; 2013), JR51 (James Clark Ross; 2000), JR106 (James Clark Ross; 2004), KN158-4 (Knorr; 1998), POS175 (Poseidon; 1990), HLY0601 (USCGC Healy; 2006), HLY0702 (USCGC Healy; 2007), M13/2 (Meteor; 1990), M 21/2 (Meteor; 1992). The locations of the surface sediment samples are shown in Supplementary Data 1.

2.2 Next-generation Sequencing of Canadian Arctic Archipelago surface sediment samples

Sequencing of the surface sediment samples were performed by Jonah Ventures, Boulder, CO, U.S.A. (https://jonahventures.com/). Genomic DNA was extracted from the samples using the DNeasy PowerSoil HTP 96, then a 2-step PCR protocol was performed. First, a portion of 18S rRNA was amplified by an adapted version of primer pair 528Flong and PRYM01+7 (F: GCGGTAATTCCAGCTCCAA, R: GATCAGTGAAAACATCCCTGG, Egge et al.(Egge et al., 2013)). The first PCR step following the program described in Egge et al.(Egge et al., 2013) was performed in 25-µl reactions containing Phusion GC buffer, 0.4 mM of each primer, 0.2 mM dNTP, DMSO 3%, 0.5 U Phusion polymerase (Thermo Scientific) and 2 µl of DNA template. After cleanup of the amplicons, a second round of PCR was performed to give each sample a unique 12-nucleotide index sequence. The final indexed amplicons were then cleaned and normalized using

SequalPrep Normalization kit (Life Technologies, Carlsbad, CA) and proceed to sequencing on an Illumina MiSeq using V2 600-cycle kit (San Diego, CA). Sequencing success and read quality was verified using FastQC v0.11.8. The forward and reverse primers were removed from the sequences, and sequences with length below 100 bp were discarded. The Amplicon Sequence Variants (ASVs) were compiled for each sample after denoising by UNOISE3 algorithm with an alpha value of 5 to remove sequencing error(Edgar, 2016). Taxonomy of the ASVs was assigned using the SILVA reference database (including 506 Isochrysidales sequences) and assign_taxonomy.py as implemented in QIIME/1.9.1(Caporaso, Kuczynski, et al., 2010).

2.3 Re-analyses of environmental sequences and phylogeny

We searched for short-read studies including the term "sea ice" on the European Nucleotide Archive (ENA), and runs from studies targeting subfragments of 18S rRNA that included sea-ice or seawater samples were downloaded. Primers were removed from the downloaded raw reads using cutadapt(Martin, n.d.), except from Roche 454 sequenced reads where forward primers were removed after quality trimming. ASVs were compiled after the reads were quality trimmed using DADA2(Callahan et al., 2016), except for studies with available quality trimmed ASVs(Enberg et al., 2018; Majaneva et al., 2019). The DADA2 parameters were adjusted based on the quality profiles of the sequencing runs. Taxonomic affiliations of the ASVs were identified using the assignTaxonomy command in DADA2 and, as reference sequences, the Protist Ribosomal Reference database(Guillou et al., 2012) (including 159 expert-curated Isochrysidales sequences from each taxonomic groups). Sequences classified to the order Isochrysidales were selected to proceed to further analysis. Close relatives of the environmental sequences were identified through BLAST search against NCBI GenBank and compiled as reference sequences for phylogeny. All

sequences were then aligned against a curated alignment from Gran-Stadniczeñko et al.(Gran-Stadniczeñko et al., 2017) using PyNast(Caporaso, Bittinger, et al., 2010). In total, the alignment contains 105 sequences, including 6 Coccolithales, 16 Group 2 and III Isochrysidales culture, 46 published environmental sequences from GenBank, and 37 recovered or re-analyzed environmental sequences from this study. A maximum-likelihood phylogeny was inferred using the RAxML(Stamatakis, 2014) program with substitution model GTRCAT with 1000 bootstraps through CIPRES(Miller et al., 2010).

2.4 Culture experiments

We obtained the RCC5486 strain (GenBank accession: MH764930) from the Roscoff Culture from the National Institute for Environmental Studies. The strain was acclimatized to 3 ℃ and 6˚C for 10 days before the start of corresponding culture experiments. The f/2 medium was prepared from filtered and sterilized seawater collected from Vineyard Sound, Woods Hole, MA, USA, adjusted to 15, 21, 26, 31, 38 ppt. Cultures were grown under a light:dark cycle set at 16:8 hours. The light intensity was 140 $\mu E \cdot m^{-2} \cdot s^{-1}$. Culture experiments under each salinity and temperature condition were triplicated.

Cultures were harvested at early stationary phase (monitored using hemocytometer counts (Hausser Scientific, PA, USA)) by filtering onto 0.7 μm glass fiber filters (Merck Millipore, MA, USA). All filters were wrapped with aluminum foils and immediately frozen at -20 ℃ before further extraction and analysis. For alkenones analyses, all of the filters were freeze-dried overnight and then dissolved in DCM and sonicated (3 × 30 min, 40 ml each time). The total extracts were separated and analyzed for alkenones as described in the section Alkenones Analyses.

2.5 Alkenones Analyses

Surface sediment samples were analyzed for lipids by extracting around 10 g of freeze-dried sediment using a Dionex^{TM} accelerated solvent extraction (ASE) system with dichloromethane (DCM):methanol mixture (9:1, v/v) to obtain a total lipid extract (TLE). The TLE was then separated into alkane, ketone and polar fractions through silica gel columns by eluents with increasing polarity: hexane, DCM, and methanol. The ketone fraction containing alkenones was analyzed by gas chromatography-flame ionization detection (GC-FID) Agilent 7890N Series instrument equipped with mid-polarity column RTX-200 (105 m × 250 μm × 0.25 μm) with the oven program described in Zheng et al(Zheng et al., 2017). This method is able to fully eliminate the co-elution between alkenones and alkenoates, as well as co-elution between C_{38} methyl and ethyl alkenones (Zheng et al., 2017). Alkenone peaks were identified and quantified based on retention time compared with standard Group 1 alkenone samples extracted from BrayaSø Lake (Greenland) through Agilent ChemStation B.03.02. A gas chromatography-mass spectrometer (GC-MS, Agilent 7890B interfaced to 5977 inert plus MSD) equipped with RTX-200 columns (105 m × 250 μm × 0.25 μm) was used to examine co-elution. Samples with compounds co-eluting with alkenones were purified using silver thiolate silica gel columns with hexane : DCM (1:1, v/v), DCM, acetone(Wang et al., 2019). Regressions of alkenone indices and environmental parameters were performed via MATLAB (R2018b).

2.6 IP_{25} analyses

Analysis of IP_{25} (Ice Proxy with 25 carbon atoms) in core M23258-2 was carried out as described by Belt et al.(Belt et al., 2012) with minor modification. An internal standard (9-octylhexadec-8-ene; 9-OHD; 0.1 μg) was added to dried sediment material (ca. 2 g), which was

extracted using dichloromethane (DCM)/methanol (MeOH) (2:1 v/v; 3 x 6 ml) and ultrasonication. Following evaporation of the total organic extract (TOE) to dryness (N_2 stream; room T), elemental S was removed according to Cabedo-Sanz and Belt(Cabedo-Sanz & Belt, 2015). Thus, the TOE was dissolved in hexane (1 ml) followed by addition of tetrabutylammonium sulfite (TBA, 1ml) and propan-2-ol (2 ml). After brief shaking by hand (1 min), ultra-high purity water (3 ml) was added, re-agitated (1 min) and centrifuged (2 min; 2500 rpm). The hexane layer was transferred to a clean vial and the procedure repeated twice more. Combined hexane extracts were dried using N_2. Partially purified TOEs were re-suspended in hexane and purified using column chromatography (SiO_2; ca. 0.5 g in a glass pipette), with fractions containing IP_{25} collected using hexane (6 ml). Final purification was achieved using Ag-ion chromatography (Supelco discovery® Ag-Ion; 0.1 g). After elution of saturated hydrocarbons (hexane; 1 ml), unsaturated hydrocarbons including IP_{25} were collected in acetone (2 ml).

Identification and quantification of IP_{25} in purified sediment extracts was carried out via gas chromatography–mass spectrometry GC–MS using established methods(Belt et al., 2012) with an Agilent 7890 gas chromatograph equipped with a HP_{5MS} fused-silica column (30 m; 0.25µm film thickness; 0.25 mm internal diameter) coupled to an Agilent 5975 series mass spectrometric detector. IP_{25} was identified by its characteristic retention index ($RI_{HP5\text{-}MS}$ = 2081) and mass spectrum. Quantification was carried out in single ion monitoring (SIM) mode. The resulting peak areas for IP_{25} were normalised to internal standard responses, instrumental response factors, and sediment mass.

3. Results and discussion

3.1 Identifying widespread ice-related alkenone producers

We sequenced the V4 region of the 18S rRNA gene from three surface sediment samples containing high $\%C_{37:4}$ (59-68%; Fig. 2. S. 2) that were collected from Victoria Strait in the Canadian Arctic Archipelago where the sea ice regime is mainly governed by first-year ice. Four Isochrysidales amplicon sequence variants (ASVs) were recovered from those surface sediments (Table 2. S. 2). We also extracted 18S-V4 sequences of Isochrysidales available from NGS datasets from high latitude oceans (20 datasets, 1216 samples). We used a phylogenetic framework to compare these data with published Isochrysidales 18S-V4 data from environmental and culture studies(Edvardsen et al., 2016)(Fig. 2. 1).

We followed the Isochrysidales classification of Theroux et al.(Theroux et al., 2010) based on habitat salinity ranges and phylogenetic divergence: Group 1 (freshwater species, uncultured), Group 2 (brackish species, e.g., *Isochrysis galbana*, *Ruttnera lamellosa*), Group 3 (marine species, *E. huxleyi* and *G. oceanica*). Our phylogenetic analysis revealed close relationships between the majority of Isochrysidales sequences recovered from marine sites with perennial or extended seasonal sea ice and those of published sequences from lakes with seasonal or perennial ice cover (Fig. 2. 1, Fig. 2. 2a). The sequences formed a monophyletic group with 80% bootstrap support, and placement of these sequences within Group 2 Isochrysidales is supported by 100% bootstrap support. We refer to this monophyletic clade as the Group 2 ice lineage Isochrysidales (Group 2i). Group 2i is distinct from any named Isochrysidales species, and potentially represents one or more new species. The sequences falling within Group 2i were detected in environments with a wide range of salinity, from freshwater to saline brine channels within sea ice, and in samples from sea-ice cores, under-ice seawater, and sediments from regions governed by multi- and first-year ice.

These distributions suggest that Group 2i is euryhaline and well-adapted to variable Arctic marine environments. *E. huxleyi* was abundant in seawater samples that were collected during the summer after ice melt in the Chukchi Sea and Barents Sea, and was not identified in any of the sea-ice samples except one sample from the central Arctic. Particularly, seawater samples collected in the Fram Strait during sea ice melting season(Fadeev et al., 2018) (June 2014) where the western part of the Fram Strait was ice-covered and eastern part was ice-free, showed *E. huxleyi* was present in both ice-covered and ice-free sites. However, Group 2i was only detected in seawater samples collected under ice-cover. The DNA data suggests the presence of Group 2i is tightly associated with sea ice.

3.2 Culture experiments show Group 2i produce predominant $C_{37:4}$

To confirm that Group 2i produces high $\%C_{37:4}$, we cultured the un-classified Isochrysidales strain RCC5486 at 3˚C and 6 ˚C in f/2 medium under salinity of 15, 21, 26, 31, 38 ppt. The RCC5486 strain falls within the Group 2i in our phylogeny and it is the most phylogenetically similar strain to the Isochrysidales found in Canadian Arctic Archipelago surface sediments that is available in pure culture (Fig. 2. 1). Live cells of RCC5486 were isolated during the algal pre-bloom and bloom-development phase in sea ice samples from Baffin Bay(Ribeiro, n.d.) (67.47˚N, 63.78˚W; May-July 2016). The alkenones produced by RCC5486 showed exceptionally high $\%C_{37:4}$ (~80%) at both 3 and 6 ˚C (Fig. 2. S. 2), and salinity does not have any significant influence on $\%C_{37:4}$ (Fig. 2. S. 3). This further validates that physiological response to decreased salinity would not result in increased $C_{37:4}$ production. Published DNA sequences that falls into Group 2i in our phylogenetic analyses were also observed in water and sediment samples from lakes in China(Theroux et al., 2010; Yao et al., 2019), Canada(Plancq et al., 2019),

U.S.A.(Theroux et al., 2010) and Antarctica(Coolen, 2004), where $C_{37:4}$ was the predominant alkenone. High $\%C_{37:4}$ alkenone production is thus likely a shared characteristic across Group 2i Isochrysidales. Culture of RCC5486 also showed an absence of C_{38} methyl alkenones (C_{38}Me), matching alkenone production by other Group 2 Isochrysidales and differing from *E. huxleyi*(Zheng et al., 2019). However, C_{38}Me was present in the Canadian Arctic Archipelago surface sediments, even though Group 2i was the only Isochrysidales detected through NGS. The C_{38}Me detected in Canadian Arctic Archipelago is likely produced by *E.huxleyi* even though their DNA was not detected. The discrepancy between DNA and alkenone preservation could result from differences in the life cycles of Group 2i compared to *E. huxleyi*: the former potentially forms cysts and enters a resting stage in surface sediment(Ellegaard et al., 2016; Toney et al., 2012) while the latter does not form resting spores during winter(Hegseth & Sundfjord, 2008), after the bloom they die and disaggregate during downward transportation into sea-floor(Rosell-Mele & Comes, 2000).

3.3 Implications for sea ice, SSS and SST reconstructions

The identification of the novel and widespread Group 2i Isochrysidales gives rise to the possibility of using $\%C_{37:4}$ as a reliable sea ice proxy. Elevated $\%C_{37:4}$ from surface sediment and seawater POM(Bendle et al., 2005; Harada et al., 2003) is located at regions with seasonal sea ice in the Northern Hemisphere (Fig. 2. 2b). $\%C_{37:4}$ in both POM and surface sediment were positively and significantly correlated with sea ice concentrations (Fig. 2. 3a, 2. 3c). Differences in the calibration could be results of stronger seasonality of POM, uncertainty in the age of the surface sediment and advection influencing the linkage between sediment and overlying surface water(Conte et al., 2006). The positive correlation between sea ice concentration and $\%C_{37:4}$ most

likely reflect increasing alkenone contribution from Group 2i Isochrysidales with increasing sea ice. $\%C_{37:4}$ showed negative and significant correlations with SSS in POM and surface sediments (Fig. 2. 3b, 2. 3d), consistent with prior research(Harada et al., 2003; Rosell-Melé, 1998). However, this relationship is a byproduct of the negative correlation between SSS and sea ice concentrations in the above sample sites, which reflects the temporal influence of melting sea ice on near-surface salinity (Fig 2. S. 5). Thus variations in $\%C_{37:4}$ cannot be attributed to SSS changes, and regional relationship between $\%C_{37:4}$ and SSS should not be extrapolated for global-scale SSS reconstruction. So far there is no mechanistic explanation that supports a direct response of $\%C_{37:4}$ to changes in SSS, except in low salinity (0-6 ppt) or estuarine environments where Group 1 Isochrysidales are present and contribute to elevated $\%C_{37:4}$(Kaiser et al., 2019; Longo et al., 2016; Theroux et al., 2010). Group 1 Isochrysidales are typically found in freshwater to oligosaline environments and predominantly produce $C_{37:4}$(Longo et al., 2018). Alkenone contribution from Group 1 can be identified through the presence of $C_{37:3b}$ isomer, which is not produced by Group 2 and 3 (Longo et al., 2018). Our results show that both Group 1 and the Group 2i are present in brackish water underlying sea ice in the northwest of Gulf of Finland, Baltic Sea(Enberg et al., 2018) (Fig. 2. S. 6). However, Group 1 Isochrysidales are very sparse within sea ice in the Baltic Sea and are absent in other sea ice samples examined in this study (Fig. 2. 2). Thus, we conclude that the majority of $C_{37:4}$ production in the northern high latitude oceans distal from coast can be attributed to the presence of sea ice and Group 2i Isochrysidales.

Alkenones produced by the Group 2i are also a potential source of bias in $U_{37}^{K\prime}$-SST reconstructions. Surface sediment samples from regions covered by winter sea ice in the North Atlantic experience significant warm bias in $U_{37}^{K\prime}$-SST(Filippova et al., 2016; Tierney & Tingley, 2018). A similar warm bias is also observed in calculated SSTs from surface sediments examined

in this study, including the Canadian Arctic Archipelago samples where Group 2i was detected (Fig. 2. 2c), however the exact mechanism leading to the warm bias is still a question. Group 2i may produce alkenones within multi-year sea ice, but there is no prior report of alkenones detected from the surface sediments in the central Arctic. Bloom of Group 2i has been observed upon ice melt in Lake George, U.S.A., followed by a bloom of non-ice lineage Isochrysidales(Theroux et al., 2019). Group 2i and other Group 2 Isochrysidales are able to form cysts in sediments and potentially re-emerge to surface water during water-overturning under increased insolation(Ellegaard et al., 2016; Toney et al., 2012), which could occur in blooms during ice-melt. Prolonged seasonal sea ice and the Group 2i Isochrysidales within sea ice could potentially shift the phenology of *E. huxleyi* from colder to warmer seasons. They are also likely to have a $U_{37}^{K\prime}$-SST calibration different from *E. huxleyi*. The bias in $U_{37}^{K\prime}$-SST introduced by Group 2i could thus be more prominent during periods with extended seasonal sea ice coverage in downcore records. More experimental and field studies are needed to fully understand the causes for the warm SST bias inferred by $U_{37}^{K\prime}$ in high latitude oceans.

3.4 Validation of $\%C_{37:4}$ as paleo sea ice proxy in downcore sediments

Elevated $\%C_{37:4}$ has long been observed in concordance with other sea ice proxies, such as IRD (Bachem et al., 2017; Stein et al., 2014; Risebrobakken et al., 2010; Sánchez-Montes et al., 2020; Seki, 2005), diatoms (Stein et al., 2014; Horikawa et al., 2015), foraminifera assemblages (Lochte et al., 2019; McClymont et al., 2008) and IP_{25} (Łącka et al., 2019) in sediment records spanning the Late Pliocene to the Holocene. However, the interpretations of $\%C_{37:4}$ were essentially derived from long-term SSS change instead of the occurrence of sea ice in previous studies (Table 2. S. 1).

To further evaluate $\%C_{37:4}$ as a sea ice proxy within a paleoceanographic context, we compared $\%C_{37:4}$ records with the widely applied sea ice proxy IP_{25} and coarse fraction contents (% of grain size > 63 μm) in the Svalbard area during the past ca. 14.5 kyr (Fig. 2. 4, Fig. 2. 5). IP_{25} is a C_{25} isoprenoid lipid synthesized by certain Arctic sea ice diatoms and is deposited in underlying sediments following ice melt in spring (Belt, 2018; Belt et al., 2007; Brown et al., 2014). Coarse sediment fraction at this site is largely composed of lithic grains and foraminifera, reflecting sea ice formation off the western Barents shelf (Sarnthein. et al., 2003). The Fram Strait is the major gateway between the North Atlantic and the Arctic Ocean, and sea ice distribution in our study area is highly sensitive to surface temperature variability in modern time (Comiso et al., 2008). Over longer timeframes such as the Holocene, variations in sea-ice extent in the Fram strait, the Greenland Sea and the northern Barents Sea, co-occurred with changes in Northern Hemisphere solar insolation and changes in Greenland air temperature (Berben et al., 2017; J. Müller et al., 2009, 2012; Syring et al., 2020; Werner et al., 2016). Marine sediment core M23258-2(Sarnthein. et al., 2003; Martrat et al., 2003) (74.99˚N, 13.97˚E) is located close to the modern maximum winter sea ice extent in the northeastern Norwegian Sea where temporal variations of sea ice conditions have been identified (Belt et al., 2015). Alkenones were not detected prior to 14.1 kyr BP in M23258-2, likely due to seasonally extended sea-ice cover limiting productivity.The general trend of $\%C_{37:4}$ from M23258-2 (Martrat et al., 2003) is in direct agreement with inferred-temperature trends from the $\delta^{18}O$ values of Renland ice core located in east Greenland (Johnsen et al., 2001), with increasing $\%C_{37:4}$ corresponding to decreasing temperature, and is positively correlated with IP_{25} concentration and coarse fraction content in M23258-2 (Fig. 2. S. 7). The high values of $\%C_{37:4}$ in both M23258-2 and JM09-020-GC (Łącka et al., 2019) (76.31˚N, 19.70˚E) located in the glacial trough of Storfjordrenna during the Bølling-

Allerød (13.95-12.8 kyr BP) may represent partial sea-ice cover and a retreating ice edge; high coarse fraction content during this time in M23258-2 suggests rapid breakup of the Svalbard-Barents Sea Ice Sheet. The highest peak in $\%C_{37:4}$ in M23258-2 occurs at the beginning of the Younger Dryas (YD, ~12.8 kyr BP), indicating an expansion of sea ice. This is in agreement with increases in the coarse grain-size fraction and IP_{25} from M23258-2 and increases in IP_{25} at nearby site JM09-KA11-GC (Berben et al., 2014) (74.87˚N, 16.48˚E). The gradual decrease in $\%C_{37:4}$ observed in M23258-2 and JM09-020-GC after the termination of YD (~11.7 kyr BP) is coincident with increasing Northern Hemisphere summer insolation and temperature. Low $\%C_{37:4}$ in M23258-2 and the closely adjacent core SV04 (Rigual-Hernández et al., 2017) (74.957˚N, 13.899˚E) suggests that sea ice extent retreated and was present in low concentrations at these sites between 10.8-4 kyr BP during the Holocene Thermal Maximum, while the fluctuating $\%C_{37:4}$ in JM09-020-GC suggests a variable ice-edge condition at Storfjordrenna during this period. $\%C_{37:4}$ in M23258-2 increased after ca. 4 kyr BP indicating a slight expansion of the sea ice margin during the Neoglacial cooling period in the Northern Hemisphere, as the coarse fraction contents in this core also increased, reflecting sediment injections caused by cascades of dense brine water down the Barents shelf induced by seasonal sea ice (Sarnthein. et al., 2003). IP_{25} in M23258-2 is, however, absent (or below detection limit) during this time period. The return to partial seasonal sea ice cover during Neoglaciation is also evident in the rapid IP_{25} increase in the Fram Strait (Werner et al., 2016) (MSM5/5-723-2; 79.16˚N, 5.33˚E) and northern Barents Sea records (Köseoğlu et al., 2018) (NP05-11-70GC; 78.40˚N, 32.42˚E), as well as the re-emergence of IP_{25} in JM09-KA11-GC.

In this study we demonstrate that $\%C_{37:4}$ is a reliable and sensitive indicator for paleo sea ice, and has the potential for quantitative sea ice concentration reconstructions based on surface

sediment calibrations. As alkenones are solely produced by Isochrysidales, $\%C_{37:4}$ directly reflects proportion of Group 2i Isochrysidales within Isochrysidales community induced by sea ice, and is not affected by variations in total productivity or sedimentation rates as IP_{25}. $\%C_{37:4}$ is also less likely to be affected by diagenetic factors due to the strong diagenetic stability of alkenones, and does not suffer from dissolution like microfossil sea-ice proxies such as diatoms, ostracods, and foraminifers. As an example of the durability of the $\%C_{37:4}$ proxy, a gradual increase of $\%C_{37:4}$ from 0 to 10% was observed in Bering Sea after the onset of MIS M2 glaciation (~3.3Ma) in concordance with an increase in sea-ice-related diatoms (Horikawa et al., 2015). In addition, $\%C_{37:4}$ provides site-specific sea ice information which is different from proxies such as methanesulfonic acid and sea salt in ice from glaciers and ice sheets that records the averaged sea ice condition at a variable (e.g., depending on wind direction and speed) sector of ocean. Future work combining molecular biology and organic geochemistry analyses in culture experiments and large-scale analyses of seawater, sea ice and sediment samples will improve the $\%C_{37:4}$-sea ice calibration and shed light on other sea-ice properties such as seasonality.

Data availability

Raw sequence data generated in this study were archived in NCBI GenBank with accession number PRJNA650544, assembled Isochrysidales sequences were archived in NCBI GenBank with accession number MT647637-MT647640. Re-analyzed NGS data can be found through European Nucleotide Archive (ENA) with accession codes provided in Supplementary Data 2. Reference database SILVA is available at https://www.arb-silva.de/, and PR2 is available at https://github.com/pr2database/pr2database.

Acknowledgements

This work was supported by the United States National Science Foundation (NSF) EAR-1762431 and an IBES seed grant to Yongsong Huang, IBES Graduate Research, Training & Travel Award to Karen Wang, and NSF DEB-1930820 to Tyler R. Kartzinel. We would like to thank Dr. Beth Caissie for surface sediment samples from Bering Sea, and Dr. Daniel Sigman, , Dr. Cara Manning, Dr. Anissa Merzouk, Dr. Alexandre Forest, Dr. Camille Wilhelmy, Dr. Philippe-Olivier Dumais, Dr. Diana Saltymakova, Dr. Katarzyna Polcwiartek and Dr. Cindy Grant for surface sediment samples from Amundsen cruise. We would like to thank GEOMAR Helmholtz Centre for Ocean Research, BOSCORF repository and Lamont-Doherty Core Repository, Columbia University for other surface sediment samples. We would also like to thank Dr. Robert Spielhagen for sediment samples from core M23258-2.

Author Contributions

Y.H. initiated the research idea. K.J.W. and Y.H. co-designed the study after discussions with T.R.K., T.D.H. and S.T.B; K.J.W., M.M., T.R.K. and N.R. analyzed the DNA and the phylogenetic data; S.L. conducted the culture experiment; J.N., S.L., K.J.W., Y.H. and T.D.H. conducted the alkenone analyses; S.T.B. and P.C. conducted the IP_{25} analyses; K.J.W. and Y.H. co-wrote the manuscript with contributions from co-authors.

Competing Interests

The authors declare no competing interests.

Reference

Anon. 2014. *Earth and Life Processes Discovered from Subseafloor Environments - A Decade of Science Achieved by the Integrated Ocean Drilling Program (IODP)*. Vol. 7. Elsevier.

Bachem, Paul E., Bjørg Risebrobakken, Stijn De Schepper, and Erin L. McClymont. 2017. "Highly Variable Pliocene Sea Surface Conditions in the Norwegian Sea." *Climate of the Past* 13(9):1153–68. doi: 10.5194/cp-13-1153-2017.

Belt, Simon T. 2018. "Source-Specific Biomarkers as Proxies for Arctic and Antarctic Sea Ice." *Organic Geochemistry* 125:277–98. doi: 10.1016/j.orggeochem.2018.10.002.

Belt, Simon T., Thomas A. Brown, Alba Navarro Rodriguez, Patricia Cabedo Sanz, Andrew Tonkin, and Rebecca Ingle. 2012. "A Reproducible Method for the Extraction, Identification and Quantification of the Arctic Sea Ice Proxy IP25 from Marine Sediments." *Analytical Methods* 4(3):705. doi: 10.1039/c2ay05728j.

Belt, Simon T., Patricia Cabedo-Sanz, Lukas Smik, Alba Navarro-Rodriguez, Sarah M. P. Berben, Jochen Knies, and Katrine Husum. 2015. "Identification of Paleo Arctic Winter Sea Ice Limits and the Marginal Ice Zone: Optimised Biomarker-Based Reconstructions of Late Quaternary Arctic Sea Ice." *Earth and Planetary Science Letters* 431:127–39. doi: 10.1016/j.epsl.2015.09.020.

Belt, Simon T., Guillaume Massé, Steven J. Rowland, Michel Poulin, Christine Michel, and Bernard LeBlanc. 2007. "A Novel Chemical Fossil of Palaeo Sea Ice: IP25." *Organic Geochemistry* 38(1):16–27. doi: 10.1016/j.orggeochem.2006.09.013.

Bendle, James, and Antoni Rosell-Melé. 2004. "Distributions of U^{K}_{37} and $U^{K}_{37'}$ in the Surface Waters and Sediments of the Nordic Seas: Implications for Paleoceanography:

DISTRIBUTIONS OF U^{K}_{37} AND $U^{K}_{37'}$." *Geochemistry, Geophysics, Geosystems* 5(11):n/a-n/a. doi: 10.1029/2004GC000741.

Bendle, James, Antoni Rosell-Melé, and Patrizia Ziveri. 2005. "Variability of Unusual Distributions of Alkenones in the Surface Waters of the Nordic Seas: PERCENT $C_{37:4}$ IN THE NORDIC SEAS." *Paleoceanography* 20(2):n/a-n/a. doi: 10.1029/2004PA001025.

Berben, S. M. P., K. Husum, P. Cabedo-Sanz, and S. T. Belt. 2014. "Holocene Sub-Centennial Evolution of Atlantic Water Inflow and Sea Ice Distribution in the Western Barents Sea." *Climate of the Past* 10(1):181–98. doi: 10.5194/cp-10-181-2014.

Berben, Sarah M. P., Katrine Husum, Alba Navarro-Rodriguez, Simon T. Belt, and Steffen Aagaard-Sørensen. 2017. "Semi-Quantitative Reconstruction of Early to Late Holocene Spring and Summer Sea Ice Conditions in the Northern Barents Sea: HOLOCENE SEA ICE CONDITIONS IN THE NORTHERN BARENTS SEA." *Journal of Quaternary Science* 32(5):587–603. doi: 10.1002/jqs.2953.

Brassell, S. C., G. Eglinton, I. T. Marlowe, U. Pflaumann, and M. Sarnthein. 1986. "Molecular Stratigraphy: A New Tool for Climatic Assessment." *Nature* 320(6058):129–33. doi: 10.1038/320129a0.

Brown, T. A., S. T. Belt, A. Tatarek, and C. J. Mundy. 2014. "Source Identification of the Arctic Sea Ice Proxy IP25." *Nature Communications* 5(1). doi: 10.1038/ncomms5197.

Cabedo-Sanz, Patricia, and Simon T. Belt. 2015. "Identification and Characterisation of a Novel Mono-Unsaturated Highly Branched Isoprenoid (HBI) Alkene in Ancient Arctic Sediments." *Organic Geochemistry* 81:34–39. doi: 10.1016/j.orggeochem.2015.01.009.

Callahan, Benjamin J., Paul J. McMurdie, Michael J. Rosen, Andrew W. Han, Amy Jo A. Johnson, and Susan P. Holmes. 2016. "DADA2: High-Resolution Sample Inference from Illumina Amplicon Data." *Nature Methods* 13(7):581–83. doi: 10.1038/nmeth.3869.

Caporaso, J. G., K. Bittinger, F. D. Bushman, T. Z. DeSantis, G. L. Andersen, and R. Knight. 2010. "PyNAST: A Flexible Tool for Aligning Sequences to a Template Alignment." *Bioinformatics* 26(2):266–67. doi: 10.1093/bioinformatics/btp636.

Caporaso, J Gregory, Justin Kuczynski, Jesse Stombaugh, Kyle Bittinger, Frederic D. Bushman, Elizabeth K. Costello, Noah Fierer, Antonio Gonzalez Peña, Julia K. Goodrich, Jeffrey I. Gordon, Gavin A. Huttley, Scott T. Kelley, Dan Knights, Jeremy E. Koenig, Ruth E. Ley, Catherine A. Lozupone, Daniel McDonald, Brian D. Muegge, Meg Pirrung, Jens Reeder, Joel R. Sevinsky, Peter J. Turnbaugh, William A. Walters, Jeremy Widmann, Tanya Yatsunenko, Jesse Zaneveld, and Rob Knight. 2010. "QIIME Allows Analysis of High-Throughput Community Sequencing Data." *Nature Methods* 7(5):335–36. doi: 10.1038/nmeth.f.303.

Chivall, David, Daniela M'Boule, Daniëlle Sinke-Schoen, Jaap S. Sinninghe Damsté, Stefan Schouten, and Marcel T. J. van der Meer. 2014. "Impact of Salinity and Growth Phase on Alkenone Distributions in Coastal Haptophytes." *Organic Geochemistry* 67:31–34. doi: 10.1016/j.orggeochem.2013.12.002.

Comiso, Josefino C., Claire L. Parkinson, Robert Gersten, and Larry Stock. 2008. "Accelerated Decline in the Arctic Sea Ice Cover." *Geophysical Research Letters* 35(1). doi: 10.1029/2007GL031972.

Conte, Maureen H., Marie-Alexandrine Sicre, Carsten Rühlemann, John C. Weber, Sonja Schulte, Detlef Schulz-Bull, and Thomas Blanz. 2006. "Global Temperature Calibration of the

Alkenone Unsaturation Index ($U^{K'}_{37}$) in Surface Waters and Comparison with Surface Sediments: ALKENONE UNSATURATION INDEX." *Geochemistry, Geophysics, Geosystems* 7(2):n/a-n/a. doi: 10.1029/2005GC001054.

Conte, Maureen H., Anthony Thompson, Geoffrey Eglinton, and John C. Green. 1995. "LIPID BIOMARKER DIVERSITY IN THE COCCOLITHOPHORID EMILIANIA HUXLEYI (PRYMNESIOPHYCEAE) AND THE RELATED SPECIES GEPHYROCAPSA OCEANICA1." *Journal of Phycology* 31(2):272–82. doi: 10.1111/j.0022-3646.1995.00272.x.

Coolen, M. 2004. "Combined DNA and Lipid Analyses of Sediments Reveal Changes in Holocene Haptophyte and Diatom Populations in an Antarctic Lake." *Earth and Planetary Science Letters* 223(1–2):225–39. doi: 10.1016/j.epsl.2004.04.014.

Edgar, Robert C. 2016. *UNOISE2: Improved Error-Correction for Illumina 16S and ITS Amplicon Sequencing*. *preprint*. Bioinformatics. doi: 10.1101/081257.

Edvardsen, Bente, Elianne Sirnæs Egge, and Daniel Vaulot. 2016. "Diversity and Distribution of Haptophytes Revealed by Environmental Sequencing and Metabarcoding – a Review." *Perspectives in Phycology* 3(2):77–91. doi: 10.1127/pip/2016/0052.

Egge, Elianne, Lucie Bittner, Tom Andersen, Stéphane Audic, Colomban de Vargas, and Bente Edvardsen. 2013. "454 Pyrosequencing to Describe Microbial Eukaryotic Community Composition, Diversity and Relative Abundance: A Test for Marine Haptophytes" edited by S. Lin. *PLoS ONE* 8(9):e74371. doi: 10.1371/journal.pone.0074371.

Ellegaard, Marianne, Øjvind Moestrup, Thorbjørn Joest Andersen, and Nina Lundholm. 2016. "Long-Term Survival of Haptophyte and Prasinophyte Resting Stages in Marine Sediment." *European Journal of Phycology* 51(3):328–37. doi: 10.1080/09670262.2016.1161243.

Enberg, S., M. Majaneva, R. Autio, J. Blomster, and Jm Rintala. 2018. “Phases of Microalgal Succession in Sea Ice and the Water Column in the Baltic Sea from Autumn to Spring.” *Marine Ecology Progress Series* 599:19–34. doi: 10.3354/meps12645.

Fadeev, Eduard, Ian Salter, Vibe Schourup-Kristensen, Eva-Maria Nöthig, Katja Metfies, Anja Engel, Judith Piontek, Antje Boetius, and Christina Bienhold. 2018. “Microbial Communities in the East and West Fram Strait During Sea Ice Melting Season.” *Frontiers in Marine Science* 5. doi: 10.3389/fmars.2018.00429.

Filippova, A., M. Kienast, M. Frank, and R. R. Schneider. 2016. “Alkenone Paleothermometry in the North Atlantic: A Review and Synthesis of Surface Sediment Data and Calibrations: ALKENONE PALEOTHERMOMETRY.” *Geochemistry, Geophysics, Geosystems* 17(4):1370–82. doi: 10.1002/2015GC006106.

Gran-Stadniczeñko, Sandra, Luka Šupraha, Elianne D. Egge, and Bente Edvardsen. 2017. “Haptophyte Diversity and Vertical Distribution Explored by 18S and 28S Ribosomal RNA Gene Metabarcoding and Scanning Electron Microscopy.” *Journal of Eukaryotic Microbiology* 64(4):514–32. doi: 10.1111/jeu.12388.

Guillou, Laure, Dipankar Bachar, Stéphane Audic, David Bass, Cédric Berney, Lucie Bittner, Christophe Boutte, Gaétan Burgaud, Colomban de Vargas, Johan Decelle, Javier del Campo, John R. Dolan, Micah Dunthorn, Bente Edvardsen, Maria Holzmann, Wiebe H. C. F. Kooistra, Enrique Lara, Noan Le Bescot, Ramiro Logares, Frédéric Mahé, Ramon Massana, Marina Montresor, Raphael Morard, Fabrice Not, Jan Pawlowski, Ian Probert, Anne-Laure Sauvadet, Raffaele Siano, Thorsten Stoeck, Daniel Vaulot, Pascal Zimmermann, and Richard Christen. 2012. “The Protist Ribosomal Reference Database

(PR2): A Catalog of Unicellular Eukaryote Small Sub-Unit RRNA Sequences with Curated Taxonomy." *Nucleic Acids Research* 41(D1):D597–604. doi: 10.1093/nar/gks1160.

Harada, Naomi, Miyako Sato, and Tatsuhiko Sakamoto. 2008. "Freshwater Impacts Recorded in Tetraunsaturated Alkenones and Alkenone Sea Surface Temperatures from the Okhotsk Sea across Millennial-Scale Cycles: MILLENNIAL CYCLES IN OKHOTSK SST AND SSS." *Paleoceanography* 23(3):n/a-n/a. doi: 10.1029/2006PA001410.

Harada, Naomi, Kyung Hoon Shin, Akihiko Murata, Masao Uchida, and Tomoko Nakatani. 2003. "Characteristics of Alkenones Synthesized by a Bloom of Emiliania Huxleyi in the Bering Sea." *Geochimica et Cosmochimica Acta* 67(8):1507–19. doi: 10.1016/S0016-7037(02)01318-2.

Hegseth, Else Nøst, and Arild Sundfjord. 2008. "Intrusion and Blooming of Atlantic Phytoplankton Species in the High Arctic." *Journal of Marine Systems* 74(1–2):108–19. doi: 10.1016/j.jmarsys.2007.11.011.

Herbert, Timothy D., Kira T. Lawrence, Alexandrina Tzanova, Laura Cleaveland Peterson, Rocio Caballero-Gill, and Christopher S. Kelly. 2016. "Late Miocene Global Cooling and the Rise of Modern Ecosystems." *Nature Geoscience* 9(11):843–47. doi: 10.1038/ngeo2813.

Hernández-Almeida, Iván, Demetrio Boltovskoy, Svetlana B. Kruglikova, and Giuseppe Cortese. 2020. "A New Radiolarian Transfer Function for the Pacific Ocean and Application to Fossil Records: Assessing Potential and Limitations for the Last Glacial-Interglacial Cycle." *Global and Planetary Change* 190:103186. doi: 10.1016/j.gloplacha.2020.103186.

Horikawa, Keiji, Ellen E. Martin, Chandranath Basak, Jonaotaro Onodera, Osamu Seki, Tatsuhiko Sakamoto, Minoru Ikehara, Saburo Sakai, and Kimitaka Kawamura. 2015. "Pliocene

Cooling Enhanced by Flow of Low-Salinity Bering Sea Water to the Arctic Ocean." *Nature Communications* 6(1). doi: 10.1038/ncomms8587.

Jakobsson, Martin, Larry Mayer, Bernard Coakley, Julian A. Dowdeswell, Steve Forbes, Boris Fridman, Hanne Hodnesdal, Riko Noormets, Richard Pedersen, Michele Rebesco, Hans Werner Schenke, Yulia Zarayskaya, Daniela Accettella, Andrew Armstrong, Robert M. Anderson, Paul Bienhoff, Angelo Camerlenghi, Ian Church, Margo Edwards, James V. Gardner, John K. Hall, Benjamin Hell, Ole Hestvik, Yngve Kristoffersen, Christian Marcussen, Rezwan Mohammad, David Mosher, Son V. Nghiem, Maria Teresa Pedrosa, Paola G. Travaglini, and Pauline Weatherall. 2012. "The International Bathymetric Chart of the Arctic Ocean (IBCAO) Version 3.0: IBCAO VERSION 3.0." *Geophysical Research Letters* 39(12):n/a-n/a. doi: 10.1029/2012GL052219.

Johnsen, Sigfus J., Dorthe Dahl-Jensen, Niels Gundestrup, Jørgen P. Steffensen, Henrik B. Clausen, Heinz Miller, Valerie Masson-Delmotte, Arny E. Sveinbjörnsdottir, and James White. 2001. "Oxygen Isotope and Palaeotemperature Records from Six Greenland Ice-Core Stations: Camp Century, Dye-3, GRIP, GISP2, Renland and NorthGRIP: OXYGEN ISOTOPE AND PALEOTEMPERATURE RECORDS FROM SIX GREENLAND ICE-CORES." *Journal of Quaternary Science* 16(4):299–307. doi: 10.1002/jqs.622.

Kaiser, Jérôme, Karen J. Wang, Derek Rott, Gaoyuan Li, Yinsui Zheng, Linda Amaral-Zettler, Helge W. Arz, and Yongsong Huang. 2019. "Changes in Long Chain Alkenone Distributions and Isochrysidales Groups along the Baltic Sea Salinity Gradient." *Organic Geochemistry* 127:92–103. doi: 10.1016/j.orggeochem.2018.11.012.

Köseoğlu, Denizcan, Simon T. Belt, Katrine Husum, and Jochen Knies. 2018. "An Assessment of Biomarker-Based Multivariate Classification Methods versus the PIP25 Index for Paleo

Arctic Sea Ice Reconstruction." *Organic Geochemistry* 125:82–94. doi: 10.1016/j.orggeochem.2018.08.014.

Łącka, Magdalena, Min Cao, Antoni Rosell-Melé, Joanna Pawłowska, Małgorzata Kucharska, Matthias Forwick, and Marek Zajączkowski. 2019. "Postglacial Paleoceanography of the Western Barents Sea: Implications for Alkenone-Based Sea Surface Temperatures and Primary Productivity." *Quaternary Science Reviews* 224:105973. doi: 10.1016/j.quascirev.2019.105973.

Laskar, J., P. Robutel, F. Joutel, M. Gastineau, A. C. M. Correia, and B. Levrard. 2004. "A Long-Term Numerical Solution for the Insolation Quantities of the Earth." *Astronomy & Astrophysics* 428(1):261–85. doi: 10.1051/0004-6361:20041335.

Liu, Z., M. Pagani, D. Zinniker, R. DeConto, M. Huber, H. Brinkhuis, S. R. Shah, R. M. Leckie, and A. Pearson. 2009. "Global Cooling During the Eocene-Oligocene Climate Transition." *Science* 323(5918):1187–90. doi: 10.1126/science.1166368.

Lochte, Annalena Antonia, Janne Repschläger, Marit-Solveig Seidenkrantz, Markus Kienast, Thomas Blanz, and Ralph R. Schneider. 2019. "Holocene Water Mass Changes in the Labrador Current." *The Holocene* 29(4):676–90. doi: 10.1177/0959683618824752.

Longo, William M., Yongsong Huang, Yuan Yao, Jiaju Zhao, Anne E. Giblin, Xian Wang, Roland Zech, Torsten Haberzettl, Ludwig Jardillier, Jaime Toney, Zhonghui Liu, Sergey Krivonogov, Marina Kolpakova, Guoqiang Chu, William J. D'Andrea, Naomi Harada, Kana Nagashima, Miyako Sato, Hitoshi Yonenobu, Kazuyoshi Yamada, Katsuya Gotanda, and Yoshitsugu Shinozuka. 2018. "Widespread Occurrence of Distinct Alkenones from Group I Haptophytes in Freshwater Lakes: Implications for Paleotemperature and

Paleoenvironmental Reconstructions." *Earth and Planetary Science Letters* 492:239–50. doi: 10.1016/j.epsl.2018.04.002.

Longo, William M., Susanna Theroux, Anne E. Giblin, Yinsui Zheng, James T. Dillon, and Yongsong Huang. 2016. "Temperature Calibration and Phylogenetically Distinct Distributions for Freshwater Alkenones: Evidence from Northern Alaskan Lakes." *Geochimica et Cosmochimica Acta* 180:177–96. doi: 10.1016/j.gca.2016.02.019.

M., Sarnthein, S. Van Kreveld, Erlenkeuser H., P. M. Grootes, Kucera M., Pflaumann U., and Schulz M. 2003. "Centennial-to-Millennial-Scale Periodicities of Holocene Climate and Sediment Injections off the Western Barents Shelf, 75°N." *Boreas* 32(3):447–61. doi: 10.1080/03009480310003351.

Majaneva, M., S. Enberg, R. Autio, J. Blomster, and Jm Rintala. 2019. "Mamiellophyceae Shift in Seasonal Predominance in the Baltic Sea." *Aquatic Microbial Ecology* 83(2):181–87. doi: 10.3354/ame01915.

Martin, Marcel. n.d. "&XWDGDSW UHPRYHV DGDSWHU VHTXHQFHV IURP KLJK WKURXJKSXW VHTXHQFLQJ UHDGV." 3.

Martrat, Belen, Joan O. Grimalt, Joan Villanueva, Shirley van Kreveld, and Michael Sarnthein. 2003. "Climatic Dependence of the Organic Matter Contributions in the North Eastern Norwegian Sea over the Last 15,000 Years." *Organic Geochemistry* 34(8):1057–70. doi: 10.1016/S0146-6380(03)00084-6.

McClymont, Erin L., Antoni Rosell-Melé, Gerald H. Haug, and Jerry M. Lloyd. 2008. "Expansion of Subarctic Water Masses in the North Atlantic and Pacific Oceans and Implications for Mid-Pleistocene Ice Sheet Growth: MID-PLEISTOCENE POLAR/ARCTIC WATERS." *Paleoceanography* 23(4):n/a-n/a. doi: 10.1029/2008PA001622.

Miller, Mark A., Wayne Pfeiffer, and Terri Schwartz. 2010. "Creating the CIPRES Science Gateway for Inference of Large Phylogenetic Trees." Pp. 1–8 in *2010 Gateway Computing Environments Workshop (GCE)*. New Orleans, LA, USA: IEEE.

Mishonov, Alexey. n.d. "NOAA Atlas NESDIS 61." 53.

Mishonov, Alexey. n.d. "NOAA Atlas NESDIS 61." 47.

Müller, Juliane, Guillaume Massé, Rüdiger Stein, and Simon T. Belt. 2009. "Variability of Sea-Ice Conditions in the Fram Strait over the Past 30,000 Years." *Nature Geoscience* 2(11):772–76. doi: 10.1038/ngeo665.

Müller, Juliane, Kirstin Werner, Ruediger Stein, Kirsten Fahl, Matthias Moros, and Eystein Jansen. 2012. "Holocene Cooling Culminates in Sea Ice Oscillations in Fram Strait." *Quaternary Science Reviews* 47:1–14. doi: 10.1016/j.quascirev.2012.04.024.

Müller, Peter J., Georg Kirst, Götz Ruhland, Isabel von Storch, and Antoni Rosell-Melé. 1998. "Calibration of the Alkenone Paleotemperature Index U37K′ Based on Core-Tops from the Eastern South Atlantic and the Global Ocean (60°N-60°S)." *Geochimica et Cosmochimica Acta* 62(10):1757–72. doi: 10.1016/S0016-7037(98)00097-0.

Ono, Makiko, Ken Sawada, Masako Kubota, and Yoshihiro Shiraiwa. n.d. "Change of the Unsaturation Degree of Alkenone and Alkenoate during Acclimation to Salinity Change in Emiliania Huxleyi and Gephyrocapsa Oceanica with Reference to Palaeosalinity Indicator." 8.

Ono, Makiko, Ken Sawada, Yoshihiro Shiraiwa, and Masako Kubota. 2012. "Changes in Alkenone and Alkenoate Distributions during Acclimatization to Salinity Change in Isochrysis Galbana: Implication for Alkenone-Based Paleosalinity and Paleothermometry." *GEOCHEMICAL JOURNAL* 46(3):235–47. doi: 10.2343/geochemj.2.0203.

Peng, G., W. N. Meier, D. J. Scott, and M. H. Savoie. 2013. “A Long-Term and Reproducible Passive Microwave Sea Ice Concentration Data Record for Climate Studies and Monitoring.” 8.

Plancq, Julien, Jillian M. Couto, Umer Z. Ijaz, Peter R. Leavitt, and Jaime L. Toney. 2019. “Next Generation Sequencing to Identify Lacustrine Haptophytes in the Canadian Prairies: Significance for Temperature Proxy Applications.” *Journal of Geophysical Research: Biogeosciences*. doi: 10.1029/2018JG004954.

Prahl, F. G., and S. G. Wakeham. 1987. “Calibration of Unsaturation Patterns in Long-Chain Ketone Compositions for Palaeotemperature Assessment.” *Nature* 330(6146):367–69. doi: 10.1038/330367a0.

Prahl, Fredrick G., Laurel A. Muehlhausen, and Debra L. Zahnle. 1988. “Further Evaluation of Long-Chain Alkenones as Indicators of Paleoceanographic Conditions.” *Geochimica et Cosmochimica Acta* 52(9):2303–10. doi: 10.1016/0016-7037(88)90132-9.

Ribeiro, Catherine Gérikas. n.d. “Culturable Diversity of Arctic Phytoplankton during Pack Ice Melting.” 23.

Rigual-Hernández, A. S., E. Colmenero-Hidalgo, B. Martrat, M. A. Bárcena, A. de Vernal, F. J. Sierro, J. A. Flores, J. O. Grimalt, M. Henry, and R. G. Lucchi. 2017. “Svalbard Ice-Sheet Decay after the Last Glacial Maximum: New Insights from Micropalaeontological and Organic Biomarker Paleoceanographical Reconstructions.” *Palaeogeography, Palaeoclimatology, Palaeoecology* 465:225–36. doi: 10.1016/j.palaeo.2016.10.034.

Risebrobakken, Bjørg, Matthias Moros, Elena V. Ivanova, Natalia Chistyakova, and Reinhild Rosenberg. 2010. “Climate and Oceanographic Variability in the SW Barents Sea during the Holocene.” *The Holocene* 20(4):609–21. doi: 10.1177/0959683609356586.

Rosellmele, A. 2002. “Appraisal of a Molecular Approach to Infer Variations in Surface Ocean Freshwater Inputs into the North Atlantic during the Last Glacial.” *Global and Planetary Change* 34(3–4):143–52. doi: 10.1016/S0921-8181(02)00111-X.

Rosell-Melé, Antoni. 1998. “Interhemispheric Appraisal of the Value of Alkenone Indices as Temperature and Salinity Proxies in High-Latitude Locations.” *Paleoceanography* 13(6):694–703. doi: 10.1029/98PA02355.

Rosell-Mele, Antoni, and Pau Comes. 2000. “Alkenone Fluxes and Anomalous U3K7X Values during 1989–1990 in the Northeast Atlantic Ž488N 218W/.” 14.

Sánchez-Montes, Maria Luisa, Erin L. McClymont, Jeremy M. Lloyd, Juliane Müller, Ellen A. Cowan, and Coralie Zorzi. 2020. “Late Pliocene Cordilleran Ice Sheet Development with Warm Northeast Pacific Sea Surface Temperatures.” *Climate of the Past* 16(1):299–313. doi: 10.5194/cp-16-299-2020.

Seki, O., K. Kawamura, M. Ikehara, T. Nakatsuka, and T. Oba. 2004. “Variation of Alkenone Sea Surface Temperature in the Sea of Okhotsk over the Last 85 Kyrs.” *Organic Geochemistry* 35(3):347–54. doi: 10.1016/j.orggeochem.2003.10.011.

Seki, Osamu. 2005. “Decreased Surface Salinity in the Sea of Okhotsk during the Last Glacial Period Estimated from Alkenones.” *Geophysical Research Letters* 32(8). doi: 10.1029/2004GL022177.

Sicre, Marie-Alexandrine, Edouard Bard, Ullah Ezat, and Frauke Rostek. 2002. “Alkenone Distributions in the North Atlantic and Nordic Sea Surface Waters: UNUSUAL DISTRIBUTION OF ALKENONES.” *Geochemistry, Geophysics, Geosystems* 3(2):1 of 13–13 13. doi: 10.1029/2001GC000159.

Stamatakis, Alexandros. 2014. “RAxML Version 8: A Tool for Phylogenetic Analysis and Post-Analysis of Large Phylogenies.” *Bioinformatics* 30(9):1312–13. doi: 10.1093/bioinformatics/btu033.

Syring, Nicole, Ruediger Stein, Kirsten Fahl, Maximilian Vahlenkamp, Marc Zehnich, Robert F. Spielhagen, and Frank Niessen. 2020. “Holocene Changes in Sea-Ice Cover and Polynya Formation along the Eastern North Greenland Shelf: New Insights from Biomarker Records.” *Quaternary Science Reviews* 231:106173. doi: 10.1016/j.quascirev.2020.106173.

Theroux, Susanna, William J. D’Andrea, Jaime Toney, Linda Amaral-Zettler, and Yongsong Huang. 2010. “Phylogenetic Diversity and Evolutionary Relatedness of Alkenone-Producing Haptophyte Algae in Lakes: Implications for Continental Paleotemperature Reconstructions.” *Earth and Planetary Science Letters* 300(3–4):311–20. doi: 10.1016/j.epsl.2010.10.009.

Theroux, Susanna, Yongsong Huang, Jaime L. Toney, Robert Andersen, Paul Nyren, Rick Bohn, Jeffrey Salacup, Leslie Murphy, and Linda Amaral-Zettler. 2019. “Successional Blooms of Alkenone-producing Haptophytes in Lake George, North Dakota: Implications for Continental Paleoclimate Reconstructions.” *Limnology and Oceanography*. doi: 10.1002/lno.11311.

Tierney, Jessica E., and Martin P. Tingley. 2018. “BAYSPLINE: A New Calibration for the Alkenone Paleothermometer.” *Paleoceanography and Paleoclimatology* 33(3):281–301. doi: 10.1002/2017PA003201.

Toney, Jaime L., Susanna Theroux, Robert A. Andersen, Annette Coleman, Linda Amaral-Zettler, and Yongsong Huang. 2012. “Culturing of the First 37:4 Predominant Lacustrine

Haptophyte: Geochemical, Biochemical, and Genetic Implications." *Geochimica et Cosmochimica Acta* 78:51–64. doi: 10.1016/j.gca.2011.11.024.

Volkman, John K., Geoffrey Eglinton, Eric D. S. Corner, and T. E. V. Forsberg. 1980. "Long-Chain Alkenes and Alkenones in the Marine Coccolithophorid Emiliania Huxleyi." *Phytochemistry* 19(12):2619–22. doi: 10.1016/S0031-9422(00)83930-8.

Wang, Li, William M. Longo, James T. Dillon, Jiaju Zhao, Yinsui Zheng, Matthias Moros, and Yongsong Huang. 2019. "An Efficient Approach to Eliminate Steryl Ethers and Miscellaneous Esters/Ketones for Gas Chromatographic Analysis of Alkenones and Alkenoates." *Journal of Chromatography A* 1596:175–82. doi: 10.1016/j.chroma.2019.02.064.

Werner, Kirstin, Juliane Müller, Katrine Husum, Robert F. Spielhagen, Evgenia S. Kandiano, and Leonid Polyak. 2016. "Holocene Sea Subsurface and Surface Water Masses in the Fram Strait – Comparisons of Temperature and Sea-Ice Reconstructions." *Quaternary Science Reviews* 147:194–209. doi: 10.1016/j.quascirev.2015.09.007.

Xu, L., C. M. Reddy, J. W. Farrington, G. S. Frysinger, R. B. Gaines, C. G. Johnson, R. K. Nelson, and T. I. Eglinton. 2001. "Identification of a Novel Alkenone in Black Sea Sediments." *Organic Geochemistry* 32(5):633–45. doi: 10.1016/S0146-6380(01)00019-5.

Yao, Yuan, Jiaju Zhao, William M. Longo, Gaoyuan Li, Xian Wang, Richard S. Vachula, Karen J. Wang, and Yongsong Huang. 2019. "New Insights into Environmental Controls on the Occurrence and Abundance of Group I Alkenones and Their Paleoclimate Applications: Evidence from Volcanic Lakes of Northeastern China." *Earth and Planetary Science Letters* 527:115792. doi: 10.1016/j.epsl.2019.115792.

Zhao, Jiaju, Chengbang An, William M. Longo, James T. Dillon, Yongtao Zhao, Chao Shi, Yufeng Chen, and Yongsong Huang. 2014. "Occurrence of Extended Chain Length C41 and C42 Alkenones in Hypersaline Lakes." *Organic Geochemistry* 75:48–53. doi: 10.1016/j.orggeochem.2014.06.006.

Zheng, Yinsui, Patrick Heng, Maureen H. Conte, Richard S. Vachula, and Yongsong Huang. 2019. "Systematic Chemotaxonomic Profiling and Novel Paleotemperature Indices Based on Alkenones and Alkenoates: Potential for Disentangling Mixed Species Input." *Organic Geochemistry* 128:26–41. doi: 10.1016/j.orggeochem.2018.12.008.

Zheng, Yinsui, Rafael Tarozo, and Yongsong Huang. 2017. "Optimizing Chromatographic Resolution for Simultaneous Quantification of Long Chain Alkenones, Alkenoates and Their Double Bond Positional Isomers." *Organic Geochemistry* 111:136–43. doi: 10.1016/j.orggeochem.2017.06.013.

Figures

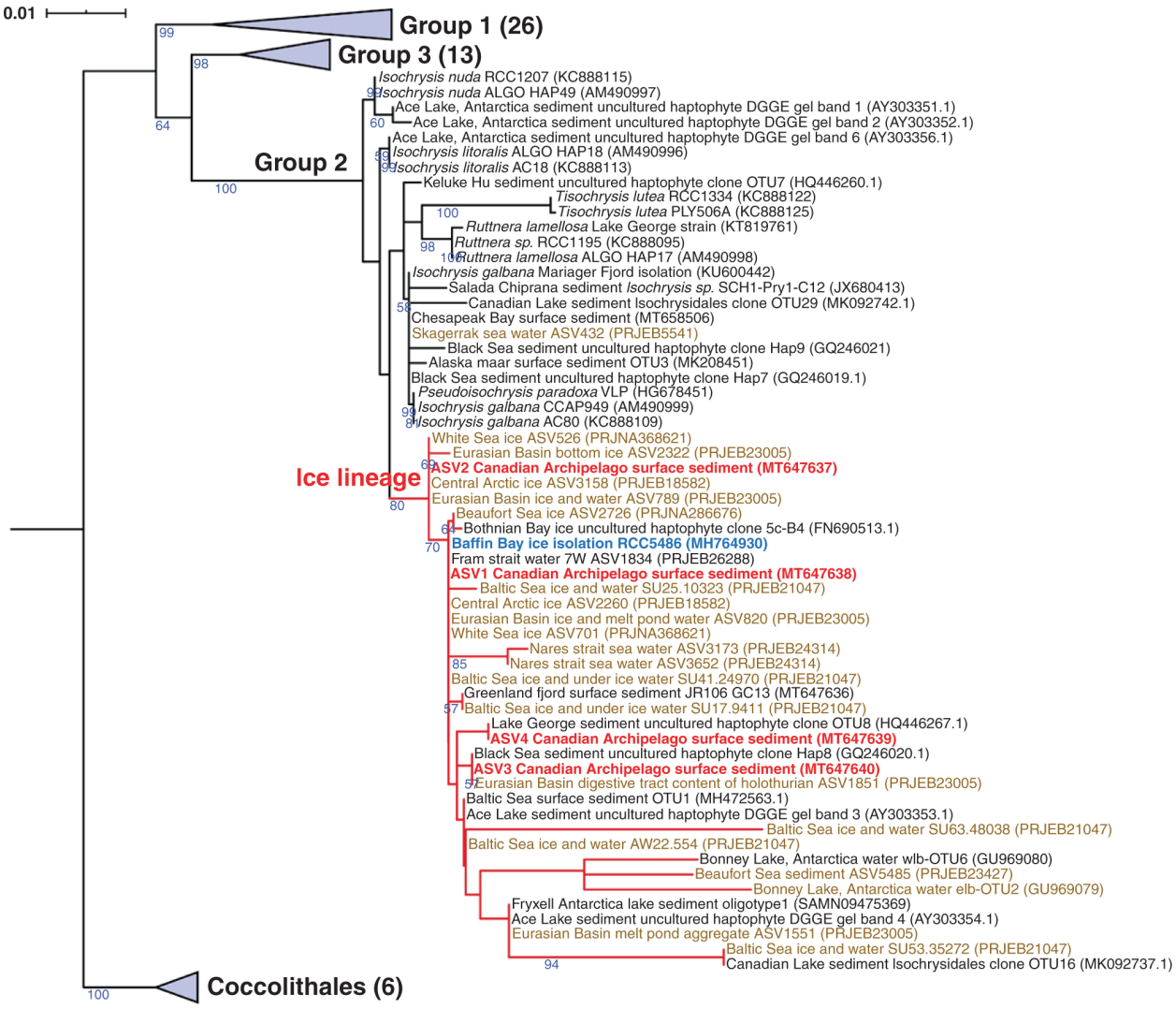

Figure 2.1. Phylogenetic position of the novel Group 2 ice lineage (Group 2i) Isochrysidales. Maximum-likelihood tree based on 18S rRNA gene from 99 sequences spanning three groups of Isochrysidales and 6 from the Coccolithales outgroup. The numbers shown on branches represent bootstrap support for the node (only those >50% are shown). Numbers in the parentheses represent numbers of sequences included in the collapsed groups, and the expanded version of this tree can be found in Supplementary Figure 4. The scale bar represent substitution/site. Sequences generated from Canadian Arctic Archipelago surface sediments in this study are highlighted in red, and sea-ice isolated strain RCC5486 cultured in this study is highlighted in blue. Sequences from re-analyzed NGS datasets are highlighted in brown, and other sequences were obtained from NCBI GenBank. The branches of the ice-lineage is marked in red.

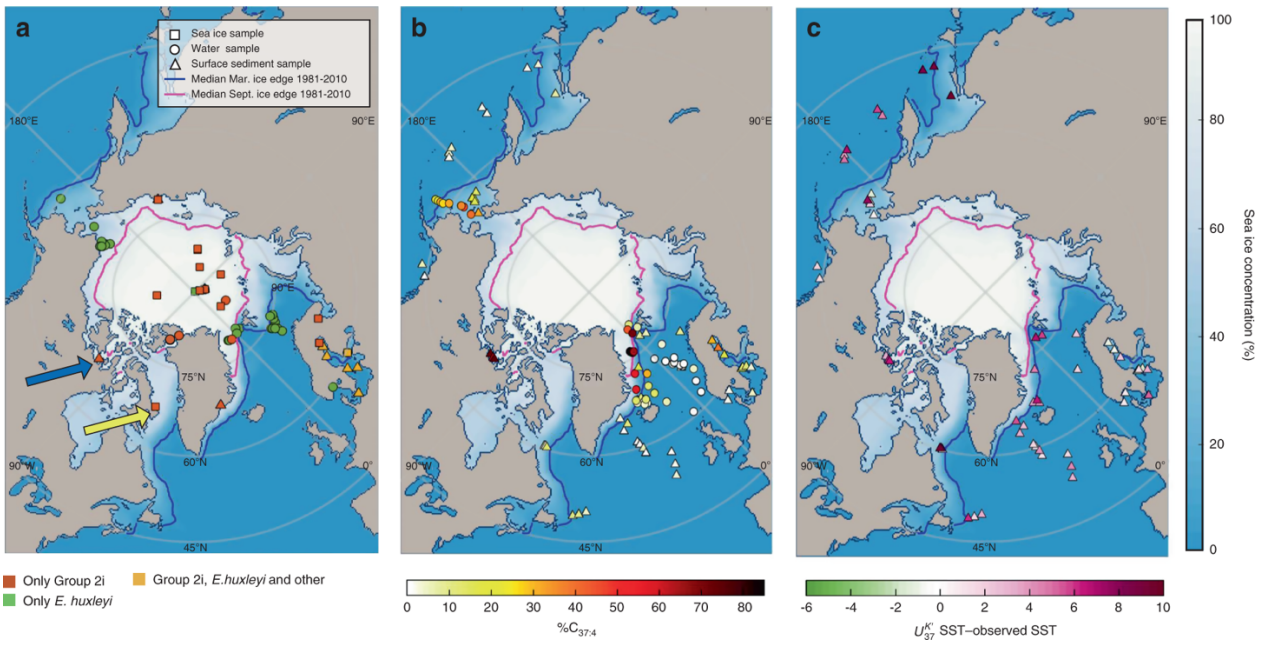

Figure 2.2. Distribution of the Group 2i Isochrysidales, $\%C_{37:4}$ values and $U^{K\prime}_{37}$-sea surface temperature bias. a) Distribution of Group 2i in northern high latitude marine environment from DNA sequencing in this study, re-analyzed NGS datasets, and NCBI GenBank based on phylogeny. Orange represent samples with Group 2i detected, yellow represent samples with both Group 2i and other Isochrysidales detected, and green represent samples with occurrence of other Isochrysidales and absence of Group 2i (details of samples can be found in Supplementary Data 2). Blue arrow indicate surface sediment samples where both DNA sequencing and alkenone analyses were conducted in this study. Yellow arrow denotes the location where strain RCC5486 cultured in this study was isolated from. b) $\%C_{37:4}$ values of water filter POM compiled from Harada et al.(Harada et al. 2003) and Bendle et al.(Bendle and Rosell-Melé 2004) are shown in circles. $\%C_{37:4}$ values of surface sediment samples from this study are shown in triangles. c) Differences between $U^{K\prime}_{37}$ reconstructed SST in surface sediment and 1981-2010 mean annual SST (WOA)(Mishonov n.d.). The contour shows annual mean sea ice concentration during 1980-2010 from National Snow and Ice Data Center (NSIDC) Climate Data Record of Passive Microwave Sea Ice Concentration, Version 3 with a spatial resolution of 25 km × 25 km(Peng et al. 2013) (https://doi.org/10.7265/N59P2ZTG). The blue and magenta lines shows 1980-2010 median sea ice extent during March and September respectively (NSIDC).

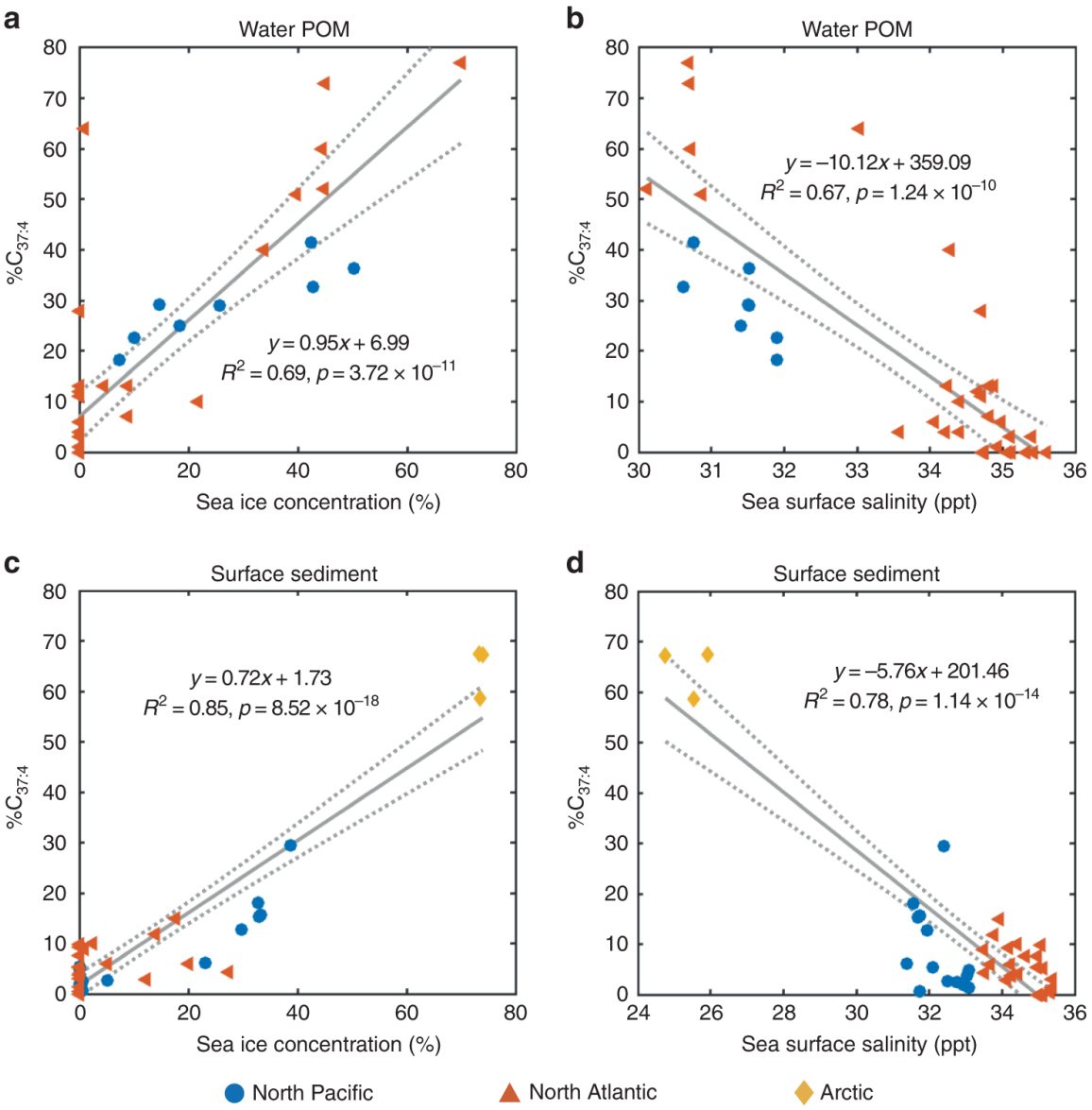

Figure 2.3. $\%C_{37:4}$ showing significant positive correlation with annual mean sea ice concentration and negative correlation with sea surface salinity. a) Linear regression between water filter POM $\%C_{37:4}$ compiled from previous studies(Bendle and Rosell-Melé 2004; Harada et al. 2003) and mean sea ice concentration 12-month prior to sample collection (n=40 independent samples). b) Linear regression between water filter POM $\%C_{37:4}$ and measured SSS during collection(Bendle and Rosell-Melé 2004; Harada et al. 2003) (n=40 independent samples). c) Linear regression between surface sediment $\%C_{37:4}$ and 1980-2010 annual mean sea ice concentration (n=42 independent samples). d) Linear regression between surface sediment $\%C_{37:4}$ and 1980-2010 annual mean SSS(Mishonov n.d.) (n=42 independent samples). Surface sediment samples from Baltic Sea are not included in the regressions in c) and d). Sea ice concentrations were obtained from NOAA/NSIDC Climate Data Record of Passive Microwave Sea Ice Concentration, Version 3 with a spatial resolution of 25 km × 25 km(Peng et al. 2013) (https://doi.org/10.7265/N59P2ZTG). The dashed lines denote 95% confidence interval for the regression.

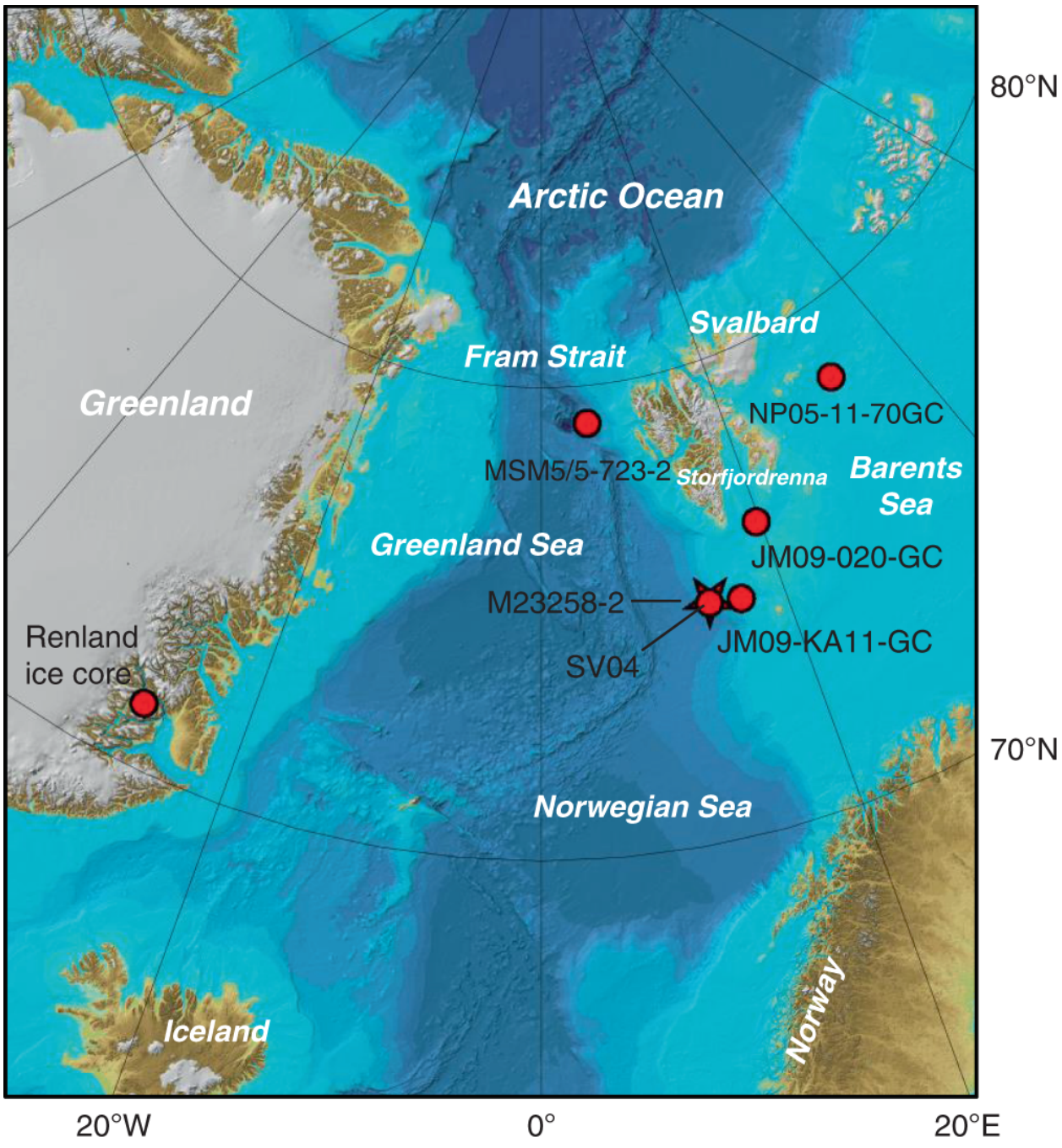

Figure 2.4. Locations of the cores discussed in the paper with bathymetry adapted from IBCAO version 3(Jakobsson et al. 2012).

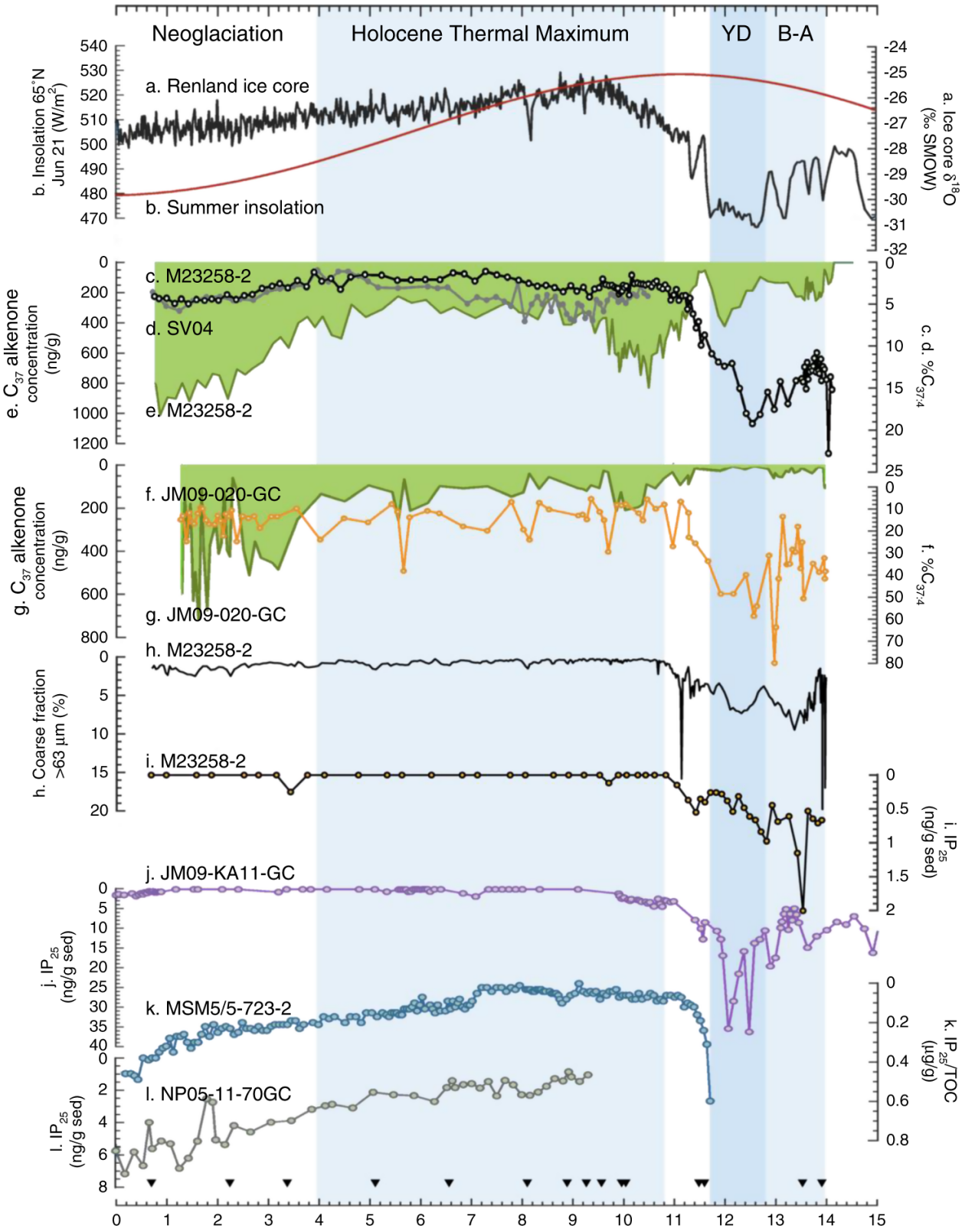
Neoglaciation
Holocene Thermal Maximum
YD
B-A
a. Renland ice core
b. Summer insolation
b. Insolation 65°N Jun 21 (W/m²)
a. Ice core δ18O (‰ SMOW)
c. M23258-2
d. SV04
e. M23258-2
e. C37 alkenone concentration (ng/g)
c. d. %C37:4
f. JM09-020-GC
g. JM09-020-GC
g. C37 alkenone concentration (ng/g)
f. %C37:4
h. M23258-2
i. M23258-2
h. Coarse fraction >63 µm (%)
i. IP25 (ng/g sed)
j. JM09-KA11-GC
k. MSM5/5-723-2
l. NP05-11-70GC
j. IP25 (ng/g sed)
l. IP25 (ng/g sed)
k. IP25/TOC (µg/g)

Figure 2.5. Sea ice reconstructions at the Svalbard region during the past ca. 14.5 kyr. a) $\delta^{18}O$ from Renland ice core(Johnsen et al. 2001). b) Mid-July 65˚N insolation(Laskar et al. 2004). c) $\%C_{37:4}$ from M23258-2(Martrat et al. 2003). d) $\%C_{37:4}$ from SV04(Rigual-Hernández et al. 2017). e) C_{37} methyl alkenone concentration from M23258-2(Martrat et al. 2003). f) $\%C_{37:4}$ from JM09-020-GC(Łącka et al. 2019). g) C_{37} methyl alkenone concentration from JM09-020-GC(Łącka et al. 2019). h) Coarse fraction from M23258-2(M. et al. 2003). i-l) IP_{25} concentration from M23258-2 (this study), JM09-KA11-GC(Belt et al. 2015; Berben et al. 2014), MSM5/5-723-2(Werner et al. 2016) and NP05-11-70GC(Köseoğlu et al. 2018:25). Black triangles represent age control points in M23258-2(M. et al. 2003).

Supplementary Information

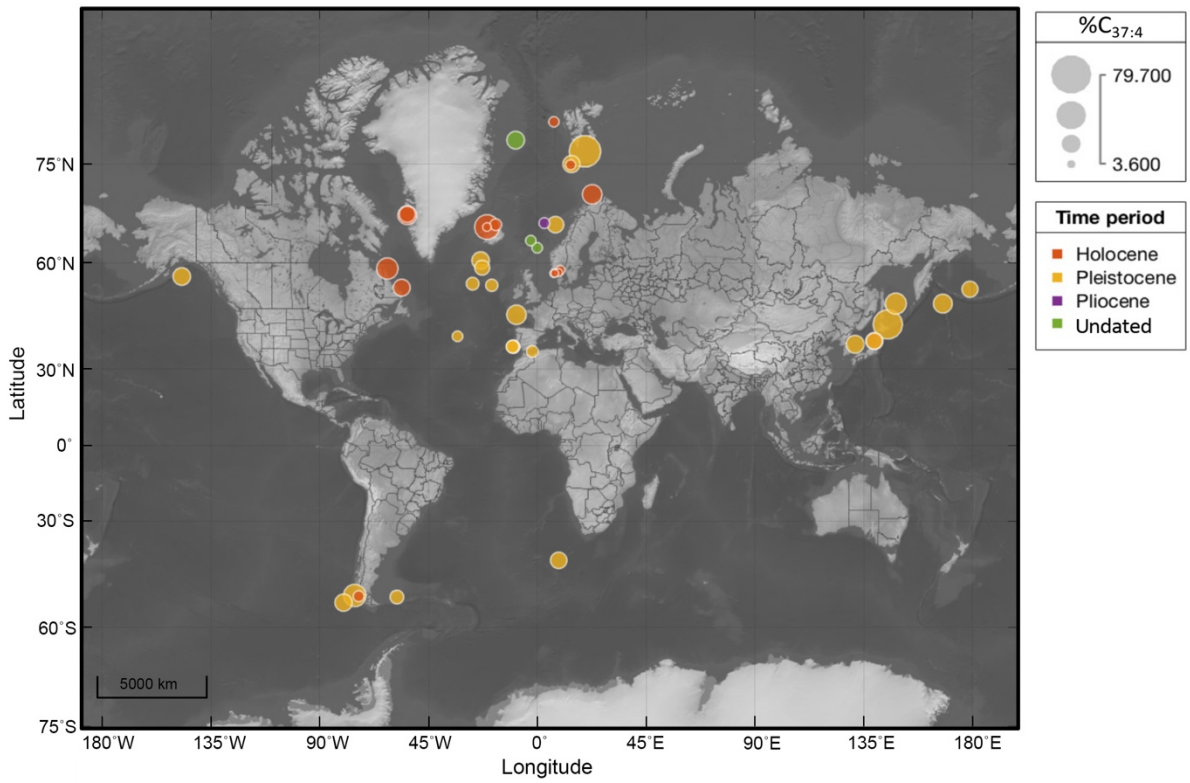

Figure 2.S.1 Compilation of reported $\%C_{37:4}$ records listed in **Table 1.S.1**. The bubble size represent highest $\%C_{37:4}$ value reported in the record, and the color represent the time period of the highest value reported.

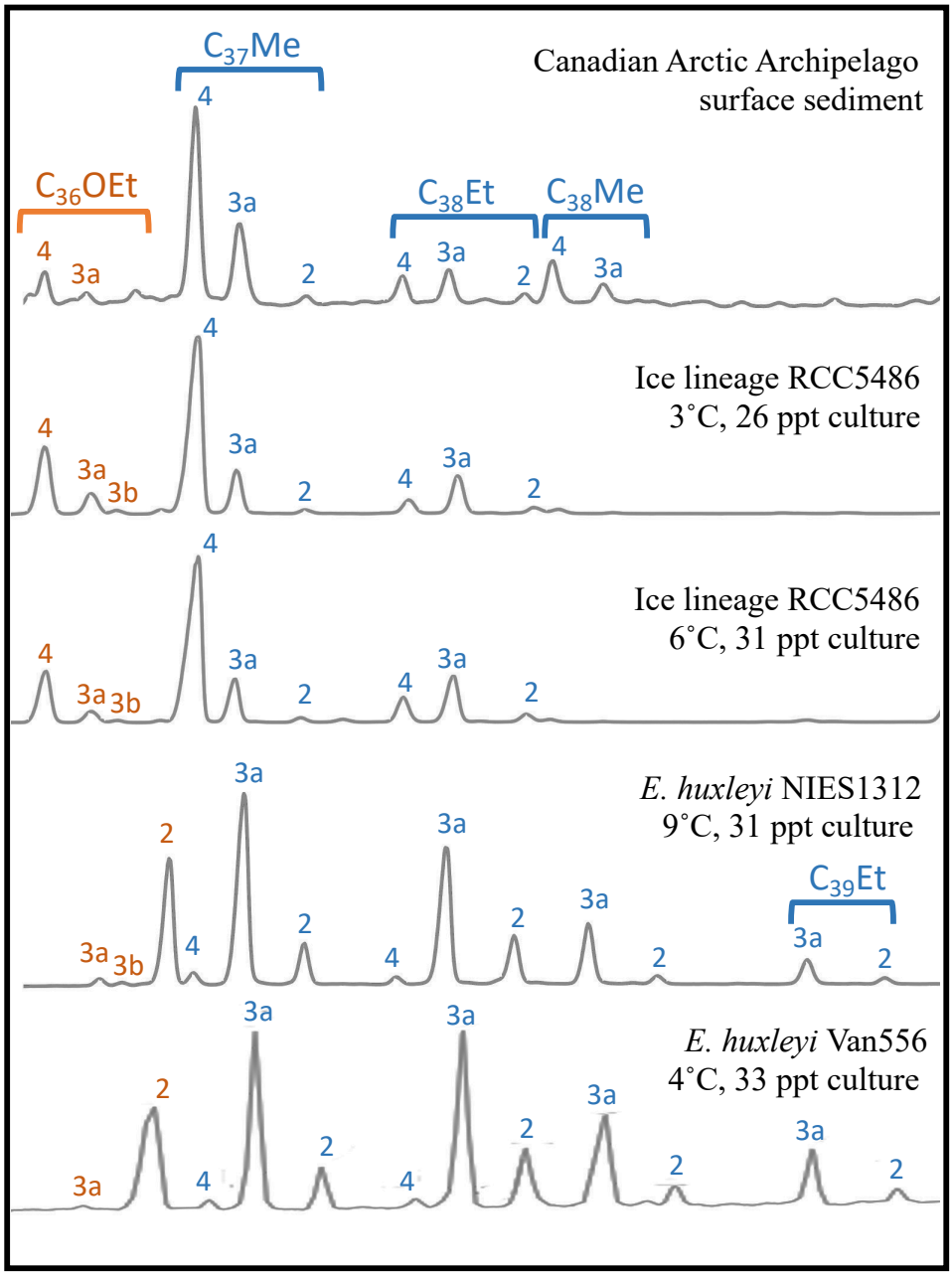

Figure 2.S.2. Gas chromatograms showing alkenone and alkenoate profiles generated from Canadian Arctic Archipelago surface sediments, RCC5486 cultures, *E. huxleyi* strain NIES1312 (Liao et al., unpublished) and Van 556 cultures(Zheng et al., 2019). C_n represent the number of carbon; Me = methyl ketone, Et = ethyl ketone, OEt = ethyl alkenoate; number above each peaks indicate the number of double bonds; 3a and 3b are tri-unsaturated double bond positional isomers.

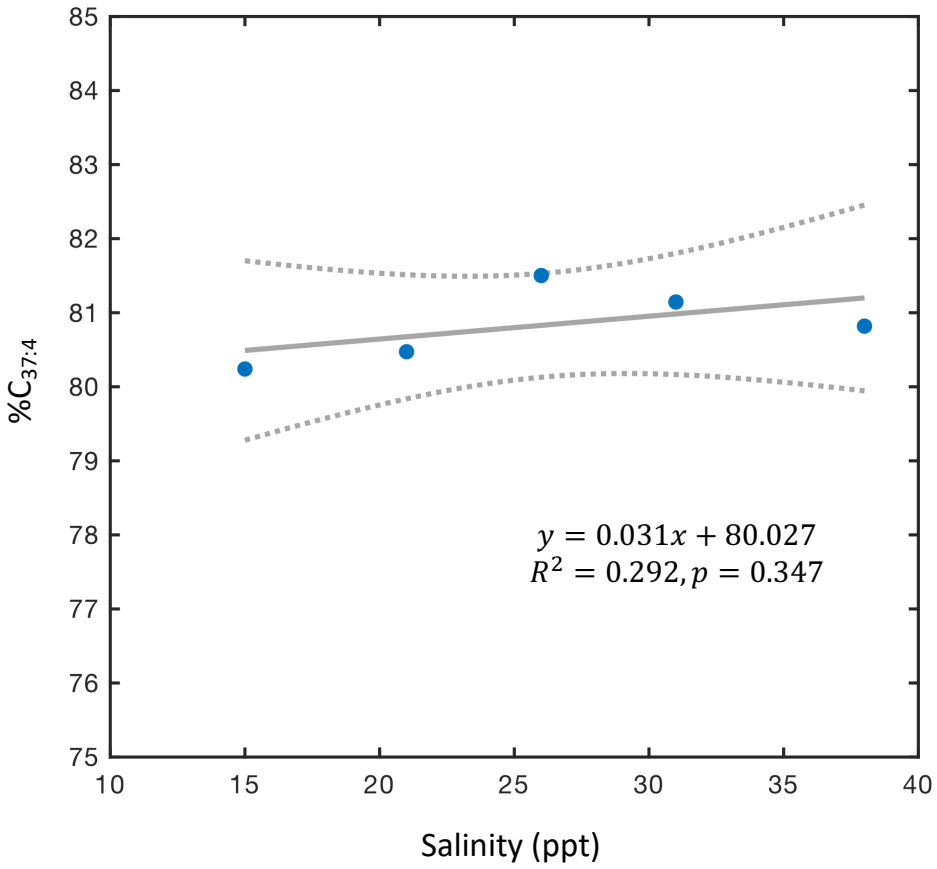

Figure 2.S.3. $\%C_{37:4}$ produced by RCC5486 under 3˚C does not show any significant correlation with salinity. Each data point represent the averaged value of the triplicated culture experiments. The dashed lines denote 95% confidence interval for the regression.

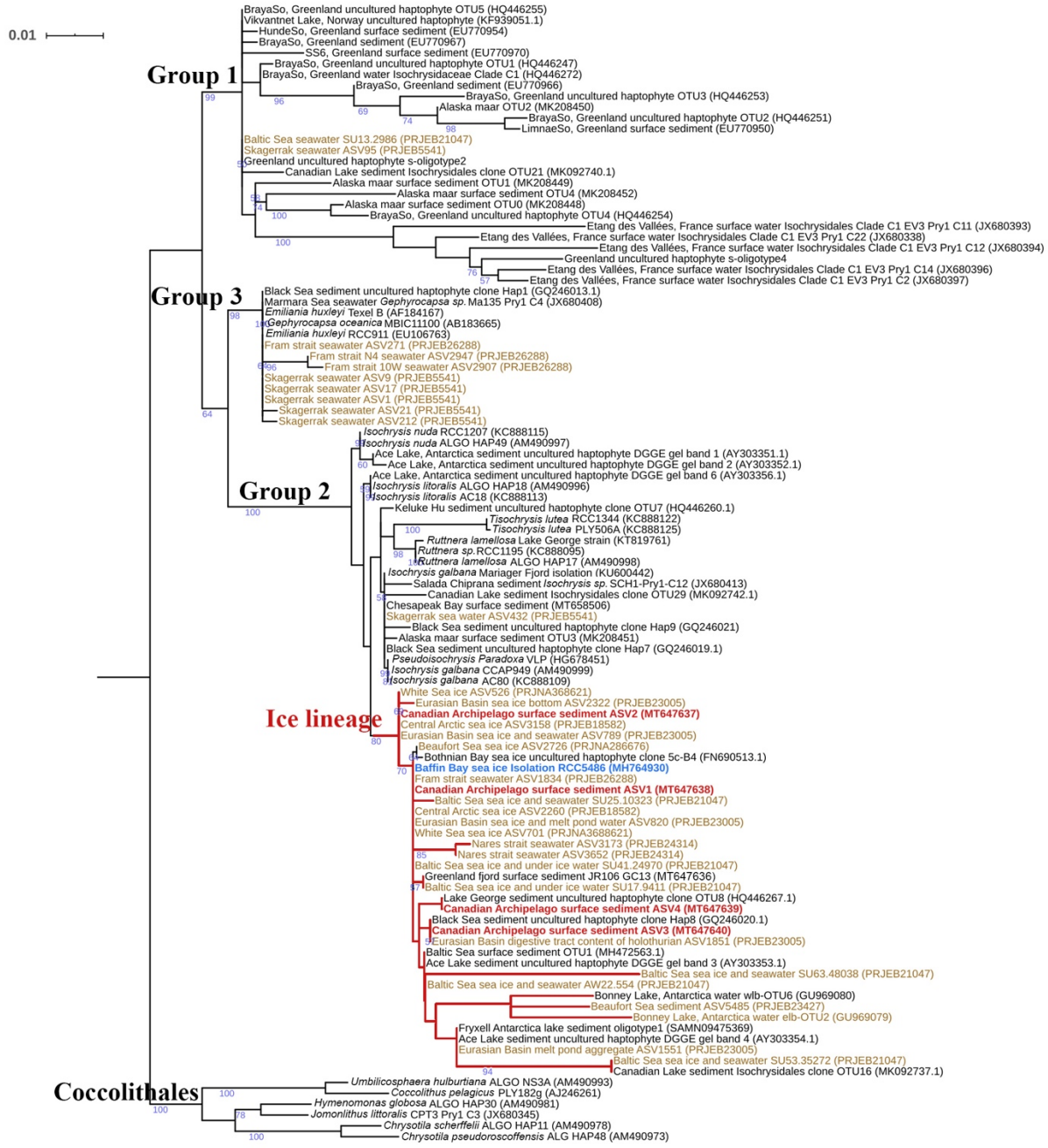

Figure 2.S.4. The full phylogenetic tree showing the position of the novel ice-lineage Isochrysidales. This maximum-likelihood tree is based on 18S rRNA gene from 99 sequences spanning three groups of Isochrysidales and 6 from the Coccolithales outgroup. The numbers shown on branches represent % bootstrap support for the node (only those >50% are shown). The scale bar represents substitutions per site. Sequences generated from Canadian Arctic Archipelago surface sediments in this study are highlighted in red, and sea-ice isolated strain RCC5486 cultured in this study is highlighted in blue font. Sequences from re-analyzed NGS datasets are indicated by brown font, and other sequences were obtained from NCBI GenBank. The branches of the ice-lineage Isochrysidales are highlighted in red. A version of this tree with collapsed nodes for easy viewing is provided in **Figure 1.1** of the main text.

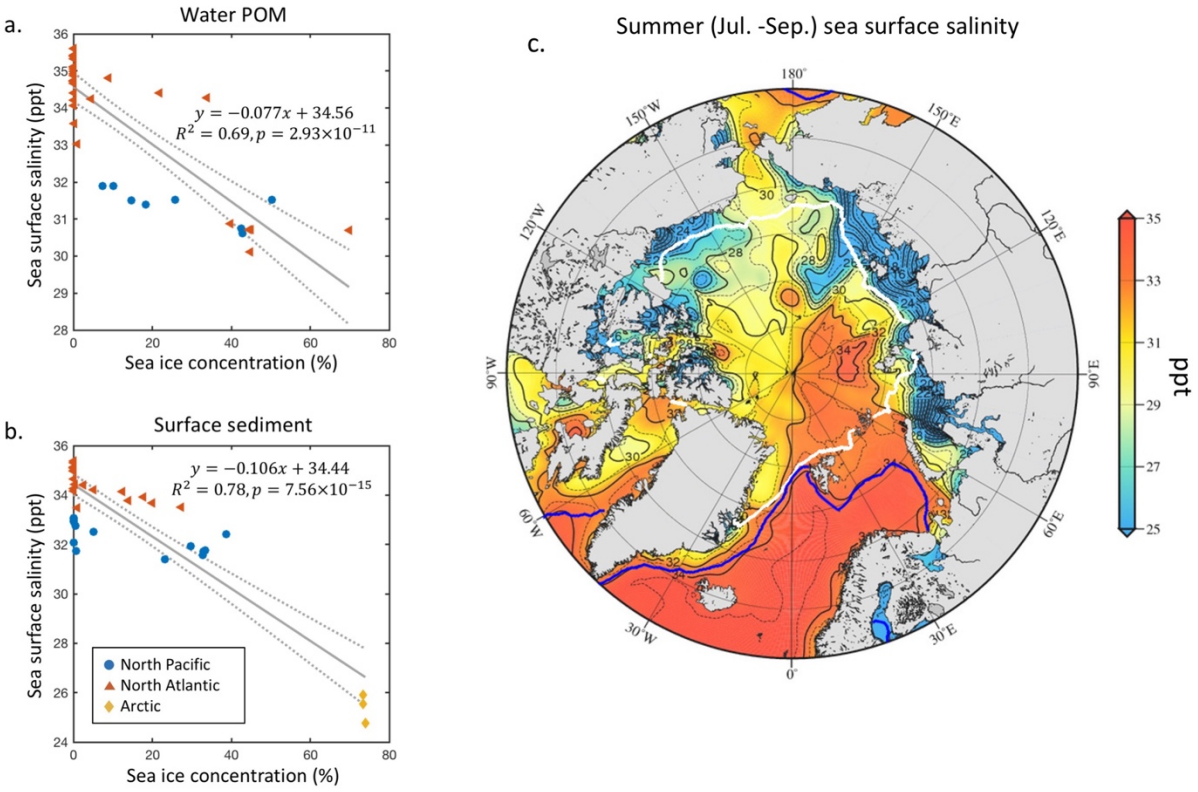

Figure 2.S.5. a) Linear regression between mean sea ice concentration 12-month prior to POM sample collection and measured SSS during sample collection compiled from previous studies(J. Bendle et al., 2005; Harada et al., 2003) (n=40 independent samples). b) Linear regression between 1981-2010 annual mean sea ice concentration and 1981-2010 annual mean SSS(Mishonov, n.d.) at surface sediment sites in this study (n=42 independent samples). The dashed lines denote 95% confidence interval for the regression in a) and b). c) shows modern summer (Jul.- Sep.) SSS in the circum-Arctic region adapted from https://www.nodc.noaa.gov/OC5/regional_climate/arctic/, with the blue and white lines indicating March and September median sea ice extent respectively (NSIDC).

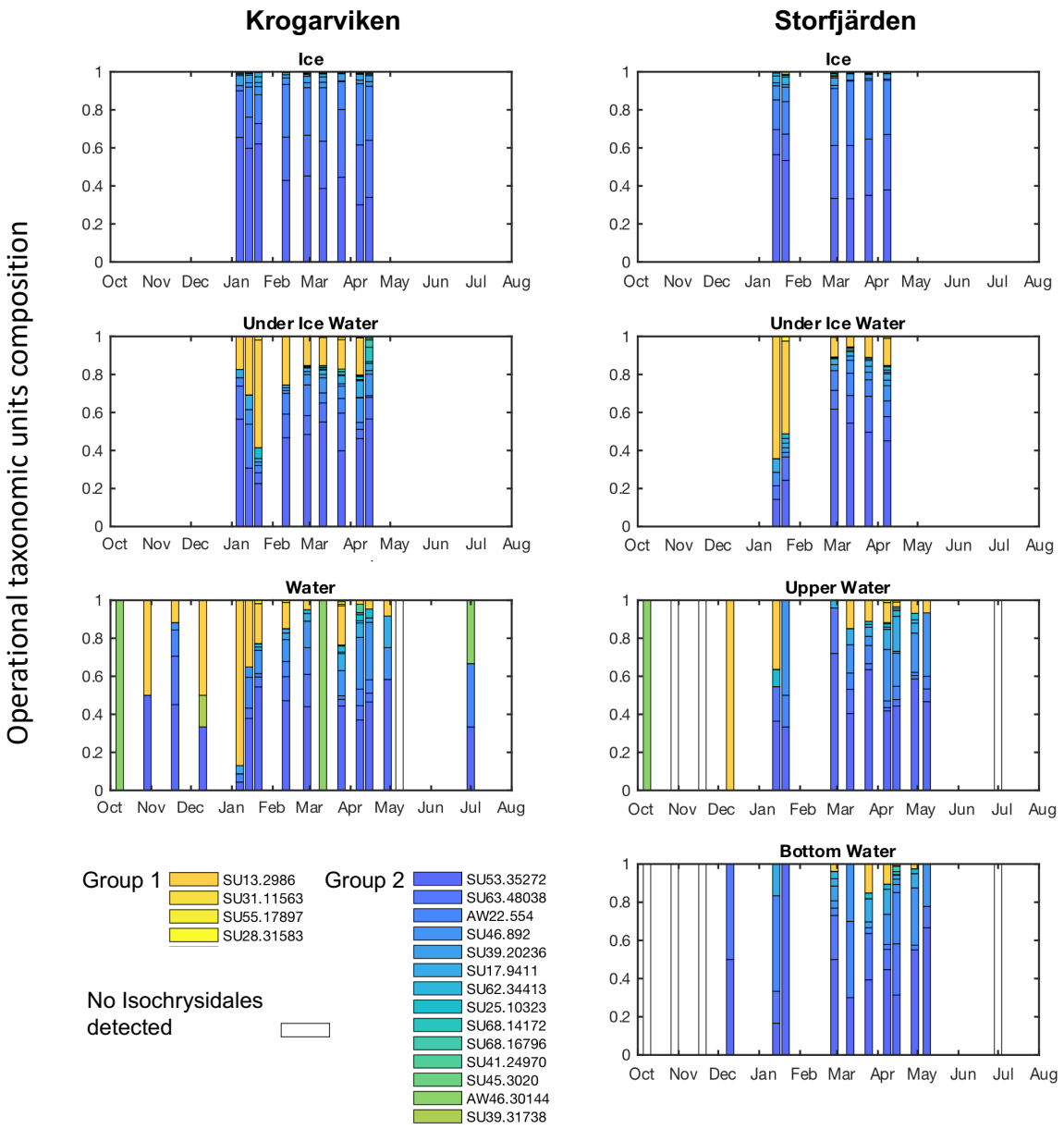

Figure 2.S.6. Seasonal succession of Isochrysidales from Autumn to Spring in the northwest of Gulf of Finland, Baltic Sea, from re-analyzed NGS data(Enberg et al., 2018). OTU composition (% of OTU reads to total Isochrysidales reads) in ice, under ice water, 0-3m water, 3-15m water at Krogarviken (59° 50.650' N, 23° 15.100' E) and Storfjärden (59° 51.250' N, 23° 15.815' E). Notably, Group 2i are the only Isochrysidales species detected within the ice in Krogarviken and compose >99% reads within the ice in Storfjärden; Group 1 species are mostly found in water samples with only a few reads (1-3) detected within ice samples from Storfjärden.

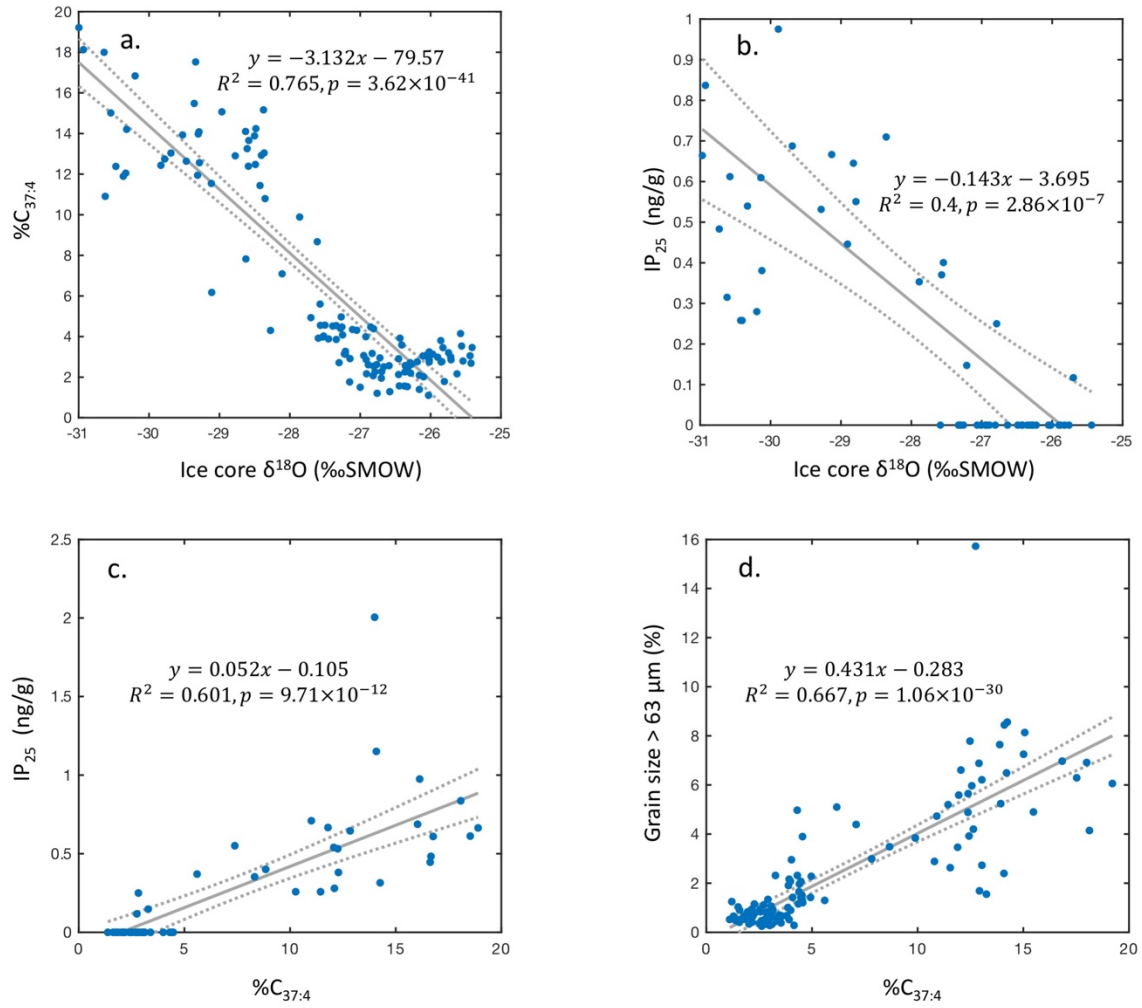

Figure 2.S.7. a) Linear regression between $\%C_{37:4}$ from M23258-2(Martrat et al., 2003) and $\delta^{18}O$ from Renland ice core(Johnsen et al., 2001) (n=127 independent samples). b) Linear regression between IP_{25} from M23258-2 and $\delta^{18}O$ from Renland ice core(Johnsen et al., 2001) (n=54 independent samples). c) Linear regression between $\%C_{37:4}$(Martrat et al., 2003) and IP_{25} in core M23258-2 (n=53 independent samples). d) Linear regression between $\%C_{37:4}$(Martrat et al., 2003) and >63 µm grain size(M. et al., 2003) in core M23258-2 (n=123 independent samples). The dashed lines denote 95% confidence interval for the regression.

Table 2.S.1 List of published $\%C_{37:4}$ sediment-core records shown in **Figure 1.S.1** and the paleoclimate interpretations.

Core	Reference	Region	Published interpretation	Lat.	Lon.	Highest $\%C_{37:4}$	Record length
GS15-198-33	Perner et al., 2019	north Icelandic shelf	freshwater flux	66.6	-20.9	5	1850-2014 AD
MSM05/05-712-1	Rueda et al., 2013	Fram Strait	colder and fresher water	78.9	6.8	8	0-2000 AD
MSM45-31-1	Lochte et al., 2020	Labrador Shelf	sea-ice or meltwater	54.4	-56.0	22	0-6.2 kyr BP
372610	Krossa et al., 2015	west Skagerrak	low salinity Baltic outflow	57.7	6.7	4	0-4 kyr BP
225514	Krossa et al., 2015	central Skagerrak	low salinity Baltic outflow	57.8	8.7	4	0-4 kyr BP
372650	Krossa et al., 2015	northeast Skagerrak	low salinity Baltic outflow	58.5	9.6	6	0-5 kyr BP
242940	Krossa et al., 2015	west Skagerrak	low salinity Baltic outflow	57.7	7.2	4	0-4 kyr BP
343310	Moros et al., 2016	west Greenland	low SSS due to meltwater input	68.6	-53.8	20	0-3.5 kyr BP
343300	Moros et al., 2016	west Greenland	low SSS due to meltwater input	68.5	-54.0	28	0-8 kyr BP
SV04	Rigual-Hernández et al., 2017	north eastern Norwegian Sea	-	75.0	13.9	7	0.73-10.49 kyr BP
MSM45-19-2	Lochte et al., 2019	Labrador Shelf	sea-ice or meltwater	58.8	-61.9	36	0-8.9 kyr BP
JR51-GC35	Bendle & Rosell-Melé, 2007	north Icelandic shelf	polar water mass	67.0	-17.2	10	0.06-10.17 kyr BP
PC03	Harada et al., 2013	Chilean Patagonia fjords	low salinity	-52.9	-74.1	9	0-12 kyr BP
PC-9	Ishiwatari et al., 2001	Japan Sea	potentially low salinity	39.6	139.4	23	1.0-36 kyr BP
MD99-2269	Kristjánsdóttir et al., 2017	Icelandic shelf	potentially low salinity	66.6	-20.9	49	0.4-11.38 kyr BP
Psh-5159	Risebrobakken et al., 2010	south western Barents Sea	freshwater influence	71.4	22.7	30	0-11.42 kyr BP
JM-09-020	Łącka et al., 2019	Storfjordrenna, west Barents Sea	polar water mass	76.3	19.7	80	1.29-13.99 kyr BP
M23258-2	Martrat et al., 2003	north eastern Norwegian Sea	polar water mass	75.0	14.0	23	0.76-14.12 kyr BP
MD95-2011	Calvo et al., 2002	NE Norwegian Sea	polar water mass (colder and fresher)	67.0	7.6	21	0.52-15 kyr BP
MD09 2002	Menot et al., 2006	Bay of Biscay	low salinity from iceberg from British-Irish ice sheet	47.5	-8.5	30	5.0-30 kyr BP
MD07-3128	Caniupán et al., 2011	Chilean Patagonia fjords	low salinity	-52.7	-75.6	40	0-60 kyr BP
JR244-GC528	Roberts et al., 2017	Drake passage	indicating alkenone-SST bias	-53.0	-58.0	14	1-25.44 kyr BP

M23415	Rosellmele, 2002	North Atlantic	freshening of surface waters in response to incoming freshwater from sea-ice and/or icebergs	55.0	-19.0	11	0-50 kyr BP
M17049	Rosellmele, 2002	North Atlantic	freshening of surface waters in response to incoming freshwater from sea-ice and/or icebergs	55.3	-26.7	12	0-50 kyr BP
U1313	Naafs et al., 2012	North Atlantic	influence of polar water	41.0	-33.0	8	5.0-70 kyr BP
BOFS 16K	Weaver et al., 1999	North Atlantic	There is no advantage of including $C_{37:4}$ in SST reconstruction	59.0	-23.0	17	0-120 kyr BP
MD01-2412	Harada et al., 2008	Okhotsk Sea	low SSS due to declining supply of saline water /strengthening freshwater supply from the river/ increasing precipitation /effect of melting sea ice	44.5	145.0	69	0-115 kyr BP
PC-2	Seki et al., 2005	Okhotsk Sea	low salinity	50.4	148.3	35	0-85 kyr BP
ODP 977A	Martrat et al., 2004	west Mediterranian	low salinity during Heinrich events	36.0	-2.0	10	0-250 kyr BP
MD01-2408	Fujine et al., 2006	Japan Sea	U_{37}^{K} is more suitable than $U_{37}^{K'}$	39.6	139.4	20	0-170 kyr BP
MD01-2444	Martrat et al., 2007	Iberian margin	advection of cold surface water	37.6	-10.1	13	135.1-185.7 kyr BP
PC05-21	Lee et al., 2008	Japan Sea	unclear	38.4	131.5	25	0-200 kyr BP
PS75/034-2	Ho et al., 2012	Southern Ocean	U_{37}^{K} is more suitable than $U_{37}^{K'}$	-54.4	-80.1	23	0-700 kyr BP
U1385	Rodrigues et al., 2017 Bajo et al., 2020	Iberian margin	freshwater input from melting iceberg during glacial extreme cold events	37.6	-10.1	15	0-1 Ma
U1341	Horikawa et al., 2015	Bering Sea	colder and fresher water	54.0	179.0	20	0-4.3 Ma
ODP 983C	McClymont et al., 2008	North Atlantic	polar water mass	60.4	-23.6	24	0.5-1.5 Ma
ODP 882	Martinez-Garcia et al., 2010	Sub-Arctic Pacific	polar/subpolar extent	50.4	167.6	28	0-3.5 Ma
ODP 1090	Martinez-Garcia et al., 2010	sub-Antarctic Atlantic	polar/subpolar extent	-42.9	8.9	21	0-3.5 Ma
U1417	Sánchez-Montes et al., 2020	Gulf of Alaska	cold and/or freshwater	57.0	-147.1	24	1.7-4 Ma
104-642B	Bachem et al., 2017	Norwegian Sea	cooler (potentially less saline) surface water	67.2	2.9	8	3.14-5.32 Ma
ACEX	Stein et al.(*Earth and Life Processes Discovered from Subseafloor Environments - A Decade of Science Achieved by the Integrated Ocean*	Arctic	decrease in salinity (melting of sea ice and/or icebergs during summer?)	87.9	137.5	10	37-48 Ma

	Drilling Program (IODP), 2014)						
HM83-06	Rosell-Melé et al., 2011	North Sea Fan	-	64.3	-2.7	8	-
HM79-08	Rosell-Melé et al., 2011	North Sea Fan	-	62.9	0.0	8	-
162-986B	Rosell-Melé et al., 2011	Svalbard margin	-	77.3	-9.1	24	-

Table 2.S.2. List of Canadian Arctic Archipelago surface sediment samples used in DNA sequencing and the amplicon sequence variants (ASVs) resolved.

Sample	Lat.	Lon.	ASV1	ASV2	ASV3	ASV4
QMG1	68.49	-99.89	0	34	0	0
QMG2	68.31	-100.80	0	0	20	0
312	69.17	-100.70	121	45	0	17

Supplementary References

Bachem, P. E., Risebrobakken, B., De Schepper, S., & McClymont, E. L. (2017). Highly variable Pliocene sea surface conditions in the Norwegian Sea. Climate of the Past, 13(9), 1153–1168. https://doi.org/10.5194/cp-13-1153-2017

Bajo, P., Drysdale, R. N., Woodhead, J. D., Hellstrom, J. C., Hodell, D., Ferretti, P., Voelker, A. H. L., Zanchetta, G., Rodrigues, T., Wolff, E., Tyler, J., Frisia, S., Spötl, C., & Fallick, A. E. (2020). Persistent influence of obliquity on ice age terminations since the Middle Pleistocene transition. Science, 367(6483), 1235–1239. https://doi.org/10.1126/science.aaw1114

Bendle, J. A. P., & Rosell-Melé, A. (2007). High-resolution alkenone sea surface temperature variability on the North Icelandic Shelf: Implications for Nordic Seas palaeoclimatic development during the Holocene. The Holocene, 17(1), 9–24. https://doi.org/10.1177/0959683607073269

Bendle, J., Rosell-Melé, A., & Ziveri, P. (2005). Variability of unusual distributions of alkenones in the surface waters of the Nordic seas: PERCENT C 37:4 IN THE NORDIC SEAS. Paleoceanography, 20(2), n/a-n/a. https://doi.org/10.1029/2004PA001025

Calvo, E., Grimalt, J., & Jansen, E. (2002). High resolution U37K sea surface temperature reconstruction in the Norwegian Sea during the Holocene. Quaternary Science Reviews, 21(12–13), 1385–1394. https://doi.org/10.1016/S0277-3791(01)00096-8

Caniupán, M., Lamy, F., Lange, C. B., Kaiser, J., Arz, H., Kilian, R., Baeza Urrea, O., Aracena, C., Hebbeln, D., Kissel, C., Laj, C., Mollenhauer, G., & Tiedemann, R. (2011). Millennial-scale sea surface temperature and Patagonian Ice Sheet changes off southernmost Chile (53°S) over the past ∼60 kyr: SST CHANGES OFF SOUTHERN CHILE. Paleoceanography, 26(3), n/a-n/a. https://doi.org/10.1029/2010PA002049

Earth and Life Processes Discovered from Subseafloor Environments—A Decade of Science Achieved by the Integrated Ocean Drilling Program (IODP) (Vol. 7). (2014). Elsevier. https://doi.org/10.1016/C2011-0-08498-3

Enberg, S., Majaneva, M., Autio, R., Blomster, J., & Rintala, J. (2018). Phases of microalgal succession in sea ice and the water column in the Baltic Sea from autumn to spring. Marine Ecology Progress Series, 599, 19–34. https://doi.org/10.3354/meps12645

Fujine, K., Yamamoto, M., Tada, R., & Kido, Y. (2006). A salinity-related occurrence of a novel alkenone and alkenoate in Late Pleistocene sediments from the Japan Sea. Organic Geochemistry, 37(9), 1074–1084. https://doi.org/10.1016/j.orggeochem.2006.05.004

Harada, N., Ninnemann, U., Lange, C. B., Marchant, M. E., Sato, M., Ahagon, N., & Pantoja, S. (2013). Deglacial–Holocene environmental changes at the Pacific entrance of the Strait of Magellan. Palaeogeography, Palaeoclimatology, Palaeoecology, 375, 125–135. https://doi.org/10.1016/j.palaeo.2013.02.022

Harada, N., Sato, M., & Sakamoto, T. (2008). Freshwater impacts recorded in tetraunsaturated alkenones and alkenone sea surface temperatures from the Okhotsk Sea across millennial-scale cycles: MILLENNIAL CYCLES IN OKHOTSK SST AND SSS. Paleoceanography, 23(3), n/a-n/a. https://doi.org/10.1029/2006PA001410

Harada, N., Shin, K. H., Murata, A., Uchida, M., & Nakatani, T. (2003). Characteristics of alkenones synthesized by a bloom of emiliania huxleyi in the Bering Sea. Geochimica et Cosmochimica Acta, 67(8), 1507–1519. https://doi.org/10.1016/S0016-7037(02)01318-2

Ho, S. L., Mollenhauer, G., Lamy, F., Martínez-Garcia, A., Mohtadi, M., Gersonde, R., Hebbeln, D., Nunez-Ricardo, S., Rosell-Melé, A., & Tiedemann, R. (2012). Sea surface

temperature variability in the Pacific sector of the Southern Ocean over the past 700 kyr: THE 700 KYR SOUTH PACIFIC SST VARIABILITY. Paleoceanography, 27(4). https://doi.org/10.1029/2012PA002317

Horikawa, K., Martin, E. E., Basak, C., Onodera, J., Seki, O., Sakamoto, T., Ikehara, M., Sakai, S., & Kawamura, K. (2015). Pliocene cooling enhanced by flow of low-salinity Bering Sea water to the Arctic Ocean. Nature Communications, 6(1). https://doi.org/10.1038/ncomms8587

Ishiwatari, R., Houtatsu, M., & Okada, H. (2001). Alkenone-sea surface temperatures in the Japan Sea over the past 36 kyr: Warm temperatures at the last glacial maximum. Organic Geochemistry, 32(1), 57–67. https://doi.org/10.1016/S0146-6380(00)00151-0

Johnsen, S. J., Dahl-Jensen, D., Gundestrup, N., Steffensen, J. P., Clausen, H. B., Miller, H., Masson-Delmotte, V., Sveinbjörnsdottir, A. E., & White, J. (2001). Oxygen isotope and palaeotemperature records from six Greenland ice-core stations: Camp Century, Dye-3, GRIP, GISP2, Renland and NorthGRIP: OXYGEN ISOTOPE AND PALEOTEMPERATURE RECORDS FROM SIX GREENLAND ICE-CORES. Journal of Quaternary Science, 16(4), 299–307. https://doi.org/10.1002/jqs.622

Kristjánsdóttir, G. B., Moros, M., Andrews, J. T., & Jennings, A. E. (2017). Holocene Mg/Ca, alkenones, and light stable isotope measurements on the outer North Iceland shelf (MD99-2269): A comparison with other multi-proxy data and sub-division of the Holocene. The Holocene, 27(1), 52–62. https://doi.org/10.1177/0959683616652703

Krossa, V. R., Moros, M., Blanz, T., Jansen, E., & Schneider, R. (2015). Late Holocene Baltic Sea outflow changes reconstructed using C 37:4 content from marine cores: Late

Holocene Baltic Sea outflow changes. Boreas, 44(1), 81–93. https://doi.org/10.1111/bor.12093

Łącka, M., Cao, M., Rosell-Melé, A., Pawłowska, J., Kucharska, M., Forwick, M., & Zajączkowski, M. (2019). Postglacial paleoceanography of the western Barents Sea: Implications for alkenone-based sea surface temperatures and primary productivity. Quaternary Science Reviews, 224, 105973. https://doi.org/10.1016/j.quascirev.2019.105973

Lee, K. E., Bahk, J. J., & Choi, J. (2008). Alkenone temperature estimates for the East Sea during the last 190,000 years. Organic Geochemistry, 39(6), 741–753. https://doi.org/10.1016/j.orggeochem.2008.02.003

Lochte, A. A., Repschläger, J., Seidenkrantz, M.-S., Kienast, M., Blanz, T., & Schneider, R. R. (2019). Holocene water mass changes in the Labrador Current. The Holocene, 29(4), 676–690. https://doi.org/10.1177/0959683618824752

Lochte, A. A., Schneider, R., Kienast, M., Repschläger, J., Blanz, T., Garbe-Schönberg, D., & Andersen, N. (2020). Surface and subsurface Labrador Shelf water mass conditions during the last 6000 years. Climate of the Past, 16(4), 1127–1143. https://doi.org/10.5194/cp-16-1127-2020

M., S., Kreveld, S. V., H., E., Grootes, P. M., M., K., U., P., & M., S. (2003). Centennial-to-millennial-scale periodicities of Holocene climate and sediment injections off the western Barents shelf, 75°N. Boreas, 32(3), 447–461. https://doi.org/10.1080/03009480310003351

Martinez-Garcia, A., Rosell-Mele, A., McClymont, E. L., Gersonde, R., & Haug, G. H. (2010). Subpolar Link to the Emergence of the Modern Equatorial Pacific Cold Tongue. Science, 328(5985), 1550–1553. https://doi.org/10.1126/science.1184480

Martrat, B., Grimalt, J. O., Lopez-Martinez, C., Cacho, I., Sierro, F. J., Flores, J. A., Zahn, R., Canals, M., Curtis, J. H., & Hodell, D. A. (2004). Abrupt Temperature Changes in the Western Mediterranean over the Past 250,000 Years. Science, 306(5702), 1762–1765. https://doi.org/10.1126/science.1101706

Martrat, B., Grimalt, J. O., Shackleton, N. J., de Abreu, L., Hutterli, M. A., & Stocker, T. F. (2007). Four Climate Cycles of Recurring Deep and Surface Water Destabilizations on the Iberian Margin. Science, 317(5837), 502–507. https://doi.org/10.1126/science.1139994

Martrat, B., Grimalt, J. O., Villanueva, J., van Kreveld, S., & Sarnthein, M. (2003). Climatic dependence of the organic matter contributions in the north eastern Norwegian Sea over the last 15,000 years. Organic Geochemistry, 34(8), 1057–1070. https://doi.org/10.1016/S0146-6380(03)00084-6

McClymont, E. L., Rosell-Melé, A., Haug, G. H., & Lloyd, J. M. (2008). Expansion of subarctic water masses in the North Atlantic and Pacific oceans and implications for mid-Pleistocene ice sheet growth: MID-PLEISTOCENE POLAR/ARCTIC WATERS. Paleoceanography, 23(4), n/a-n/a. https://doi.org/10.1029/2008PA001622

Menot, G., Bard, E., Rostek, F., Weijers, J. W. H., Hopmans, E. C., Schouten, S., & Damste, J. S. S. (2006). Early Reactivation of European Rivers During the Last Deglaciation. Science, 313(5793), 1623–1625. https://doi.org/10.1126/science.1130511

Mishonov, A. (n.d.). NOAA Atlas NESDIS 61. 47.

Moros, M., Lloyd, J. M., Perner, K., Krawczyk, D., Blanz, T., de Vernal, A., Ouellet-Bernier, M.-M., Kuijpers, A., Jennings, A. E., Witkowski, A., Schneider, R., & Jansen, E. (2016). Surface and sub-surface multi-proxy reconstruction of middle to late Holocene palaeoceanographic changes in Disko Bugt, West Greenland. Quaternary Science Reviews, 132, 146–160. https://doi.org/10.1016/j.quascirev.2015.11.017

Naafs, B. D. A., Hefter, J., Acton, G., Haug, G. H., Martínez-Garcia, A., Pancost, R., & Stein, R. (2012). Strengthening of North American dust sources during the late Pliocene (2.7Ma). Earth and Planetary Science Letters, 317–318, 8–19. https://doi.org/10.1016/j.epsl.2011.11.026

Perner, K., Moros, M., Otterå, O. H., Blanz, T., Schneider, R. R., & Jansen, E. (2019). An oceanic perspective on Greenland's recent freshwater discharge since 1850. Scientific Reports, 9(1). https://doi.org/10.1038/s41598-019-53723-z

Rigual-Hernández, A. S., Colmenero-Hidalgo, E., Martrat, B., Bárcena, M. A., de Vernal, A., Sierro, F. J., Flores, J. A., Grimalt, J. O., Henry, M., & Lucchi, R. G. (2017). Svalbard ice-sheet decay after the Last Glacial Maximum: New insights from micropalaeontological and organic biomarker paleoceanographical reconstructions. Palaeogeography, Palaeoclimatology, Palaeoecology, 465, 225–236. https://doi.org/10.1016/j.palaeo.2016.10.034

Risebrobakken, B., Moros, M., Ivanova, E. V., Chistyakova, N., & Rosenberg, R. (2010). Climate and oceanographic variability in the SW Barents Sea during the Holocene. The Holocene, 20(4), 609–621. https://doi.org/10.1177/0959683609356586

Roberts, J., McCave, I. N., McClymont, E. L., Kender, S., Hillenbrand, C.-D., Matano, R., Hodell, D. A., & Peck, V. L. (2017). Deglacial changes in flow and frontal structure

through the Drake Passage. Earth and Planetary Science Letters, 474, 397–408. https://doi.org/10.1016/j.epsl.2017.07.004

Rodrigues, T., Alonso-García, M., Hodell, D. A., Rufino, M., Naughton, F., Grimalt, J. O., Voelker, A. H. L., & Abrantes, F. (2017). A 1-Ma record of sea surface temperature and extreme cooling events in the North Atlantic: A perspective from the Iberian Margin. Quaternary Science Reviews, 172, 118–130. https://doi.org/10.1016/j.quascirev.2017.07.004

Rosellmele, A. (2002). Appraisal of a molecular approach to infer variations in surface ocean freshwater inputs into the North Atlantic during the last glacial. Global and Planetary Change, 34(3–4), 143–152. https://doi.org/10.1016/S0921-8181(02)00111-X

Rosell-Melé, A., Balestra, B., Kornilova, O., Mcclymont, E. L., Russell, M., Monechi, S., Troelstra, S., & Ziveri, P. (2011). Alkenones and coccoliths in ice-rafted debris during the Last Glacial Maximum in the North Atlantic: Implications for the use of U K 37 ′ as a sea surface temperature proxy: ALKENONES AND COCCOLITHS IN ICE-RAFTED DEBRIS. Journal of Quaternary Science, 26(6), 657–664. https://doi.org/10.1002/jqs.1488

Rueda, G., Fietz, S., & Rosell-Melé, A. (2013). Coupling of air and sea surface temperatures in the eastern Fram Strait during the last 2000 years. The Holocene, 23(5), 692–698. https://doi.org/10.1177/0959683612470177

Sánchez-Montes, M. L., McClymont, E. L., Lloyd, J. M., Müller, J., Cowan, E. A., & Zorzi, C. (2020). Late Pliocene Cordilleran Ice Sheet development with warm northeast Pacific sea surface temperatures. Climate of the Past, 16(1), 299–313. https://doi.org/10.5194/cp-16-299-2020

Seki, O. (2005). Decreased surface salinity in the Sea of Okhotsk during the last glacial period estimated from alkenones. Geophysical Research Letters, 32(8). https://doi.org/10.1029/2004GL022177

Weaver, P. P. E., Chapman, M. R., Eglinton, G., Zhao, M., Rutledge, D., & Read, G. (1999). Combined coccolith, foraminiferal, and biomarker reconstruction of paleoceanographic conditions over the past 120 kyr in the northern North Atlantic (59°N, 23°W). Paleoceanography, 14(3), 336–349. https://doi.org/10.1029/1999PA900009

Zheng, Y., Heng, P., Conte, M. H., Vachula, R. S., & Huang, Y. (2019). Systematic chemotaxonomic profiling and novel paleotemperature indices based on alkenones and alkenoates: Potential for disentangling mixed species input. Organic Geochemistry, 128, 26–41. https://doi.org/10.1016/j.orggeochem.2018.12.008

Chapter 3: Group 2i Isochrysidales thrive in cold marine and lacustrine environments with ice cover

Karen J.Wang[1, 2],YongsongHuang[1, 2]

[1]Department of Earth, Environmental and Planetary Sciences, Brown University, Providence, RI 02912, USA

[2]Institute at Brown for Environment and Society, Brown University, Providence, RI 02912, USA

Abstract

The recently identified sea-ice related Group 2i Isochrysidales and its characteristic $C_{37:4}$-predominant alkenones have been proposed as a sea-ice proxy. However, apart from the co-occurrence of sea ice and Group 2i Isochrysidales, and the empirical relationship between $\%C_{37:4}$ alkenone and annual mean sea ice cover observed in the previous study, it is unclear if the presence of seasonal or perennial ice is a prerequisite of Group 2i in natural environments. Little was known about Group 2i's bloom phenology and survival strategies that helped its proliferation. Here we investigated Isochrysidales DNA and alkenones in sediment samples from Greenland fjords, Baltic Sea, and the Chesapeake Bay, which encompasses three thermal regimes, with the last being essentially free of sea ice. We also systematically mapped the occurrence of 2i based on environmental DNA data in lakes around the globe and compared it with lake ice occurrence. Our results show the presence of Group 2i in Greenland fjords and the Baltic Sea. Group 2i was not detected in the Chesapeake Bay surface sediment samples, even though *Isochrysis galbana* were detected abundantly. We produced maps of the global distribution of Group 2i and the other Isochrysidales. We found that the occurrence of Group 2i is highly sensitive to the presence of ice, and its growth is hindered by warm temperature. Group 2i is likely a part of the ice-algae community that relies on ice as a living substrate and part of under-ice bloom and/or spring bloom, in contrast to other Isochrysidales that bloom later in open water during the warm season. This study further supports the use of Group 2i biomarkers (e.g., $\%C_{37:4}$, the presence of $C_{39:4}$) for reconstructing the extent of past ice covers in the ocean and terrestrial environments.

1. Introduction

Sea ice is a crucial element of the Earth's climate system, with its high albedo (0.65 for bare ice and 0.85 for snow-covered sea ice) contrasted to the low albedo of open seawater (0.07) (Stroeve et al., 2012). Challenges in sea-ice modeling and paleo sea ice reconstruction call for sea-ice biomarkers. A new alkenone-based sea-ice proxy has been proposed by Wang et al. (2021). Alkenones are a class of diagenetically stable algal biomarkers that have been widely used for paleo sea surface temperature (SST) reconstructions (Brassell et al., 1986; Liu et al., 2009). The progress in understanding alkenone-producing species and the chemotaxonomy has enabled alkenones to reconstruct paleoclimate properties beyond SST, such as salinity and sea-ice extent. In particular, the most recently defined subgroup – Group 2i Isochrysidales and its characteristic $C_{37:4}$-predominant alkenones are associated with sea ice (Wang et al., 2021).

Based on phylogeny and habitat, Isochrysidales can be classified into three main groups: Group 1 (freshwater), Group 2 (brackish), and Group 3 (marine), with high phylogenetic diversity within each group (Theroux et al., 2010). Group 3 includes *Emiliania huxleyi* and *Gephyrocapsa oceanica*. Group 1 can be further separated into subclades 1a ("Greenland type") and 1b ("EV type") (Richter et al., 2019). Group 2 includes well-studied species e.g., *Isochrysis galbana*, *Ruttnera lamellosa*, as well as vast environmental sequences that has not been named (Zink et al., 2001; Theroux et al., 2010; Randlett et al., 2014; Zheng et al., 2016). Wang et al. (2021) discovered a monophyletic clade (Group 2i) within Group 2 that is composed of environmental sequences and un-identified algal isolation from sea ice and ice-covered sediments. Yao et al. (2022) defined the Group 2 outside of 2i subclade collectively as Group 2w, and separated them into Group 2w1 and 2w2. However, the phylogenic robustness needs to be further examined to justify the separation between 2w1 and 2w2. The different species of

Isochrysidales have different alkenone characteristics (Zheng et al., 2019), making it possible to differentiate them through alkenones profiles from sedimentary records.

Though environmental DNA of Group 2i Isochrysidales has been detected in the Arctic Ocean and lakes with perennial and seasonal ice cover, and empirical relationship between $\%C_{37:4}$ ($C_{37:4}$/($C_{37:2}$+ $C_{37:3}$+ $C_{37:4}$)) and annual mean sea ice cover was derived (Wang et al., 2021), more information on Group 2i Isochrysidales's relationship with ice is needed for paleoclimate interpretation. Environmental controls on Group 2i occurrence and whether the occurrence of ice is a prerequisite are still elusive. How Group 2i differs from other Isochrysidales in terms of its role in phytoplankton blooms and growth condition (e.g. temperature, salinity) is also unclear.

In this paper, we examined Group 2i's spatial distribution globally, as well as its growth time in phytoplankton bloom successions. We first compared Isochrysidales community composition across estuaries and marginal seas with different temperature regimes, including Greenland fjords, Baltic Sea, and Chesapeake Bay (USA), through sedimentary DNA and alkenone analyses. We then focused on two regions in the Baltic Sea with different salinity, and analyzed its haptophyte community composition changes in ice and water columns during an annual cycle. Lastly, we compared the global distribution of Group 2i with Group 2w, as wee as other Isochrysidales, and proposed potential survival strategies adapted by Group 2i that enabled its wide distribution.

2. Methods and material

2.1 Surface sediments from the Chesapeake Bay and Greenland Fjords

Sediment samples from the Baltic Sea, Chesapeake Bay, USA, and two Greenland Fjords were collected for DNA and alkenone analyses (Table 3. 1). Surface sediment samples were collected across the Baltic Sea from Skagerrak to the Bothnian Sea during expeditions M86/1 (R/V Meteor; November 2011), P435 (R/V Poseidon; June 2012), 6EZ1215 (R/V Elisabeth Mann Borgese; July 2012), EMB046 (R/V Elisabeth Mann Borgese; May 2013) through multi-corer (Kaiser et al., 2017). Surface sediment samples were collected in the Chesapeake Bay from July-September 2017 and kept frozen prior to DNA extraction. Two sediment cores (POR13_05 and POR13_08) from Upernavik Fjord were collected in August 2013 onboard R/V Porsild with Rumohr corer (Vermassen, Wangner, et al., 2019). One surface sediment sample from Kangerlussuaq Fjord was collected during JR106 (James Clark Ross; 2004).

2.2 DNA sequencing

Surface sediment samples from the Baltic Sea are sequenced through Sanger with haptophyte-specific primers targeting 18S rRNA as described in (Kaiser et al., 2019). In short, DNA was extracted and purified from 0.5 g of dried sediments. One round of PCR was performed with primer pair Prym-429F and Prym-887R (Coolen, 2004). The PCR products were run on gel electrophoresis, and gel bands with targeted length were purified and cloned. The clone products were sequenced on an ABI 3730XL capillary sequencer (Applied Biosystems, Foster City, CA). Isochrysidales sequences were identified through BLAST search, and Operational Taxonomic Units (OTUs) were clustered by UCLUST. Representative sequences of each OTU were deposited in GenBank under accession numbers MH472563-MH472566.

The surface sediment samples from the Chesapeake Bay and Kangerlussuaq Fjord were sequenced through Next Generation Sequencing (NGS) with haptophyte-specific primers targeting 18S rRNA following methods described in Wang et al. (2021). DNA was extracted from the samples, followed by a two-step PCR. The first round of PCR used an adapted version of the primer pair 528Flong and PRYM01+7 (E. Egge et al., 2013) followed by a second round of PCR which gives each sample a unique index sequence. The cleaned and normalized amplicons were then sequenced on an Illumina Miseq with V2 600-Cycle Kit (San Diego, CA). After quality control, sequences were clustered into Amplicon Sequence Variants (ASVs), and taxonomy was assigned using the SILVA reference database.

The downcore sediment samples from Upernavik Fjord were sequenced on an Illumina MiSeq 500-cycle paired-end run with haptophyte-specific primers (HAP_LSU_F and LHapto20R_bis) targeting D1-D2 region of 28S rRNA following methods described in Richter et al. (2019). Isochrysidales sequences were selected through BLAST and aligned to 28S rRNA reference sequences by PyNAST in Richter et al. (2019). A maximum-likelihood phylogenetic tree was built by RAxML on CIPRES (Miller et al., 2010; Stamatakis, 2014).

2.3 Alkenones analyses

Freeze-dried sediment samples were extracted by an accelerated solvent extraction system with DCM: methanol mixture (9:1, v/v). The total lipid extraction was further separated into three fractions of increasing polarity by silica gel columns eluting with hexane, DCM, and methanol subsequently. The mid-polar fractions containing alkenones were analyzed on a gas chromatography–flame ionization detection Agilent 7890N Series instrument with mid-polarity

column RTX-200 (105 m × 250 μm × 0.25 μm) with the oven program described in Zheng et al. (2017).

3. Results and Discussion

3.1 Comparison of primers and sequencing methods

Isochrysidales sequences were detected in the Chesapeake Bay, Baltic Sea and the Greenland Fjords (Table 3. 1). The detection of Isochrysidales is largely influenced by the sequencing method, sequencing region, and specificity of primers. Table 3. 2 summarize published studies focused on reconstructing Isochrysidales DNA from environmental samples, including lacustrine/marine water and sediment samples. One of the most commonly used primer pairs are Prym-429F and Prym-887R designed by Coolen (2004). This haptophyte-specific primer targets a highly variable region of 18S rRNA and creates a fraction around 460 bp (Coolen, 2004). Combined with Sanger sequencing, Prym-429F and Prym-887R were able to pick up Group 1a, Group 2 (including 2i), and Group 3 even when alkenone concentrations were low. However, it has yet to amplify Group 1b from environmental samples and might have a high detection-limit for Group 3. For example, even *E.huxleyi* blooms were observed in the Baltic Sea, *E.huxleyi* DNA was not detected from sediment samples using this primer pair with Sanger sequencing due to low sequencing depth. One limitation for this primer pair is that the fraction length is relatively long compared to the limit of common next-generation sequencing platforms, so Prym-429F and Prym-887R were usually used with Sanger sequencing.

With the development of next-generation sequencing (NGS), NGS became popular in more recent studies. However, NGS requires shorter fragments compared to Sanger sequencing. Egge et al. (2013) developed haptophyte-specific primer Hap454 (528Flong and PRYM01+7), which

amplifies the V4 region of 18S rRNA with a length <400 bp. This primer, combined with NGS, is able to detect and separate Group 1a, 1b, 2 (including 2i), and 3. The requirement for primer specificity is lower in NGS as the sequencing depth is much higher than Sanger sequencing. Through NGS, Isochrysidales can also be amplified by general eukaryotic primers. However, the recovered diversity and novelty may be lower due to the signal dilution from other organisms and the high GC content of Haptophyte V4 18S rRNA (Bittner et al., 2013; Simon et al., 2013).

Though NGS can achieve high sequencing-depth, the 18S rRNA still cannot fully resolve the phylogenetic diversity. 18S rRNA in haptophyte has a relatively low evolutionary rate compared to other Eukaryotes (Bittner et al., 2013). Therefore, Bittner et al. (2013) developed a Haptophyte-specific primer set targeting the D1-D2 region of 28S rRNA, which has a higher mutation rate compared to 18S rRNA. Richter et al. (2019) compared sequencing results between V4 18S rRNA and D1-D2 28S rRNA in multiple freshwater lakes dominant by Group 1 Isochrysidales. The results showed different community composition structures, with 28S rRNA showing multiple dominant species while 18S rRNA only showing one dominant species (Richter et al., 2019). The combined use of two sequencing regions likely reveals more diversity. However, there is only limited published 28S rRNA data on Isochrysidales, which hinders the phylogenetic comparison between samples. 18S rRNA and 28S rRNA are able to differentiate between groups, but they are insufficient to differentiate *Emiliani huxleyi* and *Gephyrocapsa oceanica* (Bendif et al., 2014). The separation between those two species can be achieved by using mitochondrial DNA markers (cox1, cox2, cox3, rpl16, and dam), which have higher mutation rates (Bendif et al., 2014).

3.2 Group 2i Isochrysidales is a key alkenone producer in Greenland fjords

Group 2i was detected in two Greenland fjords—Upernavik Fjord and Kangerlussuaq Fjord (Fig. 3. 1). Upernavik Fjord is located in West Greenland and has a length of ~60 km and a width of 5-7 km (Vermassen, Andreasen, et al., 2019). West Greenland Current flows into Upernavik Fjord through a deep trough of ~ 700 m, and a significant amount of Greenland Ice Sheet is discharged through the fjord in the form of tidewater glaciers (Vermassen, Andreasen, et al., 2019). The ice-front position of the outlet glaciers has been retreating continuously since 1930 in Upernavik Fjord (Khan et al., 2013; Vermassen, Andreasen, et al., 2019).

Haptophyte-specific primer targetting 28S rRNA was able to recover Isochrysidales in 5-6 cm and 45-46 cm from POR13_05, and 48-49 cm in POR13_08. Though 28S rRNA data is more limited compared to 18S rRNA in Isochrysidales, phylogenetic analyses based on 28S rRNA were able to distinguish the three groups of Isochrysidales (Fig. 3. 2). Sequences recovered from Upernavik Fjord did not match with any known species during BLAST against NCBI GenBank and phylogenetic analyses. Instead, it clustered with dominant sequences recovered from surface sediment from Fryxell Lake, Antarctica. The dominant Isochrysidales ESVs in Fryxell Lake belong to Group 2i based on 18S rRNA (Richter et al., 2019; Wang et al., 2021). Thus, the monophyly formed by those sequences from Fryxell Lake and Upernavik Fjord likely represents Group 2i Isochrysidales. Isochrysidales sequences recovered from Upernavik Fjord all belong to Group 2i.

Kangerdlugssuaq Fjord, located in southeastern Greenland, is influenced by the warm and salty Irminger Current and sea-ice baring East Greenland Current (Andresen et al., 2017). Kangerdlugssuaq Glacier, which is an important outlet of the Greenland Ice Sheet, has been retreating in the past decades (Bevan et al., 2019). The Alkenone profile from site GC13 suggests

a mixed alkenone source for both Group 2 and 3 (Fig. 3. 3). Group 2i Isochrysidales has been detected through 18S rRNA from surface sediment at site GC13 (Wang et al., 2021). This suggests that Group 2i is capable of surviving in ice mélange-influenced regions where sea ice and icebergs are mixed together. So far, the DNA of Group 2w has yet to be found in Greenland fjords.

Alkenone reconstructed SST in Greenland Fjords such as Nørre Skjoldungesund, Sermilik Fjord, and Kangerlussuaq Fjord show significant warm bias compared to the surface water measured in situ when applying U^{K}_{37}' global calibration (Andresen et al., 2013, 2017; Vermassen et al., 2020; Wangner et al., 2020). Previous studies generally attribute this warm bias to the advection of alkenones from shelf waters, particularly the warm water from upstream Irminger Current. Our DNA results suggest that, though the fluctuation of surface water salinity in fjords might not be favorable for *E. huxleyi* alkenone production, Group 2i are capable of surviving the dynamic environments in fjords and are key species for *in situ* alkenone productions in fjords. The alkenones in fjords are likely a mixture of in situ production and shelf water advection. Thus the SST reconstruction in fjords should be cautious, especially at the presence of $C_{37:4}$ alkenone.

3.3Species mixing in the Baltic Sea

The Baltic Sea is an intra-continental shelf sea characterized by a strong salinity gradient (Fig. 3. 4). The south of the Baltic Sea is connected with the North Sea that is around 35 psu, and the northern end of Bothnian Bay and the Gulf of Finland has a salinity of around 2 psu. During winter, Bothnian Bay is covered by consolidated ice. Moving along the transect, winter ice cover transitions to more fractured ice, and open water connecting to the North Sea (Lépy, 2012). In

Skagerrak, only two Isochrysidales sequences were detected from the surface sediment, and both of them belong to Group 2i (Table 3. 1). However, the presence of C_{38}Me alkenones and absence of $C_{37:3b}$Me, as well as ecological survey in previous studies, indicate *E.huxleyi* is one of the main alkenone producers in Skagerrak (E. S. Egge et al., 2015; Kaiser et al., 2019). Both Group 1 and Group 2i were detected in Arkona Basin, Eastern Gotland Basin, Landsort Deep, Bothnian Sea, and Bothnian Bay. In the transect from the North Sea to Bothnian Bay, the alkenone profiles show a disappearing and re-emergence of C_{38}Me; a continuous increase of the absolute abundance of $C_{37:4}$; an emergence of $C_{37:3b}$ and $C_{38:3b}$ isomers (Fig. 3. 3; Kaiser et al., 2019). The alkenone profiles combined with DNA results indicate the alkenone producers in the Baltic Sea transitioned from a mixture of Group 3 and Group 2i, to predominantly Group 2i, to a mixture of Group 2i and Group 1 along the salinity gradient from Skagerrak to Bothnian Bay (Kaiser et al., 2019).

Enberg et al. (2018) examined the microalgal community in ice and water column during the cold-water season (Oct.-May) in the northwest of the Gulf of Finland-- Krogarviken and Storfjärden (Fig. 3. 4). Krogarviken has an average depth of 3m, while Storfjärden has an average depth of 30m. Both of the sites are covered by sea ice from January to April, and haptophytes compose a significant fraction of the spring bloom during ice melt in April (Enberg et al., 2018). NGS of ice, under ice water, upper water, and bottom water samples detected Group 2i and Group 1 Isochrysidales at both sites (Fig. 3. S. 6 in Wang et al., 2021). Abundant Group 2i DNA reads were detected in all ice samples, while zero or only a few (<5 reads) Group 1 were detected in each ice sample (Fig. 3. S. 6 in Wang et al., 2021). Group 2i are the predominant haptophyte in the ice samples, taking up 40-85% and 59-86% of total haptophyte reads in Krogarviken and Storfjärden sea ice from January to April (Fig. 3. 5). Both Group 2i and

Group 1 occur in the under-ice water during winter. Group 2i were most abundant (32% in Krogarviken, 22% in Storfjärden) in under-ice water during February as the ice thickness steadily increased. Group 1 relative abundance in under-ice water ranged between 1-12%. This indicates that Group 2i are able to thrive within sea ice with variable brine salinity from approximately 4-45 psu, but Group 1 only inhabits the low salinity (~4 psu) water in Gulf of Finland and occasionally gets entrapped into sea ice during ice formation. The relative abundance of Group 2i decreased in the water column as water temperature rose up, and was absent in the majority of water samples collected during July-November at both sites. Thus Group 2i is not a part of the summer phytoplankton bloom; instead, it is part of the ice algae assemblage and potentially seeded the under-ice bloom through brine drainage in spring. This is consistent with the isolation of active Group 2i cells from an ice core in Baffin bay during pre-bloom and bloom development (Ribeiro et al., 2019), and the detection of Group 2i DNA in melt ponds and throughout sea ice in the Central Arctic (Rapp et al., 2018). Interestingly, Group 2w was not detected in Enberg et al. (2018) through NGS. This could be due to the low number of samples examined in warm-season water columns. Nevertheless, Group 2w might not be present at this site, potentially due to the cold temperature.

Egge et al.(2015) sampled water at 1 m depth monthly in outer Oslofjorden (59.19˚N, 10.69˚E) near Skagerrak from Sep 2009 to June 2011 and investigated the haptophyte community composition through NGS. Group 1, 2i, 2w, and 3 were all detected at this site. *E. huxleyi* was detected in all months except April and is one of the predominant species during high-temperature months from summer to early autumn (Fig. 3. 6). Group 2w (OTU 109 in Egge et al., 2015) was only detected in September 2009 and May 2011 when the surface temperature reached 16˚C. Group 2i (OTU 110 in Egge et al., 2015), on the contrary, was absent in warm

seasons, but detected during December 2010-April 2011 when the surface water temperature was around freezing for this prolonged time period and the upper Oslofjorden was frozen extensively. The relatively low sequence reads of Group 2i at this site suggest Group 2i might be transported from the ice in Upper Oslofjorden. Group 1 (OTU 53 in Egge et al., 2015) was detected in February and May 2010, and March-May 2011 likely controlled by freshwater input and reduced surface salinity during those time periods. The sequence in Oslofjorden further demonstrates the substantial difference between the key environmental controls on bloom phenology of the three groups.

3.4 Absence of Group 2i Isochrysidales in temperate estuary – Chesapeake Bay

To further understand the control of Group 2i occurrence, we compared the Isochrysidales community structure in Greenland Fjords and the Baltic Sea with temperate estuary environments, where salinity gradient is a prominent feature. Chesapeake Bay is a nutrient-rich estuary located in the Mid-Atlantic region of North America, and has a length of ~300km (Fig. 3. 7; Schwab & Sachs, 2011). The surface water temperature ranges between approximately 5-25˚C annually. Freshwater input by several major rivers to the bay is mixed with seawater from the Atlantic Ocean, creating a salinity gradient through the Chesapeake Bay. Peak alkenone production is in May, and a secondary peak is in August (Mercer et al., 2005). The spring algal bloom in the Chesapeake Bay is largely controlled by nutrient input from rivers, and haptophytes bloom after diatoms and dinoflagellates due to nutrient competition (Mercer et al., 2005).

Isochrysidales DNA was recovered from seven surface sediment samples in the lower part of Chesapeake Bay. *E. huxleyi* was only detected in 1CB near the mouth of the bay (Fig. 3. 8). The

dominant species in all samples were *I. galbana* which was in agreement with microscopic identification conducted in a previous study (Schwab & Sachs, 2011). The unidentified ESVs recovered all have 99.2-99.7% similarity to *I. galbana*. No Group 2i were identified in these samples. Alkenones in examined samples have a mixed source of Group 2w and Group 3 of different ratios. Thus the U^{K}_{37} and U^{K}_{37}' differed from site to site even though they are under the same temperature regime (Table 3. 3).

Alkenones in Chesapeake Bay are characterized by high $C_{38}Et$ compared to $C_{37}Me$ (Table 3. 3). This could be a characteristic trait of Group 2w alkenones. Yao et al. (2022) observed predominance of $C_{38}Et$ over $C_{37}Me$ in multiple lakes in China where Group 2w was detected. The predominance of $C_{38}Et$ over $C_{37}Me$ is not typically observed in known Group 2w culture experiments including those involving *I. nuda*, *I. litoralis*, *R. lamellose*, *I. galbana*, *T. lutea* (Liao et al., 2020; Zheng et al., 2019). Theroux et al. (2019) cultured Hap-A (Group 2i) and Hap-B (Group 2w) isolated from Lake George, and observed Hap-A has $C_{37}Me/C_{38}Et>1$, while Hap-B has $C_{37}Me/C_{38}Et<1$. High $C_{38}Et$ observed in Chinese lakes and the Chesapeake Bay could either be produced by phylotypes similar to Hap-B isolated from Lake George, or controlled by environmental factors that were not reproduced in most culture experiments.

3.5 Survival strategy of Group 2i Isochrysidales

Figure 3. 9a shows the map of the global distribution of Group 1 and 2 Isochrysidales based on environmental DNA studies. Group 2i is widespread in the high latitude oceans and lacustrine environments where lake ice is present in the winter (Fig. 3. 9b). Combining the absence of Group 2i in temperate environments and its occurrence in ice, Group 2i likely relies on ice as a living substrate and is a part of ice algae bloom and/or under-ice bloom at the onset of ice melt,

in contrast to other Group 2 and Group 3 which bloom in open water. Group 2i DNA was observed in the Canadian Arctic Archipelago, Baffin Bay, and Greenland fjords. The bathymetry of those regions enhances vertical mixing from tidal energy that replenishes nutrients (Ardyna et al., 2020; Ribeiro et al., 2019; Wang et al., 2021). During late spring, melt ponds form, and ice begins to melt, light availability under ice increases rapidly (Ardyna et al., 2020). Group 2i should be able to utilize nutrients delivered to the photic zone from mixing and upwelling quickly. Group 2i DNA is also found across the high Arctic, where surviving the Polar night is an additional challenge. There are three potential reasons why Group 2i is adapted to those harsh environments: 1) the forming of resting stages that allows cells to stay in sea ice or surface sediment for a longer time; 2) mixotrophy reduces the reliance on solar radiance; 3) a preference for low growing temperature and flexibility with salinity.

In an enrichment experiment, Group 2i (Hap-A) in Lake George, Canada, was triggered out of the resting stage (during which the cells were not active and alkenone production was paused) from deep sediment. In contrast, water column samples collected during the end of the algal bloom season were able to yield non-2i Group 2 but unable to yield Group 2i (Toney et al., 2012). Group 2i DNA decreased to zero in water columns quickly after the initial bloom in Lake George. In time-series samples from the Baltic Sea, Group 2i DNA was either absent or of extremely low abundance in water columns during summer and fall. This suggests that water suspension may not be a main overwinter strategy for Group 2i; instead, it is able to form resting spores in sediment that can be re-suspended into the water column in shallow environments such as continental shelves or lakes.

The Group 2i Isochrysidales might also stay active within ice during prolonged darkness through mixotrophy. Multiple Isochrysidales species are capable of mixotrophy, including

Emiliania huxleyi, *Gephyrocapsa oceanica*, *Isochrysis galbana*, and *Tisochrysis lutea* (Alkhamis & Qin, 2013, 2015, 2016; Godrijan et al., 2020). Increased biomass production and nutrient conversion efficiency under mixotrophic conditions with glycerol as carbon source has been reported in Group 2 species *Isochrysis galbana* and *Tisochrysis lutea* (Alkhamis & Qin, 2015, 2016). Group 2i could be mixotrophic, which would explain the detection of their DNA in the Central Arctic Ocean, where perennial sea ice exists, and light is extremely limited (Wang et al., 2021). Mixotrophic haptophytes have been reported to be important bacteria grazers in oligotrophic marine environments (Unrein et al., 2014). Under-ice bloom of mixotrophic brackish-water haptophytes (Chrysochromulina and Prymnesium) has been observed in freshwater-influenced Young Sound Fjord, northeastern Greenland. Those mixotrophs are able to utilize organic carbon from the prey, which gives them a competitive advantage during the beginning of spring bloom in low-light and low-nutrient brackish water under 1-m thick sea ice (Søgaard et al., 2021).

In addition to potential mixotrophy, the temperature and salinity preference for Group 2i are also crucial to its survival in sea ice. Liao et al. (in prep.) cultured RCC5486 at different temperatures from 0-12 ˚C at 31 ppt under light: dark cycle of 16:8 and found that RCC5486 was able to thrive at high growth rates at 0, 3, 6, 9 ˚C, but failed to grow at 10.5 and 12 ˚C. Liao et al. (in prep.) also tested different salinity (15, 21, 26, 31, and 38 ppt) under 3˚C and did not observe a significant difference in growth rate between different salinity. This suggests that Group 2i may have a low-temperature preference and is not sensitive to fluctuations in salinity. Those traits enable Group 2i to survive in sea ice brine channels, melt ponds, and under-ice water, where the temperature is low and salinity fluctuates while ice forms and melts.

So far, the DNA evidence of Group 2i in the Arctic Ocean is all modern samples (Wang et al., 2021). Whether Group 2i is a local species in the polar region or a sub-polar species that recently intruded in the high Arctic remains unknown. Temperate species *E. huxleyi* has expanded poleward through bio-advection, transported by North Atlantic Water through European Arctic Corridor and North Pacific Water through Bering Strait (Winter et al., 2014; Oziel et al., 2020; Ardyna & Arrigo, 2020). Understanding Group 2i's habitat and tracing them in downcore sediment in the Arctic could help understand the bio-transport and ecological changes in the Arctic Ocean.

4. Conclusions

We examined the occurrence of Group 2i Isochrysidales across a global spatial scale and an annual cycle, and confirmed its close relationship with ice. Group 2i was detected across the Baltic Sea, while absent in temperate estuary the Chesapeake Bay, suggesting ice and low temperature are prerequisites for its growth. Excitingly, Group 2i was also detected in fjords located on both west and east Greenland, which indicates the potential of *in situ* alkenone production within Greenland fjords contrary to advection from Irminger Current suggested in previous studies. Group 2i has significantly different bloom phenology compared to other Isochrysidales that are part of the haptophyte bloom typically following diatom bloom in spring (Mercer et al., 2005; E. S. Egge et al., 2015). Instead, Group 2i is a part of the ice-algae community, which can further act as a seed for under-ice bloom and spring bloom upon ice melt. Its exact role in bloom succession and alkenone production efficiency likely vary between sites based on the sea-ice extent, light and nutrient availability, temperature, and competitors. Our synthesis of reported Group 2i DNA shows its wide range of habitats around the globe, from

lacustrine environments to continental shelves and the center Arctic. Formation of resting stage, mixotrophy, low growth temperature, and flexibility with salinity are potential survival strategies that enabled Group 2i's growth in high latitude environments. The growth of Group 2i in the Arctic region is likely sensitive to light availability beneath the ice, which is affected by ice thickness, snow cover, melt ponds, etc. (Horvat et al., 2017). Reconstructing the occurrence and abundance of Group 2i in the past can shed light on the past sea ice occurrence and albedo, as well as primary productivity in the Arctic. DNA analyses coupled with alkenone analyses on time-series samples of sea ice and water during ice melt would further improve our understanding of the Group 2i growth phenology. Culture experiments under low light mixotrophic conditions would be useful to understand Group 2i's overwinter strategy.

Reference

Alkhamis, Y., & Qin, J. G. (2013). Cultivation of Isochrysis galbana in Phototrophic, Heterotrophic, and Mixotrophic Conditions. *BioMed Research International*, 2013, 1–9. https://doi.org/10.1155/2013/983465

Alkhamis, Y., & Qin, J. G. (2015). Comparison of N and P requirements of Isochrysis galbana under phototrophic and mixotrophic conditions. *Journal of Applied Phycology*, 27(6), 2231–2238. https://doi.org/10.1007/s10811-014-0501-5

Alkhamis, Y., & Qin, J. G. (2016). Comparison of pigment and proximate compositions of Tisochrysis lutea in phototrophic and mixotrophic cultures. *Journal of Applied Phycology*, 28(1), 35–42. https://doi.org/10.1007/s10811-015-0599-0

Andresen, C. S., Kokfelt, U., Sicre, M.-A., Knudsen, M. F., Dyke, L. M., Klein, V., Kaczmar, F., Miles, M. W., & Wangner, D. (2017). Exceptional 20th century glaciological regime of a major SE Greenland outlet glacier. *Scientific Reports*, 7(1). https://doi.org/10.1038/s41598-017-13246-x

Andresen, C. S., Sicre, M.-A., Straneo, F., Sutherland, D. A., Schmith, T., Hvid Ribergaard, M., Kuijpers, A., & Lloyd, J. M. (2013). A 100-year long record of alkenone-derived SST changes by Southeast Greenland. *Continental Shelf Research*, 71, 45–51. https://doi.org/10.1016/j.csr.2013.10.003

Ardyna, M., & Arrigo, K. R. (2020). Phytoplankton dynamics in a changing Arctic Ocean. *Nature Climate Change*, 10(10), 892–903. https://doi.org/10.1038/s41558-020-0905-y

Ardyna, M., Mundy, C. J., Mills, M. M., Oziel, L., Grondin, P.-L., Lacour, L., Verin, G., van Dijken, G., Ras, J., Alou-Font, E., Babin, M., Gosselin, M., Tremblay, J.-É., Raimbault, P., Assmy, P., Nicolaus, M., Claustre, H., & Arrigo, K. R. (2020). Environmental drivers

of under-ice phytoplankton bloom dynamics in the Arctic Ocean. *Elementa: Science of the Anthropocene*, 8, 30. https://doi.org/10.1525/elementa.430

Bendif, E. M., Probert, I., Carmichael, M., Romac, S., Hagino, K., & de Vargas, C. (2014). Genetic delineation between and within the widespread coccolithophore morpho-species Emiliania huxleyi and Gephyrocapsa oceanica (Haptophyta). *Journal of Phycology*, 50(1), 140–148. https://doi.org/10.1111/jpy.12147

Bevan, S. L., Luckman, A. J., Benn, D. I., Cowton, T., & Todd, J. (2019). Impact of warming shelf waters on ice mélange and terminus retreat at a large SE Greenland glacier. *The Cryosphere*, 13(9), 2303–2315. https://doi.org/10.5194/tc-13-2303-2019

Bittner, L., Gobet, A., Audic, S., Romac, S., Egge, E. S., Santini, S., Ogata, H., Probert, I., Edvardsen, B., & de Vargas, C. (2013). Diversity patterns of uncultured Haptophytes unravelled by pyrosequencing in Naples Bay. *Molecular Ecology*, 22(1), 87–101. https://doi.org/10.1111/mec.12108

Brassell, S. C., Eglinton, G., Marlowe, I. T., Pflaumann, U., & Sarnthein, M. (1986). Molecular stratigraphy: A new tool for climatic assessment. *Nature*, 320(6058), 129–133. https://doi.org/10.1038/320129a0

Coolen, M. (2004). Combined DNA and lipid analyses of sediments reveal changes in Holocene haptophyte and diatom populations in an Antarctic lake. *Earth and Planetary Science Letters*, 223(1–2), 225–239. https://doi.org/10.1016/j.epsl.2004.04.014

Egge, E., Bittner, L., Andersen, T., Audic, S., de Vargas, C., & Edvardsen, B. (2013). 454 Pyrosequencing to Describe Microbial Eukaryotic Community Composition, Diversity and Relative Abundance: A Test for Marine Haptophytes. *PLoS ONE*, 8(9), e74371. https://doi.org/10.1371/journal.pone.0074371

Egge, E. S., Johannessen, T. V., Andersen, T., Eikrem, W., Bittner, L., Larsen, A., Sandaa, R.-A., & Edvardsen, B. (2015). Seasonal diversity and dynamics of haptophytes in the Skagerrak, Norway, explored by high-throughput sequencing. *Molecular Ecology*, 24(12), 3026–3042. https://doi.org/10.1111/mec.13160

Enberg, S., Majaneva, M., Autio, R., Blomster, J., & Rintala, J. (2018). Phases of microalgal succession in sea ice and the water column in the Baltic Sea from autumn to spring. *Marine Ecology Progress Series*, 599, 19–34. https://doi.org/10.3354/meps12645

Godrijan, J., Drapeau, D., & Balch, W. M. (2020). Mixotrophic uptake of organic compounds by coccolithophores. *Limnology and Oceanography*, 65(6), 1410–1421. https://doi.org/10.1002/lno.11396

Horvat, C., Jones, D. R., Iams, S., Schroeder, D., Flocco, D., & Feltham, D. (2017). The frequency and extent of sub-ice phytoplankton blooms in the Arctic Ocean. *Science Advances*, 3(3), e1601191. https://doi.org/10.1126/sciadv.1601191

Kaiser, J., van der Meer, M. T. J., & Arz, H. W. (2017). Long-chain alkenones in Baltic Sea surface sediments: New insights. *Organic Geochemistry*, 112, 93–104. https://doi.org/10.1016/j.orggeochem.2017.07.002

Kaiser, J., Wang, K. J., Rott, D., Li, G., Zheng, Y., Amaral-Zettler, L., Arz, H. W., & Huang, Y. (2019). Changes in long chain alkenone distributions and Isochrysidales groups along the Baltic Sea salinity gradient. *Organic Geochemistry*, 127, 92–103. https://doi.org/10.1016/j.orggeochem.2018.11.012

Khan, S. A., Kjaer, K. H., Korsgaard, N. J., Wahr, J., Joughin, I. R., Timm, L. H., Bamber, J. L., van den Broeke, M. R., Stearns, L. A., Hamilton, G. S., Csatho, B. M., Nielsen, K., Hurkmans, R., & Babonis, G. (2013). Recurring dynamically induced thinning during

1985 to 2010 on Upernavik Isstrøm, West Greenland: THINNING ON UPERNAVIK ISSTRØM. *Journal of Geophysical Research: Earth Surface*, 118(1), 111–121. https://doi.org/10.1029/2012JF002481

Lépy, É. (2012). Baltic Sea ice and environmental and societal implications from the comparative analysis of the Bay of Bothnia and the Gulf of Riga. Fennia - *International Journal of Geography*, 190(2), 90–101. https://doi.org/10.11143/4403

Liao, S., Yao, Y., Wang, L., Wang, K. J., Amaral-Zettler, L., Longo, W. M., & Huang, Y. (2020). C41 methyl and C42 ethyl alkenones are biomarkers for Group II Isochrysidales. *Organic Geochemistry*, 147, 104081. https://doi.org/10.1016/j.orggeochem.2020.104081

Liu, Z., Pagani, M., Zinniker, D., DeConto, R., Huber, M., Brinkhuis, H., Shah, S. R., Leckie, R. M., & Pearson, A. (2009). Global Cooling During the Eocene-Oligocene Climate Transition. *Science*, 323(5918), 1187–1190. https://doi.org/10.1126/science.1166368

Mercer, J. L., Zhao, M., & Colman, S. M. (2005). Seasonal variations of alkenones and UK37 in the Chesapeake Bay water column. Estuarine, *Coastal and Shelf Science*, 63(4), 675–682. https://doi.org/10.1016/j.ecss.2005.01.011

Miller, M. A., Pfeiffer, W., & Schwartz, T. (2010). Creating the CIPRES Science Gateway for inference of large phylogenetic trees. 2010 Gateway Computing Environments Workshop (GCE), 1–8. https://doi.org/10.1109/GCE.2010.5676129

Oziel, L., Baudena, A., Ardyna, M., Massicotte, P., Randelhoff, A., Sallée, J.-B., Ingvaldsen, R. B., Devred, E., & Babin, M. (2020). Faster Atlantic currents drive poleward expansion of temperate phytoplankton in the Arctic Ocean. *Nature Communications*, 11(1). https://doi.org/10.1038/s41467-020-15485-5

Randlett, M.-È., Coolen, M. J. L., Stockhecke, M., Pickarski, N., Litt, T., Balkema, C., Kwiecien, O., Tomonaga, Y., Wehrli, B., & Schubert, C. J. (2014). Alkenone distribution in Lake Van sediment over the last 270 ka: Influence of temperature and haptophyte species composition. *Quaternary Science Reviews*, 104, 53–62. https://doi.org/10.1016/j.quascirev.2014.07.009

Rapp, J. Z., Fernández-Méndez, M., Bienhold, C., & Boetius, A. (2018). Effects of Ice-Algal Aggregate Export on the Connectivity of Bacterial Communities in the Central Arctic Ocean. *Frontiers in Microbiology*, 9. https://doi.org/10.3389/fmicb.2018.01035

Ribeiro, C. G. (n.d.). Culturable diversity of Arctic phytoplankton during pack ice melting. 23.

Richter, N., Longo, W. M., George, S., Shipunova, A., Huang, Y., & Amaral‐Zettler, L. (2019). Phylogenetic diversity in freshwater‐dwelling Isochrysidales haptophytes with implications for alkenone production. *Geobiology*, 17(3), 272–280. https://doi.org/10.1111/gbi.12330

Schwab, V. F., & Sachs, J. P. (2011). Hydrogen isotopes in individual alkenones from the Chesapeake Bay estuary. *Geochimica et Cosmochimica Acta*, 75(23), 7552–7565. https://doi.org/10.1016/j.gca.2011.09.031

Simon, M., López-García, P., Moreira, D., & Jardillier, L. (2013). New haptophyte lineages and multiple independent colonizations of freshwater ecosystems. *Environmental Microbiology Reports*, 5(2), 322–332. https://doi.org/10.1111/1758-2229.12023

Søgaard, D. H., Sorrell, B. K., Sejr, M. K., Andersen, P., Rysgaard, S., Hansen, P. J., Skyttä, A., Lemcke, S., & Lund-Hansen, L. C. (2021). An under-ice bloom of mixotrophic haptophytes in low nutrient and freshwater-influenced Arctic waters. *Scientific Reports*, 11(1), 2915. https://doi.org/10.1038/s41598-021-82413-y

Stamatakis, A. (2014). RAxML version 8: A tool for phylogenetic analysis and post-analysis of large phylogenies. *Bioinformatics*, 30(9), 1312–1313. https://doi.org/10.1093/bioinformatics/btu033

Stroeve, J. C., Serreze, M. C., Holland, M. M., Kay, J. E., Malanik, J., & Barrett, A. P. (2012). The Arctic's rapidly shrinking sea ice cover: A research synthesis. *Climatic Change*, 110(3–4), 1005–1027. https://doi.org/10.1007/s10584-011-0101-1

Theroux, S., D'Andrea, W. J., Toney, J., Amaral-Zettler, L., & Huang, Y. (2010). Phylogenetic diversity and evolutionary relatedness of alkenone-producing haptophyte algae in lakes: Implications for continental paleotemperature reconstructions. *Earth and Planetary Science Letters*, 300(3–4), 311–320. https://doi.org/10.1016/j.epsl.2010.10.009

Toney, J. L., Theroux, S., Andersen, R. A., Coleman, A., Amaral-Zettler, L., & Huang, Y. (2012). Culturing of the first 37:4 predominant lacustrine haptophyte: Geochemical, biochemical, and genetic implications. *Geochimica et Cosmochimica Acta*, 78, 51–64. https://doi.org/10.1016/j.gca.2011.11.024

Unrein, F., Gasol, J. M., Not, F., Forn, I., & Massana, R. (2014). Mixotrophic haptophytes are key bacterial grazers in oligotrophic coastal waters. *The ISME Journal*, 8(1), 164–176. https://doi.org/10.1038/ismej.2013.132

Vermassen, F., Andreasen, N., Wangner, D. J., Thibault, N., Seidenkrantz, M.-S., Jackson, R., Schmidt, S., Kjær, K. H., & Andresen, C. S. (2019). A reconstruction of warm-water inflow to Upernavik Isstrøm since 1925 CE and its relation to glacier retreat. *Climate of the Past*, 15(3), 1171–1186. https://doi.org/10.5194/cp-15-1171-2019

Vermassen, F., Bjørk, A. A., Sicre, M., Jaeger, J. M., Wangner, D. J., Kjeldsen, K. K., Siggaard-Andersen, M., Klein, V., Mouginot, J., Kjær, K. H., & Andresen, C. S. (2020). A Major

Collapse of Kangerlussuaq Glacier' s Ice Tongue Between 1932 and 1933 in East Greenland. *Geophysical Research Letters*, 47(4). https://doi.org/10.1029/2019GL085954

Vermassen, F., Wangner, D. J., Dyke, L. M., Schmidt, S., Cordua, A. E., Kjær, K. H., Haubner, K., & Andresen, C. S. (2019). Evaluating ice‐rafted debris as a proxy for glacier calving in Upernavik Isfjord, NW Greenland. *Journal of Quaternary Science*, 34(3), 258–267. https://doi.org/10.1002/jqs.3095

Wang, K. J., Huang, Y., Majaneva, M., Belt, S. T., Liao, S., Novak, J., Kartzinel, T. R., Herbert, T. D., Richter, N., & Cabedo-Sanz, P. (2021). Group 2i Isochrysidales produce characteristic alkenones reflecting sea ice distribution. *Nature Communications*, 12(1). https://doi.org/10.1038/s41467-020-20187-z

Wangner, D. J., Sicre, M., Kjeldsen, K. K., Jaeger, J. M., Bjørk, A. A., Vermassen, F., Sha, L., Kjær, K. H., Klein, V., & Andresen, C. S. (2020). Sea Surface Temperature Variability on the SE‐Greenland Shelf (1796–2013 CE) and Its Influence on Thrym Glacier in Nørre Skjoldungesund. *Paleoceanography and Paleoclimatology*, 35(3). https://doi.org/10.1029/2019PA003692

Winter, A., Henderiks, J., Beaufort, L., Rickaby, R. E. M., & Brown, C. W. (2014). Poleward expansion of the coccolithophore Emiliania huxleyi. *Journal of Plankton Research*, 36(2), 316–325. https://doi.org/10.1093/plankt/fbt110

Yao, Y., Zhao, J., Vachula, R. S., Liao, S., Li, G., Pearson, E. J., & Huang, Y. (2022). Phylogeny, alkenone profiles and ecology of Isochrysidales subclades in saline lakes: Implications for paleosalinity and paleotemperature reconstructions. *Geochimica et Cosmochimica Acta*, 317, 472–487. https://doi.org/10.1016/j.gca.2021.11.001

Zheng, Y., Heng, P., Conte, M. H., Vachula, R. S., & Huang, Y. (2019). Systematic chemotaxonomic profiling and novel paleotemperature indices based on alkenones and alkenoates: Potential for disentangling mixed species input. *Organic Geochemistry*, 128, 26–41. https://doi.org/10.1016/j.orggeochem.2018.12.008

Zheng, Y., Huang, Y., Andersen, R. A., & Amaral-Zettler, L. A. (2016). Excluding the di-unsaturated alkenone in the UK37 index strengthens temperature correlation for the common lacustrine and brackish-water haptophytes. *Geochimica et Cosmochimica Acta*, 175, 36–46. https://doi.org/10.1016/j.gca.2015.11.024

Zheng, Y., Tarozo, R., & Huang, Y. (2017). Optimizing chromatographic resolution for simultaneous quantification of long chain alkenones, alkenoates and their double bond positional isomers. *Organic Geochemistry*, 111, 136–143. https://doi.org/10.1016/j.orggeochem.2017.06.013

Zink, K.-G., Leythaeuser, D., Melkonian, M., & Schwark, L. (2001). Temperature dependency of long-chain alkenone distributions in recent to fossil limnic sediments and in lake waters. *Geochimica et Cosmochimica Acta*, 65(2), 253–265. https://doi.org/10.1016/S0016-7037(00)00509-3

Figures

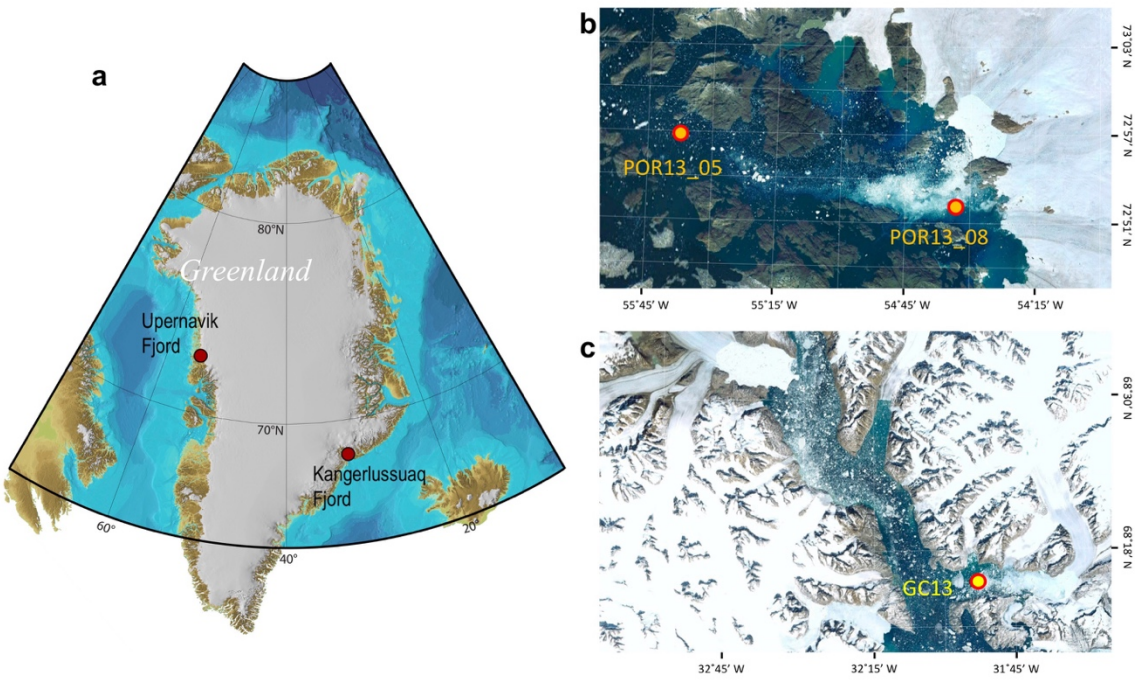

Figure 3. 1. Maps of Group 2i detected in Greenland fjords. a) locations of Upernavik Fjord and Kangerlussuaq Fjord with bathymetry adapted from IBCAO Version 3. b, c) Maps of Upernavik Fjord and Kangerlussuaq Fjord (Image U.S. Geological Survey, Image IBCAO, Google Earth).

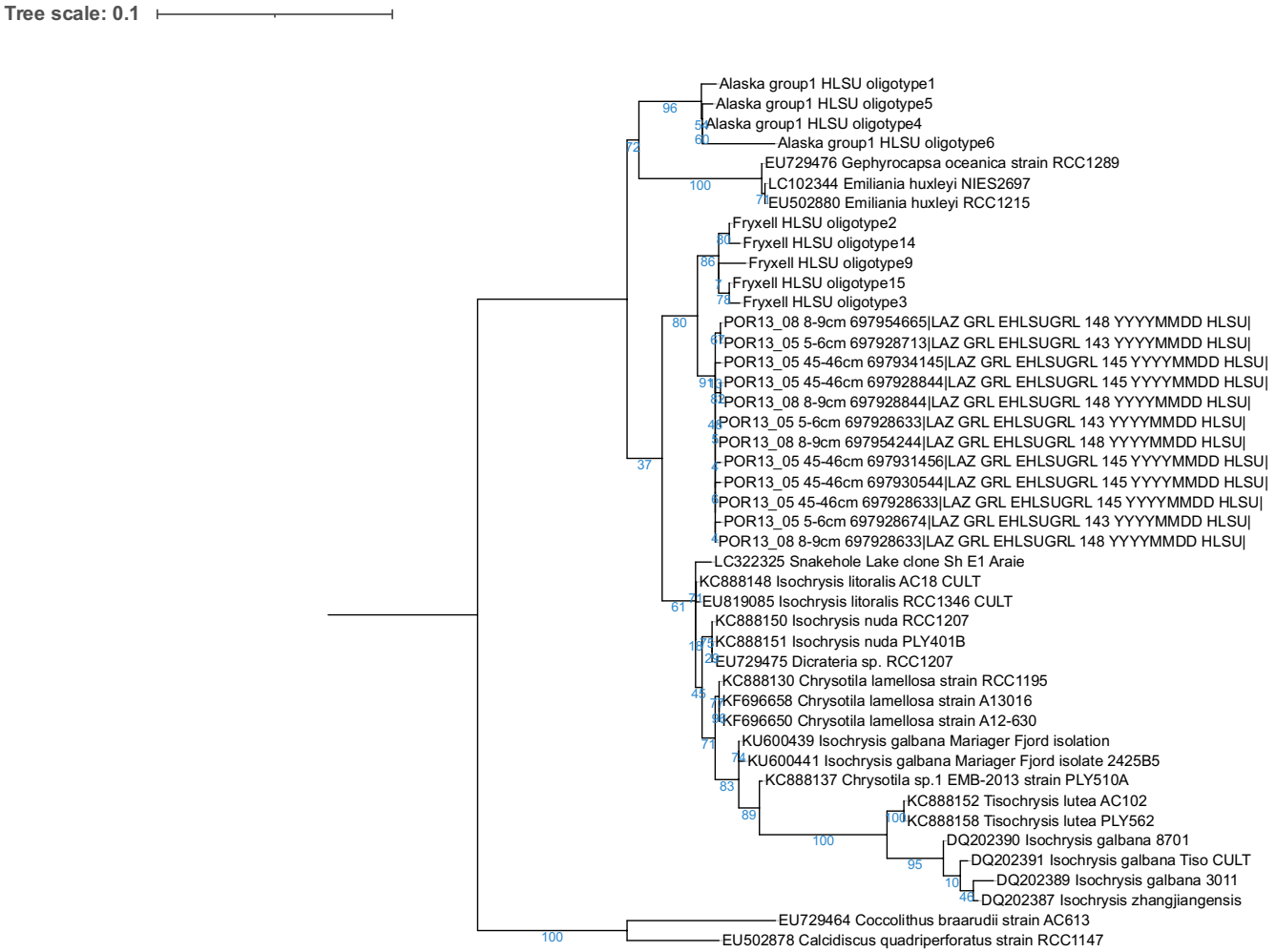

Figure 3. 2. Phylogenetic tree of Isochrysidales 28S rRNA.

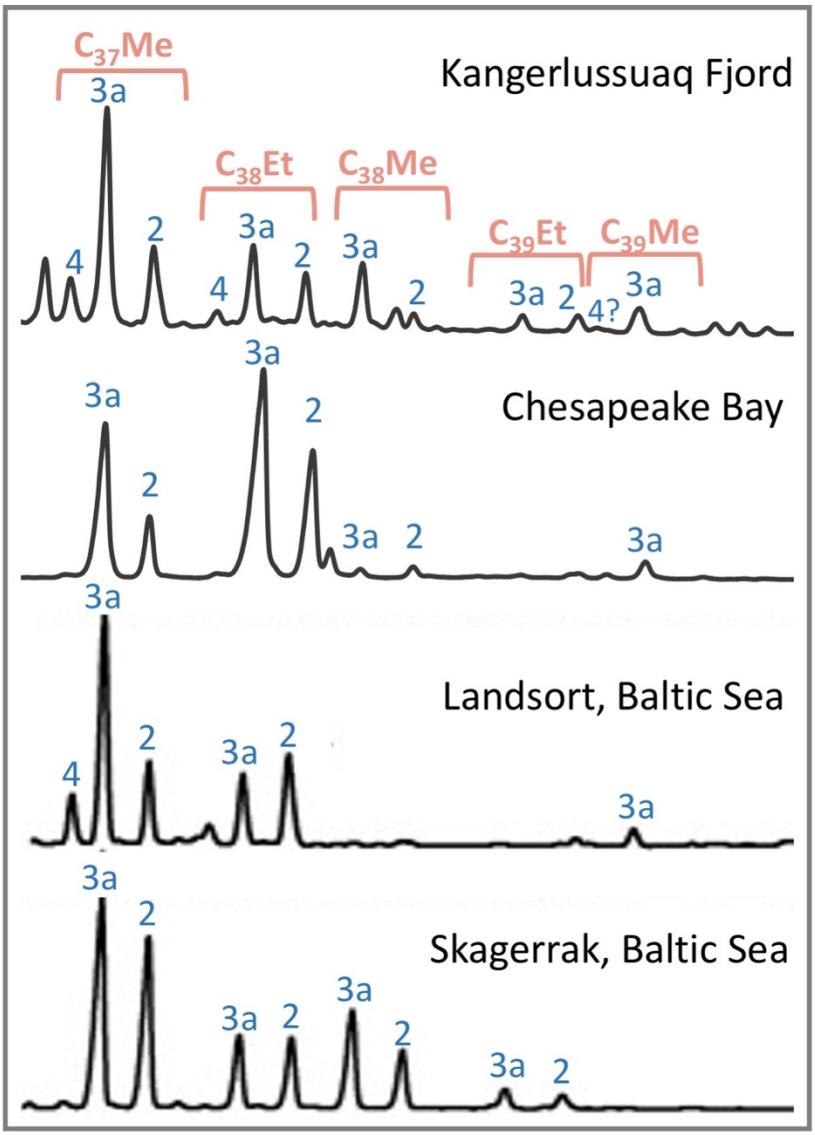

Figure 3. 3. Representative GC-FID chromatograms of alkenones in surface sediment from Kangerlussuaq Fjord (GC13), Chesapeake Bay (RB12), central Baltic Sea (Landsort Deep), western Baltic Sea (Skagerrak).

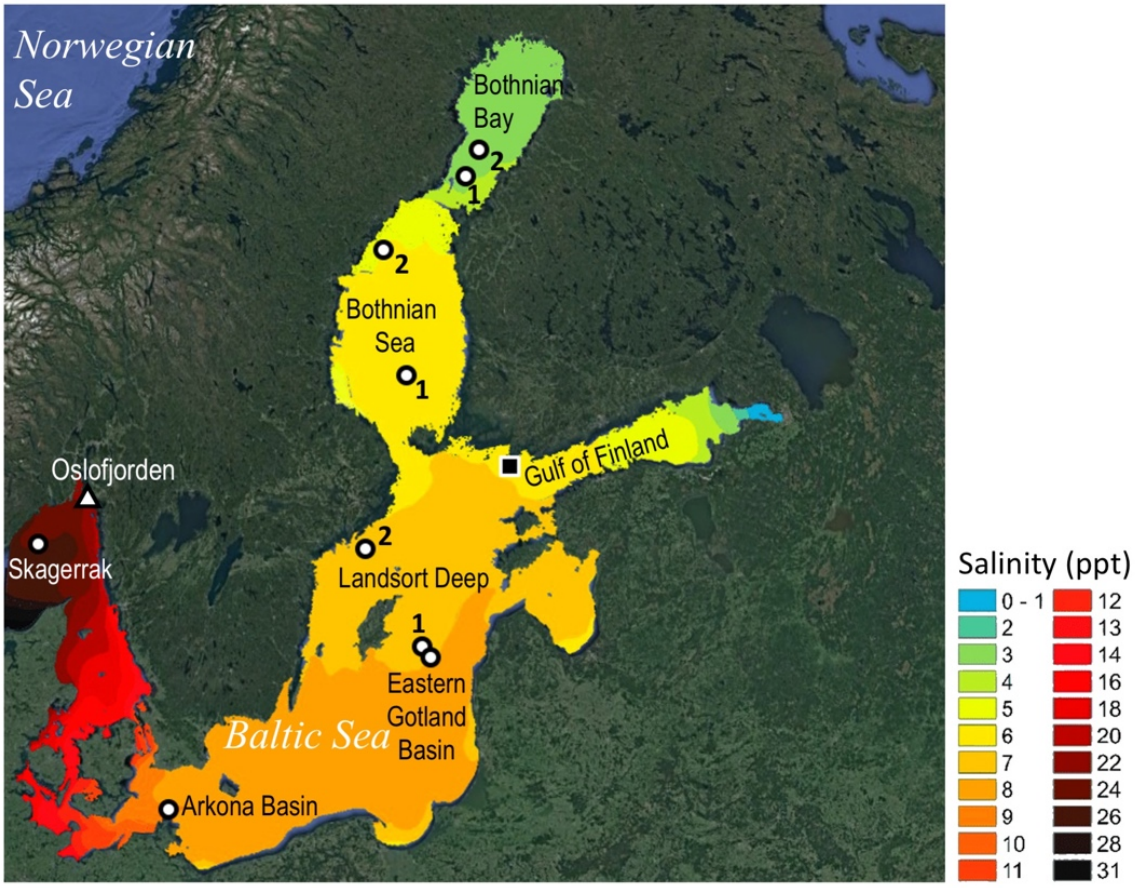

Figure 3. 4. Map of samples examined in the Baltic Sea, the base map is 2015-2019 average surface salinity adapted from Jaspers et al. (2021). Circle: surface sediments analyzed in this study and (Kaiser et al., 2019). Square and triangle: study site of Enberg et al. (2018) and Egge et al., (2015)

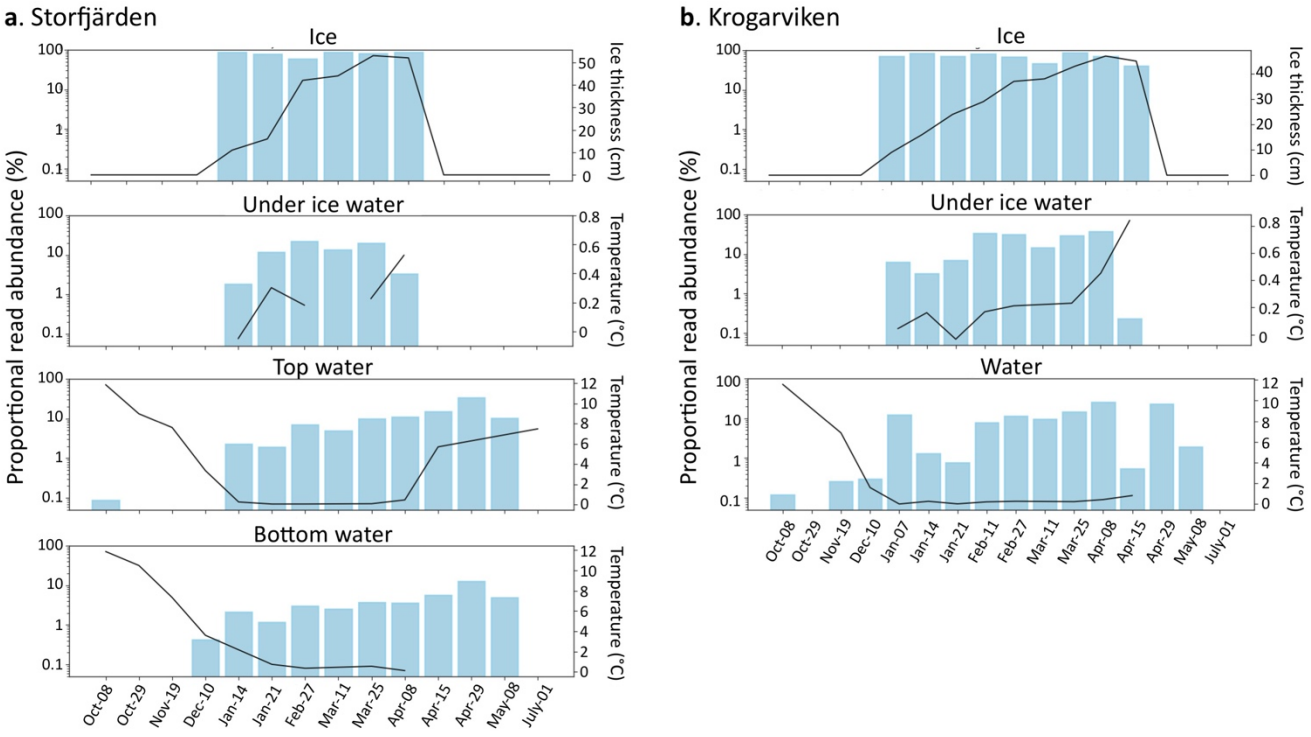

Figure 3. 5. Barplots of Group 2i relative abundance to total haptophytes based on proportional reads from ice and water samples collected during Oct. 2012-July 2013, note the y-axis are in log-scale. The black line represents the ice thickness of when the ice samples are collected, or the *in situ* temperature of the water samples. Data from: (Enberg et al., 2018)

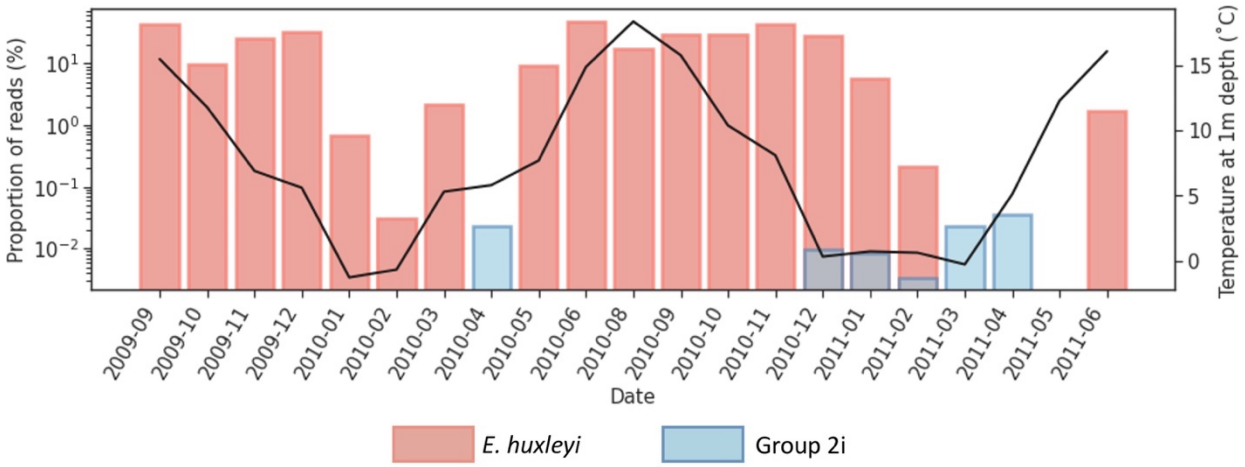

Figure 3. 6. Barplot of Group 2i and *E. huxleyi* relative abundance to total haptophytes based on proportional reads from ice and water samples collected during Sept. 2009-June 2011, note the y-axis is in log-scale, and the bars representing the two species are overlayed instead of stacked. The black line represents *in situ* water temperature at 1m depth when samples were collected. Data from: (Egge et al., 2015)

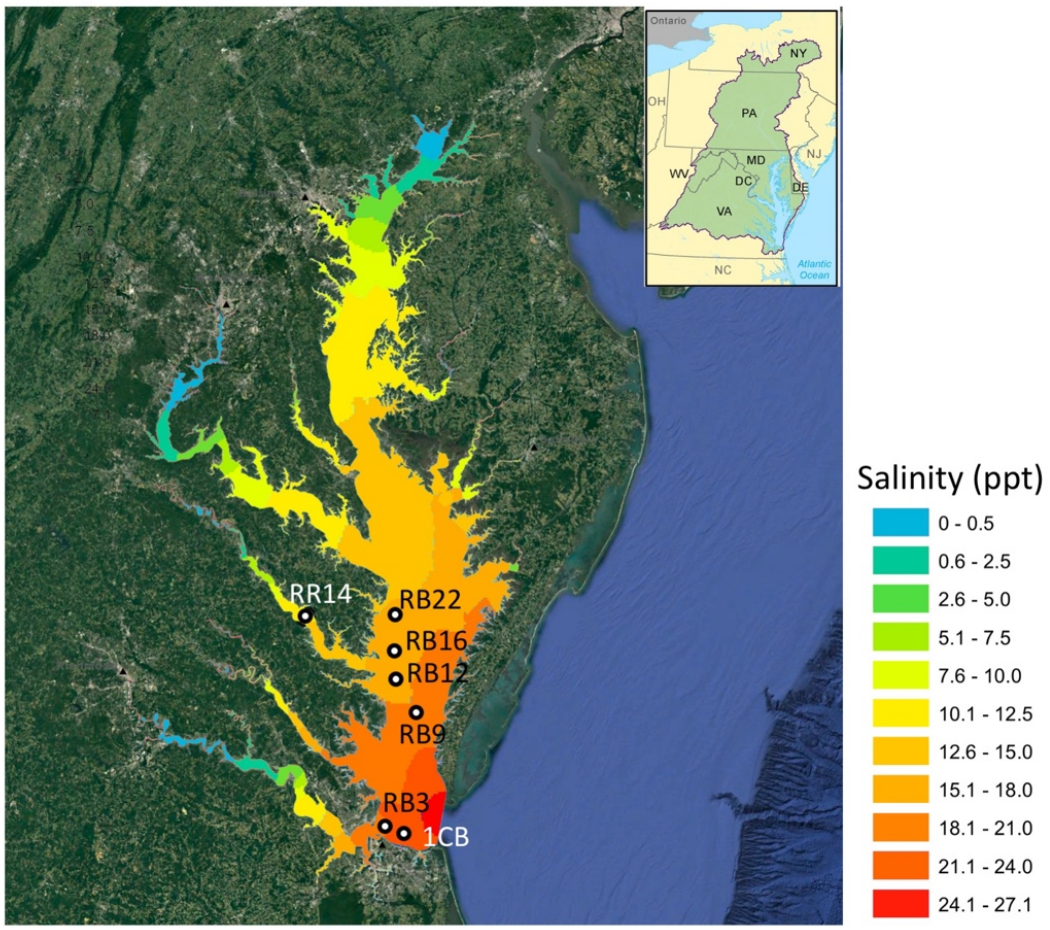

Figure 3. 7. Map of surface sediment samples examined in the Chesapeake Bay, the base map is 1985-2018 average surface salinity adapted from Wei 2019 (https://www.chesapeakebay.net/what/maps/chesapeake_bay_mean_surface_salinity_1985_2018).

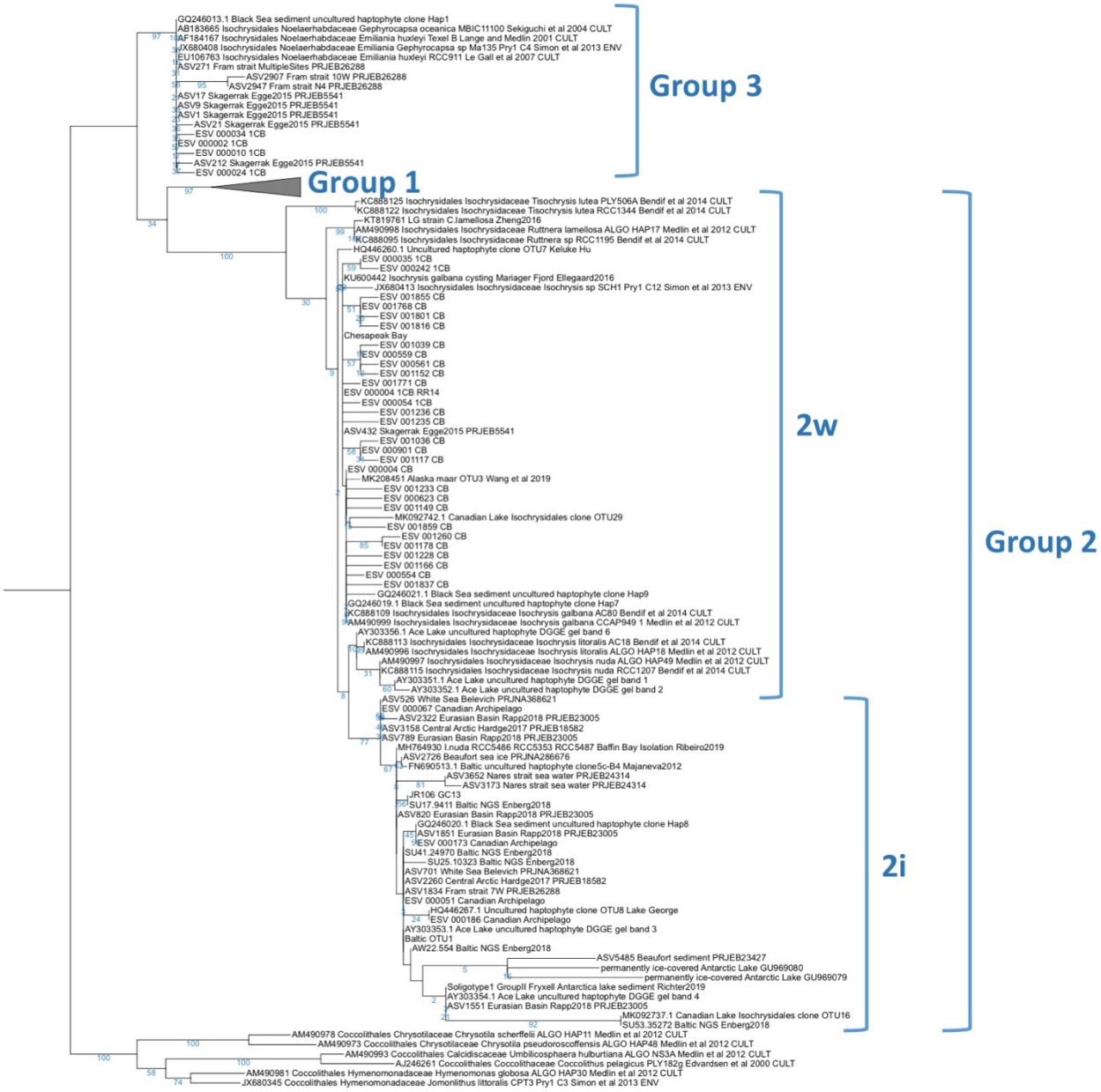

Figure 3. 8. Phylogenetic tree of Isochrysidales 18S rRNA.

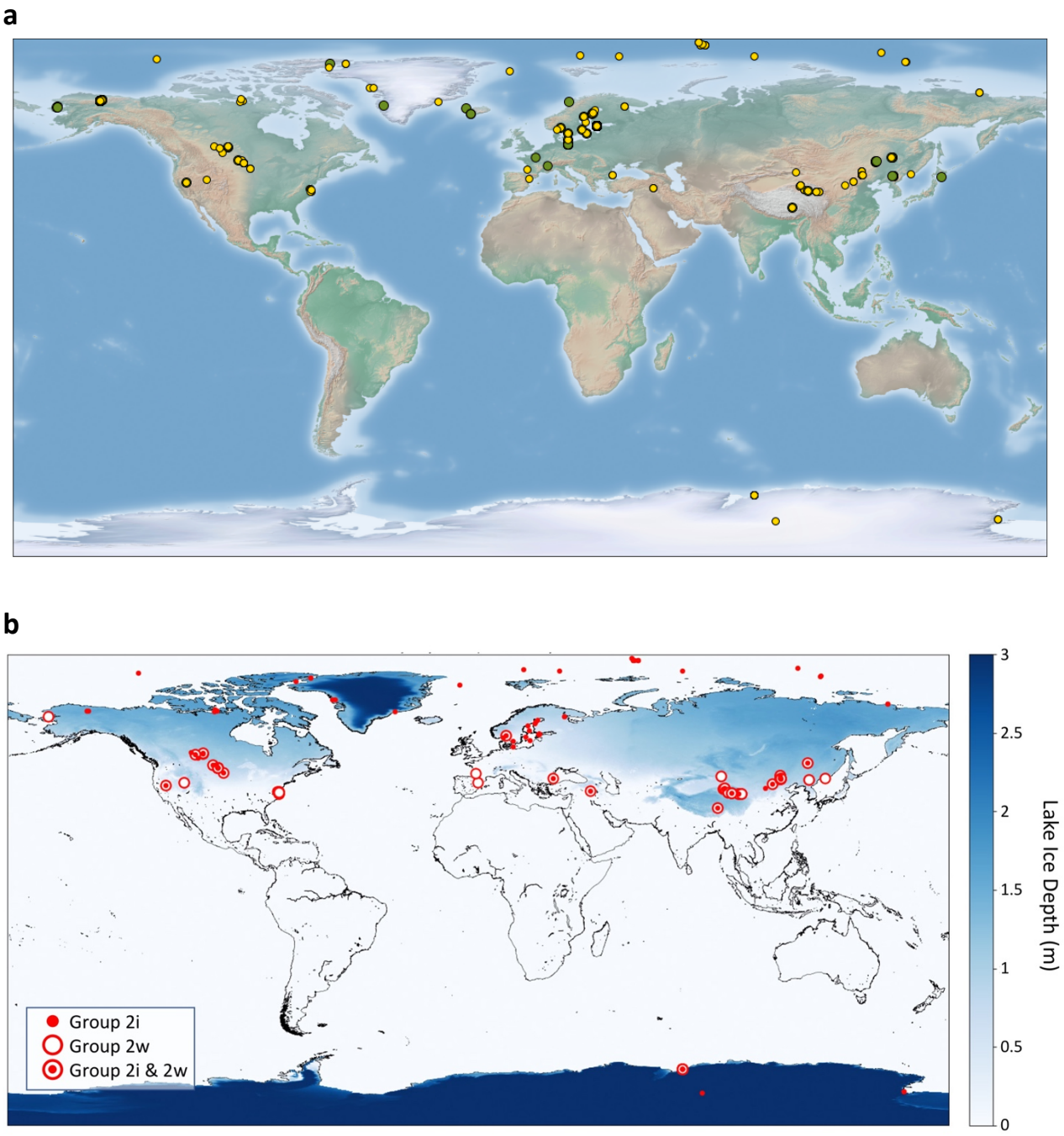

Figure 3. 9. a) Group 1 (green) and 2 (yellow) Isochrysidales detected in this study and other environmental DNA studies. Group 3 is ubiquitous in the global ocean. b) Group 2w and 2i Isochrysidales detected in this study and other environmental DNA studies, the basemap is averaged lake ice thickness in February during 2010-2020 modeled in ERA5-Land (https://www.ecmwf.int/en/era5-land).

Table 3. 1. Sediment samples examined in this study and the presence/absence of Isochrysidales (Y=yes, N=no)

Sample ID	Region	Lat.	Lon.	Salinity (psu)	# of Isochrysidales sequence reads	Sequencing method	Group 1	Group 2w	Group 2i	Group 3
1CB	Chesapeake Bay, USA	36.985	-76.166	24.3	4941	528Flong and PRYM01+7; NGS	N	Y	N	Y
RR14		37.774	-76.619	14.1	71		N	Y	N	N
RB3		37.011	-76.252		5360		N	Y	N	N
RB9		37.425	-76.109	22.8	15576		N	Y	N	N
RB12		37.549	-76.205		8626		N	Y	N	N
RB16		37.653	-76.209		45604		N	Y	N	N
RB22		37.783	-76.203		57931		N	Y	N	N
Skagerrak	Baltic Sea	58.429	9.477	34.5	2	Prym-429F and Prym-887R; Sanger	N	N	Y	N
Arkona Basin		54.852	13.433	7.6	13		Y	N	Y	N
Eastern Gotland Basin		57.083	19.985	6.9	13		Y	N	Y	N
Landsort Deep 1		57.267	19.796	6.9	9		Y	N	Y	N
Landsort Deep 2		58.641	18.265	6.8	10		Y	N	Y	N
Bothnian Sea 1		61.085	19.579	5.2	16		N	N	Y	N
Bothnian Sea 2		62.845	18.889	5	13		Y	N	Y	N
Bothnian Bay 1		63.833	21.583	3.1	50		Y	N	Y	N
Bothnian Bay 2		64.204	22.029	3	20		Y	N	Y	N
JR106 GC13	Kangerlussuaq Fjord	68.26	-31.89		336	528Flong and PRYM01+7; NGS	N	N	Y	N
POR13_05 5-6 cm	Upernavik Fjord	72.945	-55.62		45	HAP LSU F, LHapto20R bis; NGS	N	N	Y	N
POR13_05 45-46 cm		72.945	-55.62		221		N	N	Y	N
POR13_08 48-49 cm		72.869	-54.558		184		N	N	Y	N

Table 3. 2. Published environmental DNA study targeting haptophyte DNA

Region	Sample type	Sequencing method	Primers	Target region	Isochrysidales detected	Reference
Antarctica	Downcore sediment	Sanger	Prym-429F, Prym-887R (M. Coolen, 2004)	V4 18S rRNA	2 (including 2i)	(M. Coolen, 2004)
Greenland	Lake water column and surface sediment	Sanger	Prym-429F, Prym-887R (M. Coolen, 2004)	V4 18S rRNA	1 (GLD), 2w	(D'Andrea et al., 2006)
Black Sea	Downcore sediment	Sanger	Prym-429F, Prym-887R (M. Coolen, 2004)	V4 18S rRNA	2 (including 2i), 3	(M. J. L. Coolen et al., 2009)
Greenland	Lake surface sediment	Sanger	Prym-429F, Prym-887R (M. Coolen, 2004)	V4 18S rRNA	1 (GLD)	(Theroux et al., 2010)
USA	Lake surface sediment	Sanger	Prym-429F, Prym-887R (M. Coolen, 2004)	V4 18S rRNA	1 (GLD), 2 (including 2i)	(Theroux et al., 2010)
China	Lake surface sediment	Sanger	Prym-429F, Prym-887R (M. Coolen, 2004)	V4 18S rRNA	1, 2 (including 2i)	(Theroux et al., 2010)
France & Spain	Lake water and surface sediment	Sanger	Pry421F, Pry1572R (Simon et al., 2013)	V4 18S rRNA	1 (EV), 2 (non-2i)	(Simon et al., 2013)
Gulf of Naples, Italy	Seawater	NGS	LSU1 (Lhapto8, Lhapto20R_bis)	D1-D2 28S rRNA	3	(Bittner et al., 2013)
Lake Van, Turkey	Downcore sediment	Sanger	Prym-429F, Prym-887R (M. Coolen, 2004)	V4 18S rRNA	2 (including 2i)	(Randlett et al., 2014)
Skagerrak, Norway	Seawater	NGS	528Flong, PRYM01+7 (E. Egge et al., 2013)	V4 18S rRNA	1, 2 (including 2i), 3	(E. S. Egge et al., 2015)
Norway	Lake surface sediment	Sanger	Prym-429F, Prym-887R (M. Coolen, 2004)	V4 18S rRNA	1 (GLD)	(D'Andrea et al., 2016)
Pacific Ocean	Seawater	NGS	18S rRNA gene universal forward (D'Andrea et al., 2016), PRYM01+7 (E. Egge et al., 2013)	V4 18S rRNA	3	(Endo et al., 2018)
Japan	Lake surface sediment	Sanger	EukA(F) (Medlin et al., 1988), 887Deg(R)(Plancq et al., 2018)	18S rRNA	1 (not sure)	(Plancq et al., 2018)
Canada	Lake water and sediment isolated culture	Sanger	Hapto_4, Euk_34r (Liu et al., 2009); 18F, 18R (Yabuki et al., 2010)	D1-D2 28S rRNA; 18S rRNA	2 (non-2i)	(Araie et al., 2018)
China	Volcanic lake surface sediment	Sanger	Prym-429F, Prym-887R (M. Coolen, 2004)	V4 18S rRNA	1 (GLD), 2i, 2w	(Yao et al., 2019)
Baltic Sea	Marine surface sediment	Sanger	Prym-429F, Prym-887R (M. Coolen, 2004)	V4 18S rRNA	1 (GLD), 2i	(Kaiser et al., 2019)
Alaska, USA	Lake surface sediment	Sanger	Prym-429F, Prym-887R (M. Coolen, 2004)	V4 18S rRNA	1 (GLD), 2 (non-2i)	(Wang et al., 2019)

USA	Lake water column	NGS	1380F/1389F, 1510R	V9 18S rRNA	2 (including 2i)	(Theroux et al., 2019)
Canada	Lake surface sediment	NGS	528Flong, PRYM01+7 (E. Egge et al., 2013)	V4 18S rRNA	1 (GLD & EV), 2 (including 2i)	(Plancq et al., 2019)
Alaska, USA	Lake water column, surface sediment	NGS	528Flong, PRYM01+7 (E. Egge et al., 2013); HAP LSU F, LHapto20R bis 4/27/22 2:39:00 PM	V4 18S rRNA; 28S rRNA	1 (GLD & EV), 2i	(Richter et al., 2019)
Germany	Lake surface sediment	NGS	528Flong, PRYM01+7 (E. Egge et al., 2013); HAP LSU F, LHapto20R bis 4/27/22 2:39:00 PM	V4 18S rRNA; 28S rRNA	1 (GLD & EV)	(Richter et al., 2019)
Iceland	Downcore sediment	NGS	528Flong, PRYM01+7 (E. Egge et al., 2013); HAP LSU F, LHapto20R bis 4/27/22 2:39:00 PM	V4 18S rRNA; 28S rRNA	1 (GLD & EV)	(Richter et al., 2019)
Antarctica	Lake surface sediment	NGS	528Flong, PRYM01+7 (E. Egge et al., 2013); HAP LSU F, LHapto20R bis 4/27/22 2:39:00 PM	V4 18S rRNA; 28S rRNA	2i	(Richter et al., 2019)
Canadian Arctic Archipelago	Marine surface sediment	NGS	528Flong, PRYM01+7 (E. Egge et al., 2013)	V4 18S rRNA	2i	(Wang et al., 2021)
China	Lake surface sediment	Sanger	Prym-429F, Prym-887R (M. Coolen, 2004)	V4 18S rRNA	2, 2i	(Yao et al., 2022)
Chesapeake Bay, USA	Estuary surface sediment	NGS	528Flong, PRYM01+7 (E. Egge et al., 2013)	V4 18S rRNA	2, 3	This paper

Table 3. 3. Alkenone indices in Chesapeake Bay surface sediment

Sample name	U^{K}_{37}	U^{K}_{37}'	$\%C_{37:4}$	$C_{37}Me/C_{38}Et$
1CB	0.262	0.321	4.45	0.666
RB3	0.352	0.400	3.44	0.829
RB9	0.323	0.353	2.20	0.751
RB12	0.221	0.240	1.47	0.558
RB16	0.233	0.245	0.98	0.671

Chapter 4: Group I alkenones and Isochrysidales in the world's largest maar lakes and their potential paleoclimate applications

Karen J.Wang[1,*], Jonathan A.O'Donnell[2], William M.Longo[3], LindaAmaral-Zettler[1,4,5],Gaoyuan Li[6],YuanYao[1,7],YongsongHuang[1,7,*]

[1]Department of Earth, Environmental and Planetary Sciences, Brown University, Providence, RI 02912, USA

[2]Arctic Network, National Park Service, Anchorage, AK, USA

[3]Department of Marine Chemistry and Geochemistry, Woods Hole Oceanographic Institution, Woods Hole, MA 02543, USA

[4]Department of Marine Microbiology and Biogeochemistry, NIOZ Royal Netherlands Institute for Sea Research and Utrecht University, the Netherlands

[5]Department of Freshwater and Marine Ecology, Institute for Biodiversity and Ecosystem

[6]Dynamics, University of Amsterdam, the Netherlands

State Key Laboratory of Biogeology and Environmental Geology, China University of Geosciences, Beijing 100083, China

[7]State Key Laboratory of Loess and Quaternary Geology, Institute of Earth Environment, Chinese Academy of Sciences, Xi'an 710061, China

This Chapter has been published in: *Nature Communications*

Citation: Wang, K. J., O'Donnell, J. A., Longo, W. M., Amaral-Zettler, L., Li, G., Yao, Y., & Huang, Y. (2019). Group I alkenones and Isochrysidales in the world's largest maar lakes and their potential paleoclimate applications. *Organic Geochemistry, 138*, 103924.

Abstract

The Espenberg maar lakes on the Seward Peninsula, Alaska, are the largest volcanic crater lakes in the world and contain the longest known lacustrine sedimentary archives in Alaska. The lack of glacial-aged marine sedimentary archives around the Bering Land Bridge due to exposure of the shelf during sea level low-stands makes these lakes highly valuable for understanding the region's past climate and environmental changes. Located en route to humanity's last colonized American continents, the Seward Peninsula's climate and environments during the last glacial period bear major anthropological significance. However, a lack of quantitative proxies has so far hampered exploration of these lakes for paleoclimate reconstructions. Here we report, for the first time, the discovery of abundant Group I alkenones and Isochrysidales in surface sediments from three maar lakes: White Fish, North Killeak and Devil Mountain, using a combination of lipid biomarker and 18S rRNA gene sequencing analyses. Our discovery adds to the expanding list of oligotrophic freshwater lakes where Group I alkenones are found, and water chemistry data contribute to the understanding of the environmental controls on Group I Isochrysidales. Our results further confirm the use of the U_{37}^{K} index of Group I alkenones as a proxy for the mean temperature of the spring isotherm (MTSI) and RIK_{37} as a quantitative measurement for Isochrysidales group mixing. We also demonstrate the analytical challenges for analyzing alkenones in freshwater lakes and the effectiveness of eliminating coelution using silver thiolate chromatographic material (AgTCM).

1. Introduction

East Beringia is important for climatology, ecology, and anthropology (Chapin et al., 2014; Hugelius et al., 2014; Vachula et al., 2019). The regional temperature has been rising twice as fast as the global average over the last 50 years (Chapin et al., 2014), and is ecologically and climatically important with its vast tundra ecosystems underlain by carbon-rich permafrost soils (Hugelius et al., 2014). The large carbon reservoir stored in tundra soils has the potential to exert major feedback to the climate system upon thawing and subsequent carbon release to the atmosphere if the temperature continues to rise rapidly (Schuur et al., 2015). Research in this region is also critical for understanding the final voyage of modern humans from East Asia to the Americas during the last glacial period. The model and timing of human migration to Alaska are widely debated: with one hypothesis suggesting a "swift peopling" at ca. 14,000 years ago prior to the submergence of the Bering Land Bridge by the rising sea level (Gilbert et al., 2008; Goebel et al., 2008), and the other so-called "Beringian Standstill Hypothesis (BSH)" proposing a much earlier migration during the last glacial period. The BSH theorizes, based on population genetics, that Native American ancestors once inhabited east Beringia for over 10,000 years around or prior to the Last Glacial Maximum (LGM, ~21,000 years ago), before rapidly colonizing the Americas as the Laurentide Ice Sheet (LIS) retreated during the deglaciation (Tamm et al., 2007; Hoffecker et al., 2016; Moreno-Mayar et al., 2018). A recent study on fecal biomarkers and biomass burning from Northern Alaska supports the BSH, and provides new evidence of human settlement in the region at ~ 32,000 years ago (Vachula et al., 2019). Modeling studies suggest regional temperatures could have been particularly warm in comparison to other Arctic regions during the LGM, due to the potentially high elevation and topography of the LIS blocking and deflecting warm air of subtropical origin to northern Alaska

(Brady et al., 2013; Bartlein et al., 2011). As a result, ancient east Beringians living in Alaska would have benefitted from conditions that were substantially warmer than on the Siberian side of Beringia (i.e., west Beringia).

The important scientific problems detailed above cannot be addressed until long quantitative temperature reconstructions are obtained from east Beringia. Unfortunately, interpretations of the common measurable oceanographic proxies in this region are complicated by the great stratigraphic variability due to marine transgressions and influences of different water masses and freshwater input on the foraminifera isotopic composition (Knebel et al., 1974; Miller et al., 2010). Thus, lakes that hold long terrestrial sedimentary records extending to last glacial maximum and beyond are highly valuable for paleoclimate reconstructions. Espenberg maar lakes on the Seward Peninsula, Alaska, are of particular significance in this regard, as they were formed by phreatomagmatic eruptions between 7,100 yr to up to 200,000 years ago and are the world's largest crater lake complexes (Hopkins, 1988; Begét et al., 1996). Traditional paleolimnological proxies applied in lakes encounter major challenges and complications in this region: e.g., the non-analog pollen assemblages during the LGM (Bartlein et al., 2011), and chironomid assemblages potentially affected by water depth and other lake specific effects related to re-deposition and transport processes (Kurek and Cwynar, 2009). Therefore, discovering a new proxy for reconstructing past temperatures from the Espenberg maar lakes bears major paleoclimatic, paleoceanographic and anthropological significance.

We report here an initial study of lake surface sediments from three Espenberg maar lakes (White Fish, North Killeak, and Devil Mountain) and the discovery of Group I alkenones and their producers, Group I Isochrysidales, using combined organic geochemical and environmental DNA-based phylogenetic approaches. The Group I alkenones were first discovered in

southwestern Greenland (D'Andrea and Huang, 2005; D'Andrea et al., 2006). Subsequent systematic comparison of 18S rRNA gene sequences has grouped Isochrysidales, an order of haptophyte algae known to produce alkenones, into three different groups, with freshwater species being Group I, open ocean species (*Emiliania huxleyi* and *Gephyrocapsa oceanica*) as Group III, and other coastal or saline lake species (e.g., *Ruttnera lamellosa*, *Isochrysis galbana*, *Tisochrysis lutea*) as Group II (Theroux et al., 2010). Alkenones produced by Group I Isochrysidales bear distinct molecular distributions with a high abundance of $C_{37:4}$ alkenone and the presence of a set of $C_{37:3}$ double bond positional isomers, which are readily resolved using a mid-polarity gas chromatography column (Longo et al., 2013; Zheng et al., 2017). Water column particulates and survey of surface sediments from lakes in the Northern Hemisphere have yielded water temperature calibration (D'Andrea et al., 2011; Longo et al., 2016), as well as air temperature calibrations (Longo et al., 2018). Particularly, Group I Isochrysidales bloom in early spring (D'Andrea et al., 2011; Longo et al., 2016), and have been shown to record cold season air temperatures for Group I alkenones(Longo et al., 2018), which is in contrast to the majority of geochemical proxies which record warm growth season temperatures. We compared our data with previous U_{37}^{K} temperature calibrations and discussed the potential applications of alkenones in Espenberg maar lakes for paleoclimate reconstructions.

2. Material and Methods

2.1. Regional settings

The studied lakes are situated in the Devil Mountain-Cape Espenberg volcanic field, which is a segment of the northern coastal plain of the Seward Peninsula, Alaska, in the National Park Service's (NPS) Bering Land Bridge National Preserve. The maar lakes are the largest

volcanic crater lakes in the world and formed by phreatomagmatic eruptions when rising basaltic magma encounter groundwater in Cenozoic sediments beneath hundreds meters of ice-rich permafrost (Begét et al. 1996). The three maar lakes, Devil Mountain Lake, North Killeak Lake and White Fish Lake (Fig. 4. 1), where we collected surface sediments, were formed during different eruptions. The estimated age based on tephra deposition is 7,100 years for the Devil Mountain Lake, > 125,000 years for North Killeak Lake and 100,000 to 200,000 years for White Fish Lake (Hopkins, 1988; Begét et al., 1996).

The surface areas of White Fish Lake (7.68 km^2) and North Killeak Lake (9.17 km^2) are similar in size, while Devil Mountain Lake, the biggest maar lake on Earth, has a surface area of 21.23 km^2. White Fish Lake has a maximum depth of around 6 m and contains organic-rich, diatomaceous sediment, North Killeak Lake is about 25 m deep, and Devil Mountain Lake is more than 100 m deep with more complexed bathymetry surrounded by pyroclastic rocks (Begét et al., 1996).

2.2. Climate data

We retrieved climate data following the procedures described by Longo et al. (2018). Data were downloaded from the WorldClim Global Climate Database (worldclim.org; Hijmans et al., 2005) using the Senckenberg data extraction tool (dataportal-senckenberg.de/dataExtractTool). WorldClim 1.4 data were derived from monthly air temperature and precipitation data compiled from globally distributed weather stations by the Global Historical Climatology Network, the World Meteorological Organization, the Food and Agriculture Organization of the United Nations, and others (Hijmans et al., 2005). The high-resolution interpolated climate products for current condition are only available for year 1950-

2000. We therefore used these temperatures for our calibration study. Mean monthly temperatures (1950-2000) of the sites from Worldclim climatology data are shown in Figure 4.S.1.

Mean annual air temperature (MAAT), mean temperature of the warmest quarter (MTWQ) and mean temperature of the spring isothermal season (MTSI) were calculated in temperature regression of the samples from this study and its comparison between the compilation of Northern Hemisphere dataset from Longo et al. (2018). Since the sedimentation rates of the lakes in this study are unknown, the surface sediments are assumed to represent the average temperature in the past few decades, monthly mean from 1950 to 2000 climate data were used in calculations and regressions.

2.3. Sample collection

The study lakes are remote and pristine with no road access, and sample collection was carried out with aviation support from the Arctic Inventory and Monitoring Network (ARCN) program of the National Park Service. Samples and measurements were taken from Cessna 185F floatplane landing directly onto the sampling lakes in September 2017. After water depth measurement, surface sediments were collected using an Ekman dredge, wherein approximately 100 g of sediment was separated from the top ~5 to 10 cm of each sediment grab using sterile scoops and transferred into whirl-pak sampling bags for later DNA analysis. One surface sediment sample from Toolik Lake (68°38'N, 149°36'W), Northern Alaska, collected previously (Longo et al., 2016) and kept frozen at -20 °C, was also studied for comparison with the maar lakes. Water column and surface sediment samples from Toolik Lake have previously been found to contain Group I alkenones and Isochrysidales (Richter et al., 2019). The specific

sampling locations for the three lakes are: White Fish (66°22'N, 164°45'W; water depth = 2.2 m), North Killeak (66°21'N, 164°20'W; water depth = ~3 m) and Devil Mountain (66°24'N, 164°29'W; water depth = ~6 m). One surface sediment sample was taken from each lake for alkenones and phylogenetic analyses, with the assumption that these samples were representative of the alkenone profiles and genetic diversity of the individual lakes. Samples were frozen until DNA extraction.

Lake surface water samples were collected for chemical analyses as part of the National Park Service's ARCN lake monitoring program (O'Donnell et al. 2015). Chemistry data are reported in Table 4. S. 2, and represent the average (± one standard deviation) of two to three sampling dates (6/22/2013, 7/15/2015, and 9/15/2017). Water samples were collected at 0.5 m below the lake surface in the pelagic zone using a 0.45 μm high-capacity capsule filter connected to a Geopump Series II Peristaltic Pump (Geotech Environmental Equipment, Inc., Denver, CO). DOC concentrations were determined using an O.I. Analytical Model 700 TOC analyzer via the platinum catalyzed persulfate wet oxidation method (Aiken 1992). UV-visible absorbance was measured on filtered stream samples at room temperature using a quartz cell with a path length of 1 cm on an Agilent Model 8453 photodiode array spectrophotometer. Specific UV absorbance at 254 nm ($SUVA_{254}$) was determined for all stream samples by dividing the decadal UV-visible absorbance coefficient at $\lambda = 254$ nm by DOC concentration. $SUVA_{254}$ (L mgC^{-1} m^{-1}), which is typically used as an index of DOC aromaticity, provides an average absorptivity at $\lambda = 254$ nm of the dissolved organic matter (DOM; Weishaar et al., 2003). To determine DIC concentrations, stream water samples were collected without head space in a 60 mL syringe. Immediately prior to analysis, water samples were filtered using 0.45 μm nylon syringe filters into 40 mL borosilicate vials clean vials and capped by septum caps to minimize interaction with the

atmosphere. DIC concentrations were determined by acidifying with phosphoric acid and measuring on a Shimadzu TOC-VCSH Combustion Analyzer. Base cation concentrations (Ca^{2+}, Mg^{2+}, Na^{+}, K^{+}) were determined on a Shimadzu AA-7000 atomic absorption spectrophotometer, and major anions (Cl^{-}, SO_4^{2-}) were determined on a Dionex 1500 Ion Chromatograph. Alkalinity was determined via titration using a ManTech PC-Titrate Auto Titrator system. Total dissolved nitrogen was determined by persulfate digestion on a Technicon Auto-Analyzer II. pH was measured in situ using a YSI multi-parameter probe.

2.4. Alkenone analysis

Surface sediment samples were freeze-dried. Around 10 g of freeze-dried sediment were extracted by Dionex^{TM} accelerated solvent extraction (ASE) system with dichloromethane (DCM):methanol mixture (9:1 v/v). The total lipid extract was separated into alkane, ketone and polar fractions by silica gel columns based on different polarity using the following eluents: hexane, DCM, methanol. The ketone fractions that contains the alkenones and esters were saponified in 1M KOH in methanol:H_2O (95:5) solution and heated at 65 °C for 3 hours. The resulting products were acidified to pH<2 by adding drops of 3M HCl, followed by hexane extraction, and purified by silica gel columns. The alkenones were further purified using silver thiolate silica gel columns (AgTCM; Aponte et al., 2013) before analysis by gas chromatography-flame ionization detection (GC-FID) using mid-polarity GC columns VF-200 ms (Zheng et al., 2017).

2.5. DNA extraction and analysis

Genomic DNA was extracted from ~500 mg surface sediments and purified using FastDNA™ SPIN Kit for Soil (MP Biomedicals, OH, USA) and DNeasy PowerClean Pro Cleanup Kit (Qiagen, Carlsbad, CA, USA) according to the manufacturer's instructions. The V4 18S rRNA coding region was amplified using Prym-429F and Prym-887R (Coolen et al., 2004), and modified PCR conditions optimized for this sample set: denaturing 4 min at 96 °C, followed by 35 cycles including denaturing (30 s at 94 °C), 40 s of primer annealing at 61.5 °C, and primer extension (40 s at 72 °C). A final extension was performed at 72 °C (10 min). Each sample was run at three different dilutions (1:10, 1:100, 1:1000) to achieve maximum product yield, with a positive control, a negative control and an extraction blank included in each run. The PCR products were examined by gel electrophoresis and purified with the AxyPrep DNA Gel Extraction Kit (Axygen, USA). Cloning using the pGM-T Cloning Kit (Tiangen Biotech, Beijing, China) and Sanger sequencing on an ABI 3730XL capillary sequencer (Applied Biosystems, Foster City, CA) were performed by Shanghai Majorbio Bio-Pharm Technology Co., Ltd., China (www.majorbio.com). Only sequences longer than 400 bp with complete forward and reverse primer intact were retained. Sequences are deposited in GenBank under accession numbers MK208448- MK208452.

The raw capillary sequence data yielded 146 Haptophyte sequences after Chimera checking with ChimeraSlayer (Haas et al., 2011). Operational Taxonomic Units (OTUs) were clustered using UCLUST with a 97% cut-off criterion (Edgar et al., 2010). Representative sequences were picked for each OTU in QIIME/1.9.1 (Caporaso et al., 2010). Closest relatives of the OTUs were identified through BlAST queries against NCBI GenBank database. Representative sequences were then aligned against a curated alignment from Gran-Stadniczeñko et al. (2017) using PyNast (Caporaso et al., 2009). The alignment and selected outgroup

Prymnesium faveolatum (ALGO HAP79) were used to infer a phylogeny using the Randomized Axelerated Maximum (RAxML) program (Huelsenbeck and Crandall,1997; Stamatakis, 2014). Rapid bootstrapping with 1000 bootstrap replicates and an ML search under the GAMMA model of rate heterogeneity were conducted.

3. Results

3.1. Phylogenetic analysis

116 Isochrysidales sequences were recovered from the clone libraries and analyzed in total, including 26 from White Fish Lake, 9 from Devil Mountain Lake, 60 from North Killeak Lake, and 21 from Toolik Lake. The sequences were clustered into 5 OTUs, namely Alaska OTU 0-4, among which Alaska OTU0 contains all the sequences from White Fish Lake, Devil Mountain Lake, Toolik Lake and the majority of sequences from North Killeak Lake. The other 4 OTUs only include sequences from North Killeak Lake, and included 1-3 Isochrysidales sequences recovered in each OTU (Table 4. 1).

The phylogenetic tree shows that Isochrysidales sequences are clustered into three groups, with Groups I and III Isochrysidales forming a sister clade to Group II Isochrysidales (Fig. 4. 2), in consistency with the new phylogenic analyses showing common ancestry of Group I and III Isochrysidales (Richter et al, 2019). Alaska OTU 0, 1, 2, 4 were all identified as Group I Isochrysidales, with branch lengths relatively long compared to the branch lengths within Group II and Group III Isochrysidales. OTU 0 showed robust branching with the uncultured haptophyte from BrayaSo, Greenland (HQ446254) (Fig. 4. 2). Alaska OTU 3 fell into Group II and is closely related to *Isochrysis galbana*. The occurrence of Group II is very uncommon in the low salinity (1.1 psu) environment of North Killeak.

3.2. Alkenone profiles and proxy indices

Alkenones were found in the surface sediments of all three lakes. Saponification and AgTCM columns were processed sequentially in order to separate the co-eluting compounds. Saponification successfully removed the co-eluting wax esters. AgTCM columns were applied to further remove other non-ester compounds that were co-eluting mainly with $C_{37:2Me}$, $C_{38:3aEt}$, $C_{38:4Me}$. This method can efficiently separate all alkenones from co-eluting impurities such as steryl ethers and various saturated ketones with variable carbonyl positions (Fig. 4. S. 2; Wang et al., 2019). The final alkenone profiles after cleaning steps demonstrate clear Group I-type distributions including dominant $C_{37:4}$, $C_{37:3}$ isomers, and the presence of C_{38Me} alkenones (Fig. 4. 3). The results suggest it is important to remove coeluting compounds from alkenones using AgTCM (or other approaches) columns for accurate alkenones analysis.

The alkenone peaks are well resolved for accurate quantification after the saponification and AgTCM columns. Alkenone concentrations and U_{37}^{K} , $U_{37}^{K\prime}$, %$C_{37:4}$, RIK_{37} values are shown in Table 4. S. 1, as well as the MAAT, MTWQ, and MTSI of the three lakes. Calibrations between U_{37}^{K} and temperatures are calculated with data from this study and data from lakes distributed throughout the mid- and high- latitude of the Northern Hemisphere compiled by Longo et al. (2018). U_{37}^{K} yield a positive correlation with MAAT, MTWQ, and MTSI (Fig. 4. 4). Though the correlations between U_{37}^{K} and MAAT (U_{37}^{K}=0.007×T-0.4746, R^2=0.25, p=9.9e-3), MTWQ (U_{37}^{K}=0.0011×T-0.6206, R^2=0.31, p=3.4e-3) are weak, they showed significant correlation between U_{37}^{K} and MTSI (U_{37}^{K}=0.031×T-0.4858, R^2=0.5

4. Discussion

4.1. Water chemistry and the occurrence of Group I Isochrysidales

Freshwater or oligohaline conditions with relatively high pH and alkalinity have been proposed to be the key environmental factors that allow Group I Isochrysidales to thrive (Longo et al., 2016). However, not all fresh/oligohaline lakes with elevated pH host Group I Isochrysidales. Despite previous investigations including water chemistry of lakes hosting Group I Isochrysidales (.g., Longo et al., 2018; Plancq et al., 2018a), the environmental controls are not fully known. Fortunately, the ARCN program has water chemistry monitoring data for our studied lakes, providing another opportunity to explore this topic (Table 4. S. 2).

The maar lakes in this study are characterized by an elevated pH of 8.3 to 8.4, with values comparable to shallow lakes where the drainage basins are underlain by volcanic deposits in the region (Larsen et al., 2017), but are higher than those reported in freshwater lakes north of the Brooks Range, Alaska, which also contain Group I Isochrysidales and corresponding alkenones (pH 6.2 to 8.5; Longo et al., 2016). Alkalinity of the maar lakes is comparable to the northern Alaskan lakes (Table 4. S. 2; Longo et al., 2016) but significantly higher than those reported from other non-maar lakes in the Toolik region of Alaska (~0 $mgCaCO_3/L$; Luecke et al., 2014) and Russia (0-0.05 $mgCaCO_3/L$; Drake et al., 2019). The dominant cations are Na^+, Mg^{2+}, and Ca^{2+} (Table 4. S. 2). These characteristics indicate the relatively fast rate of weathering from tephra and basalt containing a high abundance of mafic minerals such as olivine, pyroxene, and plagioclase (Pecoraino et al., 2015):

CO_2+ H_2O+ sodium-rich tephra & volcanic glass + basalt (plagioclase $NaAlSi_3O_8$ + $CaAl_2Si_2O_8$; olivine $(Mg, Fe)_2SiO_4$; pyroxene $XY(Si,Al)_2O_6$)➔ clay minerals + Ca^{2+}+ Mg^{2+}+Na^++HCO_3^-

Ca^{2+} and Mg^{2+} concentrations in the maar lakes are similar to streams and rivers draining in the nearby terrain (O'Donnell et al., 2015, 2016), suggesting weathering reactions primarily take place in the surrounding soils that overlay tephra, volcanic glass, and basalt. High-purity igneous rocks are composed of silicate minerals almost devoid of anionic components such as Cl^-. Thus the high Cl^- and associated Na^+ indicate that the nearby Bering Sea exerts a strong marine influence on lake chemistry of the Seward Peninsula during the open-water period (June to September, Larsen et al., 2017), as evidenced by the relatively higher concentrations of Na^+ and Cl^- in White Fish Lake and North Killeak Lake in comparison to Devil Mountain Lake which is farther away from the coastline.

Environmental sulfur has been suggested as an essential element for all photosynthetic algae (Takahashi et al., 2011; Giordano and Prioretti, 2015; Plancq et al., 2018a), and Group I Isochrysidales have been detected in Canadian Prairies lakes with elevated sulfate content (93.43-1878.64 mg/L; Plancq et al., 2018a). However, in contrast to the Canadian Prairies lakes (Plancq et al., 2018a) and similar to the northern Alaskan lakes (Longo et al., 2016), the three maar lakes in this study all have very low sulfate concentrations, extending the lower limit of sulfate concentrations observed for Group I Isochrysidales. Some interesting spatial differences in carbon and nutrient concentration across maar lake basins have been observed. At North Killeak and Devil Mountain Lakes, dissolved inorganic nitrogen species (nitrate, ammonium) were below the detection limit, and phosphate concentrations were very low. Organic nutrient species (as reflected by total N and P, and total dissolved N and P) concentrations were also low

at North Killeak and Devil Mountain Lakes. These highly oligotrophic conditions are common in lakes of Arctic Alaska (Larsen et al., 2017; Luecke et al., 2014). However, concentrations of organic and inorganic N and P species were substantially higher at White Fish compared to the other maar lakes in this study. Further, DOC concentration and $SUVA_{254}$, which serves as an index of DOM aromaticity (Weishaar et al., 2003), are highest in White Fish Lake compared with other large lakes (N=20) surveyed in three Arctic parks as part of the NPS ARCN lake monitoring program (O'Donnell et al., 2015). Terrestrial DOM may serve as an important source of nutrients to phytoplankton in White Fish Lake, driving high rates of primary productivity in the lake. Alternately, high concentrations of DOC may originate from the decomposition of particulate carbon or algae exudate in the water column. Repeated cyanobacteria blooms were observed in White Fish Lake during a July 2018 site visit, and the organic-rich sediments collected by Ekman dredge indicate that White Fish Lake is mesotrophic.

In sum, the elevated pH, alkalinity, and low salinity of the Espenberg maar lakes are similar to the lakes hosting Group I Isochrysidales in Greenland (D'andrea et al., 2006; Theroux et al., 2010), Northern Alaska (Longo et al., 2016), Canadian Prairies (Plancq et al., 2018a), and Northeastern China (Yao et al., personal communication). However, the occurrence of Group I Isochrysidales in the mesotrophic White Fish Lake expanded our previous understanding of the environmental preference of Group I Isochrysidales which have mostly been found in oligotrophic lakes.

4.2. Genetic variation within Group I and II Isochrysidales

Longo et al. (2016) found freshwater lakes from northern Alaska featured distinct distributions of Group I alkenones. Their analysis of suspended particulate matter (SPM) from

Toolik Lake yielded the first in situ freshwater U_{37}^{K} calibration. Previous studies have examined the alkenone producers in Toolik lakes using primers targeting the eukaryotic V9 hypervariable region of the small-subunit (SSU) rRNA gene and haptophyte V4 SSU rRNA gene from water samples, showing that the alkenone producers in Toolik Lake during the sampling season belong to Group I Isochrysidales (Crump et al., 2012; Richter et al., 2019). In this study, we extracted DNA from surface sediments and applied preexisting haptophyte-specific V4 SSU rRNA gene primers (Coolen et al., 2004). The molecular data confirmed the common presence of Group I Isochrysidales DNA in sediments and showed that the alkenone producers in Espenberg maars and Toolik Lake are highly similar.

The most abundant Isochrysidales OTU in this study is Alaska OTU 0 that included all the sequences recovered from White Fish, Devil Mountain, and Toolik Lakes, and the majority of the sequence recovered from North Killeak Lake. Alaska OTU 0 is closely related to the uncultured haptophyte (HQ446254) from BrayaSo, West Greenland. OTU 1, 2, and 4 are branching among other Group I sequences from Greenland and Canadian Prairies. Those sequences grouped with Greenland phylotypes separate from a clade that consists of sequences recovered from Lakes Etang des Valles, France (EV phylotypes). Due to primer mismatches, the primer pair we used in this study cannot detect EV phylotypes (Richter et al., 2019). Therefore, it is possible that we did not recover the full Group I Isochrysidales genetic diversity present in these maar lakes. However, since the EV phylotypes are of low abundance in Toolik lake based on high-throughput sequencing data (Richter et al., 2019), and the most abundant OTU in this study branches with a Greenland phylotype with strong support, it is possible that alkenones in Toolik Lake, Alaska maar lakes and BrayaSo have similar temperature sensitivities.

There are still some lingering questions regarding the genetic diversity observed in the current data. North Killeak Lake contains all the OTUs recovered in this study, while the other lakes only contain OTU 0. Notably, Alaska OTU 3 is closely related to uncultured *Isochrysis* sp. Hap7 and Hap9 from the Black Sea during early sapropel deposition around 7140-6090 BP and 5950 BP (Coolen et al., 2009), and *Isochrysis galbana* whose optimal salinity range is around 15 ppt (strain Iso, Brand 1984). Though the salinity of North Killeak Lake is significantly lower than this range (Table 4. S. 2), it is the most saline lake among the three maar lakes, which may explain why North Killeak exhibits the highest alkenone producers diversity among the three maar lakes. Group II alkenones has been detected in a brackish lake (3.3 ppt) in Northern Alaska near the coast (Longo et al., 2016) showing that proximity to the ocean might be a source of higher salinity and Group II Isochrysidales in the lake.

4.3. Air temperature calibrations

U_{37}^{K} temperature calibrations in freshwater lacustrine environments with Group I Isochrysidales have shown the strongest correlation with the MTSI (Longo et al., 2018). The regressions between U_{37}^{K} and different temperatures shown in Fig. 4. 4 suggest this index is most correlated with MTSI. This is in agreement with previous studies of water-column filtrates from Lake George (Toney et al., 2010) and sediment trap experiment from two dimictic freshwater lakes in northern Alaska (Longo et al., 2018), which shows that alkenones are produced in the water column in early spring, shortly after ice off. The regression of U_{37}^{K} with MTSI in this study produces a slope that is within the range of slopes in previous Group I calibrations (0.021-0.030; Zink et al., 2001; D'Andrea et al., 2011, 2016; Longo et al., 2016; Longo et al., 2018). Thus, using U_{37}^{K}-MTSI instead of U_{37}^{K}-MAAT may circumvent seasonal bias and provide a season-

specific temperature reconstruction, and this compilation of North Hemisphere freshwater U_{37}^{K}-temperature calibrations would provide a good reference for paleotemperature reconstruction in freshwater systems.

The slight differences of U_{37}^{K} values in our three studied lakes might be explained by the following reasons: (1) the alkenone is extracted from a mixture of a few centimeters of sediment from the Ekman dredge, and the sedimentation rate is probably very different in the three lakes thus representing different extents of accumulation; (2) the surface area, bathymetry, and water volume of the lakes are different, which could drive spatial differences in the lake thermal regime resulting in different water temperature during the spring transition season.

4.4. Group I alkenones characteristics and RIK_{37} values

All three maar lakes investigated have shown a $C_{37:4}$ dominant (>40%) feature (White Fish: 42.5%, Devil Mountain: 48.4%, North Killeak: 60.7%) which coincide with the Group I alkenones detected in freshwater systems in Greenland (D'andrea et al., 2006; Theroux et al., 2010), Alaska (Longo et al., 2016), Canada (Plancq et al., 2018a), and Japan (Plancq et al., 2018b).

The alkenone profiles in the maar lakes also showed significant $C_{37:3b}$ concentration. In contrast to the complicated $\%C_{37:4}$ value which can't be used alone to determine either alkenone producers or salinity, the RIK_{37} value showed more potential in identifying the alkenone producers. This index is first defined by Longo et al. (2016) as the ratio of isomeric ketones, $RIK_{37}=C_{37:3a}/(C_{37:3a}+C_{37:3b})$. Group I have a RIK_{37} value of 0.44-0.60 (Plancq et al., 2018a; Longo et al., 2016), while Group II and III have RIK_{37} value of 1, mixed source alkenones would have a RIK_{37} value between 0.60-1.0. The Espenberg maar lakes all showed RIK_{37} values within

the range of pure Group I alkenones (Table 4. S. 1). The RIK_{37} is not able to detect Group II mixing in North Killeak. However, the number of Group II sequences recovered from the North Killeak is much lower than Group I sequences (only 3.3% of the total sequences) and this ratio might partly reflect the actual biomass, and it is possible that the Group II Isochrysidales only have minor contributions to the alkenones in this lake.

5. Conclusions

Our discovery of abundant Group I alkenones in three maar lakes on the Seward Peninsula, Alaska provides exciting new opportunities for quantitative paleotemperature reconstructions for this climatically, ecologically and anthropologically important region. Our findings highlight the presence of alkenones with clear Group I signatures in the maar lakes, together with their producers clustered into the same OTU with the sequences from Toolik Lake which are closely related to other Group I Isochrysidales discovered in BrayaSo, Greenland. The findings suggest that maar lakes with elevated pH and alkalinity are habitable for Group I Isochrysidales and U_{37}^{K} in these lakes are potentially powerful proxies for MTSI.

Acknowledgments

This project was supported by the United States National Science Foundation awards to Y.H. (EAR-1122749, PLR-1503846, EAR- 1502455; EAR-1762431), and in part by a grant from the NPS Shared Beringia Heritage program, the NPS Arctic Inventory and Monitoring Network, and NPS Bering Land Bridge National Preserve. The authors thank Scott Amy of Skydance Aviation who provides aviation and logistical support for the field samplings and Ben

Meyer from University of Alaska Fairbanks for the assistance in sample collection. We are grateful for the comments from the anonymous reviewers that helped to improve the manuscript.

References

Aiken, G.R., 1992. Chloride interference in the analysis of dissolved organic carbon by the wet oxidation method. Environmental Science and Technology 26, 2435-2439.

Aponte, J.C., Dillon, J.T., Huang, Y., 2013. The unique liquid chromatographic properties of Group II transition metals for the separation of unsaturated organic compounds. Journal of Separation Science 36, 2563–2570.

Arp, C.D., Jones, B.M., 2009. Geography of Alaska lake districts: Identification, description, and analysis of lake-rich regions of a diverse and dynamic state. U. S. Geological Survey.

Bartlein, P.J., Harrison, S.P., Brewer, S., Connor, S., Davis, B.A.S., Gajewski, K., Guiot, J., Harrison-Prentice, T.I., Henderson, A., Peyron, O., Prentice, I.C., 2011. Pollen-based continental climate reconstructions at 6 and 21 ka: a global synthesis. Climate Dynamics, 37(3-4), 775-802.

Begét, J., Mason, O., Anderson, P., 1992. Age, extent and climatic significance of the c. 3400 BP Aniakchak tephra, western Alaska, USA. The Holocene, 2(1), 51-56.

Begét, J.E., Hopkins, D.M., Charron, S.D., 1996. The largest known maars on Earth, Seward Peninsula, northwest Alaska. Arctic, 62-69.

Brady, E. C., Otto-Bliesner, B. L., Kay, J. E., & Rosenbloom, N. (2013). Sensitivity to glacial forcing in the CCSM4. Journal of Climate, 26(6), 1901-1925.

Brand, L.E., 1984. The salinity tolerance of forty-six marine phytoplankton isolates. Estuarine, Coastal and Shelf Science, 18(5), 543-556.

Caporaso, J.G., Bittinger, K., Bushman, F.D., DeSantis, T.Z., Andersen, G.L., Knight, R., 2009. PyNAST: a flexible tool for aligning sequences to a template alignment. Bioinformatics, 26(2), 266-267.

Caporaso, J.G., Kuczynski, J., Stombaugh, J., Bittinger, K., Bushman, F.D., Costello, E.K., Fierer, N., Pena, A.G., Goodrich, J.K., Gordon, J.I., Huttley, G.A., 2010. QIIME allows analysis of high-throughput community sequencing data. Nature methods, 7(5), 335.

Chapin III, F.S., Trainor, S.F., Cochran, P., Huntington, H., Markon, C., McCammon, M., McGuire, A.D., Serreze, M., 2014. Alaska, In: Melillo, J.M., Richmond, T.T., Yohe, G., Climate change impacts in the United States. U.S. Global Change Research Program, pp. 514-536.

Coolen, M.J., Muyzer, G., Rijpstra, W.I.C., Schouten, S., Volkman, J.K., Damsté, J.S.S., 2004. Combined DNA and lipid analyses of sediments reveal changes in Holocene haptophyte and diatom populations in an Antarctic lake. Earth and Planetary Science Letters, 223(1-2), 225-239.

Coolen, M.J., Saenz, J.P., Giosan, L., Trowbridge, N.Y., Dimitrov, P., Dimitrov, D. and Eglinton, T.I., 2009. DNA and lipid molecular stratigraphic records of haptophyte succession in the Black Sea during the Holocene. Earth and Planetary Science Letters, 284(3-4), pp.610-621.

Colinvaux, P.A., 1964. Origin of ice ages: pollen evidence from arctic Alaska. Science, 145(3633), 707-708.

Crump, B.C., Amaral-Zettler, L.A., Kling, G.W., 2012. Microbial diversity in arctic freshwaters is structured by inoculation of microbes from soils. The ISME journal, 6(9), 1629.

D'Andrea, W. J., Huang, Y., 2005. Long chain alkenones in Greenland lake sediments: Low δ 13C values and exceptional abundance. Organic Geochemistry, 36(9), 1234-1241.

D'Andrea, W.J., Lage, M., Martiny, J.B., Laatsch, A.D., Amaral-Zettler, L.A., Sogin, M.L. and Huang, Y., 2006. Alkenone producers inferred from well-preserved 18S rDNA in Greenland lake sediments. Journal of Geophysical Research: Biogeosciences, 111(G3).

D'Andrea, W. J., Huang, Y., Fritz, S. C., Anderson, N. J., 2011. Abrupt Holocene climate change as an important factor for human migration in West Greenland. Proceedings of the National academy of Sciences, 108(24), 9765-9769.

Drake, T. W., Holmes, R. M., Zhulidov, A. V., Gurtovaya, T., Raymond, P. A., McClelland, J. W., Spencer, R. G., 2019. Multidecadal climate-induced changes in Arctic tundra lake geochemistry and geomorphology. Limnology and Oceanography, 64(S1), S179-S191.

Edgar, R. C., 2010. Search and clustering orders of magnitude faster than BLAST. Bioinformatics, 26(19), 2460-2461.

Egge, E., Bittner, L., Andersen, T., Audic, S., de Vargas, C., Edvardsen, B., 2013. 454 pyrosequencing to describe microbial eukaryotic community composition, diversity and relative abundance: a test for marine haptophytes. PloS one, 8(9), e74371.

Gilbert, M.T.P., Jenkins, D.L., Götherstrom, A., Naveran, N., Sanchez, J.J., Hofreiter, M., Thomsen, P.F., Binladen, J., Higham, T.F., Yohe, R.M., Parr, R., 2008. DNA from pre-Clovis human coprolites in Oregon, North America. Science, 320(5877), 786-789.

Giordano, M., Prioretti, L., 2015. Sulphur and algae: Metabolism, ecology and evolution. In: Borowitzka, M.A., Beardall, J., Raven, J.A. (Eds.), The Physiology of Microalgae. Springer, Dordrecht, The Netherlands, pp. 185–209.

Goebel, T., Waters, M. R., O'rourke, D. H., 2008. The late Pleistocene dispersal of modern humans in the Americas. science, 319(5869), 1497-1502.

Goetcheus, V.G., Hopkins, D.M., Edwards, M.E., Mann, D.H., 1994. Window on the Bering Land Bridge: A 17,000-year-old paleosurface on the Seward Peninsula, Alaska. Current Research in the Pleistocene, 11, 131-132.

Goetcheus, V.G., Birks, H.H., 2001. Full-glacial upland tundra vegetation preserved under tephra in the Beringia National Park, Seward Peninsula, Alaska. Quaternary Science Reviews, 20(1-3), 135-147.

Gran-Stadniczeñko, S., Šupraha, L., Egge, E.D., Edvardsen, B., 2017. Haptophyte diversity and vertical distribution explored by 18S and 28S ribosomal RNA gene metabarcoding and scanning electron microscopy. Journal of Eukaryotic Microbiology, 64(4), 514-532.

Haas, B.J., Gevers, D., Earl, A.M., Feldgarden, M., Ward, D.V., Giannoukos, G., Ciulla, D., Tabbaa, D., Highlander, S.K., Sodergren, E., Methé, B., 2011. Chimeric 16S rRNA sequence formation and detection in Sanger and 454-pyrosequenced PCR amplicons. Genome research, 21(3), 494-504.

Hijmans, R. J., Cameron, S. E., Parra, J. L., Jones, P. G., Jarvis, A., 2005. Very high resolution interpolated climate surfaces for global land areas. International Journal of Climatology: A Journal of the Royal Meteorological Society, 25(15), 1965-1978.

Hoffecker, J. F., Elias, S. A., O'Rourke, D. H., Scott, G. R., Bigelow, N. H., 2016. Beringia and the global dispersal of modern humans. Evolutionary Anthropology: Issues, News, and Reviews, 25(2), 64-78.

Hopkins, D.M., 1988. The Espenberg Maars; a Record of Explosive Volcanic Activity in the Devil Mountain-Cape Espenberg Area, Seward Peninsula, Alaska. National Park Service, Alaska Regional Office.

Huelsenbeck, J.P., Crandall, K.A., 1997. Phylogeny estimation and hypothesis testing using maximum likelihood. Annual Review of Ecology, Evolution, and Systematics 28, 437–466.

Hugelius, G., Strauss, J., Zubrzycki, S., Harden, J.W., Schuur, E.A.G., Ping, C.L., Schirrmeister, L., Grosse, G., Michaelson, G.J., Koven, C.D., O'Donnell, J.A., 2014. Estimated stocks of circumpolar permafrost carbon with quantified uncertainty ranges and identified data gaps. Biogeosciences (Online), 11(23).

Knebel, H. J., Creager, J. S., Echols, R. J., 1974. Holocene sedimentary framework, east-central Bering Sea continental shelf. In: Herman, Y. (Ed.), Marine geology and oceanography of the Arctic seas. Springer, Berlin, Heidelberg, pp. 157-172

Kurek, J., Cwynar, L. C., 2009. Effects of within-lake gradients on the distribution of fossil chironomids from maar lakes in western Alaska: implications for environmental reconstructions. Hydrobiologia, 623(1), 37-52.

Larsen, A. S., O'Donnell, J. A., Schmidt, J. H., Kristenson, H. J., Swanson, D. K., 2017. Physical and chemical characteristics of lakes across heterogeneous landscapes in arctic and subarctic Alaska. Journal of Geophysical Research: Biogeosciences, 122(4), 989-1008.

Longo, W. M., Dillon, J. T., Tarozo, R., Salacup, J. M., Huang, Y., 2013. Unprecedented separation of long chain alkenones from gas chromatography with a poly (trifluoropropylmethylsiloxane) stationary phase. Organic geochemistry, 65, 94-102.

Longo, W.M., Theroux, S., Giblin, A.E., Zheng, Y., Dillon, J.T., Huang, Y., 2016. Temperature calibration and phylogenetically distinct distributions for freshwater alkenones: evidence from northern Alaskan lakes. Geochimica et Cosmochimica Acta, 180, 177-196.

Longo, W.M., Huang, Y., Yao, Y., Zhao, J., Giblin, A.E., Wang, X., Zech, R., Haberzettl, T., Jardillier, L., Toney, J., Liu, Z., 2018. Widespread occurrence of distinct alkenones from Group I haptophytes in freshwater lakes: Implications for paleotemperature and paleoenvironmental reconstructions. Earth and Planetary Science Letters, 492, 239-250.

Luecke, C., Giblin, A.E., Bettez, N.D., Burkart, G.A., Crump, B.C., Evans, M.A., Gettel, G., MacIntyre, S., O'Brien, W.J., Rublee, P.A., Kling, G.W., 2014. The response of lakes near the Arctic LTER to environmental change, In: Hobbie, J.E., Kling., G.W. (Ed.), Alaska's changing Arctic: Ecological consequences for tundra, streams, and lakes. Oxford University Press, pp. 238-286.

Miller, G.H., Brigham-Grette, J., Alley, R.B., Anderson, L., Bauch, H.A., Douglas, M.S.V., Edwards, M.E., Elias, S.A., Finney, B.P., Fitzpatrick, J.J., Funder, S.V., 2010. Temperature and precipitation history of the Arctic. Quaternary Science Reviews, 29(15-16), 1679-1715.

Moreno-Mayar, J.V., Potter, B.A., Vinner, L., Steinrücken, M., Rasmussen, S., Terhorst, J., Kamm, J.A., Albrechtsen, A., Malaspinas, A.S., Sikora, M., Reuther, J.D., 2018. Terminal Pleistocene Alaskan genome reveals first founding population of Native Americans. Nature, 553(7687), 203.

O'Donnell, J. A., G. R. Aiken, K. D. Butler, T. A. Douglas., 2015. Chemical composition of large lakes in Alaska's Arctic Network: 2013-2014. Natural Resource Data Series NPS/ARCN/NRDS— 2015/985. National Park Service, Fort Collins, Colorado.

O'Donnell, J. A., Aiken, G. R., Swanson, D. K., Panda, S., Butler, K. D., Baltensperger, A. P., 2016. Dissolved organic matter composition of Arctic rivers: Linking permafrost and parent material to riverine carbon. Global Biogeochemical Cycles, 30(12), 1811-1826.

Pecoraino, G., D'Alessandro, W., Inguaggiato, S., 2015. The other side of the coin: geochemistry of alkaline lakes in volcanic areas. In: Volcanic lakes. Springer, Berlin, Heidelberg, pp. 219-237.

Plancq, J., Cavazzin, B., Juggins, S., Haig, H.A., Leavitt, P.R., Toney, J.L., 2018a. Assessing environmental controls on the distribution of long-chain alkenones in the Canadian Prairies. Organic Geochemistry, 117, 43-55.

Plancq, J., McColl, J.L., Bendle, J.A., Seki, O., Couto, J.M., Henderson, A.C., Yamashita, Y., Kawamura, K., Toney, J.L., 2018b. Genomic identification of the long-chain alkenone producer in freshwater Lake Toyoni, Japan: implications for temperature reconstructions. Organic Geochemistry, 125, 189-195.

Prahl, F. G., Wakeham, S. G., 1987. Calibration of unsaturation patterns in long-chain ketone compositions for palaeotemperature assessment. Nature, 330(6146), 367.

Prahl, F.G., Muehlhausen, L.A., Zahnle, D.L., 1988. Further evaluation of long-chain alkenones as indicators of paleoceanographic conditions. Geochimica et Cosmochimica Acta, 52(9), 2303-2310.

Richter, N., Longo, W.M., George, S., Shipunova, A., Huang, Y., Amaral-Zettler, L., 2019. Phylogenetic diversity in freshwater-dwelling Isochrysidales haptophytes with implications for alkenone production. Geobiology, 17(3), 272-280.

Schuur, E.A., McGuire, A.D., Schädel, C., Grosse, G., Harden, J.W., Hayes, D.J., Hugelius, G., Koven, C.D., Kuhry, P., Lawrence, D.M., Natali, S.M., 2015. Climate change and the permafrost carbon feedback. Nature, 520(7546), 171.

Simon, M., López-García, P., Moreira, D. and Jardillier, L., 2013. New haptophyte lineages and multiple independent colonizations of freshwater ecosystems. Environmental microbiology reports, 5(2), 322-332.

Stamatakis, A., 2014. RaxML version 8: a tool for phylogenetic analysis and post-analysis of large phylogenies. Bioinformatics, 30(9), 1312-1313.

Takahashi, H., Kopriva, S., Giordano, M., Saito, K., Hell, R., 2011. Sulfur assimilation in photosynthetic organisms: Molecular functions and regulations of transporters and assimilatory enzymes. Annual Review of Plant Biology 62, 157–184.

Tamm, E., Kivisild, T., Reidla, M., Metspalu, M., Smith, D.G., Mulligan, C.J., Bravi, C.M., Rickards, O., Martinez-Labarga, C., Khusnutdinova, E.K., Fedorova, S.A., 2007. Beringian standstill and spread of Native American founders. PloS one, 2(9), e829.

Tarnocai, C., Canadell, J. G., Schuur, E. A., Kuhry, P., Mazhitova, G., Zimov, S., 2009. Soil organic carbon pools in the northern circumpolar permafrost region. Global biogeochemical cycles, 23(2).

Theroux, S., D'Andrea, W. J., Toney, J., Amaral-Zettler, L., Huang, Y., 2010. Phylogenetic diversity and evolutionary relatedness of alkenone-producing haptophyte algae in lakes: implications for continental paleotemperature reconstructions. Earth and Planetary Science Letters, 300(3-4), 311-320.

Toney, J.L., Huang, Y., Fritz, S.C., Baker, P.A., Grimm, E., Nyren, P., 2010. Climatic and environmental controls on the occurrence and distributions of long chain alkenones in lakes of the interior United States. Geochimica et Cosmochimica Acta, 74(5), 1563-1578.

Vachula, R. S., Huang, Y., Longo, W. M., Dee, S. G., Daniels, W. C., Russell, J. M., 2019. Evidence of Ice Age humans in eastern Beringia suggests early migration to North America. Quaternary Science Reviews, 205, 35-44.

Wang, L., Longo, W. M., Dillon, J. T., Zhao, J., Zheng, Y., Moros, M., Huang, Y., 2019. An efficient approach to eliminate steryl ethers and miscellaneous esters/ketones for gas chromatographic analysis of alkenones and alkenoates. Journal of Chromatography A , 1596, 175-182.

Weishaar, J. L., Aiken, G. R., Bergamaschi, B. A., Fram, M. S., Fujii, R., & Mopper, K., 2003. Evaluation of specific ultraviolet absorbance as an indicator of the chemical composition and reactivity of dissolved organic carbon. Environmental science & technology, 37(20), 4702-4708.

Wetterich, S., Grosse, G., Schirrmeister, L., Andreev, A.A., Bobrov, A.A., Kienast, F., Bigelow, N.H., Edwards, M.E., 2012. Late Quaternary environmental and landscape dynamics revealed by a pingo sequence on the northern Seward Peninsula, Alaska. Quaternary Science Reviews, 39, 26-44.

Zheng, Y., Tarozo, R., Huang, Y., 2017. Optimizing chromatographic resolution for simultaneous quantification of long chain alkenones, alkenoates and their double bond positional isomers. Organic Geochemistry, 111, 136-143.

Zink, K.G., Leythaeuser, D., Melkonian, M., Schwark, L., 2001. Temperature dependency of long-chain alkenone distributions in recent to fossil limnic sediments and in lake waters1. Geochimica et Cosmochimica Acta, 65(2), 253-265.

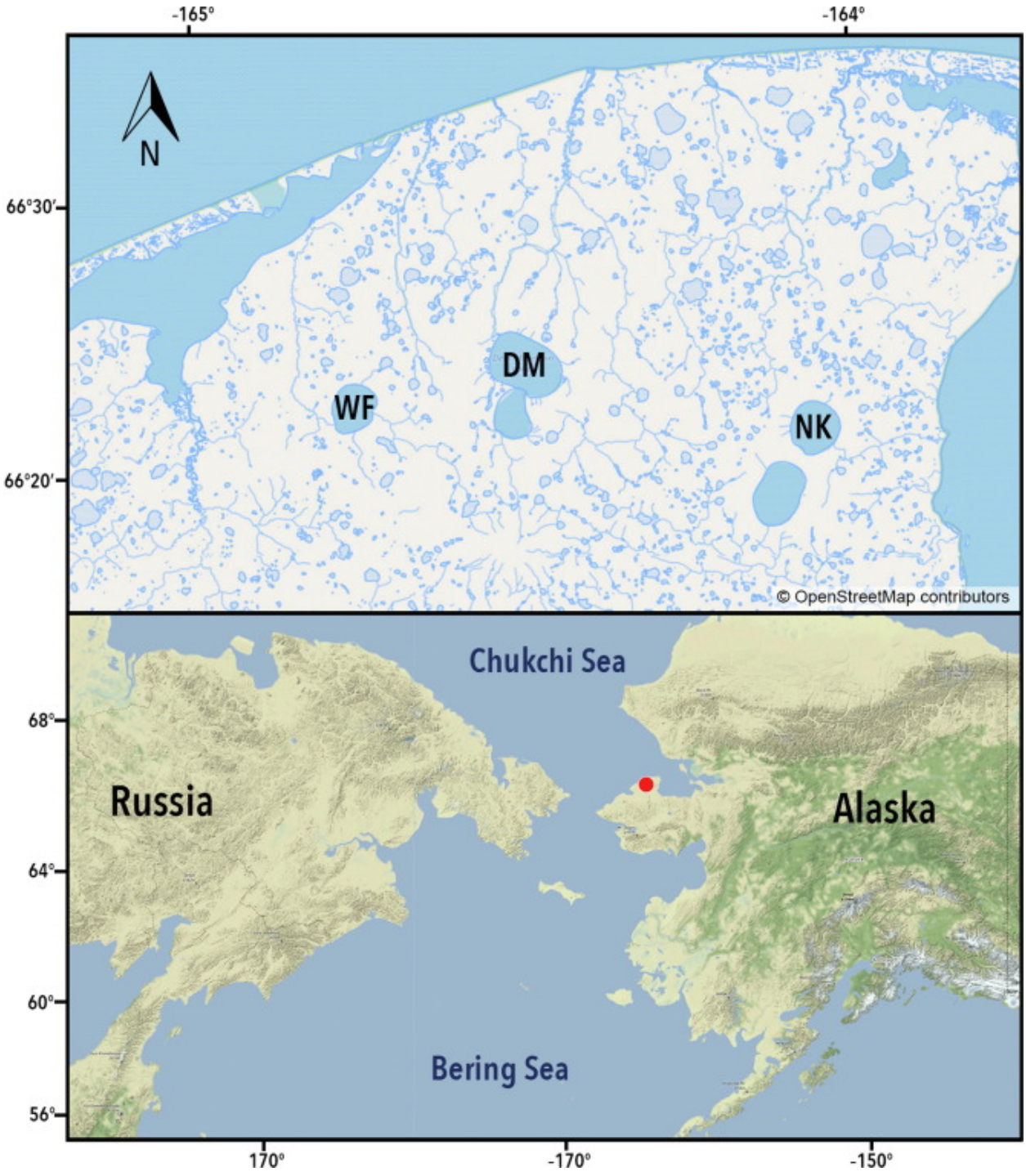

Figure 4.1. Maps of the study region and the hydrology of sampled sites. WF: White Fish Maar, DM: Devil Mountain Maar, NK: North Killeak Maar.

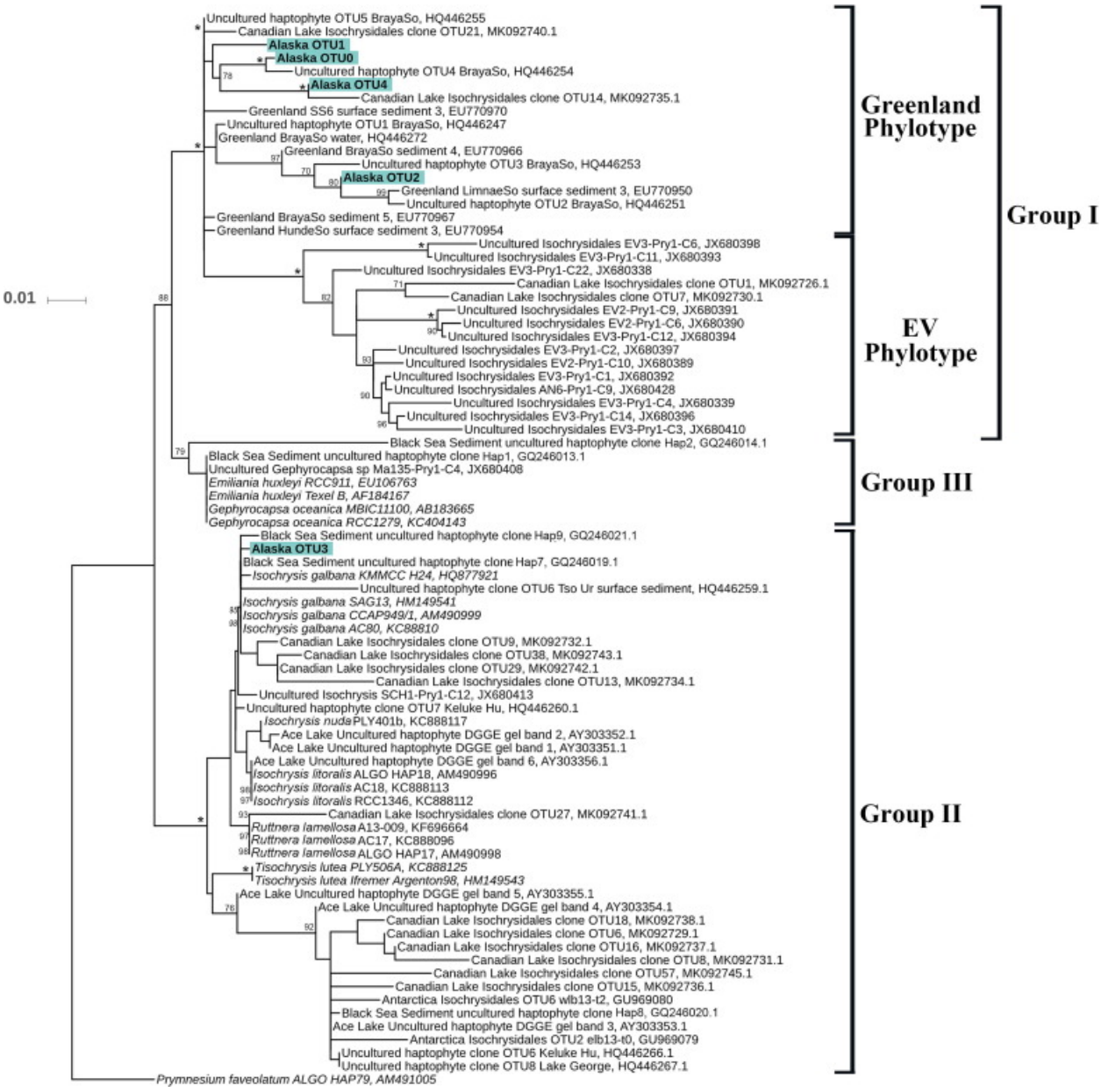

Figure. 4. 2. Maximum likelihood tree showing the phylogeny of Isochrysidales constructed from partial 18S rRNA gene sequences. Sequences recovered from this study (Alaska OTU 0–4) are in bold with GenBank number following. Groups I, II and III Isochrysidales clades are labeled after Theroux et al. (2010), Greenland phylotypes include the sequence recovered in Greenland freshwater lakes from D'Andrea et al. (2006) and four OTUs from this study, and EV phylotypes include sequences from Simon et al. (2013). Only bootstrap values > 70% are shown, asterisks represent bootstrap values equal to 100%.

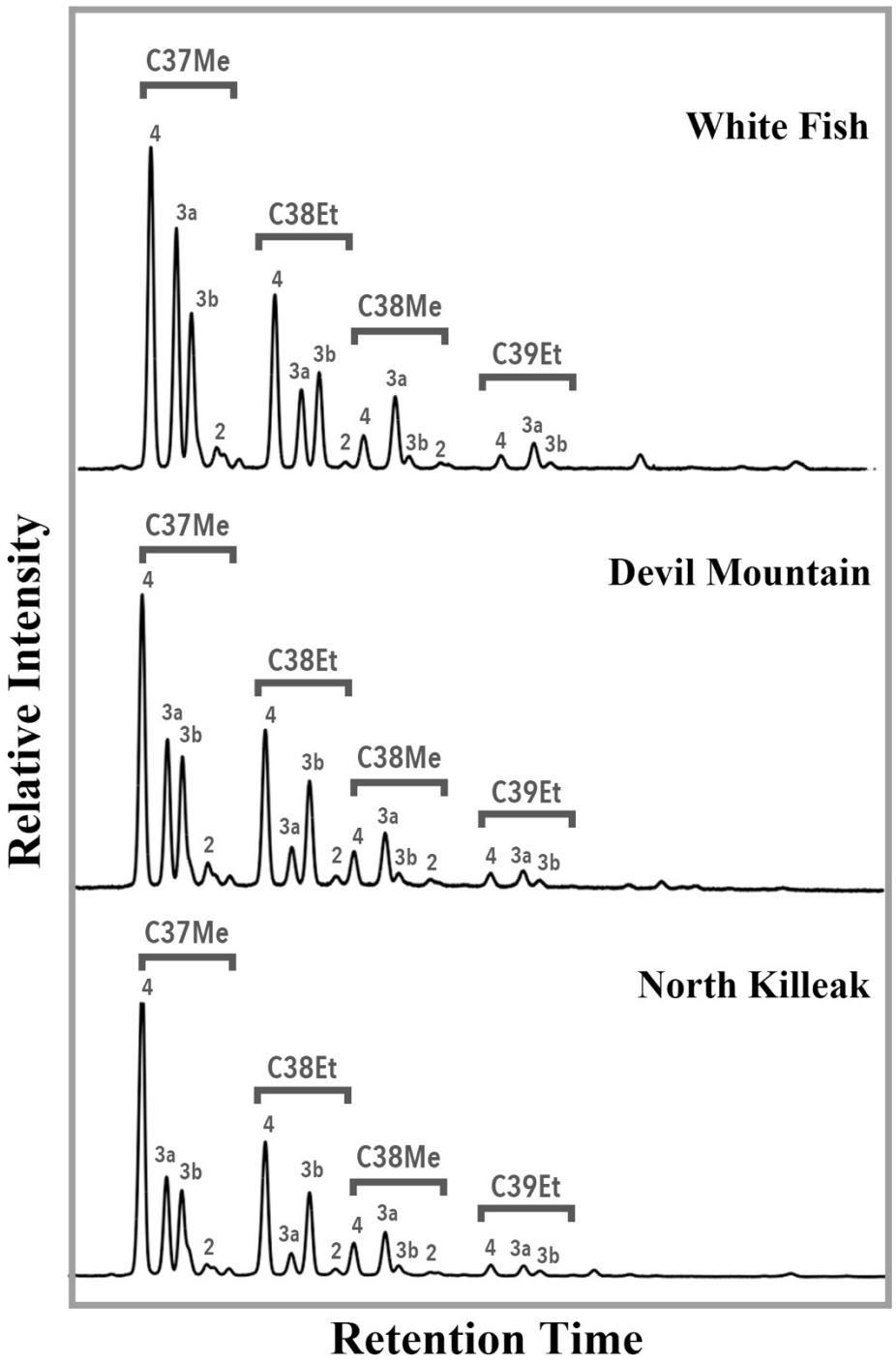

Figure 4.3. Partial chromatograms of the surface sediments from the three studied maar lakes after saponification and AgTCM column. The alkenones showed distinctive Group I characteristics.

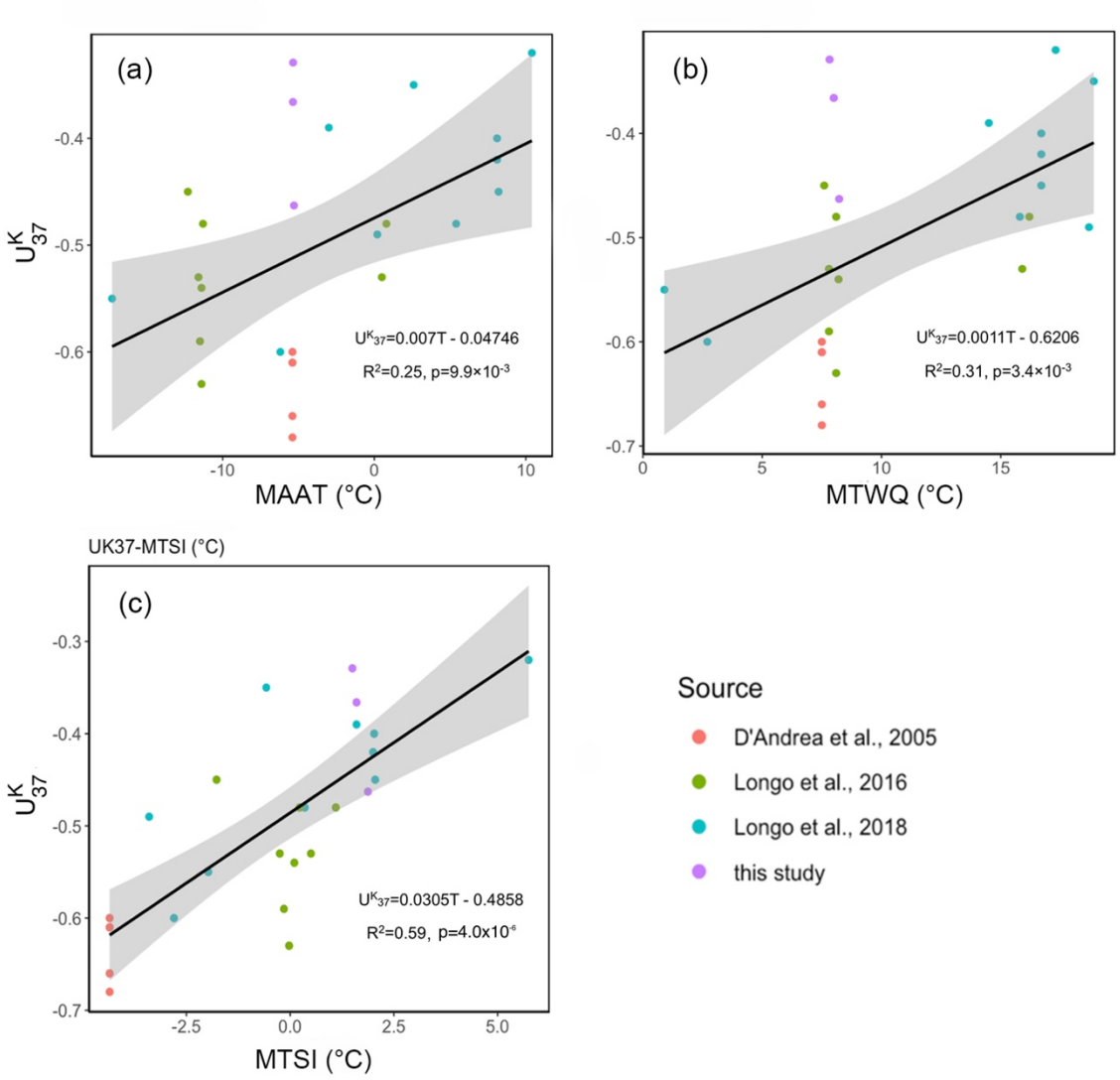

Figure 4.4. Regressions between U_{37}^K and mean annual air temperature (MAAT, a), mean temperature of the warmest quarter (MTWQ, b), and mean temperature of the spring isotherm (MTSI, c). Shaded areas represent 95% confidence interval.

Table 4.1. Summary of the sequences recovered from each sample, and their phylogenetic assignments.

Sample	Numbers of Isochrysidales sequences recovered from clone libraries					
	Total	Group I				Group II
		OTU 0	OTU 1	OTU 2	OTU 4	OTU 3
White Fish	26	26	0	0	0	0
Devil Mountain	9	9	0	0	0	0
North Killeak	60	52	2	1	3	2
Toolik	21	21	0	0	0	0

Supplementary Material

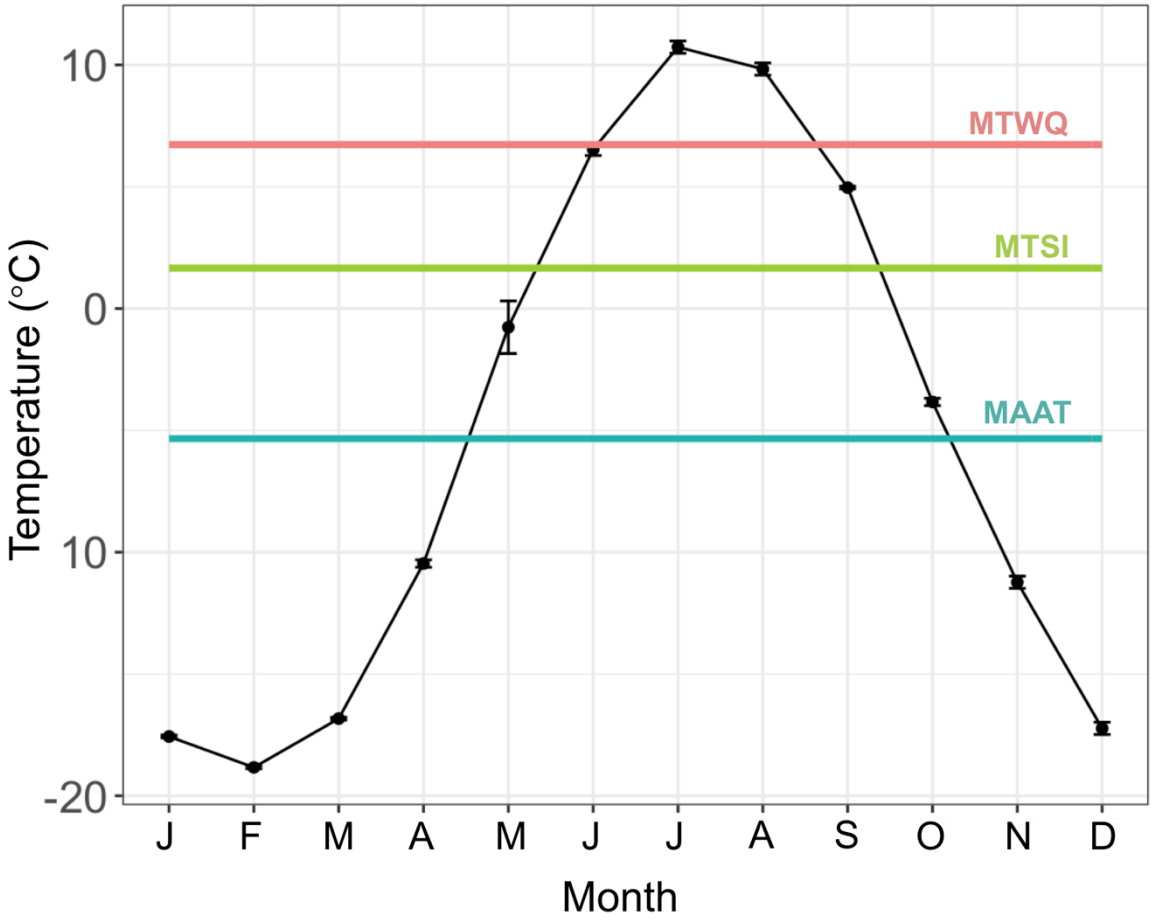

Figure 4. S. 1. Monthly air temperature of the study sites, the error bars represent the standard deviation of the temperatures from the three sites. Mean annual air temperature (MAAT), mean temperature of the warmest quarter (MTWQ) and mean temperature of the spring isothermal season (MTSI) are also shown in the figure.

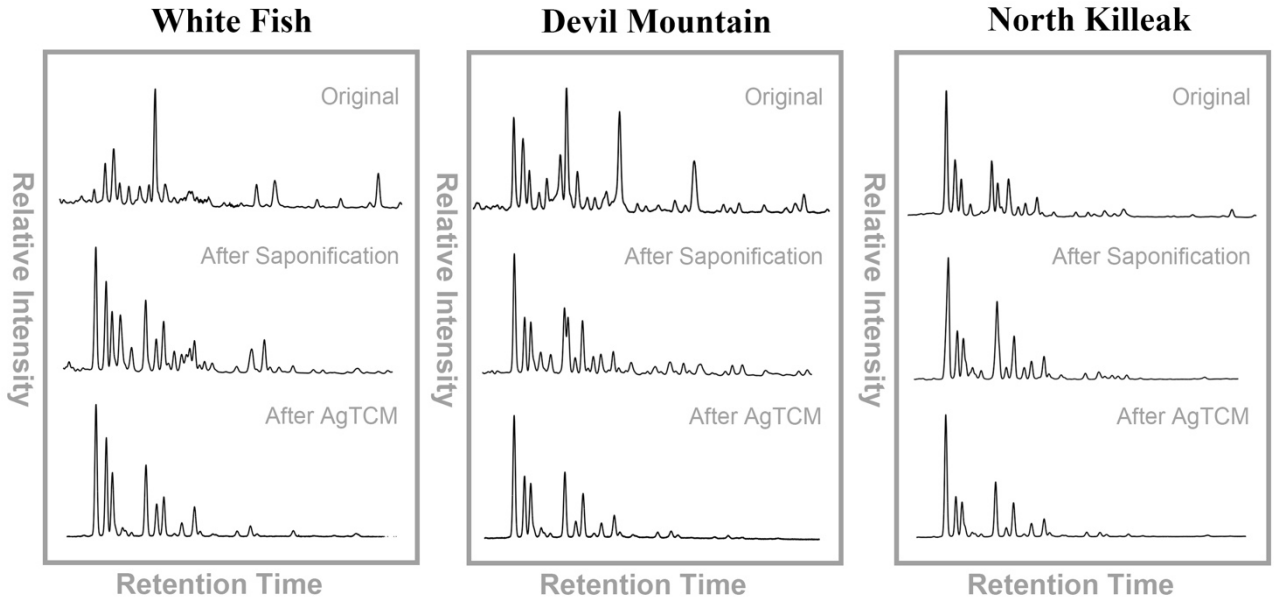

Figure 4. S. 2. Partial chromatograms of the surface sediments from the 3 studied maar lakes, showing the original DCM fraction after liquid chromatography, the same sample after saponification, and AgTCM cleaning sequentially.

Table 4. S. 1. Alkenone concentrations in freeze-dried sediments from the Espenberg maar lakes, related indices and air temperature of the study sites.

	White Fish	Devil Mountain	North Killeak
$C_{37:4\ Me}$ (µg/g)	2.3122	0.1935	8.9443
$C_{37:3a\ Me}$ (µg/g)	1.7469	0.1033	2.8871
$C_{37:3b\ Me}$ (µg/g)	1.2168	0.0868	2.6013
$C_{37:2\ Me}$ (µg/g)	0.1627	0.0167	0.3100
$C_{38:4\ Et}$ (µg/g)	1.2553	0.0996	4.2197
$C_{38:3a\ Et}$ (µg/g)	0.5966	0.0252	0.6956
$C_{38:3b\ Et}$ (µg/g)	0.7139	0.0688	2.5851
$C_{38:2\ Et}$ (µg/g)	0.0633	0.0082	0.2012
$C_{38:4\ Me}$ (µg/g)	0.2496	0.0221	1.0945
$C_{38:3a\ Me}$ (µg/g)	0.6026	0.0376	1.4447
$C_{38:3b\ Me}$ (µg/g)	0.1096	0.0093	0.3655
$C_{38:2\ Me}$ (µg/g)	0.0806	0.0074	0.1100
U_{37}^{K}	-0.3291	-0.3660	-0.4629
$U_{37}^{K\prime}$	0.0520	0.0806	0.0535
$\%C_{37:4}$	0.4251	0.4835	0.6067
RIK_{37}	0.5894	0.5434	0.5260
MAAT(°C)	-5.358	-5.367	-5.300
MTWQ(°C)	7.825	8.000	8.225
MTSI(°C)	1.500	1.600	1.875

Table 4. S. 2. Locations and water properties of the Espenberg maar lakes

	White Fish	Devil Mountain	North Killeak
sample site latitude (°N)	66.378	66.411	66.356
sample site longitude (°W)	164.751	164.499	164.042
Annual precipitation (mm)	334	302	296
Sample site depth (m)	2.2	~6	~3
salinity (ppt)*	0.317	0.039	1.077
pH	8.4 ± 0.5 (3)	8.3 ± 0.5 (3)	8.4 ± 0.2 (2)
Alkalinity ($mgCaCO_3/L$)	98.44 (1)	45.21 (1)	245.56 (1)
DIC (mgC/L)	25.76 (1)	10.95 (1)	69.56 (1)
Total dissolved N (mgN/L)	0.54 ± 0.08 (3)	0.12 ± 0.01 (2)	0.35 ± 0.04 (2)
Cl^- (mg/L)	146.3 ± 38.9 (3)	12.0 ± 1.4 (3)	658.55 ± 64.4 (2)
SO_4^{2-} (mg/L)	0.23 ± 0.18 (3)	0.76 ± 0.12 (3)	0.01 ± 0.01 (2)
Na^+ (mg/L)	69.75 ± 13.67 (3)	10.17 ± 1.13 (3)	316.19 ± 26.66 (2)
K^+ (mg/L)	4.36 ± 0.76 (3)	1.56 ± 0.31 (3)	15.99 ± 1.27 (2)
Ca^{2+} (mg/L)	21.80 ± 4.69 (3)	6.97 ± 1.10 (3)	64.93 ± 21.26 (2)
Mg^{2+} (mg/L)	19.52 ± 3.23 (3)	4.73 ± 0.61 (3)	73.49 ± 2.55 (2)
DOC (mgC/L)	11.2 ± 1.3 (3)	2.9 ± 0.5 (3)	5.2 ± 0.0 (2)
SUVA, 254 nm	3.0 ± 0.5 (3)	2.0 ± 0.5 (3)	1.7 ± 0.1 (2)

* Due to the high standard deviation of in situ salinity measurements, the salinity is estimated from the ion concentrations

Note: Values represent the average of all samples collected (± one standard deviation). The value in parentheses is the sample size.

Chapter 5: Permafrost thaw and altered carbon cycling since the 1950s based on high-resolution biogeochemical records from White Fish Lake, Seward, Alaska

Karen J.Wang[1, 2], Jonathan A.O'Donnell[3], YongsongHuang[1, 2]

[1]Department of Earth, Environmental and Planetary Sciences, Brown University, Providence, RI 02912, USA

[2]Institute at Brown for Environment and Society, Brown University, Providence, RI 02912, USA

[3]Arctic Network, National Park Service, Anchorage, AK, USA

Abstract

Recent climate change has led to widespread warming and thawing of permafrost soils across Arctic and sub-Arctic regions. Permafrost thaw remobilize previously frozen organic carbon and alters the lateral transport of carbon from terrestrial to aquatic ecosystems through thermal erosion, thermokarst, and shifting groundwater dynamics in northern catchments. However, continuous records tracking permafrost thaw and associated carbon-cycle processes in past decades are scarce. In this study, we analyzed biomarkers and bulk sediment properties from a core attained from White Fish Lake that spans the past ~60 years. White Fish Lake is a crater lake located in the Seward Peninsula where the surrounding terrain is underlain by Yedoma permafrost that is susceptible to abrupt thaw. The organic-matter-rich sediment and exceptionally high sedimentation rate (1.4 cm/yr) provided opportunity for reconstructions at an annual scale. We analyzed lipid biomarkers including fatty acids, n-alkanes, diploptene, alkenones, GDGTs, as well as bulk ^{13}C and ^{14}C isotope compositions. The radiocarbon age of the sediment averaged 3440 yr BP, suggesting contribution of old permafrost carbon in the lake catchment. GDGT-0, diploptene and C_{37} alkenone fluxes increased significantly since 2010, which suggests an increase in methanogen populations and methane production, as well as increased methane oxidizing bacteria and phytoplankton productivity. The intensified carbon cycle was also demonstrated in the bulk isotope data. The $\delta^{13}C$ content of bulk organic carbon was highly depleted (-28.87~-31.64‰, average of -30.21±0.59‰) and comparable to other thermokarst lake sediments. There is a significant decreasing trend of the $\delta^{13}C$ from 1960 to 2019 (~1.5‰), suggesting increased incorporation of a methane-derived carbon source into the aquatic biomass and sediment. Our study shows that the Seward Peninsula has undergone unprecedented changes as the Arctic warms, particularly in the past decade.

1. Introduction

Human activities are responsible for approximately 1.1 ˚C of global warming since 1850-1900, and a warming of 1.5˚C or more is projected over the next 20 years (IPCC, 2021: Climate Change 2021: The Physical Science Basis). Warming is amplified in the Arctic, where air temperatures are expected to increase more than twice the global average (IPCC, 2021: Climate Change 2021: The Physical Science Basis). The warming has led to large-scale thawing of permafrost that exposes previously frozen organic matter to microbial degradation, which in turn emits greenhouse gases that further accelerate warming (Martens et al., 2020). Yedoma which is a type of permafrost that aggraded with the deposition of wind-blown loess during the late Pleistocene (starting ~50 ka before present (B.P.) in Alaska) is widespread in Siberia and Alaska (Strauss et al., 2021). Yedoma is typically ice-rich, organic-rich, silt-dominated, and contain large syngenetic ice wedges , are particularly important as it is prone to melting and contains ~ 30% of global permafrost carbon (Anthony et al., 2014; Martens et al., 2020; Strauss et al., 2021).

Large amounts of greenhouse gases (primarily carbon dioxide (CO_2) and methane (CH_4)) have been emitted from thawing Yedoma during past warm periods such as Bølling-Allerød (14.7~12.9 ka B.P.) and early Holocene (~11.7 ka B.P.) across Siberia and Alaska (Lenz et al., 2016; Martens et al., 2020). In recent decades, landscape changes induced by the destabilization of ice-rich permafrost, including thermokarst (i.e., subsidence of the ground surface due to ground ice melt), thermal erosion and lake drainage have been observed in the northern Seward Peninsula (Strauss et al., 2021). Extensive studies have been done on carbon fluxes from lakes and ponds that are widely distributed in this region, particularly on thermokarst lakes, beaver ponds, peatland ponds and glacial/post-glacial lakes (Wik et al., 2016; Walter Anthony et al.,

2016; Engram et al., 2020; Kuhn et al., 2021). Cenozoic volcanic deposits are a common geologic feature in the Bering Sea region, spanning from the Seward Peninsula to the north to Pribilof Islands to the south. The Espenberg volcanic field in the northern Seward Peninsula includes four of the worlds' largest maar lakes with a total area of ~77 km^2 (Lanik et al., 2019). Compared to thermokarst lakes that are formed by thaw depression and emit methane from the actively expanding thaw margins (Walter et al., 2008; Walter Anthony et al., 2016), maar lakes on the Seward Peninsula are much greater in surface area and depth, and morphologically more stable (Lara & Chipman, 2021). By contrast, thermokarst lakes that are frequently influenced by erosion and deposition, drainage and subsequent infilling (Jorgenson & Shur, 2007), with disturbed sediment records reflecting these complex processes. Sediment cores from maar lakes span a longer record with clear age-depth relationships, are thus more likely to reflect lateral transport from surrounding permafrost on a larger spatial and time scale.

Here we applied organic geochemical and molecular biological methods in a sediment core collected from the center of White Fish maar, northern Seward Peninsula, Alaska, that dates back to the late 1950s. We measured the radiocarbon content of bulk total organic carbon (TOC), and investigated the abundance and $\delta^{13}C$ content of alkenones, n-alkanes, Glycerol dialkyl glycerol tetraether lipids (GDGTs), diploptene and TOC, to understand the lake's hydrological, ecological, and carbon-cycle changes in response to climate variations and permafrost thaw since the late 1950s. This is the first study to reconstruct carbon-cycle processes at annual temporal resolution from lake sediments in the Arctic.

2. Methods and material

2.1 Study site and sample collection

White Fish Lake (Fig. 5. 1; 66.38˚N, 164.75˚W) is a maar lake located in the northern Seward Peninsula in northwest Alaska, USA. The study site is in continuous permafrost zone dominant by tussock tundra, and is characterized by an abundance of thermokarst lakes (O'Donnell, 2015 ARCNlakes; Larsen et al., 2017; Nitze et al., 2018). White Fish Lake is situated within the Yedoma permafrost domain, as recently mapped by Strauss et al. (2021). The primary ecological and vegetation types in the White Fish Lake basin are Upland Dwarf Birch-Tussock Shrub, Upland Sedge-Dryas Meadow, Upland Willow Low Shrub, Lowland Sedge Fen. Dominant plant type includes deciduous shrub (e.g., *Betula nana*, *Salix reticulata*), sedge (e.g., *Eriophorum vaginatum*, *Carex aquatilis*), moss (*Sphagnum sp.*), shrubs (e.g., *Ledum decumbens*, *Vaccinium vitis-idaea*) (Jorgenson et al., 2009 ARCN report).

White Fish Lake lies on the Espenberg volcanic field and is formed by phreatomagmatic eruption when magma interacted with ice-rich permafrost around 160 ±8 kyr ago (Begét et al., 1996; Lanik et al., 2019). White Fish Lake and the nearby Devil Mountain Lake, North Killeak Lake and South Killeak Lake are the largest maar lakes on Earth (Begét et al., 1996). The shape of White Fish Lake is approximately circular with a radius of 4.3 km and a surface area of 15 km^2. The maximum depth is 8-10 m (Lanik et al., 2019). The lake water has an elevated pH of 7.8-8.8 (measured on 6/22/13 and 9/15/17, respectively) and a high DOC concentration (12.3 mgC/L) which is the highest among all large non-thermokarst lakes monitored in the region (O'Donnell, 2015 ARCNlakes). A lake outlet forms the Singeakpuk River which flows north into Shishmaref Inlet and four inlets that connect with nearby thaw ponds.

The sediment core was collected around the center of White Fish Lake (GPS) over ice cover in April 2019, using a piston corer. The total sediment core recovered is 87 cm, and was subsampled into 0.5 cm intervals for 0-50 cm, and 1 cm intervals for 50-87 cm.

2.2 Dating and chronology

The chronology of the core was determined through lead (^{210}Pb), cesium (^{137}Cs) and radium (^{226}Ra) isotopes measured at Flett Research Ltd (http://flettresearch.ca/isotopemethods.html). The sediments were measured at 0.5-cm intervals from 0-50 cm, and 1-cm intervals from 50-86 cm. Unsupported ^{210}Pb is calculated by subtracting the ^{226}Ra from each total ^{210}Pb value. A constant-rate-of-supply (CRS) model was then calibrated against the linear regression model to estimate the age at the bottom of each section and establish the final age model. ^{137}Cs measurements are used as an independent test to the CRS model. The elevated ^{137}Cs activities in 65-74 cm suggests that the majority of ^{137}Cs is from external erosion sources such as soil, instead of directly deposited from the atmosphere. Thus the 73-74 cm interval represents the year 1966 which has the highest terrestrial ^{137}Cs inventory. The CRS model is compatible with the ^{137}Cs data within reasonable uncertainty (Fig. 5. 2b).

2.3 Organic geochemical analyses

Sediment samples were first freeze-dried, and lipids were extracted from ~2g of freeze-dried sediment through Dionex™ accelerated solvent extraction system with Dichloromethane (DCM): methanol mixture (9:1, v/v). The total lipid extract was then separated into acid and neutral fractions with LC-NH_2 columns by eluting with DCM: isopropanol (2:1, v/v) and acetic acid: ether (4:96, v/v). The neutral fraction was further separated into alkane, ketone, and alcohol fractions through silica gel columns by eluting with hexane, DCM and methanol. The alkane fraction containing n-alkanes and diploptene was measured and quantified through a gas chromatograph flame ionization detector (GC-FID) with a non-polar column. The alkenone was

analyzed as described in Wang et al. (2021). The alcohol fraction was eluted through LC-Al_2O_3 column with hexane:DCM (1:1, v/v) and DCM:MeOH (1:1, v/v), the later fraction was then filtered and measured for GDGTs through High Performance Liquid Chromatography Mass Spectrometer (HPLC-MS).

2.4 Lipid biomarker indices

Lipid biomarkers produced by various Archaea, Bacteria, and Eukaryote were separated and quantified. The producers, environmental significance, and relevant indices are described below.

GDGTs: A class of large (up to 86 carbons) membrane lipids that consist ether bonds that form a monolayer (Schouten et al., 2013; Łącka et al., 2015). GDGTs can be further broken down to two categories: branched GDGTs (brGDGTs) produced by Bacteria, and Isoprenoidal GDGTs (isoGDGTs) produced by Archaea (Schouten et al., 2013). BrGDGT is denoted as I/II/III+a/b/c, where the roman numbers represent numbers of methyl branches (I:0, II:1, III:2), and the letters represent numbers of cyclopentane rings (a: 0, b:1, c:2). IsoGDGT is denoted by Arabic numbers representing the numbers of the cyclopentane rings, and crenarchaeols are unique for cyclohexane ring in addition to four cyclopentane rings. Prime and double prime represent isomers of GDGTs.

Multiple indices were developed to identify the source of GDGTs. The branched and isoprenoid tetraether (BIT) index is used to quantify the relative input from terrestrially derived tetraether lipids versus crenarchaeol is defined as Eq.1 (Hopmans et al., 2004). In freshwater environment $\sum IIIa / \sum IIa$ were shown to track relative input of aquatic and terrigenous brGDGTs (Eq. 2) (Martin et al., 2019).

$$BIT = \frac{Ia + IIa + IIIa}{Ia + IIa + IIIa + Cren} \qquad (1)$$

$$\sum IIIa / \sum IIa = \frac{IIIa + IIIa' + IIIa'' + IIIa7}{IIa + IIa' + IIa7} \qquad (2)$$

The degree of methylation (4, 5, or 6 methyl groups at position 5 or 6) of BrGDGTs are correlated with temperature. Methylation index that excludes the 6-methyl brGDGTs is defined as MBT'_{5Me} (Eq. 3; De Jonge et al., 2014), and Stefanescu et al. (2021) developed an MBT'$_{5Me}$-JJAS (June-Sept.) air temperature calibration that accounts for the influence of lake water depth based on surface sediment from high-altitude sub-alpine lakes of mid-latitude North America (Eq. 4).

$$MBT'_{5Me} = \frac{Ia + Ib + Ic}{Ia + Ib + Ic + IIa + IIb + IIc + IIIa} \qquad (3)$$

$$MBT'_{5Me} = 0.026 * \text{JJAS} - 0.065 * \ln(\text{water depth in meters}) + 0.10 \qquad (4)$$

IsoGDGT can be used to as an indicator of methanogenic and/or methanorophic activities. GDGT-0 could be produced by multiple Thaumarchaeota, Crenarchaeota, and Euryarchaeota, but is particular abundant in methanogens and methanotrophs (Pancost et al., 2001). Blaga et al. (2009) defined the ratio between GDGT-0/cren as an indicator of methanogenic GDGT-0 in lakes, a ratio >2 indicates presence of anaerobic methanogenesis (Eq. 5).

$$GDGT - 0/Cren = \frac{GDGT - 0}{Cren} \qquad (5)$$

Similarly, GDGT-1, -2, -3 presumably represents methanotrophic Euryarchaeota. Methane index (MI) is built upon a binary isoGDGT source of Crenarchaeota from water column and methanotrophic Euryarchaeota from the sediment, suggesting contribution from methanotrophic Euryarchaeota their relative abundance (Zhang et al., 2011). MI value >0.5 suggest methane-rich

environment, though the ratio was originally developed in marine environment and might not be representative in lakes with large amounts of terrigenous input (Eq. 6; Zhang et al., 2011).

$$MI = \frac{[GDGT-1]+[GDGT-2]+[GDGT-3]}{[GDGT-1]+[GDGT-2]+[GDGT-3]+[Cren]+[Cren']} \quad (6)$$

Alkenones: A class of $C_{35\text{-}42}$ methyl or ethyl ketones with two to five double bonds. They are produced exclusively by algae within the order of Isochrysidales. The producer of alkenones in freshwater lakes are mainly Group 1 Isochrysidales that is characterized by high relative abundance of $C_{37:4}$ alkenone ($\%C_{37:4}$) and presence of $C_{37:3b}$ isomers (Eq. 7 and 8; D'Andrea et al., 2006; Longo et al., 2018). The index quantifying ratio of $C_{37:3}$ isomeric ketones is defined as:

$$\%C_{37:4} = \frac{C_{37:4}}{C_{37:2}+C_{37:3a}+C_{37:3b}+C_{37:4}} \quad (7)$$

$$RIK_{37} = \frac{C_{37:3a}}{C_{37:3a}+C_{37:3b}} \quad (8)$$

The unsaturation degree of alkenones (U_{37}^{K}, Eq. 9) are correlated to temperature. Longo et al. (2018) established a correlation between U_{37}^{K} and spring transitional air temperature (average temperature of the four months centered on the spring isotherm) based on samples from global freshwater lakes where Group 1 Isochrysidales were the main alkenone producer (Eq. 10).

$$U_{37}^{K} = \frac{C_{37:2}-C_{37:4}}{C_{37:2}+C_{37:3a}+C_{37:3b}+C_{37:4}} \quad (9)$$

$$U_{37}^{K} = 0.029 * T - 0.49, r^2 = 0.60, p < 0.0001 \quad (10)$$

n-alkanes: n-alkanes are straight chain hydrocarbons that could be produced by bacteria, algae, and terrestrial plants, and are predominately odd number (Eglinton & Eglinton, 2008; Jongejans et al., 2020). The ratio between odd and even chain n-alkanes reflects the degradation

of the sediment, with decreasing odd number n-alkane corresponding to more degradation (Bray and Evans, 1961). The ratio between odd and even n-alkanes can be quantified by carbon preference index (CPI) (Eq. 11; Zech et al., 2010).

$$CPI_{23-33} = \frac{2 * \sum_{i=23}^{33} i * C_i(i = odds)}{\sum_{i=22}^{32} i * C_i + \sum_{i=24}^{34} i * C_i(i = evens)} \qquad (11)$$

The predominance chain length differs between different organisms. Algae generally produce shorter (C_{15}-C_{21}) chain length, mosses such as Sphagnum typically produce C_{23}-C_{25}, leaf waxes are mainly C_{27}-C_{29}, and grasses are C_{31}-C_{33} (Han & Calvin, 1969; Zech et al., 2010; Jongejans et al., 2020). The average chain length (ACL) thus reflects the source of n-alkane (Eq. 12; Daniels et al., 2017). Similarly, P_{aq} and P_{wax} reflect the relative contribution from macrophytes and terrestrial plants (Eq. 13, Eq. 14).

$$ACL_{20-33} = \frac{\sum_{20}^{33} i * C_i}{\sum_{20}^{33} C_i} \qquad (12)$$

$$P_{aq} = \frac{C_{23} + C_{25}}{C_{23} + C_{25} + C_{29} + C_{31}} \qquad (13)$$

$$P_{wax} = \frac{C_{27} + C_{29} + C_{31}}{\sum odd\ C_{23-31}} \qquad (14)$$

2.5 Isotopic analyses

Bulk $\delta^{13}C$ isotope was measured on the sediment remnant after lipid extraction. 2M HCl was added to the sediment samples and heated at 60˚C for 12 hours, then rinsed with deionized water to remove carbonates. The samples were then dried and analyzed on an EA IsoLink IRMS system (Thermo Scientific™), and the $\delta^{13}C$ values were reported as values in per mill compared to the standardized Vienna Pee Dee Belemnite (‰ vs. VPDB). Compound specific ^{13}C of

alkenones, n-alkanes and diploptene were measured by TRACE 1310 Gas Chromatograph coupled with Delta V Plus Isotope Ratio Mass Spectrometry (Thermo Scientific^{TM}) and reported in ‰ vs. VPDB.

Bulk ^{14}C isotope was measured on freeze-dried sediment after carbonate removal at ETH. First, carbonate was removed from sediment samples by HCl fumigation. The sediment samples were then neutralized and combusted into CO_2 and measured with a EA-AMS. Measured $^{14}C/^{12}C$ is reported in $F^{14}C$ (Reimer et al., 2004; Haghipour et al., 2019).

2.6 DNA sequencing and analyses

Three samples at depths of 1.5-2 cm, 20.5-21 cm and 63-64 cm were analyzed for Isochrysidales DNA, following the methods described in Wang et al. (2021). In short, sediment samples were frozen prior to analyses and thawed for 1-2 hours before processing. Around 0.25g of samples were extracted for genomic DNA using DNeasy PowerSoil HTP 96 Kit followed by a two-step PCR. The first PCR amplified V4 SSU rRNA with primer pair 528Flong and PRYM01+7 containing a 5' adaptor (Egge et al., 2013). The second round of PCR was performed to give each sample a unique 12-nucleotide index sequence. Final indexed amplicons from each sample were cleaned and normalized, then pooled together and sequenced on an Illumina NovaSeq (San Diego, CA) using the 6000 SP X - 2x250 v1.5 kit. Sequences were then verified and compiled after denoising. Taxonomy of ESVs was assigned using SILVA reference database. ESVs belonging to the Isochrysidales order were selected and aligned to reference sequences through PyNast (Caporaso et al., 2010; Gran-Stadniczeñko et al., 2017, p.). Phylogenetic tree including recovered sequences and representative Isochrysidales sequences available on GenBank was built through RAxML (Stamatakis, 2014). The ESVs were then

assigned to Group 1a and 1b subgroup based on the phylogeny. Shannon index of each sample was calculated after rarefying all the samples to even sampling depth (Spellerberg & Fedor, 2003).

3. Results

3.1 Age model

^{210}Pb activity showed a slight increase from 0.5 to 7 cm below the sediment surface, but decreased exponentially with depth below 7 cm (Fig. 5. 2a). The linear regression model estimated an average sediment accumulation rate of 0.3061 g/cm^2/yr, and constant-rate-of-supply (CRS) model was calibrated against the linear regression model to match the sediment accumulation rate (Fig. 5. 2b). ^{137}Cs activities in 65-74 cm are significantly above background, and decrease after 74 cm. The ^{137}Cs profile suggests the majority of the ^{137}Cs is from external erosion sources rather than direct deposition from the atmosphere, thus the maximum activity occurring at 73-74 cm section represents the maximum terrestrial ^{137}Cs inventory occurred in 1966. This result is in concordance with the CRS model, which indicates an age of 51.9 yr at 75 cm. Thus the CRS model provides a good estimate of the age of this core from 1958 (86 cm) to 2019 (0 cm).

3.2 GDGTs

The total GDGT flux ranged between 0.008-0.302 ug cm^{-2} yr^{-1}, with an increase over time (Fig. 5. 4a). GDGT distributions are shown in Fig. 5. 3. BrGDGT was the dominant GDGT in the samples (90.31±4.32%). The most abundant brGDGTs are GDGT-IIIa, GDGT-IIIa', GDGT-IIa, GDGT-IIa", GDGT-Ia, while iGDGT was mainly composed of GDGT-0 with very low

GDGT-1, 2, 3, and crenarchaeols. The overall GDGT distribution is very similar to the two river connected lakes in Mackenzie delta (Canadian Arctic) that lies in permafrost zone (Lattaud et al., 2020). The BIT index ranged from 0.99-1.00, suggesting very low crenarchaeol abundance (Fig. 5. 4b). This is similar to BIT values (0.99-1.00) reported in lake sediment and soil from MacKenzie (Canadian Arctic) and Kolyma River basin (Siberian Arctic) and active layer soil from Northern Yakutia (Siberia) (Kusch et al., 2019; Peterse et al., 2014). While Yedoma was reported to have distinctively higher relative crenarchaeol abundances and lower BIT (Kusch et al., 2019; Peterse et al., 2014), BIT values suggest limited GDGT input from Yedoma in White Fish Lake. The $\sum IIIa / \sum IIa$ ratio ranged between 1.66-2.36 (Fig. 5. 4c; mean: 2.06±0.18), which is greater than the upper limit of soil origin $\sum IIIa / \sum IIa$ (0.9), suggesting an aquatic origin of brGDGT in White Fish Lake (Lattaud et al., 2020; Martin et al., 2019). MBT'_{5Me} ranged from 0.18 to 0.26 within the core, with an increase during 1950-1990, and a decrease after 1990 (Fig. 5. 4d).

The isoGDGT is also likely from an aquatic source, supported by the near absence of crenarchaeol isomer (cren') while high-latitude soil generally has a higher cren'/(cren+cren') ratio (Daniels et al., 2021). GDGT-0 comprised the majority of isoGDGT (76.1~96.88%, mean: 88.75±3.70%). The GDGT-0/Cren in White Fish Lake is above the threshold of 2 for anaerobic methanogenesis (Fig. 5. 4e; 4.81-76.47, mean: 35.71±21.59). The MI from White Fish Lake ranged from 0.29 to 0.84 (Fig. 5. 4f; mean: 0.69±0.15). Both MI and GDGT-0/cren suggest substantial methanotrophic/methanogenic activity in White Fish Lake.

3.3Diploptene

Diploptene can originate from methane-oxidizing bacteria (MOB) or other bacteria such as cyanobacteria (Naeher et al., 2014). The flux of diploptene ranged between 0.028-0.954 ug cm^{-2} yr^{-1}, with an average of 0.225±0.188 ug cm^{-2} yr^{-1} (Fig. 5. 8b). The concentration varies annually, however, it shows a significant increase since 2000. The $\delta^{13}C$ of diploptene averaged -55.96 ±3.40‰, with a slight decreasing trend with increasing depth (Fig. 5. 9d).

3.4 Alkenones

The total alkenone flux ranged between 0.125-16.019 ug cm^{-2} yr^{-1}, with an average of 2.246±3.235 ug cm^{-2} yr^{-1} (Fig. 5. 6a). The alkenone flux was low during 1960-1970 and has shown a slight increase since the 1970s, but it has surged dramatically since 2010. The alkenone distribution in White Fish Lake is consistent with the typical Group 1 alkenone profile with predominant $C_{37:4}$Me (%$C_{37:4}$=0.388±0.055) and the presence of $C_{37:3b}$Me isomers (Fig. 5. 3; D'Andrea et al., 2006; Longo et al., 2018). The RIK_{37} ranged between 0.43-0.78, with an average of 0.613±0.068 (Fig. 5. 6b), which agrees with typical Group 1 RIK_{37}<0.63 (Longo et al., 2018). U_{37}^{K} in the sediment decreased around 1980, and increased after 2000 (Fig. 5. 6d).

DNA recovered from sediment samples are in consistent with the alkenone flux and profiles. Isochrysidales DNA was recovered from three samples at 1.5-2 cm, 10.5-11 cm, 20.5-21 cm and 63-64 cm, and 14848, 7109, 2326 and 1284 Isochrysidales reads were recovered from each sample (Table 1). All Isochrysidales sequences detected from White Fish Lake falls into Group 1 Isochrysidales based on phylogeny. The four samples share the same predominant ESV, which falls into Group 1a. Both Group 1a and Group 1b were detected in 1.5-2 cm and 10.5-11 cm, with Group 1b composing 25% and 5.9% total Isochrysidales reads. However, only Group 1a were detected from samples 20.5-21 cm (7 ESVs) and 63-64 cm (3 ESVs).

The alkenones from White Fish Lake sediment are very depleted in ^{13}C (Fig. 5. 9; $C_{37:4}Me$: -44.348±0.838, $C_{37:3}Me$: -43.172±0.924, $C_{38:4}Et$: -45.326±0.844).

3.5n-Alkanes

n-Alkanes from C_{16}-C_{33} were detected in all samples. The n-alkanes flux ranged between 1.75-11.73 ug cm^{-2} yr^{-1}, and increased over time (Fig. 5. 8a). The CPI_{23-33} index ranged between 3.86-6.36 with an average value of 5.31±0.72, no significant long term increase or decrease was detected for CPI_{23-33} (Fig. 5. 8c). The CPI value is comparable with surface sediment samples collected from 24 lakes near Toolik Field Station, Alaska (5.0±0.8, Daniels et al., 2017), reflecting limited degradation.

The ACL_{20-33} value ranged between 25.75-26.89, with an average of 26.26±0.24 (Fig. 5. 8d). C_{27} is the most abundant n-alkane in all samples, followed by C_{23} and C_{25} (Fig. 5. 7). The ACL_{20-33} decreased consistently during the 1960s to 1980s, and slightly increased during the 1990s to 2010s. P_{aq} increase overtime while P_{wax} decrease, suggesting an increase in relative contribution from the lake's production compared to surrounding plants (Fig. 5. 8e, f).

The $\delta^{13}C$ values of n-alkanes are shown below, C_{23}, C_{29} and C_{31} did not show significant trends along the core, while C_{25} and C_{27} showed slight depleting trends from the late 1950s to more recent samples (Fig. 5. 9).

3.6Bulk Isotope

The TOC $\delta^{13}C$ ranged from -28.874-31.641‰ with an average value of -30.212±0.589‰ (Fig. 5. 10a). The $\delta^{13}C$ shows a strong depleting trend over time. The $\delta^{13}C$ is comparable to the Holocene sediment from Goltsovoye Lake, Northern Siberia (range: -31.2 ~-27.0‰, median: -

28.2‰; Jongejans et al., 2020), where the section marked the transition from wetland to thermokarst lake, during which period the organic matter sourced from both in situ productivity and allochthonous Yedoma carbon, and talik expand led to Yedoma thaw creating high methane production (Jongejans et al., 2020). The TOC $\delta^{13}C$ is also similar to sediment core spanning a similar time period, from Lake T15, Seward Peninsula (1964-2010, −30.0‰ to −30.5‰, consistent decreasing trend; Medeiros et al., 2014) and Disko 2, west Greenland (~ -28‰; Stevenson et al., 2021).

The TOC $F^{14}C$ ranged from 0.5974-0.6785, corresponding to radiocarbon age ranging from 4138±72 - 3115±75 year BP (Fig. 5. 10b). The averaged radiocarbon age of the TOC is 3440 year BP, which is significantly older than ^{210}Pb dating results.

4. Discussion

4.1 The lake ecosystem

4.1.1 Methanogens

The BIT and ΣIIIa/ΣIIa index suggest *in situ* aquatic production of GDGTs and limited soil input from the catchment. We applied principal component analysis (PCA) on the fractional abundance of major GDGTs in order to track the most prominent changes in GDGTs. The results show PC1 and PC2 account for 49.38% and 20.85% of the total variance, respectively (Fig. 5. 11a). GDGT-0, -III, -III" have negative loadings on PC1 while the other GDGTs all have positive loadings. The upper 2 meters of White Fish Lake are oxygenated and the water below 3 meter is anoxic. Interestingly, GDGT-0, -IIIa, and -IIIa" are all associated with anoxic/methanogenic conditions (Weber et al., 2018; Yao et al., 2020). A study in a meromictic lake (Lake Lugano, Swizzerland) shows that while IIIa' is mainly produced in the lower part of the oxygenated water column, IIIa" is exclusively produced by anaerobic bacteria within deep water, and IIIa could be produced by both aerobic and anaerobic bacteria (Weber et al., 2018). Weber et al. (2018) also found that the $\delta^{13}C$ content of IIIa and IIIa" become significantly more depleted than $\delta^{13}C$ of IIIa' below the oxic-anoxic transition zone within the same lake, where the concentration of methane increases. Thus the production of IIIa and IIIa" is likely fueled by carbon derived from methanotrophic bacteria (Weber et al., 2018). A positive correlation between the relative abundance of IIIa compared to IIa and lake water depth has also been observed in stratified volcanic lakes in northeastern China (Yao et al., 2020). GDGT-0 is likely produced by acetoclastic methanogens in the anoxic parts of lake sediments and overlying water (Naeher et al., 2014; Lattaud et al., 2020). Thus PC1 separates GDGTs associated with different

redox states, with anoxic conditions on the left and oxic conditions on the right of the PCA biplot.

When plotting the time series of the PCs, PC1 aligns very well with MI (Fig. 5. 11b). This agrees with the sample scatter on PCA biplot, where samples from the 1950s, 1960s and 2010s are scattered on the left (anoxic), while other samples are scattered on the right (oxic). An MI value >0.5 suggests significant iGDGT contribution from methanotrophic Euryarchaeota (Zhang et al., 2011). Based on this threshold, iGDGT in sediments from ~1958-1982 and after the 2010s are affected by methanotrophic Euryarchaeota, which suggests significant anaerobic methane oxidization activities.

The reconstructed JJAS (Stefanescu et al. (2021) calibration) aligns well with instrumental record from Kotzebue Station from 1960-2000, and the MBT'$_{5Me}$ reconstructed JJAS temperature diverge from instrumental record since 2000 showing a decrease in reconstructed temperature instead (Fig. 5. 17d). There are several potential reasons for the divergent trend after 2000: 1) More brGDGT been produced in deeper part of the water column compared to shallower part leading to a bias to deep water temperature; 2) Anoxic condition at lake bottom and increased IIIa production from bacteria favoring anoxic environments (Weber et al., 2018; Yao et al., 2020; Stefanescu et al., 2021); 3) Increased stratification in the lake increases the gap between water temperature and JJAS air temperature; 4) Input of brGDGT from lake surroundings.

4.1.2 Methanotrophs

Methane can be oxidized by bacteria aerobically, where oxygen and methane are combined to form formaldehyde and incorporated into the biomass. Methane oxidizing bacteria (MOB)

produce diverse lipids, including hopanoids, such as diploptene. Though diploptene has a wide range of bacterial producers, depleted ^{13}C of diploptene can suggest a MOB origin due to the depleted ^{13}C of methane and the strong isotopic fractionation during lipid biosynthesis (Summons et al., 1994; Thiel, 2020).

Depleted $\delta^{13}C$ of diploptene interpreted as evidence for MOB has been reported in surface sediment from thermokarst lakes with methane ebullition in Alaska (-68.2~-38.8‰; Davies et al., 2016), downcore samples from a eutrophic lake in Switzerland (-60~-43‰; Naeher et al., 2014) and volcanic lake in Northeast China (-50.3‰±1.9‰), and peat samples from global peatlands (-45~-29‰; Inglis et al., 2019). The $\delta^{13}C$ content of diploptene from our site is consistent with these prior observations, with an average value of -55.96 ±3.40‰, thus suggesting a prominent MOB production. The $\delta^{13}C$ fluctuates and show a slightly enriched trend over time. Multiple potential causes can lead to fluctuation in diploptene $\delta^{13}C$: 1) different ratios between diploptene produced by ^{13}C-depleted MOB and ^{13}C-enriched heterotrophic bacteria (Davies et al., 2016); 2) different ratio between Type I and Type II MOB, where Type II MOB also use CO_2 as carbon source which can dilute the ^{13}C signal from methane (van Winden et al., 2012); 3) changes in methane availability that leads to different isotopic fractionation rate; 4) High spatial heterogeneity of MOB within the same lake (Davies et al., 2016).

The flux of ^{13}C-depleted diploptene in White Fish Lake increased drastically after 2010 (Fig. 5. 8b). A similar phenomenon has been observed in other lakes. Naeher et al. (2014) observed a high concentration of diploptene with strongly negative $\delta^{13}C$ coincides with peak CH_4 production in Lake Rotsee, Switzerland, during the 1920s-1030s. Yao et al. (2021) observed a drastic increase of ^{13}C-depleted diploptene in Wudalianchi, China, since 1975 as regional permafrost thaws and methane cycling within the lake intensified. A high-closure lake with

seasonal anoxic bottom from Canadian Arctic showed ^{13}C-depleted diploptene concentration in downcore sediment increase as regional air temperature rise since 1960 (Lattaud et al., 2020). The increased flux of diploptene since 2010 likely indicate increased aerobic methanotrophy by bacteria in White Fish Lake.

4.1.3 Primary productivity: Haptophyte algae

All DNA Isochrysidales sequences recovered from four samples from White Fish Lake sediments belong to Group 1 Isochrysidales based on the phylogenetic tree. The sequences could be further separated into 1a phylotype and 1b phylotype. Richter et al. (2019) examined a suite of oligotrophic freshwater lakes in the North Slope of Alaska. Both phylotypes were detected in all the lakes from the water column and surface sediment. The 1b phylotype was originally discovered from a eutrophic lake Etang des Vallees in France (Simon et al., 2013). Though 1a phylotype was not detected in Etang des Vallees, it was potentially due to the limitation of the primers used by Simon et al. (2013), so we cannot conclusively determine if 1b and 1a phylotypes prefer different nutrient level. In sum, while both phylotypes belong to Group 1 and live in low salinity habitats, 1a phylotype is mainly detected in oligotrophic-mesotrophic environments (Theroux et al., 2010; Longo et al., 2018), 1b phylotype is found in both oligotrophic and eutrophic environments (Simon et al., 2013; Richter et al., 2019). The alkenone production difference between the two subgroups is not larger than the differences within the subgroups. Relatively low $\%C_{37:4}$ has been observed in both 1a-dominant and 1b-dominant lakes (Baejarvotn, 1a-dominanted, $\%C_{37:4}$ =35.09, Etang des Vallees, 1b-dominanted, $\%C_{37:4}$ =36.47).

The number of Isochrysidales reads recovered increased drastically in the most recent samples, though the total read number might be influenced by preservation. This increase is

consistent with the drastic increase in alkenone flux, thus likely reflecting an actual increase in alkenone producer biomass. The most abundant Greenland phylotype sequence ESV_000278 was detected in all samples and was the dominant sequence in all samples. ESV_000278 is phylogenetically close to Soligotype 2 in Richter et al. (2019), which was the most abundant sequence in all the samples they examined from Alaska North Slope lakes. Percentage read and percentage ESVs contributed by 1a phytlotype decreased from 100% to 75.0% and 16.2% respectively from 63-64 cm to 1.5-2 cm, and the Shannon Index increased (Table 1). The DNA results suggest a drastic increase in alkenone producer diversity, and an emergence of 1b phylotypes potentially indicate lake nutrient level change .

The U_{37}^{K} from White Fish Lake yield realistic MJJA temperature based on this calibration, though the temperature range was larger than monitored MJJA air temperature from Kotzebue Station (Fig. 5. 12a). Differences between lake water temperature and air temperature, as well as changes in alkenone producer community as observed from DNA data can contribute to the discrepancy between U_{37}^{K}-reconstructed temperature and monitored air temperature. SPM samples from Toolik Lake water column collected during June-July 2013 showed a strong correlation between U_{37}^{K} and U_{38Me}^{K} (r^2=0.91, Fig. 5. 12b), but the correlation is much weaker in White Fish Lake downcore samples (r^2=0.43, Fig. 5. 12c). This proves that the alkenones in the sediment core are produced by multiple species mixing in variable ratios.

The $\delta^{13}C$ content alkenones at White Fish Lake are extremely depleted compared to Ace lake, Antarctica (averaged C37 alkenones: -31.7~-36.1‰, Schouten et al., 2001), Gulf of Alaska ($C_{37:4}$Me: -24.8~-27.79‰, $C_{37:3}$Me:-24.0~-27.4‰, unpublished) and similar to the values observed in Greenland lakes ($C_{37:4}$Me: -40.8~-41.7‰, $C_{37:3}$Me:-40.0~-41.0‰, D'Andrea & Huang, 2005). The alkenones in White Fish Lake are also significantly more depleted in $\delta^{13}C$

compared to n-alkanes (Fig. 5. 9). Both the fractionation during alkenone synthesis and CO_2 source can result in the extreme depletion: 1) Group 1 Isochrysidales might have stronger fractionation comparing to Group 2 and Group 3, which are the main alkenone producers in Ace Lake and Gulf of Alaska (Richter et al., 2019); 2) Low water temperature may result in high solubility of CO_2 in the lake, and the surplus of dissolved CO_2 leads to higher fractionation in algal productivity (Schouten et al., 2001); 3) The CO_2 might be derived from degradation of organic matter in the lake or surrounding catchment in addition to CO_2 exchange with the atmosphere during summer. During winter, ice cover on the lake would further limit the exchange of CO_2 between water column and atmosphere, potentially driving increases in dissolved CO_2 concentration (Schouten et al., 2001; D'Andrea & Huang, 2005). The averaged alkenones $\delta^{13}C$ did not show long-term trend in White Fish Lake. However, alkenone flux increased around 50 times from 1958 to 2018 which would lead to weaker fractionation and more enriched alkenones $\delta^{13}C$. A relatively stable $\delta^{13}C$ trend potentially suggests a more depleted CO_2 source in recent years.

4.1.4 Surrounding plants: *Sphagnum* and higher plants

n-alkanes deposited in the lake could originate from the autochthonous primary productivity, or through lateral hydrologic transport (e.g., runoff, groundwater) and aeolian transport from the surrounding catchment and region. The land cover surrounding the lake is dominated by herbaceous plants followed by shrubs, sparsely vegetated ground and fens (NASA ABoVE satellite data). During the period of 2000-2012, the White Fish Lake catchment has undergone a decrease in herbaceous land cover, and an increase in shrubland and fen (NASA ABoVE), consistent with both shrubification and possible permafrost thaw (Jorgenson et al., 2001; Tape et

al., 2006). Pearson correlation between the relative abundance of C21, C23 and C25 is high, suggesting they were largely contributed from the same plant source (Fig. 5. 13). The concentration of C23 and C25 are similar throughout the core and slightly higher than C21, which is similar to the n-alkane distribution of *Sphagnum* spp. mosses (Bingham et al., 2010; Ronkainen et al., 2013). C29 and C31 are highly correlated and of similar concentration, which could be contributed from shrubs such as dwarfed birch (*Betula nana*). The relative abundance of shorter chain n-alkanes C17 and C19 are negatively correlated from mid-to-long chain n-alkanes, suggesting a separate aquatic source (e.g. algae).

A similar pattern is also shown in the PCA biplot (Fig. 5. 14a). The loading directions separate n-alkanes into three origins: aquatic (C17-C19), terrestrial mosses (C21-C25), shrubs and grass (C27-C33). The oldest samples from the 1950s and 1960s are clustered on the right side of the biplot along with C27-C33, suggesting a higher contribution from herbaceous plants. The younger samples are scattered on the left side of the biplot with higher C21-C25 suggesting increased input from mosses, and particularly the most recent samples from the 2010s are clustered close to C17, suggesting an increased aquatic contribution. The most important principle component PC1 is mainly contributed by C21-C23 and C27-C31 with opposite contributions. Interestingly, the trend of PC1 shows high similarity with ACL along the core (Fig. 5. 14b). This suggests that changes in ACL is a prominent difference between samples before and after the 1980s, and those changes are driven by ratios between n-alkane contribution from mosses (C21-C23) and shrubs (C27-C31).

The *Sphagnum* derived C25 shows a slight ^{13}C-depleting trend over time, while sedge/shrub derived C29 and C31 do not show a similar trend in ^{13}C (Fig. 5. 9). This is potentially related to *Sphagnum*-associated methane oxidation (Kip et al., 2010; Inglis et al., 2019; Winden et al.,

2020). Kip et al. (2010) showed that methane oxidation is ubiquitous among submerged *Sphagnum* mosses, where endophytic methanotrophic bacteria provide methane-derived CO_2 to sphagnum and *Sphagnum* provide oxygen for methanotrophic bacteria. Increased submerged *Sphagnum* could lead to a depleted ^{13}C in *Sphagnum* n-alkanes.

However, C23 and C25 alkanes are not more depleted than C29 and C31 alkanes, suggesting that the influence from *Sphagnum*-associated methanotrophy might be limited. A similar ^{13}C depleting trend is also observed in C27 alkane, which is not abundantly produced by *Sphagnum*. Altogether, the observed trend could also be a result of changes in ratios between plants with different fractionation, e.g., aquatic vs. semi-aquatic mosses.

Combining satellite data from 2000-2012 (ABOVE), the lake catchment/basin has shown a continuous increase in areal extent of shrubland and fen (where *Sphagnum* is potentially the dominant moss) which is fed by groundwater. The ACL of n-alkanes could be explained by the continuous increase of aquatic plants and mosses since the 1950s, and an increase of shrubs since the 1990s.

4.2 Carbon cycle in the lake

To summarize the biomarker results discussed above, a schematic of the carbon cycle within White Fish Lake is illustrated in Fig. 5. 15. The $F^{14}C$ of bulk TOC is significantly older than the deposition age of the lake sediments, suggesting carbon input from surrounding permafrost and active layer. The remobilized old organic matter fuels the carbon cycle within the lake. Methanogens reside in the anoxic lake sediments and overlying bottom waters, where organic carbon from lake productivity and terrestrial C input (DOC + POM) from the catchment is transformed/mineralized into CH_4 and CO_2 through the acetoclastic pathway ($CH_3COOH \rightarrow$

$CH_4 + CO_2$; Lattaud et al., 2020; Thiel, 2020). During winter, organic matter produced by algae and other primary producers is oxidized and the exchange between atmosphere and lake water is blocked by ice, driving the drawdown of dissolved oxygen and strengthen the anoxic environment for methanogenic activity. The methane produced in anoxic sediments and surface water as well as transported from surrounding permafrost thaw then diffuse into the oxic part of the water column and oxidized into CO_2 by MOB ($CH_4 + O_2 \rightarrow 2CO_2 + 2H_2O$). MOB may be promoted by symbiosis with submerged *Sphagnum* mosses (Kip et al., 2010; Inglis et al., 2019; Winden et al., 2020). Anaerobic oxidation of methane using sulfate as electron acceptor is also possible in the lake ($CH_4 + SO_4^{2-} \rightarrow HCO_3^- + HS^- + H_2O$), however, White Fish Lake has exceedingly low sulfate concentration, which might limit this process. Thus methane is likely oxidized mostly by MOB aerobically, instead of anaerobic oxidation of methane. CO_2 produced in this process can then be utilized by algae for photosynthesis. The biomass produced by primary production is then deposited into the lake sediment, where it can be decomposed and utilized by methanogens.

The transport of DOC from the surrounding terrestrial ecosystem to White Fish Lake is likely an important component of the catchment carbon budget. DOC concentration is relatively high in lake water, ranging from 10-13 mgC L^{-1}. Lake dissolved organic matter (DOM) appears to be primarily of terrestrial origin, given the low fluorescence index values (FI = 1.2; McKnight et al., 2001) and relatively high fraction of aromatic compounds (as evidenced by specific ultraviolet absorbance at 254 nm, or $SUVA_{254}$, ranging from 2.5-3.5 L mgC^{-1} m^{-1}; Weishaar et al., 2003). Aromatic DOM absorbs light, which can influence rates of primary productivity and can contribute to lake browning (Williamson et al., 2016). The absorption of photosynthetically active radiation (PAR) in the epilimnion by aromatic DOM can facilitate thermal stratification

(Burpee & Saros, 2020). A stronger stratification leads to more prominent bottom water anoxia, which promotes methanogenesis and release of sediment phosphorus that was originally bonded to metal oxides (mainly Al and Fe; Wu et al., 2014). The phosphorus released into the water column elevates the lake's trophic state and stimulates algae bloom, forming positive feedback to redox stratification. As permafrost thaws and active layer thickness increases, a shift in subsurface hydrology can impact the concentration, age, and chemical composition of DOM in Arctic surface waters (O'Donnell et al. 2014, 2016). Some evidence indicates that increases in active layer thickening could reduce the amount and aromaticity of DOM in surface water, which in turn could alter both primary productivity and thermal stratification. Large uncertainties exist however about the fate of terrestrial DOC under climate change and permafrost thaw, and how these changes may alter lake ecosystem function.

The TOC is $\delta^{13}C$-depleted compared to other surface lake sediments and deposits reported in the region (Fig. 5. 16; Drained thermokarst lake basins: -31.8~-27.6‰; thermokarst lakes: -27.4~-30.5‰; Medeiros et al., 2014; Lenz et al., 2016; Jongejans et al., 2018). There are multiple reasons that could affect the $\delta^{13}C$ values of bulk sediment. Factors leading to enrichment include: 1) Increased incorporation of atmospheric CO_2; 2) Increased lake productivity would reduce biological fractionation leading to more enriched ^{13}C biomass that later deposits into the sediment. The factors leading to a depleting bulk ^{13}C include: 1) Direct input from decomposed permafrost released DOM and POM that has a lower $\delta^{13}C$ values and in-lake respiration of those substrates (Wild et al., 2019); 2) Input of low $\delta^{13}C$ CH_4 from degrading permafrost through diffusion (Walter et al., 2008); 3) Increased methanotrophy, as MOB preferentially utilize ^{12}C, and the fractionation could approach $\alpha_{CH4-CH3OH} \sim 1.035$ when there is an excess of methane or limitation in O_2 (Templeton et al., 2006); 4) Primary productivity incorporate methane-derived

CO_2 into biomass and the carbon recycling within the lake; 5) Suess effect that suggests a depleting trend in atmospheric CO_2 due to fossil fuel burning.

4.3Implications for changes in Yedoma permafrost

The biomarker composition and carbon isotope in White Fish Lake shed light on changes in permafrost in the Seward Peninsula. The White Fish Lake basin is situated within a region containing thick deposits of ice-rich Pleistocene permafrost, commonly referred to as Yedoma (Strauss et al., 2021). Large amounts of organic carbon are stored in Yedoma, which are sensitive to mobilization upon thaw. Warming air temperatures and changing precipitation patters can lead to permafrost thaw, both through active layer thickeningand thermokarst formation, with subsequent carbon-cycle feedbacks (Anthony et al., 2014; Strauss et al., 2021). As the air temperature rise recorded by Kotzebue Meteorology Station, averaged modeled active layer depth around White Fish Lake has increased from ~0.75 m to ~1.1 m from 1950 to 2020 (Fig. 5. 6).

Pronounced permafrost thaw and widespread thermokarst lake formation were observed at Early Holocene as the region became warmer and wetter compared to Pleistocene (Kaufman et al., 2016; Lenz et al., 2016). Lenz et al. (2016) reported a decrease of bulk $\delta^{13}C$ from -26.4 to -28.1 ‰ from a sediment core recovered from the center of a thermokarst drained basin located on northern coastal Seward (66.5658˚N, 164.4814˚W) from 11800 cal. a BP to ~1060 cal. a BP, as the thermokarst lake expand into Yedoma and release a large amount of methane that were subsequently incorporated into the aquatic system (Anthony et al., 2014; Lenz et al., 2016).

Significant changes in landscape associated with permafrost destabilization have also been observed in a much shorter timescale within decades or years (Nitze et al., 2018; Swanson,

2019). While the Northern Seward Peninsula is still covered by continuous permafrost, the middle Seward partially lies in the discontinuous permafrost zone (Debolskiy et al., n.d.). Lake T15 (65.2326˚N, 164.8232˚W) lies on the modern boundary between continuous and discontinuous permafrost zone (Medeiros et al., 2014). Since 1920, the lake surrounding has developed talik that is unfrozen year-round between the active layer and permafrost (Fig. 5. 18), and the lake basin has witnessed pronounced shrub expansion and growth since 1972 (Medeiros et al., 2014). Similar to White Fish Lake and Wudalianchi Lake in Northeastern China, T15 downcore sediment showed a depleting trend in bulk $\delta^{13}C$ from -29.2 to -30.6‰ from 1920 to 2010. Flooding and expansion of Lake T15 thermokarst basin that leads to more soil input since the late 1950s as suggested by geochemical and biotic analysis is in concordance of the emergence of talik from model.

Lake T15 can be viewed as an analog of future White Fish Lake as the boundary between continuous and discontinuous permafrost continue to shift Northward. While thermokarst lakes are underlain by talik that directly supply remobilized old carbon to the lake, maar lakes are underlain by volcanic rocks. Thus organic carbon and nutrients supplied into the lake are more likely through lateral transport from surrounding permafrost on a broader scale. The rapid changes observed in White Fish Lake may relate to large-scale destabilization of Yedoma in Northern Alaska and Siberia. Ecological changes resulted from permafrost thaw, such as enhanced shrub abundance, as already observed around White Fish Lake and broader Alaska (Myers-Smith et al., 2011). Those changes are expected to continue as Alaska gets warmer and wetter in the near future.

5. Conclusions

Carbon isotopes suggest significant permafrost carbon input into White Fish Lake since at least the late 1950s. The lipid biomarkers, including alkenones, n-alkanes, GDGTs and diploptene, as well as carbon isotope composition, were able to capture changes in primary productivity, methanogenesis, methanotrophy, and vegetation in White Fish Lake catchment since the late 1950s. GDGT and $\delta^{13}C$-depleted diploptene suggest significant methanogenic and methanotrophic activities in the lake with an increase after 2010s. Alkenone producer diversity and alkenone production increased throughout the core, with emergence of Group 1b Isochrysidales around 2010. The change of community composition could be related to change of nutrient state in the lake. The $\delta^{13}C$ of alkenones were very depleted, which is likely a combination of large fractionation during Group 1 Isochrysidales carbon fixation and biosynthesis, and recycling of CH_4-derived CO_2. The ^{14}C age of bulk TOC is significantly older than ^{210}Pb-dated age of the sediment core, suggesting older carbon source likely from permafrost thaw around the catchment. The $\delta^{13}C$ showed a depleting trend overtime, which suggest intensified carbon-cycling in the lake. Those changes are likely a result of carbon and nutrient input from thawing Yedoma permafrost, which is also consistent with observed shrubification around the lake. Air temperature and active layer thickness have drastically increased in this region since the 2010s, intensifying the changes in the past few decades. We expect the trend continues as the region becomes warmer and wetter in the coming decades (IPCC WGI Interactive Atlas: Regional information). Our study suggests maar lakes effectively capture shifts in terrestrial and aquatic ecosystem processes, including carbon-cycle processes associated with warming and permafrost thaw, and are valuable archives for permafrost research on longer timescales spanning the Late Pleistocene and Holocene.

To understand the exact age and origin of permafrost input into White Fish Lake, future work would benefit from compound-specific radiocarbon dating of terrestrial material (e.g. lignin derived from vascular plants). Mercury accumulation rate in sediment and its isotopic composition can also indicate permafrost input, as large amounts of mercury are deposited into the permafrost atmospherically, and thawing of permafrost could release mercury into lakes (Rydberg et al., 2010). Dual-carbon isotope (^{14}C and ^{13}C of bulk TOC) mixing model would be able to estimate relative contribution of carbon from permafrost source, contemporary source and *in situ* autochthonous source with reliable estimation of end-member carbon isotope composition (Mann et al., 2015). The ratio between TOC and TON (C/N) would also indicate the source of organic matter in the sediment, as terrestrial input has a higher C/N (Jongejans et al., 2018). Compound specific ^{13}C of GDGTs would quantify the methanogenic activities, as methanotrophic Archaea produce $\delta^{13}C$-depleted GDGTs (Lattaud et al., 2021). Extent of methanotrophic activity can be estimated by measuring the concentration of MOB biomarkers, such as unsaturated C16 and C18 fatty acids, and bacteriohopanepolyols (Thiel et al., 2020).

Reference

Anthony, K. M. W., Zimov, S. A., Grosse, G., Jones, M. C., Anthony, P. M., Iii, F. S. C., Finlay, J. C., Mack, M. C., Davydov, S., Frenzel, P., & Frolking, S. (2014). A shift of thermokarst lakes from carbon sources to sinks during the Holocene epoch. Nature, 511(7510), 452–456. https://doi.org/10.1038/nature13560

Begét, J. E., Hopkins, D. M., & Charron, S. D. (1996). The Largest Known Maars on Earth, Seward Peninsula, Northwest Alaska. Arctic, 49(1), 62–69.

Bingham, E. M., McClymont, E. L., Väliranta, M., Mauquoy, D., Roberts, Z., Chambers, F. M., Pancost, R. D., & Evershed, R. P. (2010). Conservative composition of n-alkane biomarkers in Sphagnum species: Implications for palaeoclimate reconstruction in ombrotrophic peat bogs. Organic Geochemistry, 41(2), 214–220. https://doi.org/10.1016/j.orggeochem.2009.06.010

Bkay, E. E. (n.d.). Distribution of n-pamlEns as a clue to recognition of source beds. 14.

Brassell, S. C., Eglinton, G., Marlowe, I. T., Pflaumann, U., & Sarnthein, M. (1986). Molecular stratigraphy: A new tool for climatic assessment. Nature, 320(6058), 129–133. https://doi.org/10.1038/320129a0

Burpee, B. T., & Saros, J. E. (2020). Cross-ecosystem nutrient subsidies in Arctic and alpine lakes: Implications of global change for remote lakes. Environmental Science: Processes & Impacts, 22(5), 1166–1189. https://doi.org/10.1039/C9EM00528E

Caporaso, J. G., Bittinger, K., Bushman, F. D., DeSantis, T. Z., Andersen, G. L., & Knight, R. (2010). PyNAST: A flexible tool for aligning sequences to a template alignment. Bioinformatics, 26(2), 266–267. https://doi.org/10.1093/bioinformatics/btp636

D'Andrea, W. J., & Huang, Y. (2005). Long chain alkenones in Greenland lake sediments: Low δ13C values and exceptional abundance. Organic Geochemistry, 36(9), 1234–1241. https://doi.org/10.1016/j.orggeochem.2005.05.001

D'Andrea, W. J., Lage, M., Martiny, J. B. H., Laatsch, A. D., Amaral-Zettler, L. A., Sogin, M. L., & Huang, Y. (2006). Alkenone producers inferred from well-preserved 18S rDNA in Greenland lake sediments. Journal of Geophysical Research, 111(G3). https://doi.org/10.1029/2005JG000121

Daniels, W. C., Castañeda, I. S., Salacup, J. M., Habicht, M. H., Lindberg, K. R., & Brigham-Grette, J. (2021). Archaeal lipids reveal climate-driven changes in microbial ecology at Lake El' gygytgyn (Far East Russia) during the Plio-Pleistocene. Journal of Quaternary Science, jqs.3347. https://doi.org/10.1002/jqs.3347

Daniels, W. C., Russell, J. M., Giblin, A. E., Welker, J. M., Klein, E. S., & Huang, Y. (2017). Hydrogen isotope fractionation in leaf waxes in the Alaskan Arctic tundra. Geochimica et Cosmochimica Acta, 213, 216–236. https://doi.org/10.1016/j.gca.2017.06.028

Davies, K. L., Pancost, R. D., Edwards, M. E., Walter Anthony, K. M., Langdon, P. G., & Chaves Torres, L. (2016). Diploptene <i>δ</i>¹³C values from contemporary thermokarst lake sediments show complex spatial variation. Biogeosciences, 13(8), 2611–2621. https://doi.org/10.5194/bg-13-2611-2016

De Jonge, C., Hopmans, E. C., Zell, C. I., Kim, J.-H., Schouten, S., & Sinninghe Damsté, J. S. (2014). Occurrence and abundance of 6-methyl branched glycerol dialkyl glycerol tetraethers in soils: Implications for palaeoclimate reconstruction. Geochimica et Cosmochimica Acta, 141, 97–112. https://doi.org/10.1016/j.gca.2014.06.013

Debolskiy, M. V., Nicolsky, D. J., Hock, R., & Romanovsky, V. E. (n.d.). Modeling Present and Future Permafrost Distribution at the Seward Peninsula, Alaska. Journal of Geophysical Research, 24.

Discussion: Reporting and Calibration of Post-Bomb 14 C Data. (2004). Radiocarbon, 46(3), 1299–1304. https://doi.org/10.1017/S0033822200033154

Egge, E., Bittner, L., Andersen, T., Audic, S., de Vargas, C., & Edvardsen, B. (2013). 454 Pyrosequencing to Describe Microbial Eukaryotic Community Composition, Diversity and Relative Abundance: A Test for Marine Haptophytes. PLoS ONE, 8(9), e74371. https://doi.org/10.1371/journal.pone.0074371

Eglinton, T. I., & Eglinton, G. (2008). Molecular proxies for paleoclimatology. Earth and Planetary Science Letters, 275(1–2), 1–16. https://doi.org/10.1016/j.epsl.2008.07.012

Engram, M., Walter Anthony, K. M., Sachs, T., Kohnert, K., Serafimovich, A., Grosse, G., & Meyer, F. J. (2020). Remote sensing northern lake methane ebullition. Nature Climate Change, 10(6), 511–517. https://doi.org/10.1038/s41558-020-0762-8

Gran-Stadniczeñko, S., Šupraha, L., Egge, E. D., & Edvardsen, B. (2017). Haptophyte Diversity and Vertical Distribution Explored by 18S and 28S Ribosomal RNA Gene Metabarcoding and Scanning Electron Microscopy. Journal of Eukaryotic Microbiology, 64(4), 514–532. https://doi.org/10.1111/jeu.12388

Haghipour, N., Ausin, B., Usman, M. O., Ishikawa, N., Wacker, L., Welte, C., Ueda, K., & Eglinton, T. I. (2019). Compound-Specific Radiocarbon Analysis by Elemental Analyzer–Accelerator Mass Spectrometry: Precision and Limitations. Analytical Chemistry, 91(3), 2042–2049. https://doi.org/10.1021/acs.analchem.8b04491

Han, J., & Calvin, M. (1969). HYDROCARBON DISTRIBUTION OF ALGAE AND BACTERIA, AND MICROBIOLOGICAL ACTIVITY IN SEDIMENTS. Proceedings of the National Academy of Sciences, 64(2), 436–443. https://doi.org/10.1073/pnas.64.2.436

Hopmans, E. C., Weijers, J. W. H., Schefuß, E., Herfort, L., Sinninghe Damsté, J. S., & Schouten, S. (2004). A novel proxy for terrestrial organic matter in sediments based on branched and isoprenoid tetraether lipids. Earth and Planetary Science Letters, 224(1–2), 107–116. https://doi.org/10.1016/j.epsl.2004.05.012

Inglis, G. N., Naafs, B. D. A., Zheng, Y., Schellekens, J., & Pancost, R. D. (2019). Δ13C values of bacterial hopanoids and leaf waxes as tracers for methanotrophy in peatlands. Geochimica et Cosmochimica Acta, 260, 244–256. https://doi.org/10.1016/j.gca.2019.06.030

Jongejans, L. L., Mangelsdorf, K., Schirrmeister, L., Grigoriev, M. N., Maksimov, G. M., Biskaborn, B. K., Grosse, G., & Strauss, J. (2020). N-Alkane Characteristics of Thawed Permafrost Deposits Below a Thermokarst Lake on Bykovsky Peninsula, Northeastern Siberia. Frontiers in Environmental Science, 8. https://doi.org/10.3389/fenvs.2020.00118

Jongejans, L. L., Strauss, J., Lenz, J., Peterse, F., Mangelsdorf, K., Fuchs, M., & Grosse, G. (2018). Organic matter characteristics in yedoma and thermokarst deposits on Baldwin Peninsula, west Alaska. Biogeosciences, 15(20), 6033–6048. https://doi.org/10.5194/bg-15-6033-2018

Jorgenson, M. T., Racine, C. H., Walters, J. C., & Osterkamp, T. E. (n.d.). Permafrost Degradation and Ecological Changes Associated with a WarmingClimate in Central Alaska. 29.

Jorgenson, M. T., & Shur, Y. (2007). Evolution of lakes and basins in northern Alaska and discussion of the thaw lake cycle. Journal of Geophysical Research, 112(F2), F02S17. https://doi.org/10.1029/2006JF000531

Kaufman, D. S., Axford, Y. L., Henderson, A. C. G., McKay, N. P., Oswald, W. W., Saenger, C., Anderson, R. S., Bailey, H. L., Clegg, B., Gajewski, K., Hu, F. S., Jones, M. C., Massa, C., Routson, C. C., Werner, A., Wooller, M. J., & Yu, Z. (2016). Holocene climate changes in eastern Beringia (NW North America) – A systematic review of multi-proxy evidence. Quaternary Science Reviews, 147, 312–339. https://doi.org/10.1016/j.quascirev.2015.10.021

Kip, N., van Winden, J. F., Pan, Y., Bodrossy, L., Reichart, G.-J., Smolders, A. J. P., Jetten, M. S. M., Damsté, J. S. S., & Op den Camp, H. J. M. (2010). Global prevalence of methane oxidation by symbiotic bacteria in peat-moss ecosystems. Nature Geoscience, 3(9), 617–621. https://doi.org/10.1038/ngeo939

Kuhn, M. A., Varner, R. K., Bastviken, D., Crill, P., MacIntyre, S., Turetsky, M., Walter Anthony, K., McGuire, A. D., & Olefeldt, D. (2021). BAWLD-CH₄: A comprehensive dataset of methane fluxes from boreal and arctic ecosystems. Earth System Science Data, 13(11), 5151–5189. https://doi.org/10.5194/essd-13-5151-2021

Kusch, S., Winterfeld, M., Mollenhauer, G., Höfle, S. T., Schirrmeister, L., Schwamborn, G., & Rethemeyer, J. (2019). Glycerol dialkyl glycerol tetraethers (GDGTs) in high latitude Siberian permafrost: Diversity, environmental controls, and implications for proxy applications. Organic Geochemistry, 136, 103888. https://doi.org/10.1016/j.orggeochem.2019.06.009

Łącka, M., Pawłowska, J., & Zajączkowski, M. (2015). New Methods in the Reconstruction of Arctic Marine Palaeoenvironments. In T. Zielinski, M. Weslawski, & K. Kuliński (Eds.), Impact of Climate Changes on Marine Environments (pp. 127–148). Springer International Publishing. https://doi.org/10.1007/978-3-319-14283-8_10

Lara, M. J., & Chipman, M. L. (2021). Periglacial Lake Origin Influences the Likelihood of Lake Drainage in Northern Alaska. Remote Sensing, 13(5), 852. https://doi.org/10.3390/rs13050852

Larsen, A. S., O'Donnell, J. A., Schmidt, J. H., Kristenson, H. J., & Swanson, D. K. (2017). Physical and chemical characteristics of lakes across heterogeneous landscapes in arctic and subarctic Alaska: Lake Basin Types of Alaska. Journal of Geophysical Research: Biogeosciences, 122(4), 989–1008. https://doi.org/10.1002/2016JG003729

Lattaud, J., De Jonge, C., Elling, F., Pearson, A., & Eglinton, T. (2020). Microbial lipid signatures in Arctic deltaic sediments—Insights into methane cycling and climate variability [Preprint]. Earth Sciences. https://doi.org/10.31223/X5B01W

Lenz, J., Wetterich, S., Jones, B. M., Meyer, H., Bobrov, A., & Grosse, G. (2016). Evidence of multiple thermokarst lake generations from an 11 800-year-old permafrost core on the northern S eward P eninsula, A laska. Boreas, 45(4), 584–603. https://doi.org/10.1111/bor.12186

Longo, W. M., Huang, Y., Yao, Y., Zhao, J., Giblin, A. E., Wang, X., Zech, R., Haberzettl, T., Jardillier, L., Toney, J., Liu, Z., Krivonogov, S., Kolpakova, M., Chu, G., D'Andrea, W. J., Harada, N., Nagashima, K., Sato, M., Yonenobu, H., … Shinozuka, Y. (2018). Widespread occurrence of distinct alkenones from Group I haptophytes in freshwater

lakes: Implications for paleotemperature and paleoenvironmental reconstructions. Earth and Planetary Science Letters, 492, 239–250. https://doi.org/10.1016/j.epsl.2018.04.002

Martens, J., Wild, B., Muschitiello, F., O'Regan, M., Jakobsson, M., Semiletov, I., Dudarev, O. V., & Gustafsson, Ö. (2020). Remobilization of dormant carbon from Siberian-Arctic permafrost during three past warming events. Science Advances, 6(42), eabb6546. https://doi.org/10.1126/sciadv.abb6546

Martin, C., Ménot, G., Thouveny, N., Davtian, N., Andrieu-Ponel, V., Reille, M., & Bard, E. (2019). Impact of human activities and vegetation changes on the tetraether sources in Lake St Front (Massif Central, France). Organic Geochemistry, 135, 38–52. https://doi.org/10.1016/j.orggeochem.2019.06.005

Mann, P. J., Eglinton, T. I., McIntyre, C. P., Zimov, N., Davydova, A., Vonk, J. E., ... & Spencer, R. G. (2015). Utilization of ancient permafrost carbon in headwaters of Arctic fluvial networks. Nature Communications, 6(1), 1-7.

McKnight, D. M., Boyer, E. W., Westerhoff, P. K., Doran, P. T., Kulbe, T., & Andersen, D. T. (2001). Spectrofluorometric characterization of dissolved organic matter for indication of precursor organic material and aromaticity. Limnology and Oceanography, 46(1), 38–48. https://doi.org/10.4319/lo.2001.46.1.0038

Medeiros, A. S., Taylor, D. J., Couse, M., Hall, R. I., Quinlan, R., & Wolfe, B. B. (2014). Biological and nutrient responses to catchment disturbance and warming in small lakes near the Alaskan tundra–taiga boundary. The Holocene, 24(10), 1308–1319. https://doi.org/10.1177/0959683614540955

Myers-Smith, I. H., Forbes, B. C., Wilmking, M., Hallinger, M., Lantz, T., Blok, D., Tape, K. D., Macias-Fauria, M., Sass-Klaassen, U., Lévesque, E., Boudreau, S., Ropars, P.,

Hermanutz, L., Trant, A., Collier, L. S., Weijers, S., Rozema, J., Rayback, S. A., Schmidt, N. M., … Hik, D. S. (2011). Shrub expansion in tundra ecosystems: Dynamics, impacts and research priorities. Environmental Research Letters, 6(4), 045509. https://doi.org/10.1088/1748-9326/6/4/045509

Naeher, S., Niemann, H., Peterse, F., Smittenberg, R. H., Zigah, P. K., & Schubert, C. J. (2014). Tracing the methane cycle with lipid biomarkers in Lake Rotsee (Switzerland). Organic Geochemistry, 66, 174–181. https://doi.org/10.1016/j.orggeochem.2013.11.002

Nitze, I., Cooley, S. W., Duguay, C. R., Jones, B. M., & Grosse, G. (2018). The catastrophic thermokarst lake drainage events of 2018 in northwestern Alaska: Fast-forward into the future. The Cryosphere, 19.

O'Donnell, J. A., Aiken, G. R., Swanson, D. K., Panda, S., Butler, K. D., & Baltensperger, A. P. (2016). Dissolved organic matter composition of Arctic rivers: Linking permafrost and parent material to riverine carbon: DOM Composition in Arctic Rivers. Global Biogeochemical Cycles, 30(12), 1811–1826. https://doi.org/10.1002/2016GB005482

O'Donnell, J. A., Aiken, G. R., Walvoord, M. A., Raymond, P. A., Butler, K. D., Dornblaser, M. M., & Heckman, K. (2014). Using dissolved organic matter age and composition to detect permafrost thaw in boreal watersheds of interior Alaska. Journal of Geophysical Research: Biogeosciences, 119(11), 2155–2170. https://doi.org/10.1002/2014JG002695

Pancost, R. D., Hopmans, E. C., & Sinninghe Damsté, J. S. (2001). Archaeal lipids in Mediterranean cold seeps: Molecular proxies for anaerobic methane oxidation. Geochimica et Cosmochimica Acta, 65(10), 1611–1627. https://doi.org/10.1016/S0016-7037(00)00562-7

Peterse, F., Vonk, J. E., Holmes, R. M., Giosan, L., Zimov, N., & Eglinton, T. I. (2014). Branched glycerol dialkyl glycerol tetraethers in Arctic lake sediments: Sources and implications for paleothermometry at high latitudes: Branched GDGTs in Arctic lakes. Journal of Geophysical Research: Biogeosciences, 119(8), 1738–1754. https://doi.org/10.1002/2014JG002639

Richter, N., Longo, W. M., George, S., Shipunova, A., Huang, Y., & Amaral-Zettler, L. (2019). Phylogenetic diversity in freshwater-dwelling Isochrysidales haptophytes with implications for alkenone production. Geobiology, 17(3), 272–280. https://doi.org/10.1111/gbi.12330

Ronkainen, T., McClymont, E. L., Väliranta, M., & Tuittila, E.-S. (2013). The n-alkane and sterol composition of living fen plants as a potential tool for palaeoecological studies. Organic Geochemistry, 59, 1–9. https://doi.org/10.1016/j.orggeochem.2013.03.005

Rydberg, J., Klaminder, J., Rosén, P., & Bindler, R. (2010). Climate driven release of carbon and mercury from permafrost mires increases mercury loading to sub-arctic lakes. Science of the total environment, 408(20), 4778-4783.

Schouten, S., Hopmans, E. C., & Sinninghe Damsté, J. S. (2013). The organic geochemistry of glycerol dialkyl glycerol tetraether lipids: A review. Organic Geochemistry, 54, 19–61. https://doi.org/10.1016/j.orggeochem.2012.09.006

Schouten, S., Rijpstra, W. I. C., Kok, M., Hopmans, E. C., Summons, R. E., Volkman, J. K., & Sinninghe Damsté, J. S. (2001). Molecular organic tracers of biogeochemical processes in a saline meromictic lake (Ace Lake). Geochimica et Cosmochimica Acta, 65(10), 1629–1640. https://doi.org/10.1016/S0016-7037(00)00627-X

Sc'Mmons, R. E., Jahnke, L. I. L., & Roksandic', Z. (n.d.). Carbon isotopic fractionation in lipids from methsnotrophic bacteria: Relevance for interpretation of the geochemical record of biomarkers. 11.

Service, N. P. (n.d.). Bering Land Bridge National Preserve: Geologic Resources Inventory Report. 122.

Simon, M., López-García, P., Moreira, D., & Jardillier, L. (n.d.). New haptophyte lineages and multiple independent colonizations of freshwater ecosystems. Environmental Microbiology Reports, 5(2), 322–332. https://doi.org/10.1111/1758-2229.12023

Spellerberg, I. F., & Fedor, P. J. (2003). A tribute to Claude Shannon (1916-2001) and a plea for more rigorous use of species richness, species diversity and the 'Shannon-Wiener' Index: On species richness and diversity. Global Ecology and Biogeography, 12(3), 177–179. https://doi.org/10.1046/j.1466-822X.2003.00015.x

Stamatakis, A. (2014). RAxML version 8: A tool for phylogenetic analysis and post-analysis of large phylogenies. Bioinformatics, 30(9), 1312–1313. https://doi.org/10.1093/bioinformatics/btu033

Stefanescu, I. C., Shuman, B. N., & Tierney, J. E. (2021). Temperature and water depth effects on brGDGT distributions in sub-alpine lakes of mid-latitude North America. Organic Geochemistry, 152, 104174. https://doi.org/10.1016/j.orggeochem.2020.104174

Strauss, J., Laboor, S., Schirrmeister, L., Fedorov, A. N., Fortier, D., Froese, D., Fuchs, M., Günther, F., Grigoriev, M., Harden, J., Hugelius, G., Jongejans, L. L., Kanevskiy, M., Kholodov, A., Kunitsky, V., Kraev, G., Lozhkin, A., Rivkina, E., Shur, Y., … Grosse, G. (2021). Circum-Arctic Map of the Yedoma Permafrost Domain. Frontiers in Earth Science, 9, 758360. https://doi.org/10.3389/feart.2021.758360

Swanson, D. K. (2019). Thermokarst and precipitation drive changes in the area of lakes and ponds in the National Parks of northwestern Alaska, 1984–2018. Arctic, Antarctic, and Alpine Research, 51(1), 265–279. https://doi.org/10.1080/15230430.2019.1629222

Tape, K., Sturm, M., & Racine, C. (2006). The evidence for shrub expansion in Northern Alaska and the Pan-Arctic: SHRUB EXPANSION IN NORTHERN ALASKA AND PAN-ARCTIC. Global Change Biology, 12(4), 686–702. https://doi.org/10.1111/j.1365-2486.2006.01128.x

Templeton, A. S., Chu, K.-H., Alvarez-Cohen, L., & Conrad, M. E. (2006). Variable carbon isotope fractionation expressed by aerobic CH4-oxidizing bacteria. Geochimica et Cosmochimica Acta, 70(7), 1739–1752. https://doi.org/10.1016/j.gca.2005.12.002

Theroux, S., D'Andrea, W. J., Toney, J., Amaral-Zettler, L., & Huang, Y. (2010). Phylogenetic diversity and evolutionary relatedness of alkenone-producing haptophyte algae in lakes: Implications for continental paleotemperature reconstructions. Earth and Planetary Science Letters, 300(3–4), 311–320. https://doi.org/10.1016/j.epsl.2010.10.009

Thiel, V. (2020). Methane Carbon Cycling in the Past: Insights from Hydrocarbon and Lipid Biomarkers. In H. Wilkes (Ed.), Hydrocarbons, Oils and Lipids: Diversity, Origin, Chemistry and Fate (pp. 781–810). Springer International Publishing. https://doi.org/10.1007/978-3-319-90569-3_6

van Winden, J. F., Talbot, H. M., De Vleeschouwer, F., Reichart, G.-J., & Sinninghe Damsté, J. S. (2012). Variation in methanotroph-related proxies in peat deposits from Misten Bog, Hautes-Fagnes, Belgium. Organic Geochemistry, 53, 73–79. https://doi.org/10.1016/j.orggeochem.2012.07.001

Walter Anthony, K., Daanen, R., Anthony, P., Schneider von Deimling, T., Ping, C.-L., Chanton, J. P., & Grosse, G. (2016). Methane emissions proportional to permafrost carbon thawed in Arctic lakes since the 1950s. Nature Geoscience, 9(9), 679–682. https://doi.org/10.1038/ngeo2795

Walter, K. M., Chanton, J. P., Chapin, F. S., Schuur, E. A. G., & Zimov, S. A. (2008). Methane production and bubble emissions from arctic lakes: Isotopic implications for source pathways and ages. Journal of Geophysical Research, 113, G00A08. https://doi.org/10.1029/2007JG000569

Wang, K. J., Huang, Y., Majaneva, M., Belt, S. T., Liao, S., Novak, J., Kartzinel, T. R., Herbert, T. D., Richter, N., & Cabedo-Sanz, P. (2021). Group 2i Isochrysidales produce characteristic alkenones reflecting sea ice distribution. Nature Communications, 12(1). https://doi.org/10.1038/s41467-020-20187-z

Weber, Y., Sinninghe Damsté, J. S., Zopfi, J., De Jonge, C., Gilli, A., Schubert, C. J., Lepori, F., Lehmann, M. F., & Niemann, H. (2018). Redox-dependent niche differentiation provides evidence for multiple bacterial sources of glycerol tetraether lipids in lakes. Proceedings of the National Academy of Sciences, 115(43), 10926–10931. https://doi.org/10.1073/pnas.1805186115

Weishaar, J. L., Aiken, G. R., Bergamaschi, B. A., Fram, M. S., Fujii, R., & Mopper, K. (2003). Evaluation of Specific Ultraviolet Absorbance as an Indicator of the Chemical Composition and Reactivity of Dissolved Organic Carbon. Environmental Science & Technology, 37(20), 4702–4708. https://doi.org/10.1021/es030360x

Wik, M., Varner, R. K., Anthony, K. W., MacIntyre, S., & Bastviken, D. (2016). Climate-sensitive northern lakes and ponds are critical components of methane release. Nature Geoscience, 9(2), 99–105. https://doi.org/10.1038/ngeo2578

Wild, B., Andersson, A., Bröder, L., Vonk, J., Hugelius, G., McClelland, J. W., Song, W., Raymond, P. A., & Gustafsson, Ö. (2019). Rivers across the Siberian Arctic unearth the patterns of carbon release from thawing permafrost. Proceedings of the National Academy of Sciences, 116(21), 10280–10285. https://doi.org/10.1073/pnas.1811797116

Williamson, C. E., Overholt, E. P., Pilla, R. M., Leach, T. H., Brentrup, J. A., Knoll, L. B., Mette, E. M., & Moeller, R. E. (2016). Ecological consequences of long-term browning in lakes. Scientific Reports, 5(1), 18666. https://doi.org/10.1038/srep18666

Winden, J. F., Talbot, H. M., Reichart, G., McNamara, N. P., Benthien, A., & Sinninghe Damst é, J. S. (2020). Influence of temperature on the δ 13 C values and distribution of methanotroph‐related hopanoids in Sphagnum ‐dominated peat bogs. Geobiology, 18(4), 497–507. https://doi.org/10.1111/gbi.12389

Wu, Y., Wen, Y., Zhou, J., & Wu, Y. (2014). Phosphorus release from lake sediments: Effects of pH, temperature and dissolved oxygen. KSCE Journal of Civil Engineering, 18(1), 323–329. https://doi.org/10.1007/s12205-014-0192-0

Yao, Y., Huang, Y., Zhao, J., Wang, L., Ran, Y., Liu, W., & Cheng, H. (2021). Permafrost thaw induced abrupt changes in hydrology andcarbon cycling in Lake Wudalianchi, northeastern China. Geology. https://doi.org/10.1130/G48891.1

Yao, Y., Zhao, J., Vachula, R. S., Werne, J. P., Wu, J., Song, X., & Huang, Y. (2020). Correlation between the ratio of 5-methyl hexamethylated to pentamethylated branched

GDGTs (HP5) and water depth reflects redox variations in stratified lakes. Organic Geochemistry, 147, 104076. https://doi.org/10.1016/j.orggeochem.2020.104076

Zech, M., Buggle, B., Leiber, K., Marković, S., Glaser, B., Hambach, U., Huwe, B., Stevens, T., Sümegi, P., Wiesenberg, G., & Zöller, L. (2010). Reconstructing Quaternary vegetation history in the Carpathian Basin, SE-Europe, using n-alkane biomarkers as molecular fossils: Problems and possible solutions, potential and limitations. E&G Quaternary Science Journal, 58(2), 148–155. https://doi.org/10.3285/eg.58.2.03

Zhang, Y. G., Zhang, C. L., Liu, X.-L., Li, L., Hinrichs, K.-U., & Noakes, J. E. (2011). Methane Index: A tetraether archaeal lipid biomarker indicator for detecting the instability of marine gas hydrates. Earth and Planetary Science Letters, 307(3–4), 525–534. https://doi.org/10.1016/j.epsl.2011.05.031

Figures and Tables

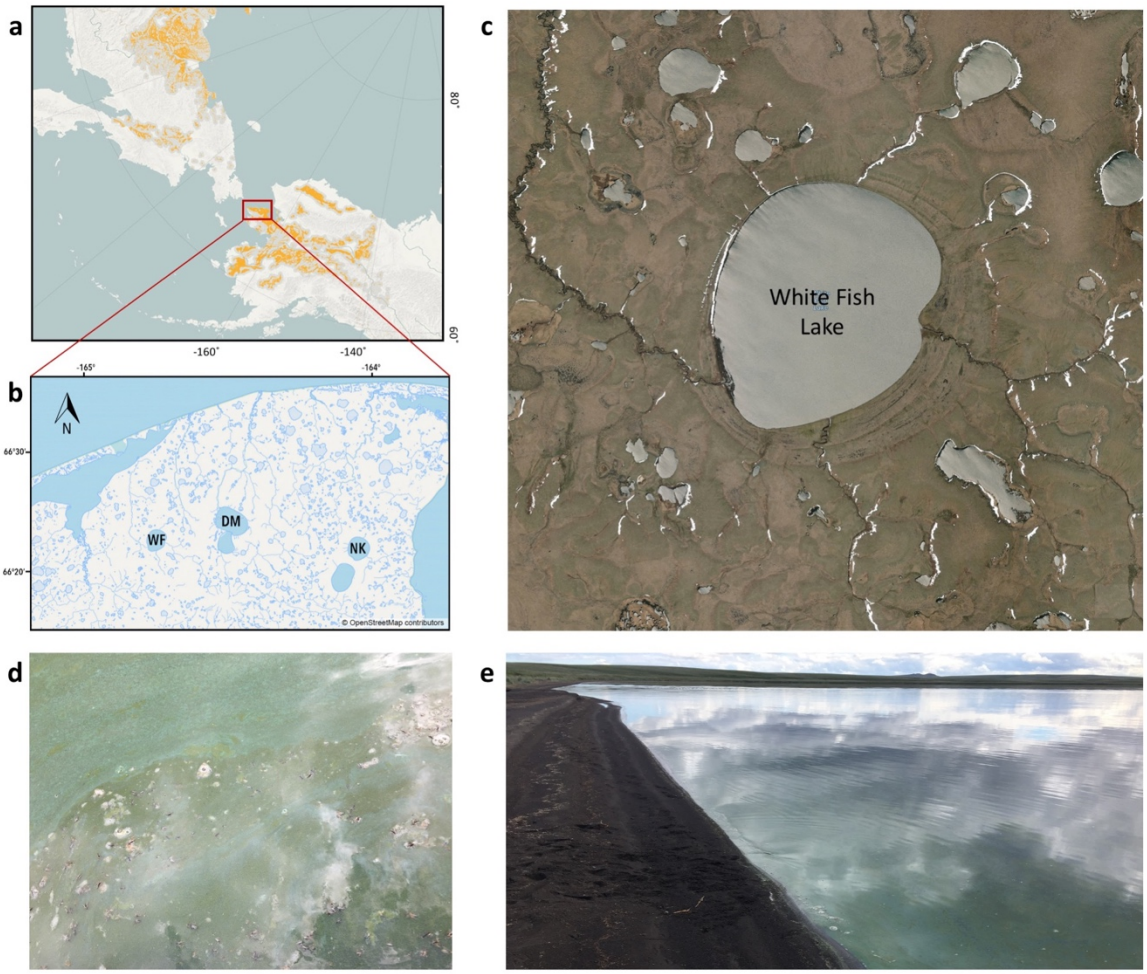

Figure 5. 1. Map of White Fish Lake and the studied region. a) Yedoma (shaded orange) distribution map in the Bering Land Bridge from Strauss et al. (2021). b) Hydrological map of the northern Seward Peninsula, WF: White Fish Lake, DM: Devil Mountain Lake, NK: North Killeak Lake. c) Satellite image of White Fish Lake catchment. d, e) Photos of White Fish Lake covered by cyanobacteria bloom on July 15h, 2018.

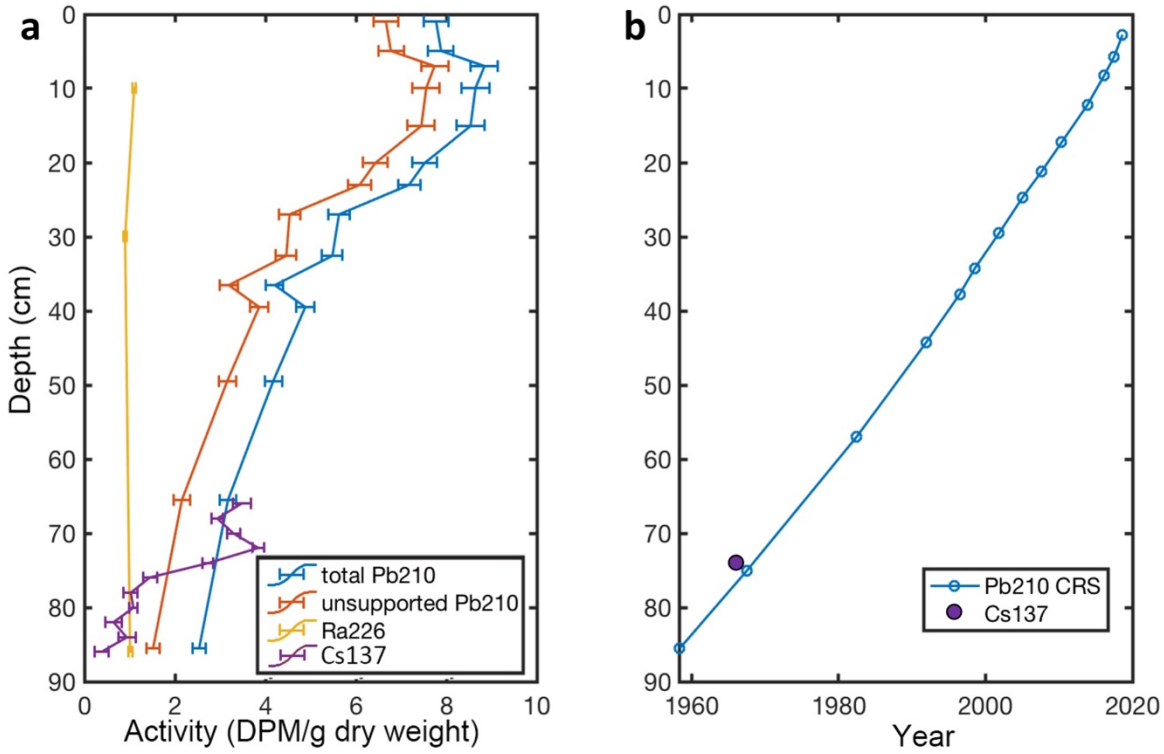

Figure 5. 2. Age model of White Fish Lake. a) Activity of ^{210}Pb, ^{226}Ra, ^{137}Cs and the calculated unsupported ^{210}Pb, the error bars represent +/-σ in measurments. b) Reconstructed chronology based on CRS model and the ^{137}Cs peak fixed at year 1966.

a

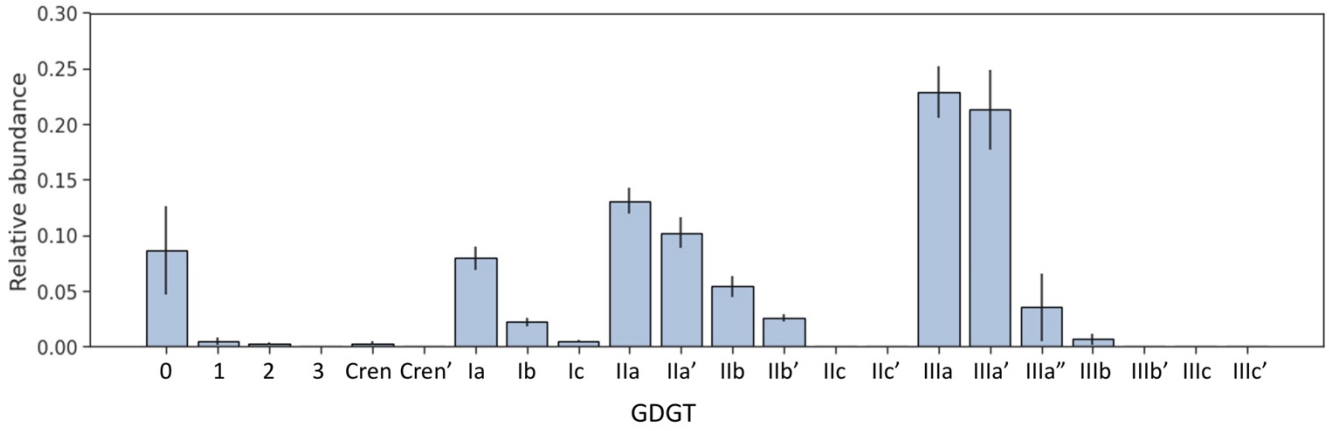

b

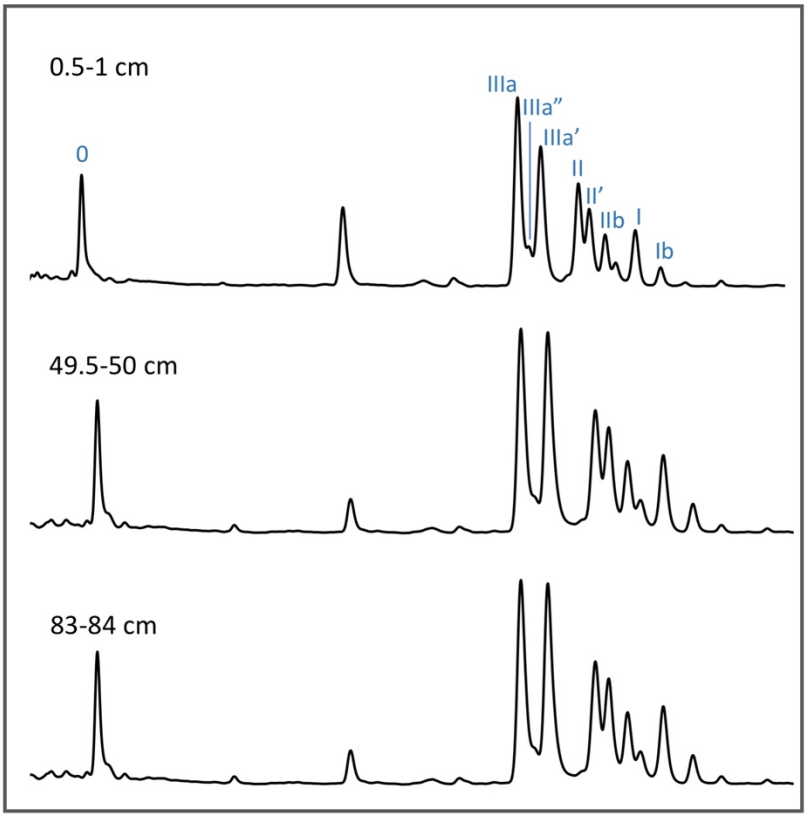

Figure 5. 3. a) Averaged relative abundance of GDGTs in the sediment core, the black error bar denotes the standard deviation along the core. b) Representative HPLC-MS chromatograms of GDGTs.

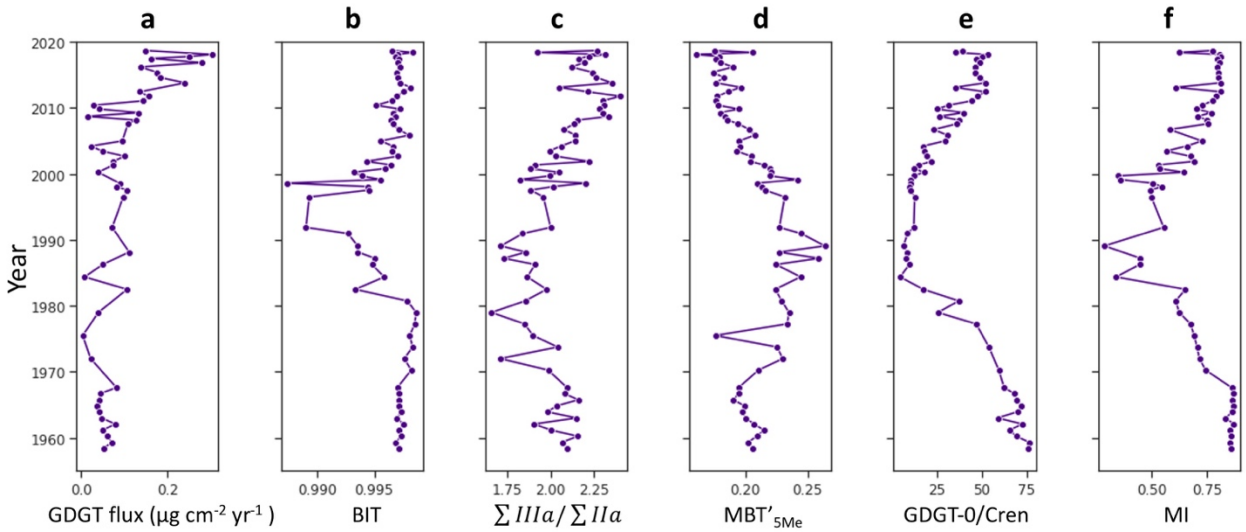

Figure 5. 4. GDGT indices along the core. a) total brGDGT and isoGDGT flux. b-f) BIT, ΣIIIa/ΣIIa, MBT'$_{5Me}$, GDGT-0/Cren, MI indices.

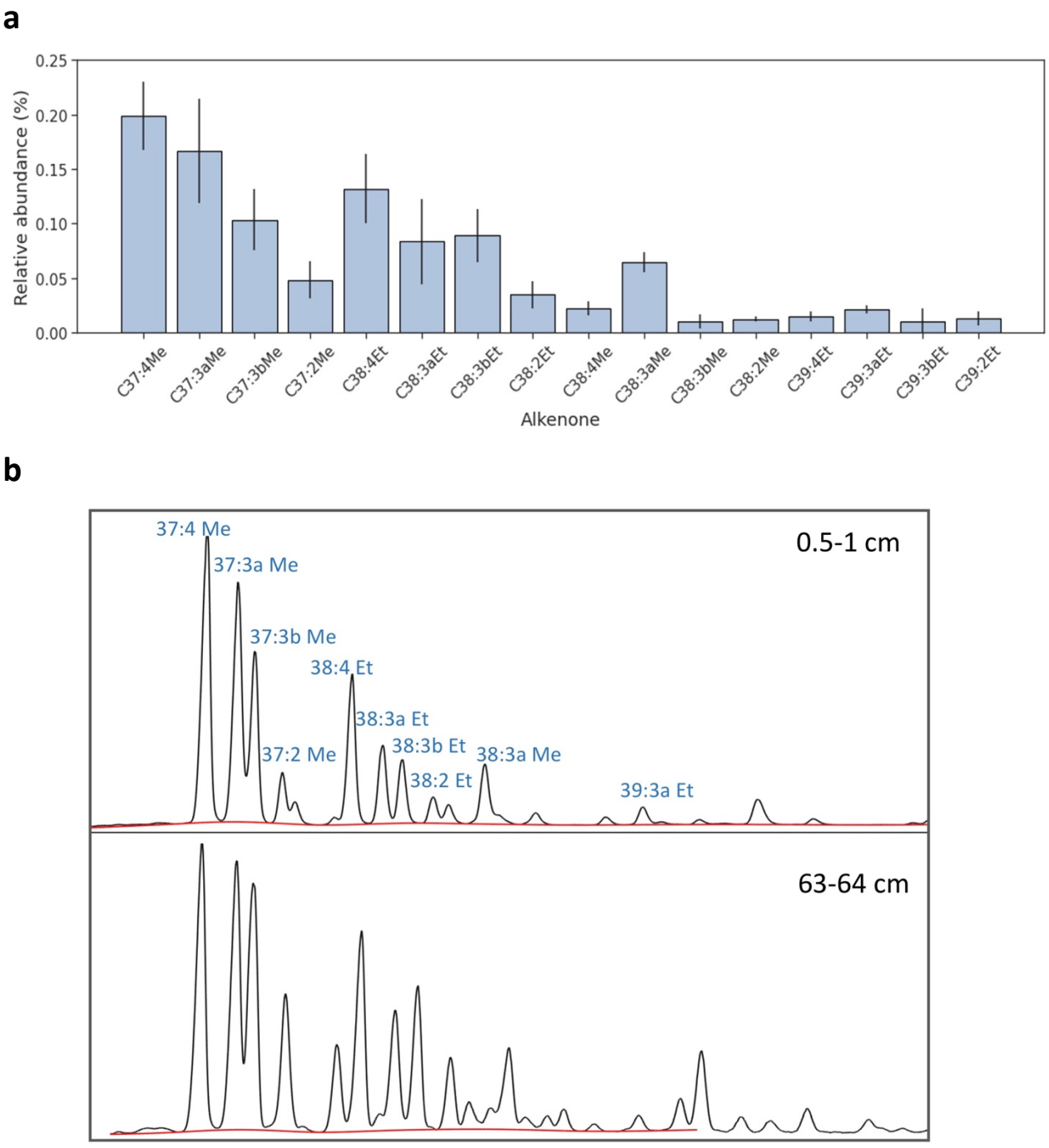

Figure 5. 5. a) Averaged relative abundance of alkenones in the sediment core, the black error bar denotes the standard deviation along the core. b) Representative GC-FID chromatograms of alkenones.

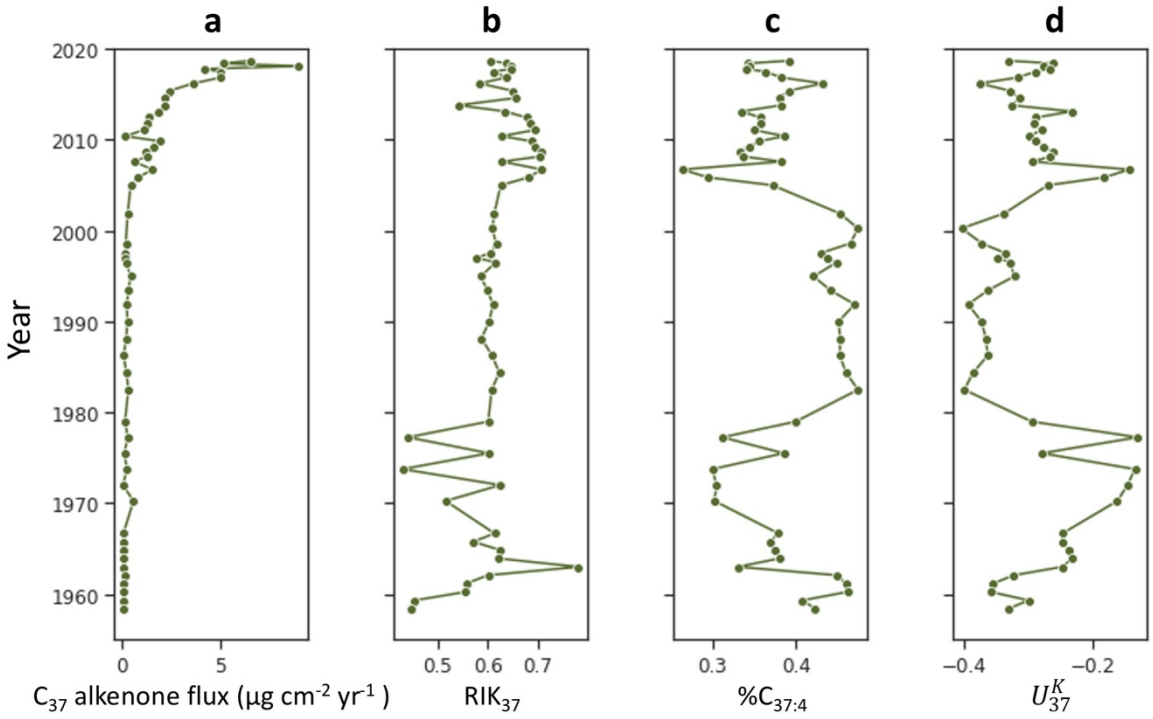

Figure 5. 6. a-d) C_{37} alkenone flux and RIK_{37}, $\%C_{37:4}$, and U_{37}^{K} indices along the core.

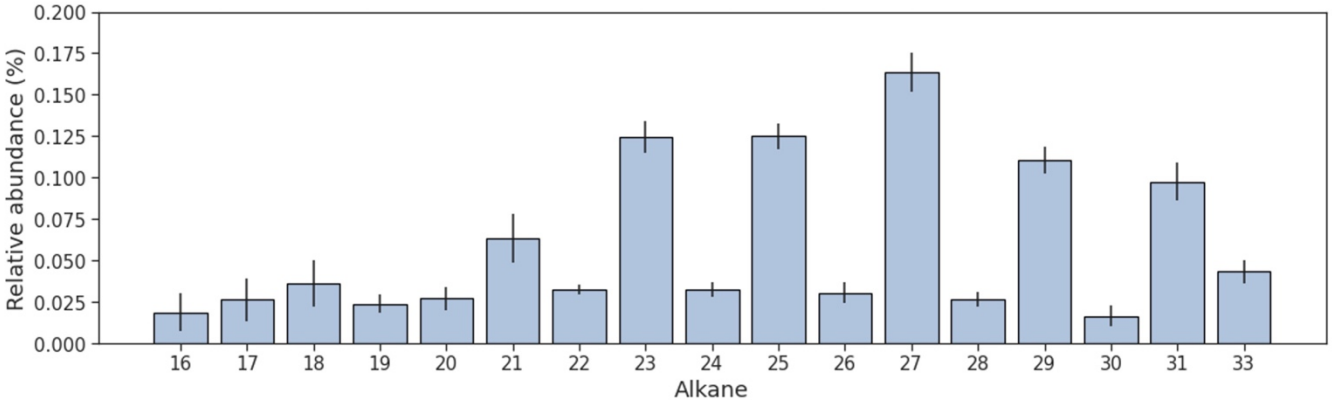

Figure 5. 7. Averaged relative abundance of n-alkanes (C_{16}-C_{33}), the black error bar denotes the standard deviation along the core.

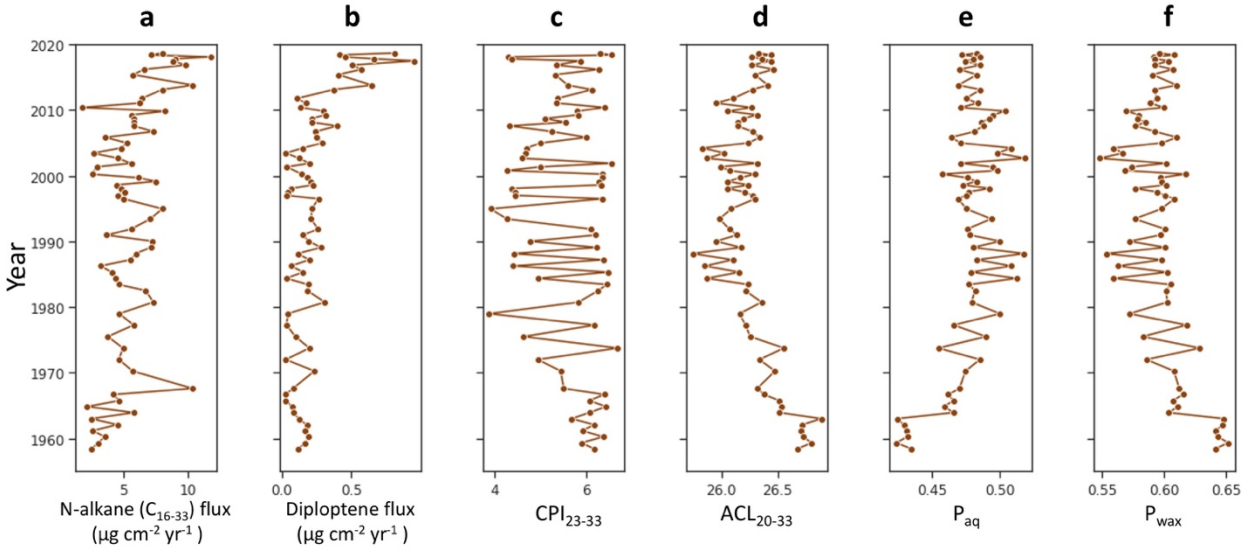

Figure 5. 8. a, b) C_{16-33} n-alkane flux and diploptene flux. c-f) CPI_{23-33}, ACL_{20-33}, P_{aq}, and P_{wax} indices along the core.

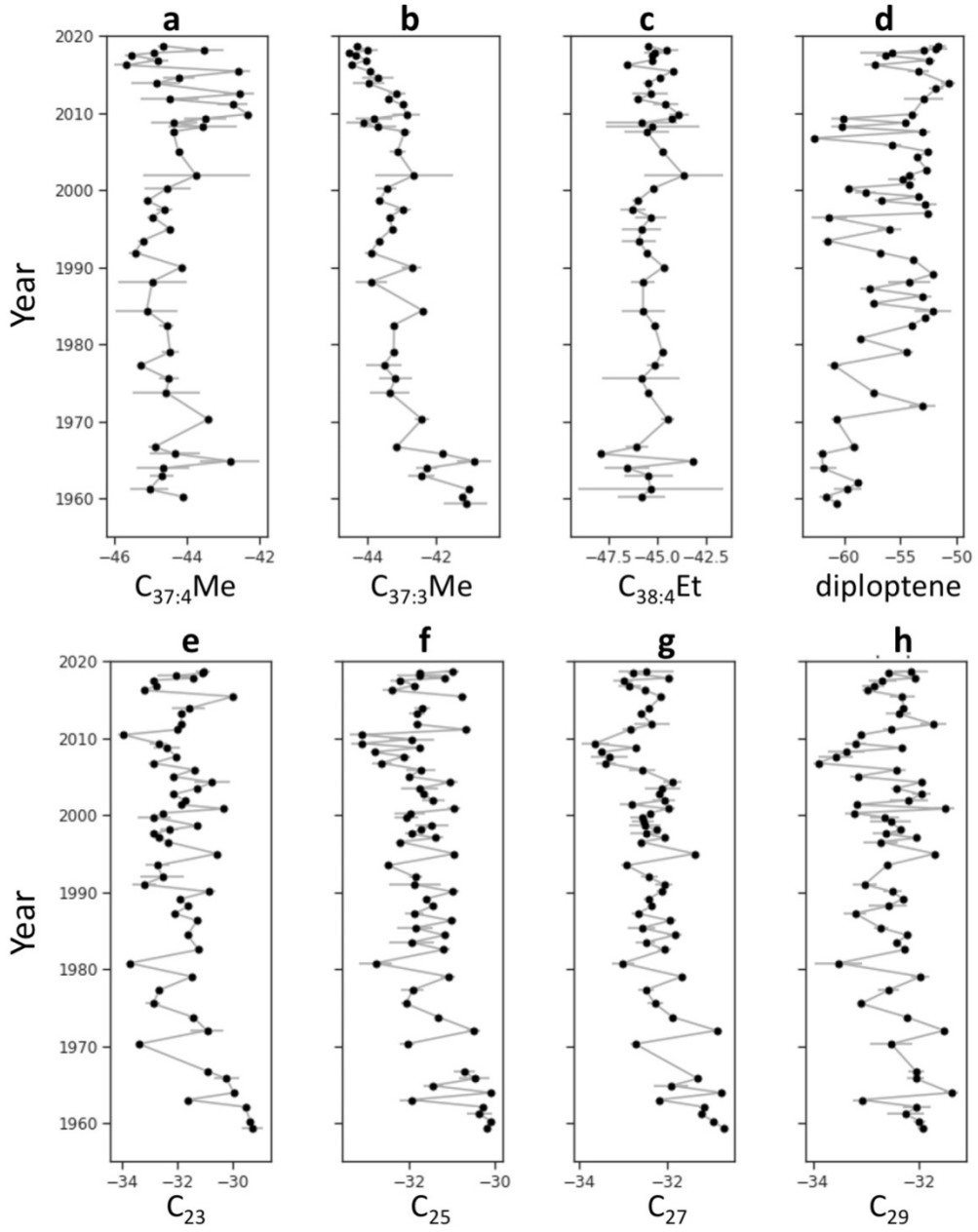

Figure 5. 9. a-h) $\delta^{13}C$ (‰VPDB) of $C_{37:4}Me$, $C_{37:3}Me$, $C_{38:4}Et$ alkenones, diploptene, and C_{23}, C_{25}, C_{27}, C_{29} alkanes.

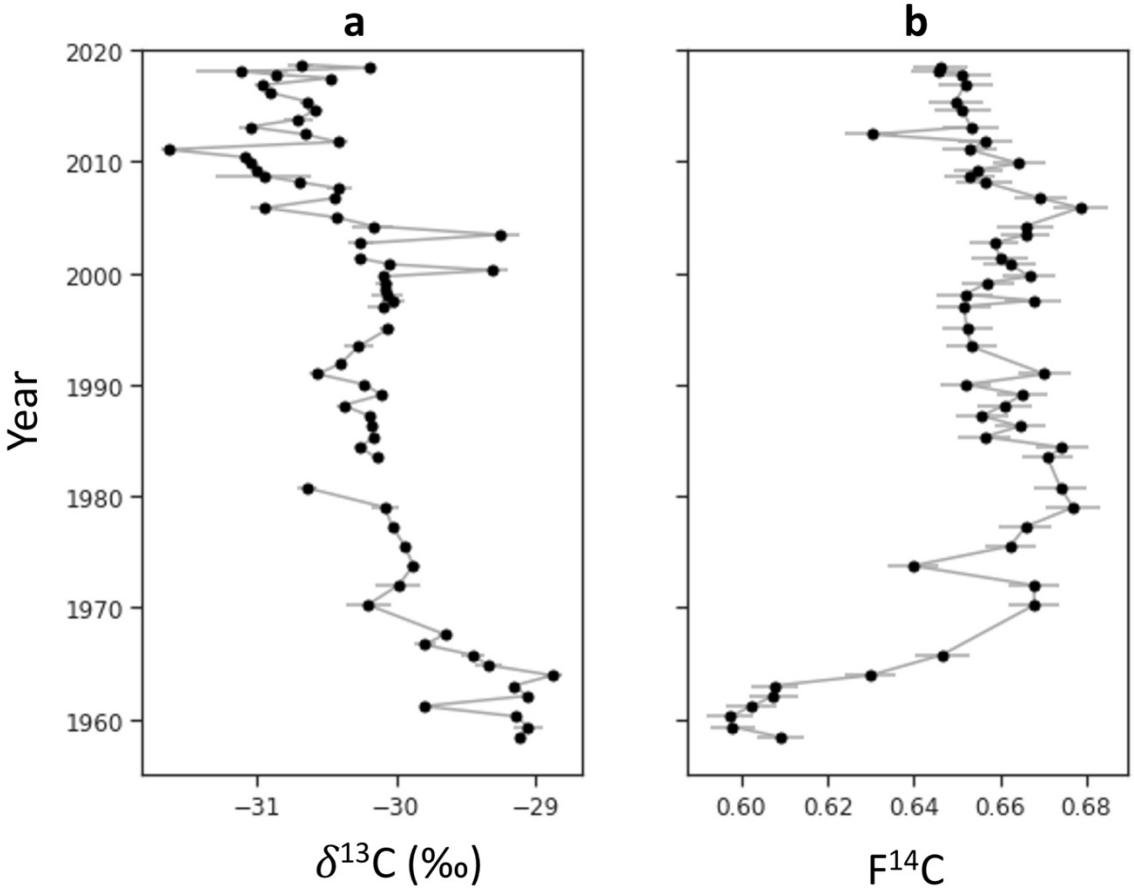

Figure 5. 10. a, b) bulk TOC stable and radiocarbon isotopes $\delta^{13}C$ (‰VPDB) and $F^{14}C$.

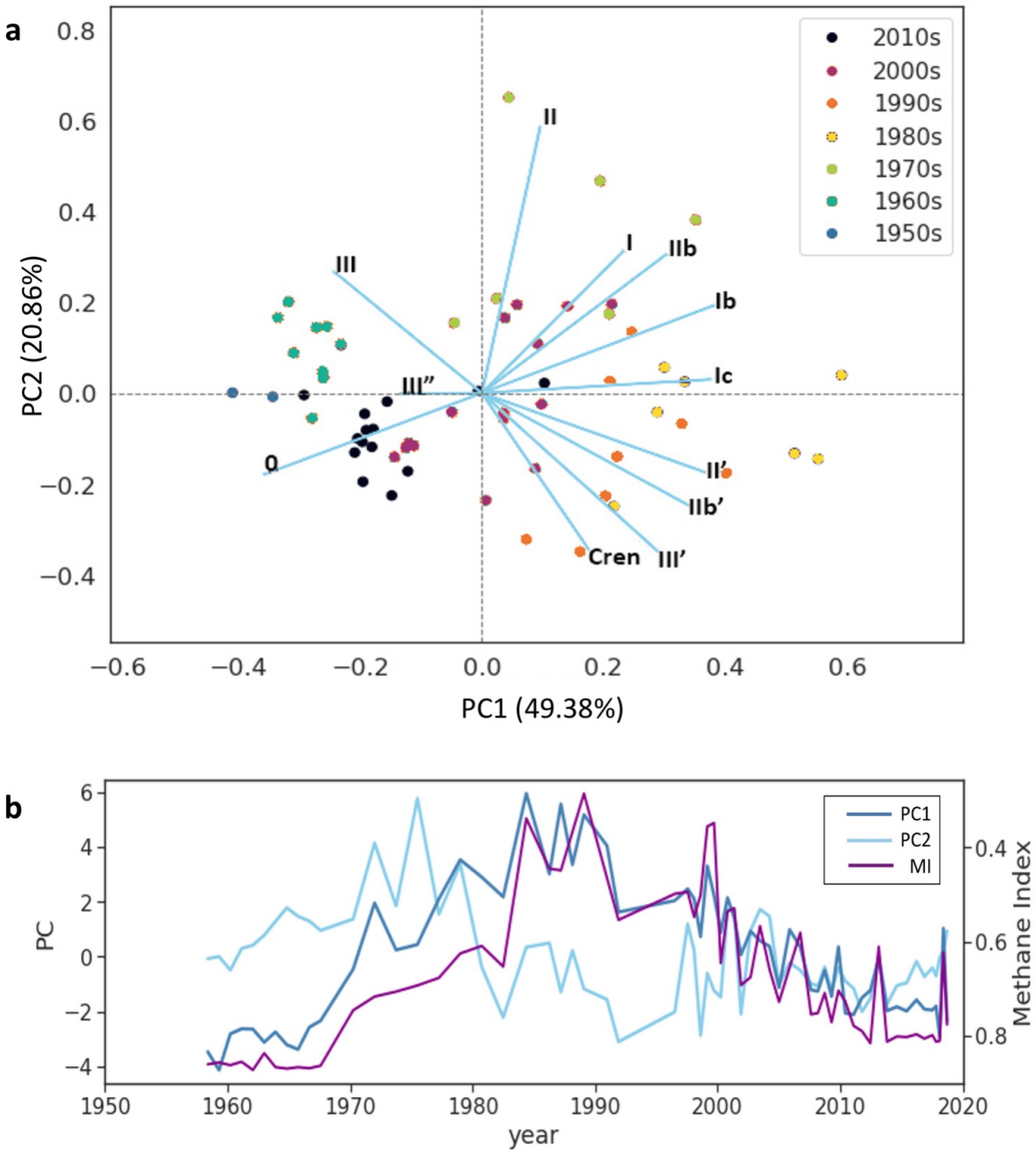

Figure 5. 11. a) PCA biplot of GDGT relative abundance. Scattered point denotes individual sediment samples. b) Time series of PC1 and PC2, and methane index (MI).

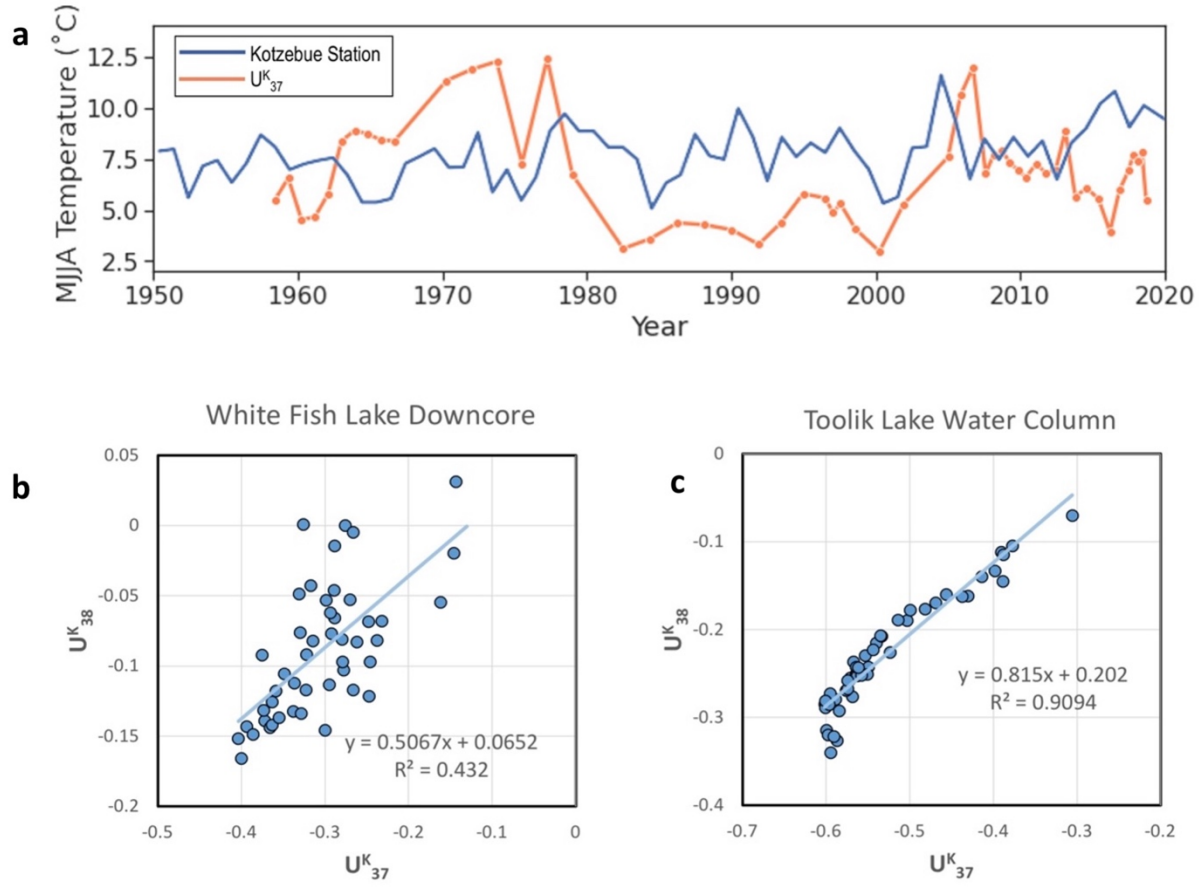

Figure 5. 12. a) MJJA air temperature record from Kotzebue Airport Meteorology Station (blue) comparing with U^K_{37} reconstructed MJJA temperature using Longo et al. (2018) calibration. b, c) Linear regression between U^K_{37} and U^K_{38Me} from White Fish Lake downcore samples and Toolik Lake water column samples (Longo et al., 2016).

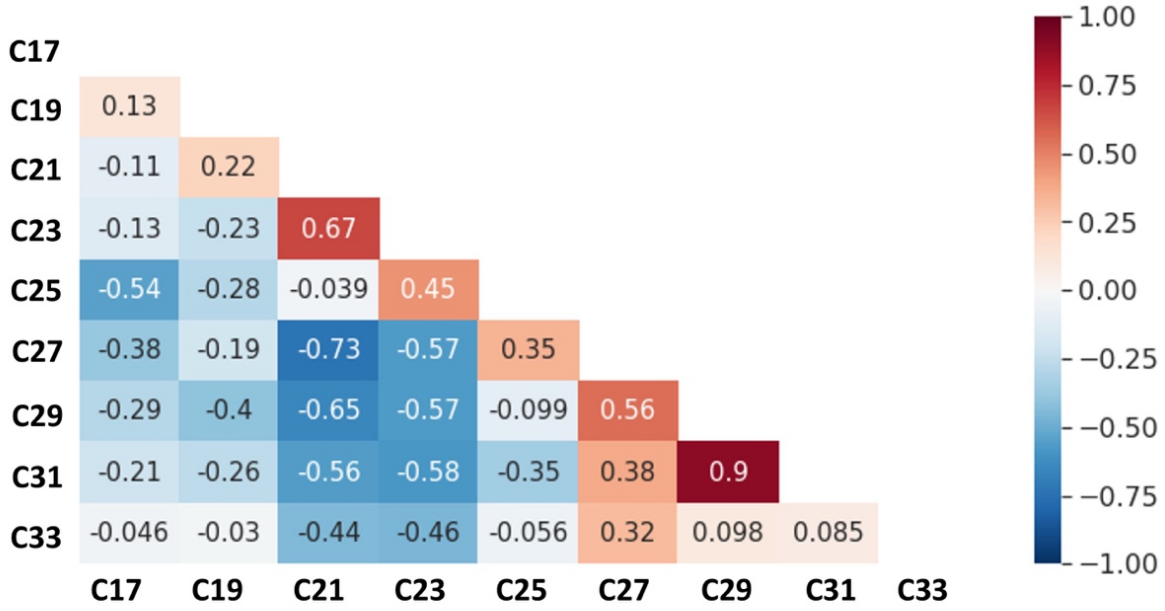

Figure 5. 13. Pearson correlation between the relative abundance of C17-C33 odd number n-alkane.

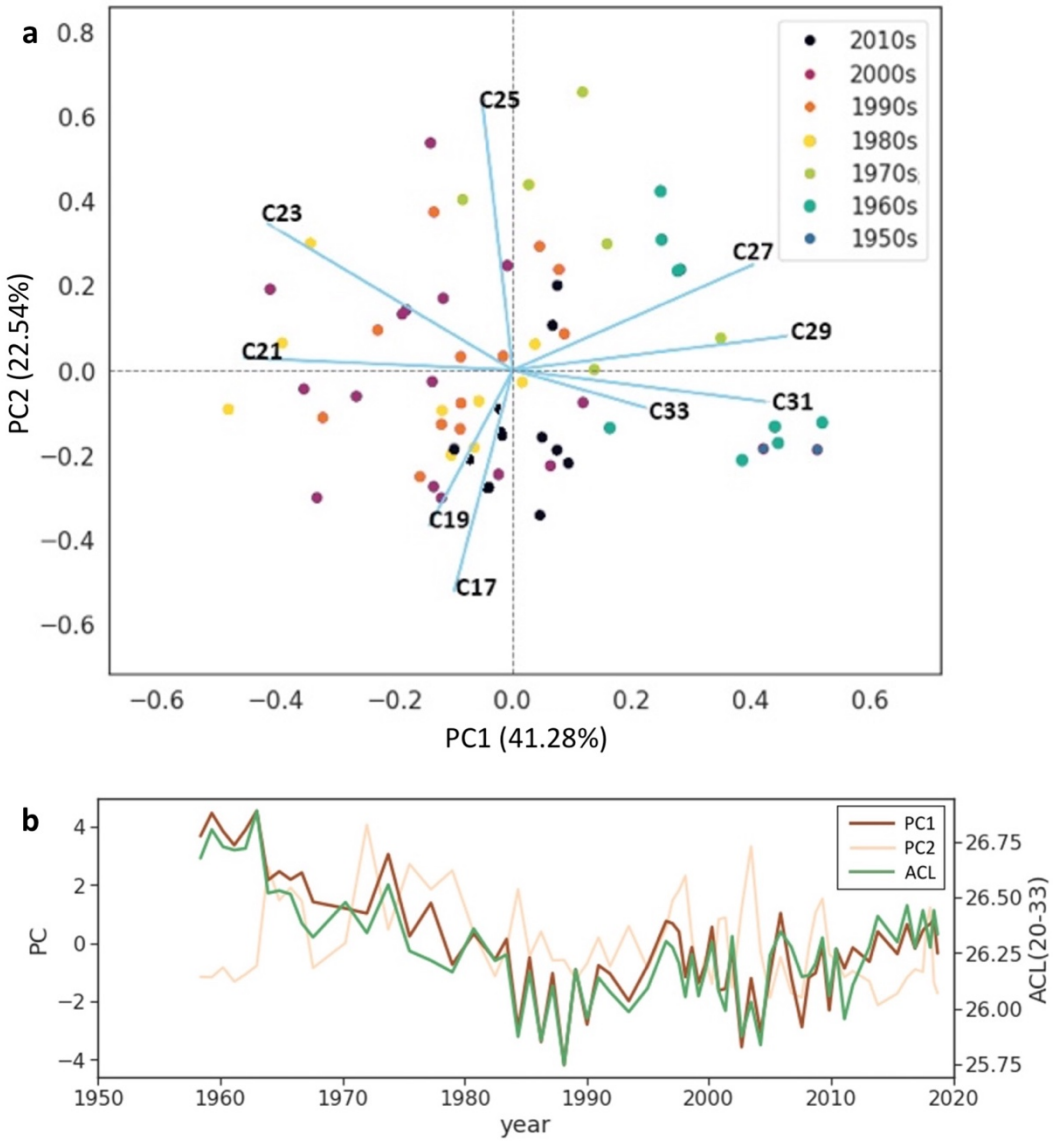

Figure 5. 14. a) PCA biplot of n-alkanes relative abundance. Scattered point denotes individual sediment samples. b) Time series of PC1 and PC2 plotted with average chain length ($ACL_{20\text{-}33}$).

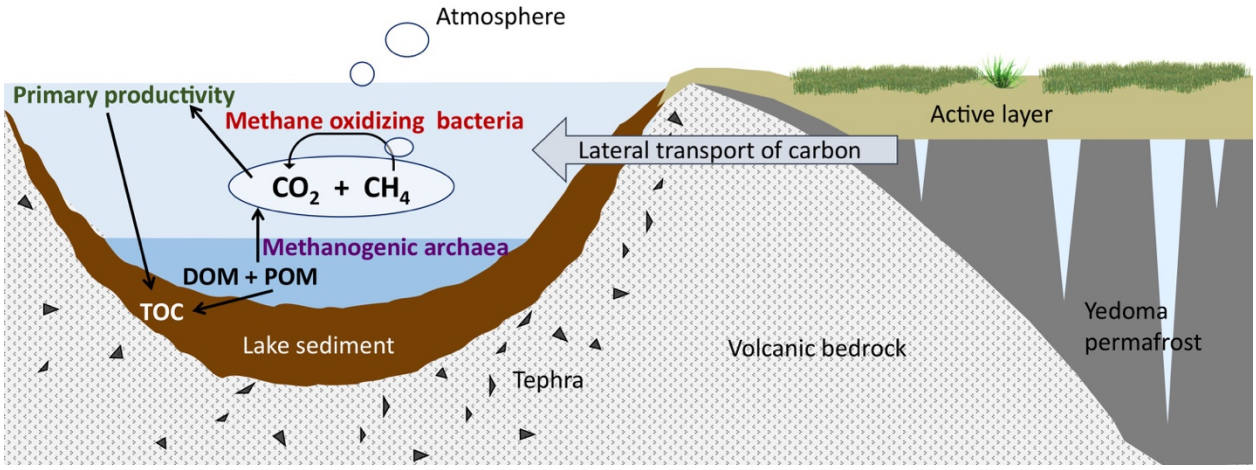

Figure 5. 15. Schematics of the carbon cycle within White Fish Lake.

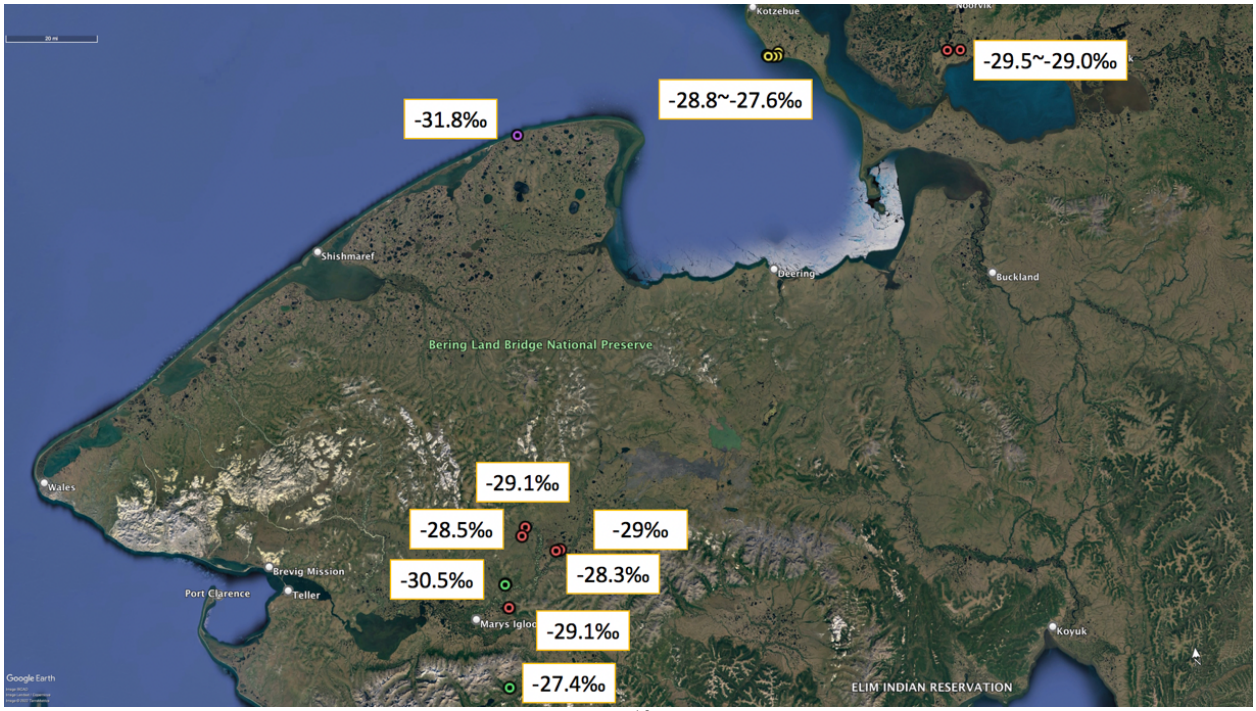

Figure 5. 16. Map of the surface lake sediment $\delta^{13}C$ reported in previous studies (yellow: Jongejans et al., 2018; red: Lenz et al., 2018; purple: Lenz et al., 2016; green: Medeiros et al., 2014).

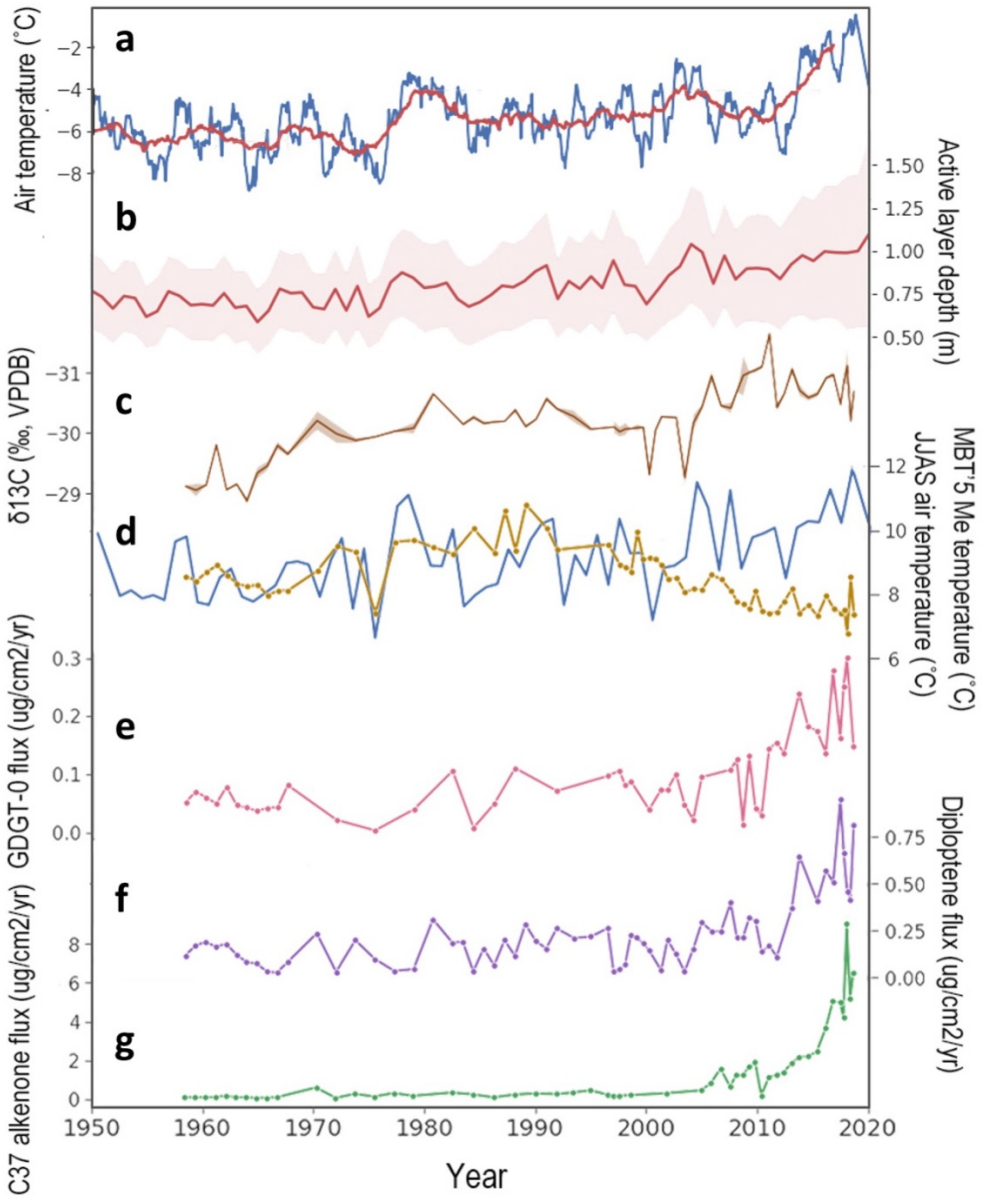

Figure 5. 17. Temperature and active layer depth in comparison with biomarker results in White Fish Lake since late 1950s. a) Air temperature recorded in Kotzebue Airport Meteorology Station (https://www.ncdc.noaa.gov/cdo-web/datasets), the blue line is the mean monthly air temperature, and the red line is the 3-yr running mean. b) Modeled average active layer thickness within 2km radius of White Fish Lake, the shaded area denotes standard deviation within the 2km radius (https://ngee-arctic.ornl.gov/data/pages/NGA196.html). c) $\delta^{13}C$ of bulk organic carbon, shaded area denotes the standard deviation between measurements. d) JJAS air temperature record from Kotzebue Airport Meteorology Station (blue) comparing with MBT'_{5Me} reconstructed JJAS temperature using Stefanescu et al. (2021) calibration. e) GDGT-0 flux. f) Diploptene flux. g) C37 alkenone flux.

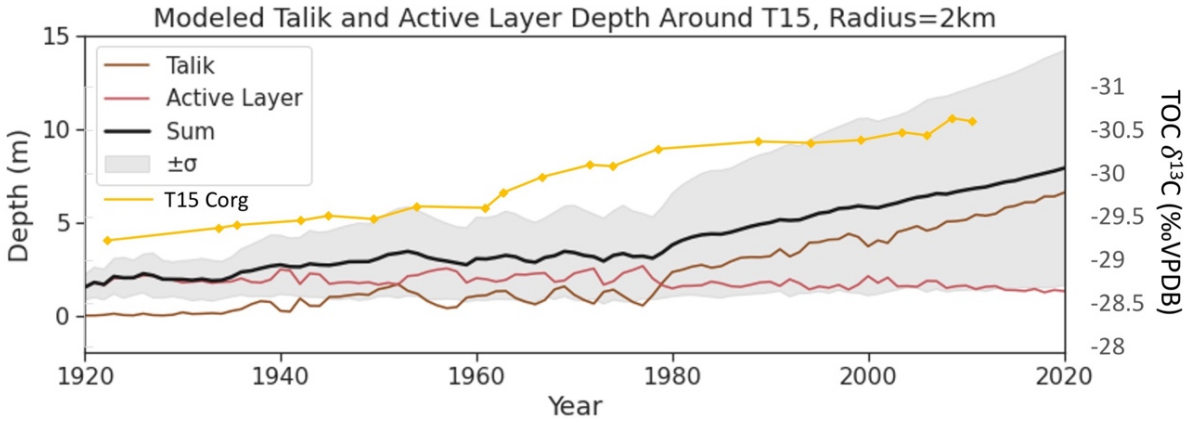

Figure 5. 18. Modeled talik and active layer depth around 2km radius of Lake T15, the black line denotes the sum of talik and active layer depth, and the shaded area is the standard deviation within 2km-radius examined region. The yellow line is the bulk TOC $\delta^{13}C$ of Lake T15 (Medeiros et al., 2014).

Table 5. 1. Isochrysidales sequence reads recovered from three downcore samples

	1.5-2 cm	**10.5-11 cm**	**20.5-21 cm**	**63-64 cm**
Total reads	14848	7109	2326	1284
Total ESVs	37	19	7	3
1a phylotype % reads	75.0%	94.1%	100%	100%
1a phylotype % ESVs	16.2%	84.2%	100%	100%
Shannon Index	1.32±0.04	1.22±0.04	0.44±0.03	0.15±0.02